



HAL
open science

CE platform for assaying enzymatic activity and modulation : application to lipases and nucleoside kinases

Ghassan Al Hamoui Dit Banni

► **To cite this version:**

Ghassan Al Hamoui Dit Banni. CE platform for assaying enzymatic activity and modulation : application to lipases and nucleoside kinases. Analytical chemistry. Université d'Orléans, 2021. English. NNT : 2021ORLE3122 . tel-03463674

HAL Id: tel-03463674

<https://theses.hal.science/tel-03463674>

Submitted on 2 Dec 2021

HAL is a multi-disciplinary open access archive for the deposit and dissemination of scientific research documents, whether they are published or not. The documents may come from teaching and research institutions in France or abroad, or from public or private research centers.

L'archive ouverte pluridisciplinaire **HAL**, est destinée au dépôt et à la diffusion de documents scientifiques de niveau recherche, publiés ou non, émanant des établissements d'enseignement et de recherche français ou étrangers, des laboratoires publics ou privés.

UNIVERSITÉ D'ORLÉANS
ÉCOLE DOCTORALE
SANTÉ, SCIENCES BIOLOGIQUES ET CHIMIE DU VIVANT (SSBCV)
INSTITUT DE CHIMIE ORGANIQUE ET ANALYTIQUE

THÈSE présentée par :

Ghassan AL HAMOUI DIT BANNI

soutenue le : 25 mai 2021

pour obtenir le grade de : **Docteur de l'Université d'Orléans**
Discipline/ Spécialité : Chimie analytique

**Suivi de l'activité enzymatique et de sa
modulation par CE : application à l'étude
des lipases et nucléosides kinases**

THÈSE dirigée par :
Pr. NEHME Reine

Professeur, Université d'Orléans

RAPPORTEURS :
Pr. PERRIN Catherine
Pr. CLAROT Igor

Professeur, Université de Montpellier
Professeur, Université Lorraine

JURY :

Pr. CLAROT Igor
Pr. PERRIN Catherine
Pr. HAMACEK Josef
Dr. SEBBAN Muriel
Dr. ROY Vincent
Pr. NEHME Reine

Professeur, Université Lorraine (Président)
Professeur, Université de Montpellier
Professeur, Université d'Orléans
Maître de conférences, Université de Rouen
Maître de conférences, Université d'Orléans
Professeur, Université d'Orléans



“and ye have not been vouchsafed of knowledge save a little.”
Surat Al Isra, Verse 85

To the memory of my father

To my mother and siblings

Acknowledgments

I would describe this thesis as one of the most remarkable and exciting experiences I have ever lived. It has allowed me to grow and mature both on a scientific and personal level. Throughout the duration of this thesis, I have had the absolute honor of encountering many wonderful people whom I would like to thank for partaking in this journey with me.

First and foremost, I would like to thank all the members of the thesis defense jury who have accepted to review my thesis, Pr. Catherine Perrin and Pr. Igor Clarot for having accepted to be reporters and Dr. Muriel Sebban, Pr. Josef Hamacek and Dr. Vincent Roy for having accepted to be examiners of this thesis.

I would like to thank the Region Centre-Val de Loire for financing this PhD.

I would especially like to thank Pr. Reine Nehmé for her wise and concise direction of this thesis. Thank you Reine for entrusting me with this responsibility and for being there to guide me and offer me precious advice, for the motivational boosts throughout the years particularly during the last few months. Your ability to turn data from a few experiments into an intriguing, fascinating story will never cease to impress me. I would also like to thank Pr. Philippe Morin for all his help, advice and support, Dr. Rouba Nasreddine for all her help and scientific advice especially those regarding MST operation and Dr. Bérengère Claude for her continuous aid, valuable discussions and support.

This thesis took place at the institute of organic and analytical chemistry (ICOA), which had become my second home for the last 4 years. I would like to thank Pr. Sylvain Routier and Pr. Pascal Bonnet, current and past directors of ICOA, for hosting this project at the institute and providing necessities for all students and employees.

I would like to thank all of our collaborators who have fruitfully contributed to this work through their scientific expertise: Pr. Luigi Agrofoglio, Dr. Vincent Roy, Dr. Nicolas Biteau, Pr. Josef Hamacek, Pr. Francesco Piazza and Pr. Chrystelle Lopin-Bon from the university of Orléans, Pr. Axel Marchal and Dr. Syntia Fayad from the university of Bordeaux, Pr. Hervé Cottet, Dr. Laurent Leclercq and Dr. Phu Cao-Ngoc from the university of Montpellier, Dr. Rawi Ramautar and Dr. Nicolas Drouin from the university of Leiden- The Netherlands. I would also like to thank the Nanotemper community and support team for their quick and decisive responses for issues related to MST.

I would like to thank all the permanent employees of ICOA for all their administrative aid and technical assistance: Marie-Madeleine, Sophie, Christophe, Stéphane, Alain-Michel, Véronique and Laurent. Florian, thank you for designing the 3D scaffold for the conductivity detection cell that has greatly facilitated our work. Cédric, thank you

for your availability whenever technical issues ensued (and they did a lot!) and also for your help with the design of the 3D scaffold.

I would like to thank Cyril for all the interesting discussions (scientific or not), advices and aid for MS and other analyses.

I would like to thank all the permanent members of the SAAB team of ICOA: Bérengère, Sandrine, Laetitia, David, Caroline, Emilie, Eric, Agnès, Pierre-Eric and Christelle. Thank you all for all your support, advice and discussions. Bérengère, thank you for all your kind words of support and encouragement and for your scientific aid. David, thank you for all the interesting discussions, scientific aid and the memories shared in the break room. Sandrine, thank you for your words of motivation and encouragement, particularly on Mondays!

I would like to thank all current and past colleagues in the SAAB team for all their aid, support and memories. Syntia, thank you for all your help at the beginning and throughout my thesis and for having been my first friend upon my arrival here! Adrien, Adad is simply the best gamer out there! Thank you for all the CS:GO and LOL memories, your humor, impulsiveness and kindness. Angeline, thank you for your extreme "gentillesse". I am glad you won the rights to the computer! Nhi, my little Vietnamese herb! Thank you for all the hilarious moments at the university restaurant, for your sympathy and kindness. Thibault, thank you habibi for all the good laughs, memories and memes "You know what they say..". Souhila: "Sho ya 7elo?!" Thank you for all the good times and memories, and your scientific and personal aid. Jeremy, one of the gentlest and kindest people I have ever met. Thanks to you, I can engage in a conversation in French! Thank you for being there to answer my questions. All the best for your thesis. Quentin, my favorite Toulousian! Thank you for all the positive energy you diffuse through the lab. I wish you have a blast in Japan! Laurine, Thank you for all the morning horoscopes, Covid-19 infection stats and miscellaneous information. All the best for your defense! Rouba, Thank you for your aid and support and all the discussions, about CE, MST and most importantly, food! Farah, Thank you for all your support, advices and kindness during the short period of your stay. Sirine, thank you for all the great food review moments with Rouba. All the best for your thesis. Solweig, Thank you for all the interesting discussions during smoking breaks. Best of luck for your thesis! "May your hats fly as high as your dreams". Gaëlle, thank you for your sportsmanship, my fellow pétanque championess. Cécile, thank you for your energy and enthusiasm. I would also like to thank Elise, Amal, Lucija, Batiste, Coralie, Magdalena, Andra, Sofiane, Vanille, Vanessa and Chloé who were for a brief period, a part of our family. Marta, Jossipa, Katia and Mathieu, I wish you all the best for your future endeavors!

I would like to thank on behalf of the PA 800+ CE instrument Thibault, Adrien, Jérémy, Quentin and Laurine for their aid in transporting the CE instrument for MS hyphenation.

From outside the analytical lab, I would like to thank all my colleagues from the organic synthesis, biochemistry and modulation laboratories. Vincent, my fellow pétanque champion and gig-mate! Thank you for all the awesome times especially during preparation for the Christmas eve gig. I would like to thank Mazarine, Abdul Aziz and Pierre for all their help. I would also like to thank Dr. Pierre Lafitte for his advices and insight about protein purification and Mateja for her help using microplate reader. I would also like to thank Cosmin, Giuliano, Romain, Celia, Benjamin, Abdugheni, Soukaina and Janwa.

I would like to thank Aurélien Bonnamy, Gisèle Tong, David Da Silava, Martine Beaufour and Bérengère Claude from IUT Orléans for their help and advices during practical teaching sessions. I would also like to thank all of Zoé, Clémentine, Estelle, Ninon, Sophia, Maxime and Laetitia from Lycée Voltaire-Orléans, for their participation in the EDIFICE program.

I would like to thank my friends outside of the work environment. Georges, thank you for being a brother of mine, providing me with daily doses of support and encouragement ever since I first met you 5 years ago. I will cherish all the awesome adventures we've been through and I look forward to those of the future. A Special thanks to Marc and Chady, my first Dota 2 comrades. Thank you for all the good times and memories, I hope to see you soon. Dany, thank you for all the "support" and great times. I think you are on the path of becoming my friend rather than my brother's friend ☺. I wish you all the best for your future. I would also like to thank my M2 colleagues Nour, Mira, Samer, Antonia, Malak, Batoul, Najat and Zeinab for all the great times and memories we had back in Lebanon.

Thank you to Pr. Bassam Badran and Dr. Walid Rachidi, directors of my M2 program in Lebanon and Grenoble and Dr. Jean-Luc Ravanat, director of my M2 internship at CEA-Grenoble, for all the opportunities and expertise that you have shared with me.

I would like to thank my family to whom I am eternally grateful. If it weren't for your love and support, I wouldn't have been where I am now. Thank you, Mom, for your unconditional support and love, the consistent moral boosting and for your patience. Thanks to my siblings, Mohammed and Rawan for the much-needed laughs and jokes, their support and prayers. I would also like to dedicate this thesis to the memory of my late father. I miss all of you and I pray to see you soon. I would also like to thank my aunts, uncles, cousins and grandparents for all their support and sympathy.

Chantal (Michat), Tempo, Amélie, Thibaut, Charlie and Moka, thank you for becoming my family here in France. Your kindness, sympathy and compassion are unprecedented. Thank you for all your love, support and caring. I will cherish all the moments we have spent together.

Table of content

Abbreviations	I
Constants and symbols	IV
Introduction.....	1
Chapter I: Bibliographic introduction.....	7
Chapter II: Enzyme modulating molecules: Bioactivities and biophysical interactions.....	83
Part A: Screening for pancreatic lipase natural modulators by capillary electrophoresis hyphenated to spectrophotometric and conductometric dual detection	87
Part B: Microscale thermophoresis, complemented by capillary electrophoresis, to highlight lipase-ligand interactions	128
Part C: Bioactivity assays: investigating the complexity of modulators and reaction environment.....	161
Chapter III: Hyphenation of capillary electrophoresis to mass spectrometry	195
Part A: Capillary electrophoresis-mass spectrometry at trial by Metabo-Ring: effective electrophoretic mobility for reproducible and robust compound annotation	207
Part B: Capillary electrophoresis- mass spectrometry for monitoring nucleoside kinases activity: Applications to novel anti-viral compounds.....	225
Conclusions & perspectives.....	253

Abbreviations

3-GBA	3-O-galloylbarrinic acid
4-NP	4-nitrophenol
4-NPB	4-nitrophenyl butyrate
5-FU	5-Fluorouracil
ABTS	2,2'-azino-bis(3-ethylbenzothiazoline-6-sulfonic acid)
ACE	Angiotensin-converting enzyme
ACV	Acyclovir
ACVMP	Acyclovir monophosphate
ADP	Adenosine diphosphate
AK	Adenosine kinase
AMP	Adenosine monophosphate
APTES	(3-aminopropyl)triethoxysilane
ATP	Adenosine triphosphate
BA	Bartogenic acid
BC	Blackcurrant
BGE	Background electrolyte
BSA	Bovine serum albumin
BVDU	(E)-5-(2-bromovinyl)-2'-deoxyuridine
C ⁴ D	Capacitively coupled contactless conductivity detection
CA	<i>Chrysanthellum americanum</i>
CALB	<i>Candida antarctica</i> lipase B
CD	Cyclodextrin
CE	Capillary electrophoresis
CHES	N-cyclohexyl-2-aminoethanesulfonic acid
CMP	Cytidine monophosphate
CRL	<i>Candida rugosa</i> lipase
CS	Chondroitin sulfate
CVL	<i>Chromobacterium viscosum</i> lipase
CZE	Capillary zone electrophoresis
DAD	Diode-array detector
DG	Diglyceride
DLS	Dynamic light scattering
DMSO	Dimethyl sulfoxide
DNA	Deoxyribonucleic acid
DOL	Degree of labeling
DPPC	1,2-dipalmitoyl-sn-glycero-3-phosphocholine
DTT	Dithiothreitol
EDTA	Ethylenediaminetetraacetic acid
EGC	Epigallocatechin
EGCG	Epigallocatechin gallate
ELSD	Evaporative light scattering detector

EMMA	Electromigration microanalysis
EOF	Electroosmotic flow
ESI	Electrospray ionization
EtOH	Ethanol
FA	Fatty acid
FFA	Free fatty acid
FIA	Flow injection analysis
FT-ICR	Fourier-transform ion cyclotron resonance
GA	Glutaraldehyde
GC	Gas chromatography
GCV	Ganciclovir
GMP	Guanosine monophosphate
HA	Hyaluronic acid
HAW	Hawthorn
Hex	Hexasaccharide, HA hydrolysis product
HNE	Human neutrophil elastase
HPAC	High-performance affinity chromatography
HPLC	High-performance liquid chromatography
HRMS	High-resolution mass spectrometry
HSV	Herpes simplex virus
HTS	High throughput screening
IB	Incubation buffer
IMER	Immobilized enzyme reactor
IR	Infrared
ITC	Isothermal calorimetry
LC	Liquid chromatography
LED	Light emitting diode
LIF	Laser induced fluorescence
LOD	Limit of detection
ME	Microchip electrophoresis
MEKC	Micellar electrokinetic chromatography
MG	Monoglyceride
MOF	Metal organic framework
MOPS	3-(N-morpholino)propanesulfonic acid
MS	Mass spectrometry
MST	Microscale thermophoresis
NDPK	Nucleoside diphosphate kinase
NHS	N-hydroxysuccinimide
NMP	Nucleoside monophosphate
NMR	Nuclear magnetic resonance
NP	Nanoparticle
NTP	Nucleoside triphosphate
OPC	Proanthocyanidin oligomers content
PDA	Photodiode array

PDMS	Polydimethylsiloxane
PEG	Polyethylene glycol
PEI	Polyethylenimine
PL	Pancreatic lipase
PL*	Fluorescently labeled PL
PMMA	Pressure mediated microanalysis
PPL	Porcine pancreatic Lipase
PTFE	Polytetrafluoroethylene
Q	Quadropole
QTT-I	Quercotriterpenoside-I or 23-O-galloyl arjungenin 28-O- β -glucopyranosyl
QTT-III	Quercotriterpenoside-III or 3-O-galloyl arjungenin 28-O- β -glucopyranosyl
RMT	Relative migration time
RNA	Ribonucleic acid
ROS	Reactive oxygen species
RP	Reverse phase
RSD	Relative standard deviation
SAR	Structure-activity relationships
SDS	Sodium dodecyl sulfate
SFC	Supercritical fluid chromatography
SPE	Solid phase extraction
SPR	Surface plasmon resonance
TDLFP	Transverse diffusion of laminar flow profiles
TDP	Thymidine diphosphate
Tet	Tetrasaccharide, HA hydrolysis product
TFC	Total flavonoid content
TG	Triglyceride
TK	Thymidine kinase
TMP	Thymidine monophosphate
TMPK	Thymidine monophosphate kinase
TOF	Time of flight
TPC	Total polyphenols content
Tris	Tris (hydroxymethyl) aminomethane or 2-Amino-2-(hydroxymethylpropane-1,3-diol)
TTP	Thymidine triphosphate
UHPLC	Ultra-high-performance liquid chromatography
UV	Ultra-violet

Constants and symbols

σ_{eff}	Effective charge
μ_{app}	Apparent mobility
μ_{eff}	Effective electrophoretic mobility
μ_{EOF}	Electroosmotic mobility
‰	Parts per thousand
A	Particle size
AU	Absorbance units
CPA	Corrected peak area
Da	Dalton
E	Enzyme
I	Inhibitor
I%	Percentage of inhibition
i.d.	Inner diameter
IC ₅₀	Half maximal inhibitory concentration
K _d	Equilibrium dissociation constant
K _m	Michaelis-Menten constant
M	Modulatory compounds
<i>pI</i>	Isoelectric point
pKa	Acid dissociation constant
RSD	Relative standard deviation
S	Substrate
S/N	Signal over noise ratio
ΔS_{hyd}	Hydration entropy
ST	Soret coefficient
V _{max}	Maximum velocity
Y ₀	York number
λ	Wavelength

Introduction

The use of capillary electrophoresis (CE) has been widely spreading with applications in various industrial, medical and scientific fields. One of these applications are assays of enzymatic activity. CE introduces several advantages that makes it an interesting complementary or even an alternative technique for assaying catalytic activities of enzymes as well as their modulation by various natural or synthetic ligands.

Only few nLs of samples are injected into the capillary. The consumption of buffers and reagents necessary for capillary conditioning is minimal. Furthermore, most applications of CE-based enzymatic assays require little to no organic solvents. This economy in sample and reagent consumption promotes CE as an interesting technique for enzymatic assays especially when rare and commercially unavailable enzymes are considered.

CE can be adapted in several ways and used in different operation modes for the separation and detection of different types of molecules. It can also be hyphenated to a plethora of detection techniques. This adaptability and versatility of CE allows its utilization in assays of different types of enzymes with various mechanisms of actions towards different substrates. Additionally, different modes of reactions exist and can be carried out using CE. The offline CE-mode involves incubating the reaction components in a vial prior to their injection into the capillary. This approach is simple and easy to optimize and control. Another approach is the online CE-mode where the reaction components are mixed and incubated inside the capillary. In-capillary mixing of the analytes can be carried out by various methods amongst which, transverse diffusion of laminar flow profile (TDLFP) was used throughout this thesis. Online CE-assays are highly automated where the injection, mixing, incubation, separation and detection are all carried out in one step inside the capillary requiring minimal human intervention. Nonetheless, online CE-assays are more complex and are often more difficult to optimize and control compared to their offline counterparts.

In this dissertation, the aim was to demonstrated the power of CE used in the context of monitoring and assaying enzyme catalyzed reactions. To do so, metabolic enzymes such as pancreatic lipases (PL), nucleoside kinases and hyaluronidases were used as model enzymes. These enzymes belong to different families, catalyzing different transformation processes. PL catalyzes the hydrolysis of triglycerides and their ester analogues, hyaluronidase catalyzes the hydrolysis of hyaluronic acid (HA) polysaccharide and nucleoside kinases catalyze the transfer of a phosphate group from a nucleotide triphosphate (NTP) donor to an acceptor nucleoside or nucleotide.

The dissertation will commence by an introductory chapter (**Chapter I**) discussing the most relevant applications of CE for assays involving mainly lipases and nucleoside kinases. This chapter will review different CE reaction (offline and online) and operation modes (CZE or MKEC) as well as different detection modules (UV, C⁴D, LIF and MS) hyphenated to CE for the analyses of lipases and nucleoside kinases. This will set the ground for demonstrating the applicability of CE in enzymatic analyses for different applications and under different conditions. The CE-based enzymatic assays will be compared to chromatography-based as well as microchip- and microfluidic-based analyses of the same type highlighting the strong points of CE and bringing forward points of possible improvements.

The experimental section is divided into two main parts, namely **Chapters II and III**.

In **Chapter II**, the development and optimization of a CE-based assay for monitoring the activity of PL as well as its modulation by natural and synthetic ligands is introduced (**Chapter II; Part A**). The detection of the PL catalyzed hydrolysis products will be achieved through a dual UV/C⁴D detection couple connected in series and supported by a home-made 3D printed scaffold. The CE reaction was carried out both in the offline and the online modes, which were optimized to accommodate the requirements of the PL catalyzed reaction. The developed method permitted screening for natural modulators of PL activity in the form of purified, isolated molecules or complex plant extracts.

The binding affinity of small ligands towards lipases from crude pancreatic extracts will be evaluated through the use of a specialized biophysical technique, the microscale thermophoresis (MST) (**Chapter II; Part B**). MST permits the evaluation of the equilibrium dissociation constant (K_d) based on changes of the size, charge or hydration shell that occur upon binding. The binding assay was developed and optimized and used for the first time to measure binding interactions between lipases from the crude pancreatic extracts and natural molecules demonstrated to be modulators of lipases activity. Complementarity of use of the developed binding assays and the previous activity assay will be highlighted as a strategy to gain more insight onto the molecular mechanism through which small ligands modulate lipases and their activities.

Bioactivities of natural and synthetic enzyme modulators of different complexities, from purified molecules to crude extracts, were then investigated using CE in addition to other conventional bioactivity assays to gain better insight (**Chapter II; Part C**). The effect of biomolecular crowding, the act of mimicking the extracellular matrix through the addition of polyethylene glycol (PEG), on hyaluronidase activity and its modulation by various original

natural or synthetic purified molecules will be investigated. Additionally, the anti-hyaluronidase, anti-hypertensive and anti-oxidant bioactivities of a variety of crude plant extracts will be investigated by CE in addition to other spectrophotometric bioactivity assays. Finally, **Chapter III** will consider applications of CE hyphenated to MS along with the difficulties and challenges accompanied with such coupling and ways to overcome them. Results from an inter-laboratory study aiming to investigate the subtleness of substituting migration time scales with ones of effective electrophoretic mobility where CE-MS was applied for the separation and detection of metabolites in biological fluids without the involvement of any enzymatic action will be presented (**Chapter III; Part A**).

Furthermore, the enzymatic activity of nucleoside kinases towards endogenous and synthetic substrates will be monitored using an optimized CE-MS assay (**Chapter III; Part B**). Most of the optimizations were carried out using conventional CE-UV and the optimized conditions were then transferred onto CE-MS. The flexibility of using CE-MS for different applications is discussed.

The manuscript will end by a general conclusion (**Conclusions & perspectives**), highlighting the main points and proposing ideas for the future to expand the scope of this work.

Chapter I:

Bibliographic introduction

Summary

As an opening to my PhD thesis, this chapter will review capillary electrophoresis (CE)-based assays applied mainly to investigate lipases and nucleoside kinases as model enzymes. A brief comparison with liquid chromatography (LC) and microchips-based assays will be conducted.

CE is a powerful analytical technique continuously expanding into new fields of study and application. Operated in various modes, such as capillary zone electrophoresis (CZE) or micellar electrokinetic chromatography (MEKC), CE can be adapted for the separation and detection of a plethora of charged as well as neutral molecules of diverse sizes. Furthermore, several different detection techniques can be coupled to CE, such as UV spectrophotometry, laser induced fluorescence (LIF) detection, capacitively-coupled contactless conductivity detection (C⁴D) and mass spectrometry (MS) exploiting the physicochemical traits of molecules efficiently separated by CE to detect and quantify them. Additionally, CE analyses are rapid (few min), economic in reagent consumption (few nL required) and, prone to automatization and miniaturization. Reactions can be analyzed using various approaches such as the offline (Pre-capillary), online (In-capillary) or post-capillary approach.

This work will demonstrate the aforementioned technical merits of CE-based enzymatic studies using two model enzymes that differ considerably in their mechanism of action, lipases and nucleoside kinases. Both enzymes possess interesting properties, are implicated in biological and pathological processes and, are widely used for industrial purposes.

Lipases are implicated in the metabolism of fat and function by an intriguing mechanism where their full catalytic potential is achieved at lipid-water or organic-aqueous interfaces. Modulation of lipase activity by synthetic or natural agents has been trending in order to discover new drugs for the treatment of obesity and obesity-related conditions. Additionally, lipases have had several applications in bio-catalyzed synthesis and enantioselective reactions.

On the other hand, nucleoside kinases play a key role in the nucleoside salvage pathway and DNA replication making them crucial for cell division. They can undergo hyperactivation in some cancers or may be recruited to mediate replication of viral genomes infecting host cells. These enzymes require special substrate-associated molecules or ions in order to catalyze the phosphorylation action. Getting a grasp on the exact mechanism of action and the reaction

pathways involved in addition to probing for specific and efficient modulators aids in the development of novel anti-cancer and anti-viral therapeutics.

Outline

I. Introduction.....	12
II. Modes of CE-based enzymatic assays.....	15
III. General information about lipases and nucleoside kinases.....	24
IV. CE- and LC- based lipase assays.....	27
V. CE- and LC- based kinase assays.....	46
VI. Microchip-based lipase and kinase assays.....	65
VII. Binding affinity assays.....	68
VIII. Conclusion.....	72

I. Introduction

Enzymes are biomolecules responsible for catalyzing the transformations of specific substrate molecules into products in the context of metabolic reactions occurring in the cells of living organisms. Depending on the nature of the transformation reaction, enzymes can be classified into different groups [1]. Enzyme catalyzed reactions and abnormal perturbations in their function are implicated, either directly or indirectly, in the development of several disorders such as infections [2,3], cancers [4,5], neurodegenerative diseases, obesity [6] or skin aging [7]. Assaying the catalytic activity of enzymes expedites the elaboration of the molecular mechanisms through which enzymes function and influence the development of diseases [8]. Monitoring the kinetics of enzyme-catalyzed reactions can be achieved by observing either the consumption of substrates, formation of products or, the physiochemical changes occurring as a result of the reaction. Kinetic parameters such as the maximal velocity (V_{max}), the Michaelis-Menten constant (K_m) and the turnover number (K_{cat}) are used to characterize enzymatic reactions. V_{max} and K_m are determined by measuring the reaction's velocity at a range of different substrate concentrations *via* the Michaelis-Menten equation below (Equation I.1):

$$V_i = \frac{V_{max} \times [S]}{K_m \times [S]} \quad \text{Equation I.1}$$

where V_i is the rate of the enzymatic reaction, $[S]$ is the substrate concentration and V_{max} is the rate of the reaction when the enzyme is fully saturated with the substrate. K_m represents the affinity of an enzyme to its substrate and represents the concentration of the substrate sufficient to saturate half of the enzymes in a reaction mixture ($V = \frac{V_{max}}{2}$). The latter can be used to assess different substrates for their appropriateness to be transformed by an enzyme [9,10]. On the other hand, K_{cat} can be determined *via* Equation I.2 below:

$$K_{cat} = \frac{V_{max}}{[E]} \quad \text{Equation I.2}$$

where $[E]$ is the concentration of the enzyme. K_{cat} represent the number of transformed substrates *per unit time per enzyme concentration*.

The enzymatic activity can be measured in the presence of modulatory molecules relative to that activity in their absence to assess the type and degree of modulation exerted by such molecules. The half maximal inhibitory concentration (IC_{50}) is the amount of modulatory ligand required to reduce the enzymes activity by half and can be determined by CE-based assays using a range of ligand concentrations and measuring its influence on the activity of the enzyme. IC_{50} can be used to rank the inhibitors in terms of their potency in modulating an enzyme's activity. IC_{50} can also be used to determine another parameter, the inhibitory dissociation constant (K_i), which describes the strength of the binding interaction between the inhibitor and the enzyme.

Another approach is to elucidate the formation of molecular complexes between the enzyme and other molecules through binding interactions. Association (K_{on}) and dissociation (K_{off}) rate constants can be used to evaluate the equilibrium dissociation constant ($K_d = \frac{K_{off}}{K_{on}}$) between interaction partners. Evaluating K_d allows the prediction of the binding affinities between potential substrates/ligands and target enzymes and is an important preliminary step for drug screening [11]. Both of these approaches facilitate, through their complementarity, the establishment of a structure - activity relationship (SAR) which can then act as a guideline for prioritizing certain ligands over others for their therapeutic use [12]. In addition to being drug targets themselves, enzymes can be used in the pharmaceutical industry for the synthesis of active pharmaceutical compounds. Additionally, other industries such as the food, biofuels and chemical industries have adapted the use of enzymes in their line of production [13]. Some of the common examples for the implementation of enzymes in industrial processes may be the production of lactose free dairy through the use of lactase enzymes [14] or in the production of protease or lipase containing washing detergents [15].

For the last 10 years, various techniques have been reviewed and described for assaying enzymatic activities as well as screening for drug candidates [7,10,24,16–23]. There exists no “one technique to rule them all”. Enzymes have different physical and chemical requirements and therefore some assays may be unsuitable and must be modified or replaced. The choice of the technique depends on several factors most importantly is the relevance of the collected information, the price of the assay including the cost of reagents, enzymes and the degree of their consumption and the compatibility of the technique with the nature of the investigated reaction [25]. Enzymatic assays can be divided into homogenous and heterogeneous assays. In homogenous assays, all the reactants exist in the same physical state, usually the liquid phase. In contrast, heterogeneous assays involve

the enzyme or the substrate immobilized onto a phase distinct from that of the other reactants, usually a solid phase [26,27]. Amongst the several analytical techniques used for assaying enzymatic activity, capillary electrophoresis (CE) introduces several advantages given the low sample and reagent requirements, excellent separation efficiency and high versatility of hyphenation and operation modes associated with CE analyses [28]. CE can also be expanded to measure macromolecular binding interactions through the use of affinity CE. This mode generally exploits the different electrophoretic mobilities of unbound and bound complexes for their separation and quantification and may be fine-tuned according to the application [29,30]. Similarly, high performance affinity chromatography (HPAC) is the chromatographic equivalent of affinity CE where the retention of the ligands onto the biomolecule-immobilized solid phase are defined by binding interactions [31]. Other conventional, non-separative techniques such as isothermal titration calorimetry (ITC), surface plasmon resonance (SPR) or microscale thermophoresis (MST) have all been used to evaluate binding affinities, represented by K_d [32,33]. Miniaturization of conventional enzymatic assays through the use of microfluidic chips benefit from the several advantages compared to larger scale analytical counterparts such as considerable reduction in reagent and sample consumption, less waste production, faster analyses, automation and portability [34]. Microchip enzymatic assays have been used across several fields of application fields such as medical and environmental analysis and diagnosis [35,36]. One interesting application of miniaturized devices is single cell analysis. Cells belonging to the same population exhibit heterogeneity due to differences in the immediate environment as well as genotypic and phenotypic variations of each cell [37,38].

This chapter will summarize advances in the application of CE-based techniques using lipases and nucleoside kinases as model enzymes that will be assayed throughout this thesis. A brief comparison will be conducted with chromatographic and miniaturized assays of the same caliber, highlighting the main differences between the analytical techniques. Furthermore, recently developed binding assays of both enzymes will be briefly discussed.

II. Modes of CE-based enzymatic assays

CE-based enzymatic assays can be broadly divided into offline (pre-capillary) and online (in-capillary) assays. Furthermore, CE-based enzymatic assays can be also categorized into homogeneous (solution-based) or heterogeneous (immobilized) reactions depending on the physical state of the reactants. The different approaches used to assay enzymes by CE is presented in Figure I.1 below.

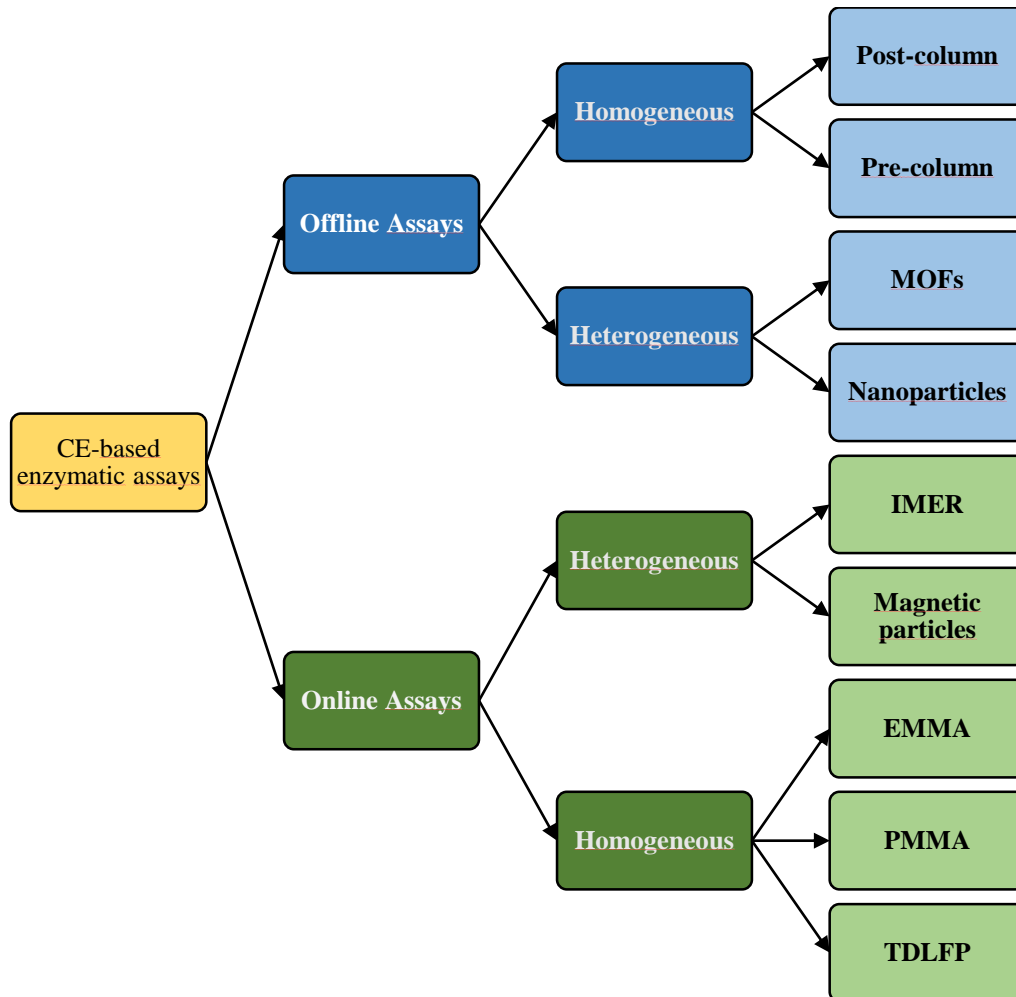


Figure I.1: Hierarchal categorization of CE-based enzymatic assays

II.a Offline homogeneous CE-mode

In the offline CE mode, the capillary serves as a vessel for the separation of the reactants from the reaction mixture. Two types of assays are categorized under offline CE assays, the pre- and post-capillary assays.

The pre-capillary mode was introduced in 1991 by N. Banke *et al.* [39]. All the reagents, except one (substrate or enzyme), are incubated in a vial outside the capillary. The reaction is initiated by adding the missing reagent (enzyme or substrate). The total volume of the reaction mixture ranges from as little as few tens of μL to 1 mL. After a sufficient incubation time at the optimal temperature of the enzymatic activity, the reaction is monitored either continuously, by injecting a given volume of the reaction mixture at regular intervals into the capillary or discontinuously by stopping the reaction. Generally, enzymatic reactions can be terminated by bringing the reaction mixture to a boil, changing the pH. of the reaction medium or, by adding protein-precipitating reagents [10].

Post-capillary assays involve the use of several capillaries connected in tandem. The first capillary is often used to separate one of the reactants, such as the enzyme, from a complex sample, such as cell lysate or fermentation broth, and the second capillary is used to separate the reaction mixture and detect the formation of product. Post-capillary assays are often incompatible with commercial CE instruments and often require the design and construction of home-made ones.

Offline CE-assays are easy to optimize since the enzymatic reaction and analyte separation occur independently. Due to this division in tasks, these assays are easy to control. Manual interventions are, however, inevitable when handling reactions offline and relatively large reaction volumes are required [39,40].

II.b Online homogeneous CE assays

II.b.1 In-capillary analyte mixing by EMMA

Introduced in 1992 by J. Bao and F. Regnier [41,42], in-capillary reactant mixing by EMMA is based on the mobility differences of the analytes. The approach is used for in-capillary mixing of two reactant plugs. The reactant with the lowest mobility is injected first, into the BGE filled capillary, followed by the reactant with a higher mobility. Through the application of a relatively low voltage for a specific period of time, the reactant plug injected last penetrates the one injected first mixing the analytes. A similar approach involves the application of multiple

consecutive voltages of alternating polarities (positive and negative). This is known as rapid polarity switching. After the application of the mixing voltage, the reactants are incubated for a pre-determined period of time at zero voltage in order to accumulate the product (zero potential amplification step). The enzymatic reaction is terminated through the application of a relatively high separation voltage which results in the separation of the enzyme from the substrate. The product of the reaction is also separated from the reactants and migrated towards the detector. The different steps of EMMA are depicted in Figure I.2.

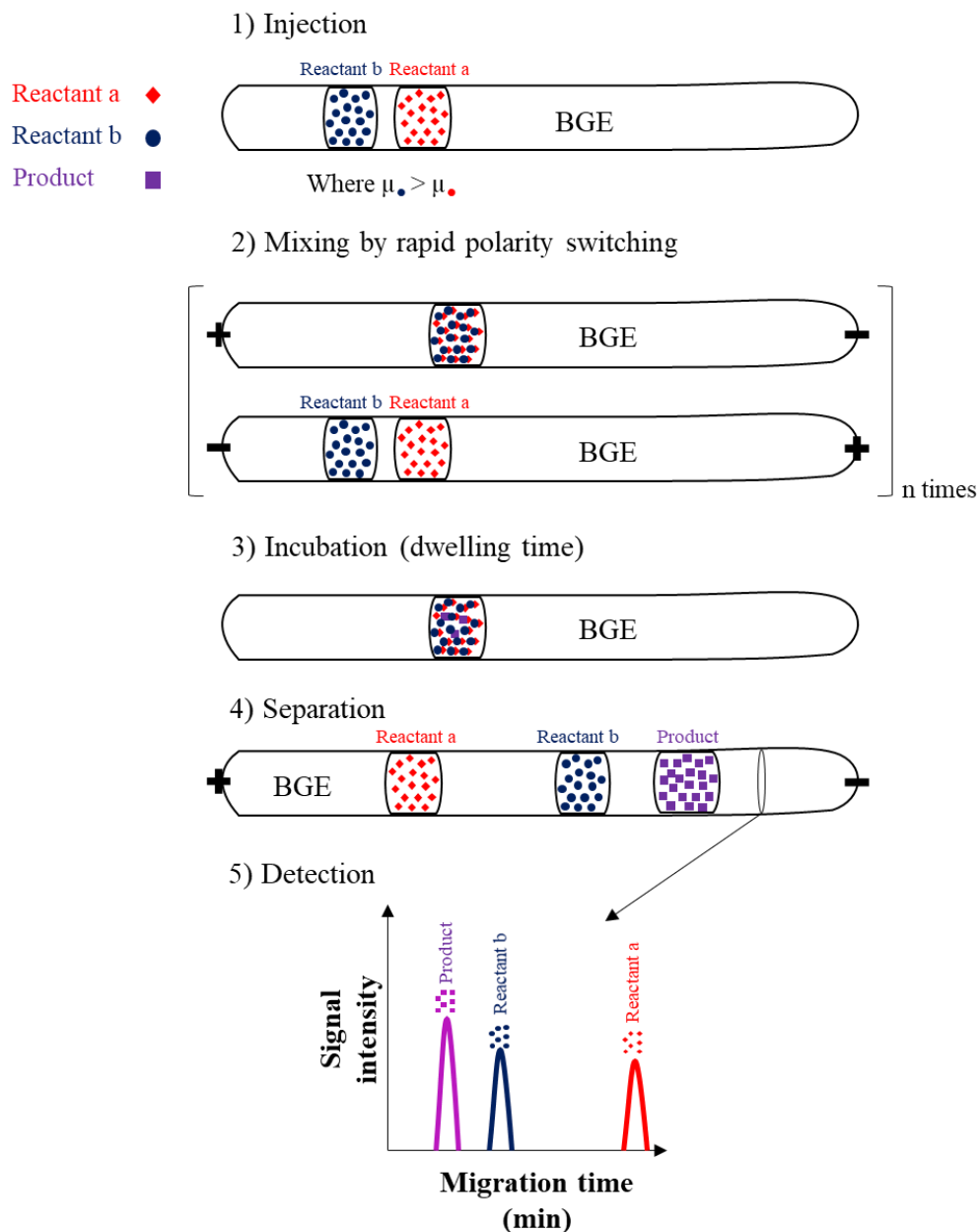


Figure I.2: Illustration of the different steps of in-capillary analysis and mixing by EMMA

Assuming that the analyte plugs are of equal lengths, the time required to obtain total interpenetration of the reactant plugs is estimated as the distance between the frontal end of the lower mobility and the terminal end of the higher mobility reactant plug divided by the difference their velocities as shown in (Equation I.3) below:

$$t_{interpenetration} = \frac{2\delta}{\Delta v} \quad \text{Equation I.3}$$

where δ is the length of each individual plug and Δv is the difference in the apparent velocities of the two reactants.

The apparent velocity of each species can be calculated by Equation I.4 below:

$$v = \frac{L}{t_m} = \mu_{app} \times E \quad \text{Equation I.4}$$

where L is the distance from the capillary inlet to the detector (effective length), t_m is the analyte's migration time, μ_{app} is the apparent mobility of the analyte, calculated as the sum of electrophoretic (μ_{eff}) and electroosmotic (μ_{EOF}) mobilities and, E is the electric field or voltage applied *per* cm of capillary length.

The EMMA approach is simple and suitable for rapid in-capillary mixing of two analyte plugs. However, the approach falls off when more than two analyte plugs are involved and prior knowledge of the reactant's mobilities is required in order to estimate plug interpenetration. Additionally, ionic strengths of the reaction/ incubation buffer (IB) and the separation buffer/ background electrolyte (BGE) should preferably be close to avoid discontinuity of the applied electric field. EMMA has been previously used by our group to assay kinetics of glycerol kinase [43] and cellular β -galactosidase [44] in addition to screening inhibitors of β -galactosidase [45].

II.b.2 In-capillary analyte mixing by PMMA

In-capillary mixing of analyte plugs by longitudinal diffusion was first introduced by A. Taga and S. Honda in 1996 [46]. The analytes were mixed solely by diffusion without the application of external forces. The diffusion was based on the analyte's D. The diffusion time necessary for a

reagent to travel a distance equal to the length of the injected plug (δ) may be elevated for analytes with low D (high molecular weights) or if the diffusion distance is great as shown in Equation I.5 below.

$$t_{diffusion} = \frac{\delta^2}{D} \quad \text{Equation I.5}$$

To overcome such limitation, the analytes can be injected in a sandwich mode where two plugs of the first analyte surround the plug of the other. This reduces the diffusion time 4-folds and enhances analyte plug mixing. A spin-off of longitudinal diffusion mixing was introduced by our group in 2012 [45] where a continuous external pressure is applied to push all reactants and products to the detection window following an incubation period. Quantification of the products in this case is only possible if they are detected selectively.

Mixing analytes by longitudinal diffusion is practical given that analytes are of low molecular weights and relatively short analyte plugs are injected. The approach is unreliable for mixing more than two plugs.

II.b.3 In-capillary analyte mixing by TDLFP

Another approach involving in-capillary analyte mixing based on the difference of their D was introduced by S. Krylov *et al.* in 2005 [47]. With TDLFP, the analytes are injected at high pressure for a short time to obtain parabolic plugs. A schematic illustration of a simple TDLFP approach is represented in Figure I.3. Due to the profiles of the analyte plugs, they may diffuse transversely along the inner radius of the capillary (r_i) which is a distance of few micrometers (25 μm). The transverse diffusion time ($t_{diffusion}$) is therefore much shorter than that of longitudinal diffusion which occurs over few millimeters. This can be concluded from Equation I.6 below. Large molecules with low D can diffuse rapidly (≈ 1 min) *via* transverse diffusion.

$$t_{diffusion} = \frac{r_i^2}{D} \quad \text{Equation I.6}$$

Typically, the injected analyte plug lengths (δ) is much greater than the inner capillary radius (r_i). Under such conditions, longitudinal diffusion is so much slower than transverse diffusion that it can be neglected completely. Therefore, the analytes mix predominantly *via* transverse diffusion

across the capillary's radius.

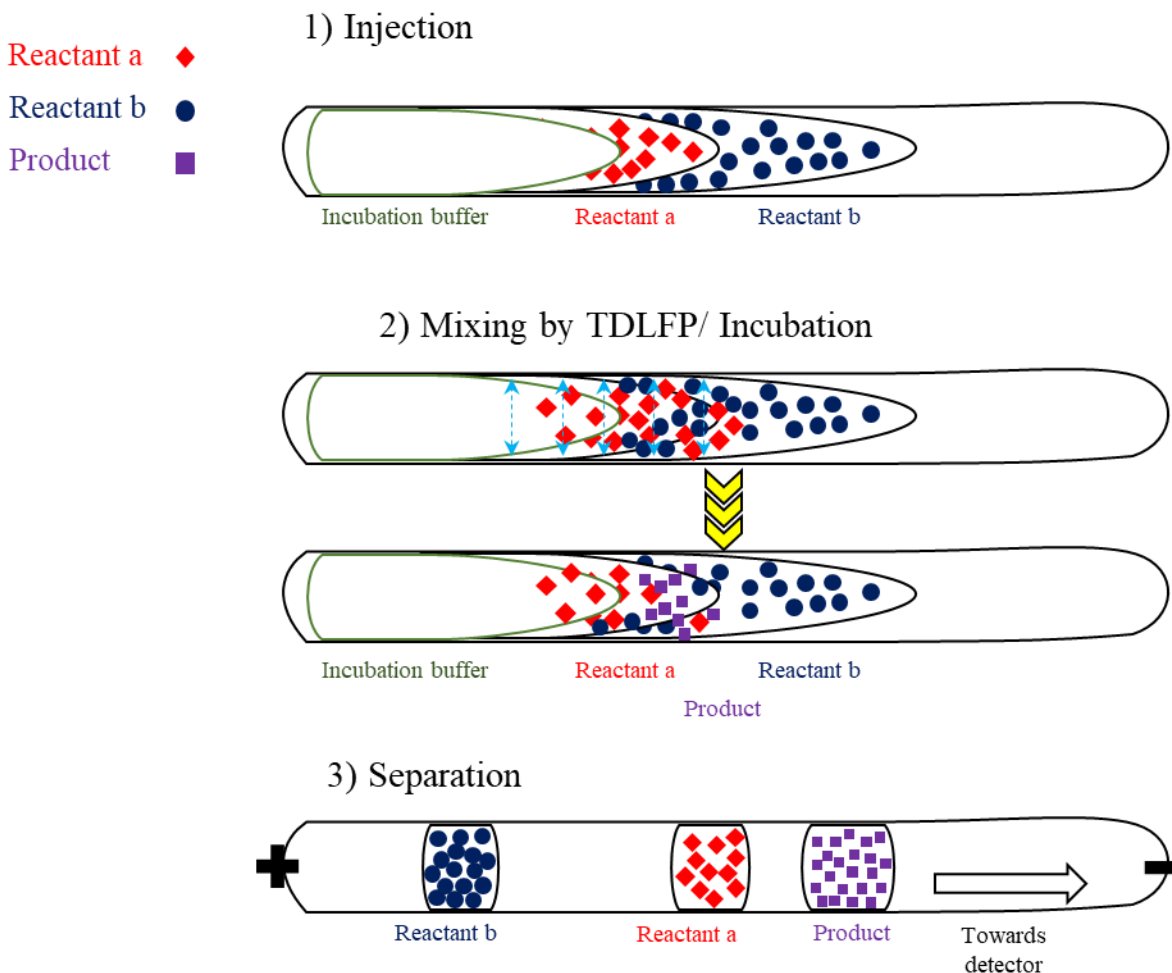


Figure I.3: Illustration of the different steps of in-capillary analysis and mixing by TDLFP

The York number (Y_0) is a dimensionless quantity used to evaluate the quality of in-capillary plug mixing calculated by Equation I.7 below:

$$Y_0 = \frac{D \times \delta}{v_{max} \times r_i^2} = \frac{D \times t_{inj}}{r_i^2} = \frac{t_{inj}}{t_{diffusion}} \quad \text{Equation I.7}$$

where v_{max} is the maximal injection velocity (cm s^{-1}) and t_{inj} is the injection time (s). Good interpenetration of plugs is achieved at low Y_0 values. Nonetheless, since Y_0 is inversely proportional to $t_{diffusion}$, longer times are expected for optimal interpenetration. Therefore, a good compromise between mixing efficiency and analyses times must be considered.

The analyte injection sequence should be carried out in the order of increasing D where, analytes with the lowest D are injected first and those with the highest D are injected last. This way, the in-capillary enzymatic reaction will be initiated only after the injection of the last reactant.

To facilitate quantitative assays of enzymatic reactions, δ of the different analytes should be equal. If the BGE and IB were of different compositions, there is a possibility that the BGE would interrupt the enzymatic reaction upon introduction of the reactants to the BGE-filled capillary. If that was the case, the injection sequence is preceded by the injection of a rectangular plug constituted of the IB by applying a low pressure for a long period of time. The IB isolated the enzyme and the other analytes from the potentially harmful BGE. This approach was introduced by S. Van Dyck and A. Van Schepdael in 2001 and is known as partial-filling [48]. It could be applied for EMMA and PMMA online mixing. The reaction sequence is typically terminated by the injection of a parabolic IB plug. This plug penetrates the preceding analyte plugs enhancing their overlap. Furthermore, the IB plug pushes all reactant plugs deeper into the capillary where thermal control is established so that the enzymatic reaction is carried out at its optimal temperature. The longer the IB plug, the better the plug overlapping but the higher the dilution of the reactants by the IB. This dilution is difficult to determine accurately and thus the length of the terminal IB plug must be chosen taking into consideration better plug overlapping and thus better analytes mixing and the dilution effect which could negatively impact the sensitivity of the method. TDLFP overcomes the limitations of EMMA and PMMA where more than two plugs can be efficiently mixed. Furthermore, the sandwich mode described previously for PMMA can be also applied for TDLFP to further enhance the efficiency of mixing. Additionally, this approach is suitable for mixing large analytes with low D since their transverse diffusion occurs rapidly. This approach has been used by our group to screen inhibitors of various kinases [5,49,50] and hyaluronidase [51] activities.

II.c Heterogeneous CE-based assays

In heterogeneous assays, a reagent, usually the enzyme, is immobilized directly onto an insoluble solid support such as monolithic devices, magnetic beads, nanoparticles or the inner wall of the capillary, creating an immobilized enzyme reactor (IMER). Generally and depending on the nature of the enzyme, solid support and the mechanism of immobilization, the stability of the enzyme is enhanced upon immobilization and its resistance to elevated temperatures and pH as well as its

reusability is improved [52]. These improvements to the enzyme's properties come in handy when immobilized enzymes are used industrially. The lifespan of the enzyme is prolonged and it can be used for an extended period of time which reduces production costs. Enzyme immobilization is implicated in both offline and online CE-assays. With the offline (pre-capillary) mode, the enzymes may be immobilized onto nanoparticles or porous material such as metal organic frameworks (MOFs) and incubated with the substrate as described for homogeneous pre-capillary assays. These particles are separated from the reaction mixture depending on their physical feature, for instance by centrifugation or the use of an external magnet, before CE analyses for their recycling. Concerning online (in-capillary) assays, the immobilization of the enzyme onto the separation capillary can be achieved either directly, within a polymer created in the capillary or, onto particles injected into the capillary and fixed in place [52]. Several approaches for enzyme immobilization have been described including physical adsorption, covalent bonding and cross-linking [53]. Figure I.4 represents a graphical illustration of the different enzyme immobilization strategies.

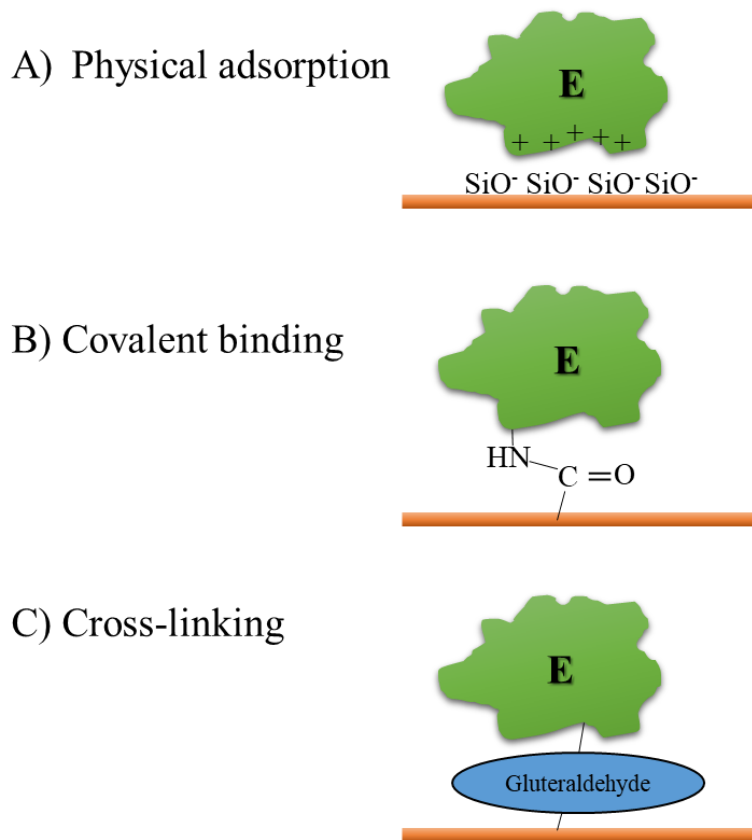


Figure I.4: Illustration of different types of enzyme immobilization strategies

II.c.1 Physical adsorption

Interactions such as Van der Waals, hydrogen, ionic and hydrophobic bonds are all weak interactions associated with physical adsorption. A physical support is immersed in the enzyme solution and then washed to remove the non-adsorbed molecules after an appropriate period of time. No specific reagents or specific activation steps of the inner surface of the capillary are required. Attachment of the enzymes *via* physical adsorption is a simple and cheap approach. However, loss of enzyme from the solid support is often encountered and the stability of the immobilized enzyme is reduced [40,53].

II.c.2 Covalent bonding

Covalently attaching the enzyme onto the support reduces the risk of detachment of the enzyme during enzymatic assays. This type of immobilization can take place between several functional groups of the enzyme, such as amino, carboxyl or alcoholic groups, with the solid support. Due to the rigid nature of such immobilization, the freedom of enzyme movement is compromised which could result in reduction of the activity of the enzyme. This may happen due the inactivation of the enzymes active site as a result of conformational changes in the enzyme influenced by the immobilization process [40,53].

II.c.3 Cross-linking

A type of covalent immobilization, cross-linking involves the indirect attachment of the enzyme to the solid support *via* functional reagents serving as linkers. Glutaraldehyde, for example, is a bifunctional reagent commonly used as a linker in cross-linking reactions [40,53].

Due to the covalent nature of the immobilization reaction, a rigid system is produced. This covalent interaction may inactivate the active site of the enzyme [53]. However, this depends on the nature of the enzyme and the immobilization protocol as most of the examples that will be reviewed in this chapter show enhanced stability and activity of the immobilized enzymes over in-solution ones.

III. General information about lipases and nucleoside kinases

CE-based enzymatic assays were used to investigate the catalytic actions of numerous enzymes with various mechanisms of actions and from different organisms. Throughout this thesis, lipases and nucleoside kinases were used as enzymatic models to demonstrate the power of CE-based enzymatic assays.

Lipases (EC 3.1.1.3) belong to the hydrolases class of enzymes that catalyze the hydrolysis of ester bonds such as those of triglycerides (TG) resulting in the release of free fatty acids (FFA) and monoglyceride (MG), facilitating the absorption of fats into the body (Figure I.5) [54].

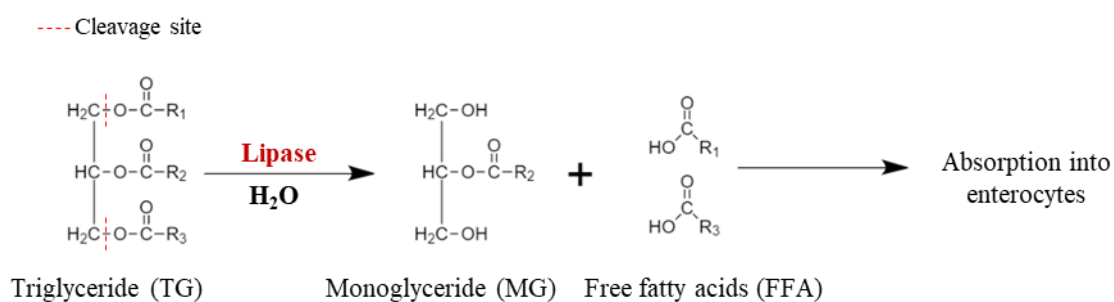


Figure I.5: An illustration of TG hydrolysis catalyzed by lipases

Lipases demonstrate higher activity towards insoluble substrates with long FA chains [55]. Their active sites are covered by an amphipathic lid domain, consisting of hydrophilic and hydrophobic segments. In highly aqueous media, the hydrophobic segment of the lid faces away from the surrounding solvent and towards the enzyme's active site sheltering the site's residues from the environment and restricting access into the site. Upon shifting to a less aqueous media (more hydrophobic) such as the lipid-water interface occurring physiologically during the contact of lipases with the micellar TG substrate or in organic media, the lid's hydrophobic segment faces away from the active site rendering it open and exposing hydrophobic amino acid residues of the active site to substrates [56,57]. Several applications have been described for lipases in different industrial fields such as in the baking, dairy and pharmaceutical industry, production of cosmetics and detergents, synthesis of bio-diesel or bioremediation processes [58–62].

Kinases (EC 2.7.x.x) differ from lipases through their mechanism of substrate transformation. They belong to the family of phosphotransferases catalyzing the transfer of an energetic phosphate group from a donor such as nucleotide triphosphates (NTP) toward an acceptor.

Kinases are further divided into classes based on the type of phosphate acceptors (*e.g.*: proteins or nucleosides). Nucleoside kinases (EC 2.7.4.x) are essential for the phosphorylation of nucleosides and nucleoside phosphates (nucleotides) playing major roles in processes such as the nucleoside salvage pathways and DNA replication [63]. Figure I.6 depicts the phosphorylation of a nucleoside, thymidine, by thymidine kinase (TK), producing thymidine monophosphate (TMP) and ADP. The phosphorylation of TMP to thymidine triphosphate (TTP) is then catalyzed by other types of cellular nucleoside kinases.

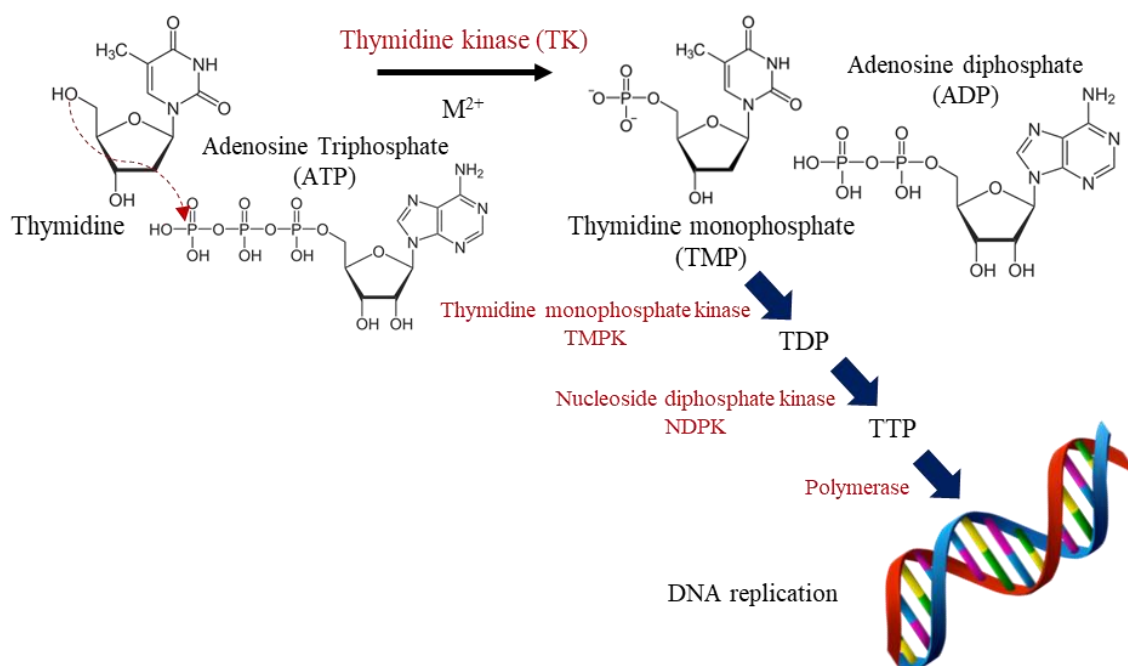


Figure I.6: Illustration of the phosphorylation cascade leading to DNA replication and involving multiple kinases. M^{2+} : Divalent metal cation such as Mg^{2+} or Mn^{2+}

As is the case with other types of kinases, this reaction requires the presence of a divalent metal cation to neutralize the negative charges of the phosphate groups [63]. Applications of these kinases are almost exclusively reserved for scientific and pharmaceutical research. For instance, certain nucleoside kinases are encoded by DNA-viruses such as the herpes simplex virus and can thus be used to phosphorylate therapeutic prodrugs used as anti-viral drugs. On the other hand, hyperactivation or overexpression of kinases may be an indication of cancer given their role in cell proliferation [64].

Lipases-catalyzed reactions are rather straightforward but operate with a unique mechanism of activation at the aqueous-fat/organic interface (interfacial activation). Reactions catalyzed by nucleoside kinases, on the other hand, are complicated and require more than one co-factor additives that can be regarded as secondary substrates since the reaction cannot proceed without them. Both enzymes are thus suitably used as models of simple and complex reactions to demonstrate CE-based approaches as interesting ones for assaying the activities of different enzymes.

In this chapter, assays of lipases and nucleoside kinases using offline and online CE assays. Immobilization of lipases for CE analysis is common and several examples will be introduced. On the other hand, studies involving immobilized nucleoside kinases are scarce given the complicated nature of the reactions catalyzed by these kinases.

IV. CE- and LC-based lipase assays

In the next segment, we will be reviewing applications based on the utilization of lipases in CE in drug screening, chiral resolution, organic synthesis and enzyme characterization.

IV.a Lipase activity and modulation

Assessment of enzymatic activity can be helpful in identifying the presence or prove the absence of an enzyme in a sample. Additionally, quantitative analyses of enzymatic reactions are crucial for the understanding of the underlying mechanisms governing this reaction as well as the subsequent biological and chemical consequences [9]. Enzymatic and inhibitor screening assays have been largely explored in conjugation with CE [52,65–69] and HPLC [70–73].

The implication of CE in lipase-related studies was as early as the 1990s for determining the purity of lipases from crude specimen [74,75]. In 1998, B. Vallejo-Cordoba *et al.* introduced a CE-UV assay to measure FFA in cream subjected to lipase hydrolysis [76]. FA with chain lengths of 4 – 12 carbons (C₄-C₁₂) were detected by adding p-anisate to the 20 mM tris BGE as a chromophore using indirect UV detection at $\lambda = 270$ nm. Methylated beta-cyclodextrin (β -CD) was added to the BGE in order to enhance the solubility of FFA in the aqueous solution through the formation of inclusion complexes, as previously described by L. Szenté *et al.* [77]. Conditions of the enzymatic reaction and CE separation are summarized in Table I.1. The kinetics of cream fat hydrolysis into FFA, catalyzed by a commercial lipase isolated from *Rhizomucor miehei*, were followed by analyzing sample aliquots at different time periods for 60 min (Figure I.7a). The released FFA were analyzed using the CE method where a good separation of the individual FFA species was obtained which allowed their quantification using pre-constructed calibration curves. Figure I.7b represents the electropherogram of resolved FFA species separated in decreasing order of carbon chain length. C₄ FFA migrated last since their electrophoretic mobility, which acts opposite to the EOF due to the anionic form of the FFA, was the highest due to their small size. Furthermore, the noisy profile may be attributed to the low sensitivity of indirect UV detection and/or the complex sample matrix. It was revealed that short chain FFA (C₄, C₆ and C₈) were the most abundant compared to larger ones at different reaction times. The adopted CE method also permitted the detection and quantification of FFA in fresh cream subjected to a MeOH extraction protocol. Compared to the FFA-extracted cream, higher quantities of all FFA, especially those with short carbon chains, were detected in the lipolyzed one. These short chain FFA play an important role

in determining the flavor of dairy products [78,79].

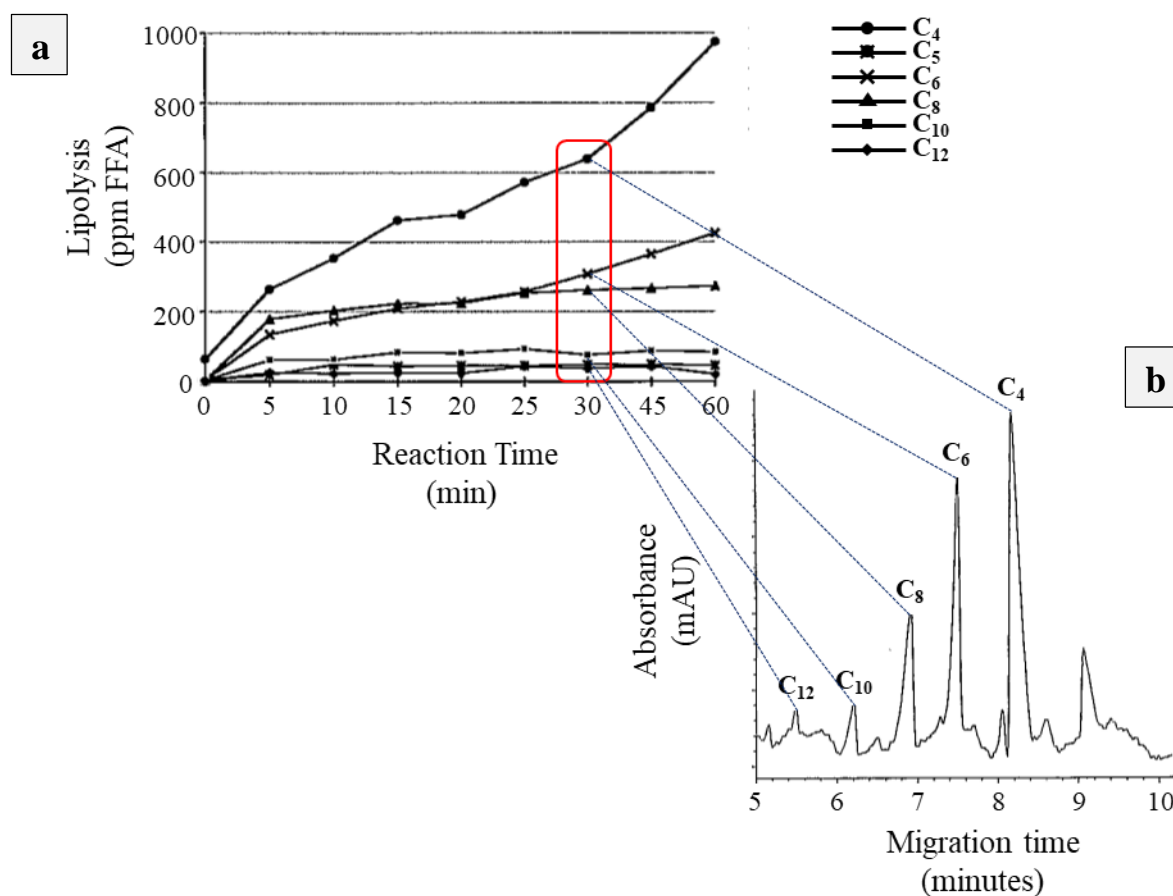


Figure I.7: Kinetics of lipase catalyzed hydrolysis of cream fat into FFA (a) and electropherogram of FFA in lipolyzed cream for 30 min (b). Adapted from [76]. Reaction and separation conditions are summarized in (Table I.1)

The developed CE method overcame the requirements of FFA derivatization or extraction, associated with chromatographic techniques such as gas chromatography (GC) and liquid chromatography (LC). Additionally, the method permitted separation and quantification of FFA standards (C₄ - C₁₂) in under 10 min. The study demonstrated the possibility of customizing dairy flavors by blocking the lipase catalyzed hydrolysis of milk fat at specific times giving emphasis to short-chains FFA production and providing an index for assessing milk quality.

Gang Hao *et al.* described an LC-quadruple time-of-flight (Q-TOF) MS method for assaying microbial lipase activity [80]. TG hydrolysis, catalyzed by lipase, was carried out offline by mixing 20 mM of triolein TG with a solution of 20% Triton X and 100 mM amino acid buffer (pH 6.0) and then adding 0.02 μg of lipase to 1 mL of the substrate solution. The reaction mixture was

incubated at 37°C before injecting aliquots of 2 µL collected at different time points into LC-MS and measuring the amount of liberated oleic FA with the help of an isotopically labeled [¹³C]-oleic acid internal standard. LC was coupled to the Q-TOF MS by an electrospray ionization (ESI) Using a reverse- phase (RP) gradient, the oleic acid product was isolated from the rest of the reaction mixture. Mass spectra of oleic acid ($m/z = 281.25$) and the internal standard ($m/z = 299.25$) were collected in the negative ionization mode at a capillary voltage of 2500 V. The method overcame the laborious radioactive or fluorescent labelling of the substrates and the high pH requirements associated with conventional assays. A limitation of the described assay compared to CE-based ones was the relatively high reagent concentrations which necessitated a 500-fold dilution of the aliquoted reaction samples prior to their analysis. Furthermore, the total injection volume of the samples collected sequentially over a period of 15 min (5 x 2 µL) was one hundred-folds lower than the total volume of the reaction mixture (1 mL), which meant that most of the sample was wasted especially since triolein hydrolyzed spontaneously and had to be freshly prepared from stocks stored at freezing temperatures.

More recently in 2013, T. Koseki *et al.* [81] assayed the lipolytic activity of a recombinant lipase from filamentous fungi *Aspergillus oryzae* (rLipAO), purified from an expression vector. Hydrolysis of tributyrin, a natural TG found in butter, into butyrate was monitored using LC hyphenated to Q-TOF-MS and CE hyphenated to TOF-MS. The lipolytic activity of rLipAO was compared to that of tannase, an enzyme catalyzing the hydrolysis of ester and depside bonds, from the same fungal species. The hydrolysis reaction was measured through the detection of lingering tributyrin after the reaction by RP-LC-MS after injecting 1 µL of reaction mixture. CE-MS was used in the negative ionization mode to monitor the release of butyric acid from tributyrin hydrolysis at m/z 87.045. Reaction and CE separation conditions are summarized in Table I.1. Butyric acid was identified by comparing its m/z to the theoretical one and its migration time to that of a standard. Figure I.8 demonstrates the tributyrin hydrolysis reaction catalyzed by rLipAO. The electropherogram represents the detection of butyrate peak at a migration time of approximately 15 min in the presence of rLipAO and the lack of the butyrate peak in the absence of rLipAO. The isolated protein (rLipAO) demonstrated lipolytic activity toward the tributyrin substrate after 5 hr incubation at 37°C whilst *A. oryzae* tannase showed no activity. Finally, an HPLC-UV approach revealed that rLipAO had no feruloyl esterase, paraben esterase or tannase activity when assayed against various substrates.

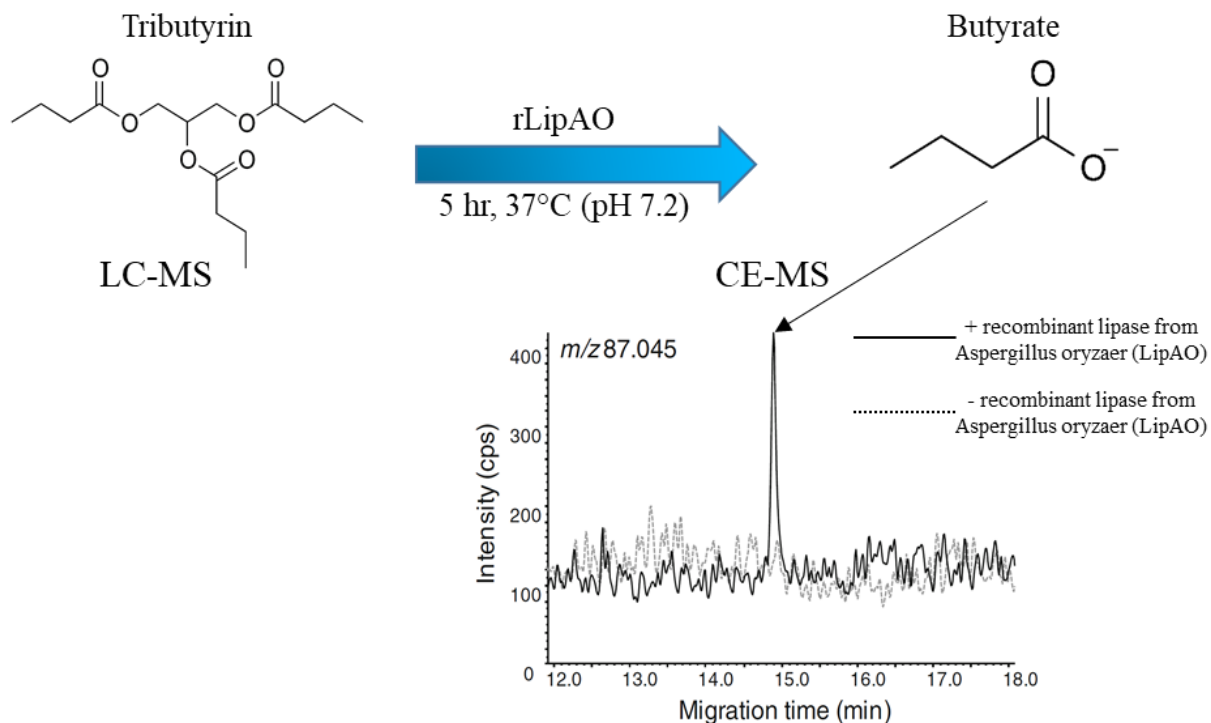
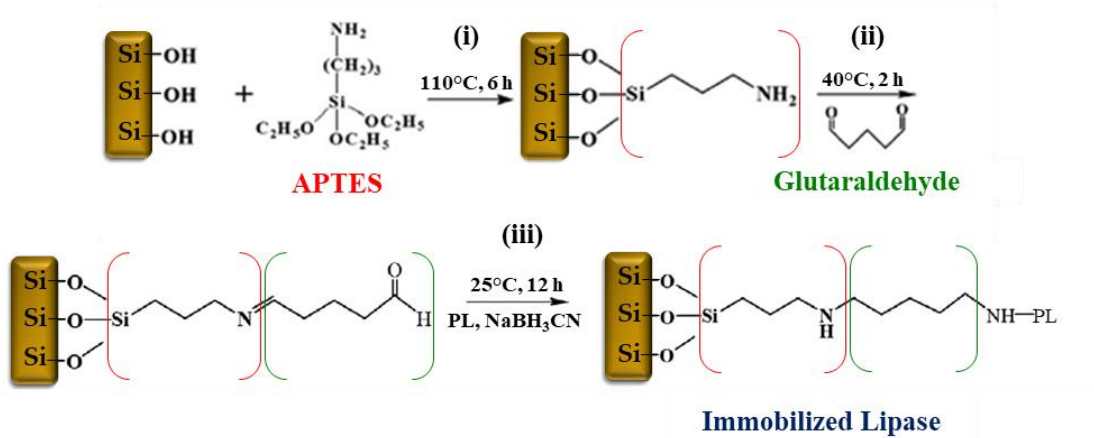


Figure I.8: Hydrolysis of tributyrin by rLipAO from *Aspergillus oryzae* into butyrate detected by CE-TOF-MS as depicted in the electropherogram. The tributyrin substrate was monitored using LC-(Q-TOF-MS). Conditions of the enzymatic reaction, LC-MS and CE-MS are summarized in (Table I.1). Adapted from [81]

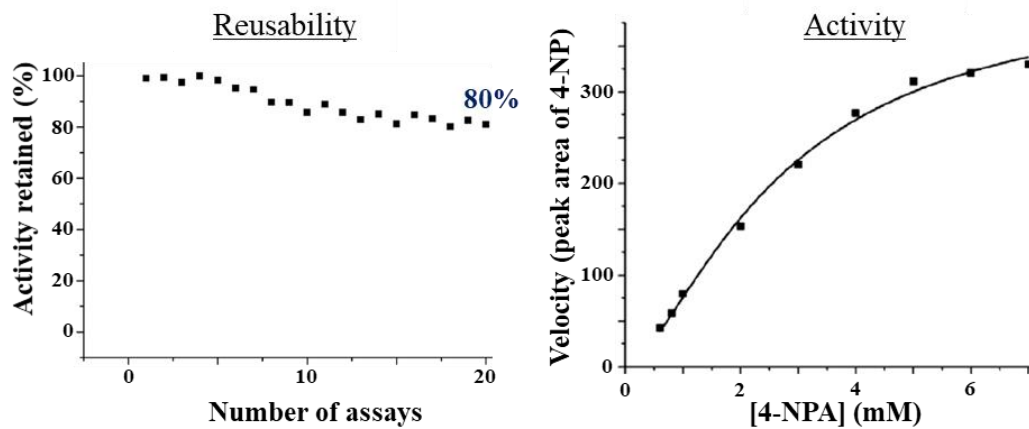
By coupling CE to MS and using it complementarily to LC-MS, the practicality of CE in characterizing the enzymatic activities of newly discovered proteins and protein fractions was demonstrated.

Immobilization offers enzymes higher tolerance to variations in temperatures and pH and provides them with better storage stability [53,82]. It is argued that this increased tolerance compared to in-solution enzymes is brought about by the lower flexibility of the amino acid conformation of the immobilized enzymes, protecting them from thermal and pH-mediated denaturation [82,83].

An online immobilized enzyme microreactor (IMER) was introduced by Y. Tang *et al.* in 2019 [84] to screen for lipase inhibitors. PL was immobilized onto (3-aminopropyl)triethoxysilane (APTES)-treated silica of the inner capillary walls *via* cross-linking to a glutaraldehyde (GA) linker in three steps as illustrated in Figure I.9a. The online enzymatic hydrolysis of 4-nitrophenyl acetate (4-NPA) was then followed by measuring the peak area of the 4-NP product spectrophotometrically at $\lambda = 400$ nm. Following the optimization of acetonitrile content, reaction pH and incubation time, the repeatabilities of the 4-NP product peak area and migration time were evaluated.

(a) PL immobilization *via* cross-linking

(b) Characterization of immobilized PL



(c) Inhibitor screening

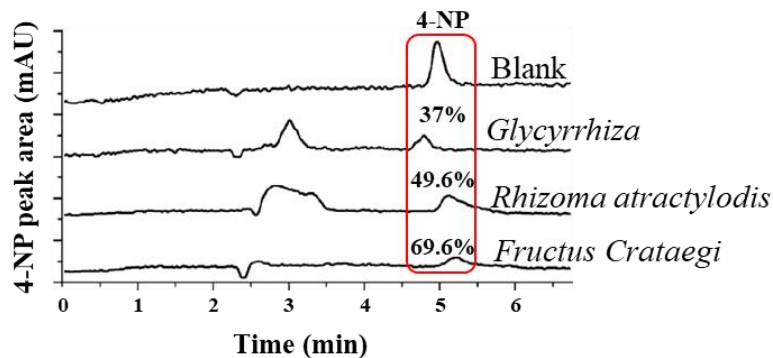


Figure I.9: Illustration of PL immobilization onto the capillary wall via cross-linking using glutaraldehyde as a bifunctional linker (a), Immobilized PL reusability over 20 assays and activity over a range of 4-NPB concentrations (0.6-7 mM) (b) and, Screening of plant extracts at 10 mg mL⁻¹ for PL inhibition (c). More conditions of enzymatic reaction, inhibition assays and CE separation are summarized in Table I.1. Adapted from [85]

Using the same capillary provided good peak areas and migration time repeatabilities (relative standard deviation or RSD < 5%) while the repeatabilities obtained using different capillaries were slightly worse and batches due to variations in the capillary surface but were within the acceptable range (< 15%) defined by international guidelines for validating analytical methodologies [86]. Immobilized lipase preserved 80% of its catalytic activity after 20 consecutive tests reflecting great stability of the immobilized enzyme (Figure I.9b, left). The affinity of immobilized PL towards 4-NPA ($K_m = 2.7 \pm 0.29$ mM) was evaluated against a range of 4-NPA concentrations (0.6 - 7 mM) as shown in Figure I.9b, right and was almost two-folds greater compared to that of PL in solution ($K_m = 4.65 \pm 1.23$ mM) due to reduced steric hindrance between the immobilized PL molecules and increased contact between them and the 4-NPA substrate. The IMER was used to assay PL inhibition by orlistat, a reference PL inhibitor, as well as ten traditional Chinese medicine extracts at 10 mg mL^{-1} by observing the decrease in 4-NP peak areas (Figure I.9c). Conditions of the enzymatic reaction and CE separation are summarized in Table I.1. IC_{50} of orlistat was evaluated as $0.0097 \text{ }\mu\text{M}$, which was globally in good agreement with literature reports of this value. Six out of the ten samples were demonstrated to possess mild to potent PPL inhibition activity ranging from 21 – 70%. Interferents in three other samples co-migrated with 4-NP thus hindering accurate integration and evaluation of inhibitory potential. This may be brought about by the short detection distance (8.5 cm) where the analytes reach the detector before being fully resolved. The developed method demonstrates the merits of enzyme immobilization, enhancing both the affinity and activity of immobilized PL towards the 4-NPA substrate compared to in-solution PL. Furthermore, the application of the method allowed rapid, automated and economic analysis of PL inhibitors in complex plant extracts. The co-migration of some plant components with the 4-NP product peak can be overcome by increasing the migratory distance to the detector or by decreasing the magnitude of the EOF.

Another lipase immobilization approach was introduced shortly after by Jai Liu *et al.* [87]. Using the offline CE mode, inhibitors of immobilized *Candida rugose* lipase (CRL) in traditional Tibetan medicines. CRL was attached *via*, electrostatic (Van der Waals) interactions, onto titanium dioxide magnetic nanoparticles ($\text{Fe}_3\text{O}_4@TiO_2$). The use of a combination of magnetic Fe_3O_4 nanoparticles (NP) and titanium dioxide provides an efficient mean of low-cost enzyme immobilization and the ability to separate the immobilized enzyme from the reaction medium due to the magnetic nature of such NP. The “enzyme-less” NPs were characterized by several techniques such as Fourier-

transform infrared (FT-IR), transmission electron microscopy (TEM) and dynamic light scattering (DLS). The group demonstrated several optimizations performed to enhance CRL immobilization such as the pH, time and enzyme concentration. Furthermore, the activity of the immobilized enzyme towards 4-nitrophenyl palmitate (4-NPP) was compared to that of in-solution CRL. The release of 4-NP as a result of CRL-catalyzed hydrolysis of 4-NPP was monitored spectrophotometrically at $\lambda = 400$ nm. Reaction and CE separation conditions are summarized in Table I.1. Compared to in-solution CRL, the immobilized enzyme was more active at different ranges of temperature (40 - 50°C) particularly at higher temperatures. Additionally, immobilized CRL preserved most of its 4-NPP hydrolyzing activity after storage at 4°C for 30 days whereas in-solution CRL lost around 65% of its activity. Furthermore, immobilized CRL demonstrated higher affinity towards 4-NPP (2.51 mM) compared to CRL in solution (9.96 mM). The inhibition kinetics of immobilized CRL were investigated against a range of orlistat concentrations. A K_i value of 13.41 μM and an IC_{50} value of 4.37 mM was obtained for orlistat. Moreover, amongst 6 methanolic extracts of traditional Chinese medicines, *Oxytropis falcate* Bunge demonstrated considerable inhibition of immobilized CRL with 54 and 68.6% inhibition at 50 and 100 mg mL^{-1} , respectively. Eleven compounds were identified and isolated from *Oxytropis falcate* Bunge and screened individually for immobilized CRL inhibition and compared to that of orlistat at 50 and 100 μM . Six out of the eleven compounds had promising CRL inhibitory potentials similar to that of orlistat, which inhibited CRL by 64 and 82% at 50 and 100 μM , respectively. Kaempferol demonstrated superior inhibition to that of orlistat (92% at 50 and 100 μM). Kaempferol has been previously demonstrated as a CRL inhibitor and its inhibition has been attributed to the high number of hydroxyl group in addition to their location on the molecule [88]. Lipase immobilization onto NP have shown to improve the enzyme's durability, stability, reusability and, its affinity and activity towards the 4-NPP substrate compared to in-solution lipases. The method was applicable for screening lipase inhibitors in samples of varying degrees of complexity from isolated, purified molecules to crude extracts.

Y.-T. Zhu *et al.* introduced a RP-HPLC-UV approach in 2014 to screen inhibition of porcine pancreatic lipase (PL) immobilized covalently onto magnetic nanoparticles (NP) [89]. Several techniques such as atomic force microscopy (AFM) and Fourier-transform infrared spectrometry (FT-IR) were used to characterize the NP and the covalent binding of PL onto them. The NP-PL demonstrated higher activities at a wider range of pH and temperatures as well as higher thermal

and storage stabilities compared to in-solution PL. Furthermore, immobilized PL demonstrated higher catalytic activity and affinity towards the synthetic 4-NPP substrate as suggested by higher V_{\max} (6.40 vs 3.16 U mg⁻¹ enzyme) and lower K_m (0.02 vs 0.29 mM) values, respectively. The amount of 4-NP liberated from the immobilized PL-catalyzed hydrolysis of 4-NPP, was monitored by HPLC-UV at $\lambda = 317$ nm in the presence of reference PL inhibitor orlistat, (-)-epigallocatechin 3-O-gallate (EGCG) and (-)-epigallocatechin (EGC) and compared to that in their absence. The incubation of immobilized PL with the inhibitors was carried out offline prior to injection and analysis of the reaction mixture by HPLC. IC₅₀ values of 0.64 ± 0.02 μM and 55 ± 0.5 μM were calculated for orlistat and EGCG, respectively, whereas no inhibitory effect was observed by EGC. Screening inhibitors of covalently immobilized PL was demonstrated using an HPLC-UV approach. As was the case in the previous examples containing immobilized lipases, NP-PL demonstrated superior endurance to pH and temperature changes as well as higher activity and affinity towards the 4-NPP substrate, compared to in-solution lipases. However, the retention time of the 4-NP product detected by HPLC-UV was relatively long (≈ 19 min) compared to the previous examples using CE-based assays (≈ 5 min) with immobilized lipases. Furthermore, the injection volume (20 μL) and the total volume of the reaction mixture (4 mL) were quite elevated. CE offers several advantages for enzymatic activity and inhibition assays. For instance, the highly efficient separation of the reaction components offered by CE comes in handy especially when the substrates and products of the reaction are indiscernible from each other by standard spectrophotometric approaches [65]. Furthermore, the low volume requirements and short analysis time promote CE as an interesting technique for high throughput screening (HTS) of enzyme modulating drugs and compounds [67]. The previous examples have all demonstrated the power of using CE compared to other techniques for assaying the catalytic activities of enzymes and screening for potential modulators, qualitatively and quantitatively, coupled to various detection techniques and using immobilized and in-solution enzymes. These advantages conveyed by CE should expand its use in different application fields of pharmaceutical and scientific research.

IV.b Enantioselective synthesis catalyzed by lipases and CE-based separation

CE has been established as a successful technique for chiral separations. Through the use of a chiral selector in the BGE, differential interactions between the selector and enantiomeric analytes with identical structural and physicochemical features results in different effective electrophoretic

mobilities and separation [90]. Additionally, lipases are known as chiral enzymes with stereo- and regioselective properties favoring the formation of either enantiomers [91].

K. Pomeisl *et al.* [92] described an offline CE-based heterogeneous lipase assay using immobilized lipase B from *Candida antarctica* (CALB) for the enantioselective resolution of *gem*-difluorinated alcohols. These alcohols serve as intermediates in the synthesis of bioactive molecules with potential anti-viral activities. The synthesis pathway of these fluorinated molecules is often complicated. Additionally, the bioactivities of these molecules strongly depend on their configuration. Lipase catalyzed enantioselective synthesis is thus an interesting approach for the synthesis of difluorinated bioactive molecules from alcohol derivatives. The group monitored the progression of the transesterification reaction with time using CE/UV at $\lambda = 206$ nm. The racemic (R and S) 3-(benzyloxy)-1-difluoropropanol alcohol substrates and subsequent racemic (R and S) ester products were detected and separated using sulfobutyl ether as a chiral selector in the 22 mM NaOH/ 35 mM phosphoric acid (pH 2.5) BGE. The peak area of each of the compounds was corrected for its migration time and quantified relative to an internal standard, sodium benzoate. The group explained a change of enantioselectivity observed upon changing the enzyme-to-substrate ratio from 1:1 to 5:1. They related these findings to the presence of three reaction steps: acetylation, hydrolysis and isomerization following the content of each of the substrate and product enantiomers with CALB under kinetic and thermodynamic control. The CE method allowed monitoring of enantiomeric substrate and products in 14 min. The injection volume was very small (1-2 nL) making the method interesting in analyzing reactions with low yields.

A. Schuchert-Shi and P. C. Hauser [93] demonstrated the enantioselective hydrolysis of serine and threonine amino acid esters by porcine PL using CE- C^4D . The use of conductimetry was essential due to the inability to detect non-aromatic amino acids such as threonine and serine by UV spectrophotometry without their prior derivatization. The enantioselectivity of the hydrolysis reaction was performed by temporal monitoring of the progression of the reaction through the formation of the D- and L- amino acid, products. An acidic BGE, 2 M acetic acid, was used as to protonate the analytes into their cationic forms and 5 mM of the chiral selector (+)-(18-crown-6)-2,3,11,12-tetracarboxylic was added to it. The separation of the DL-serine methyl esters (SME) substrate from the DL-serine products and the enantiomeric resolution of D- and L- stereofoms is demonstrated in the electropherogram in Figure I.10.

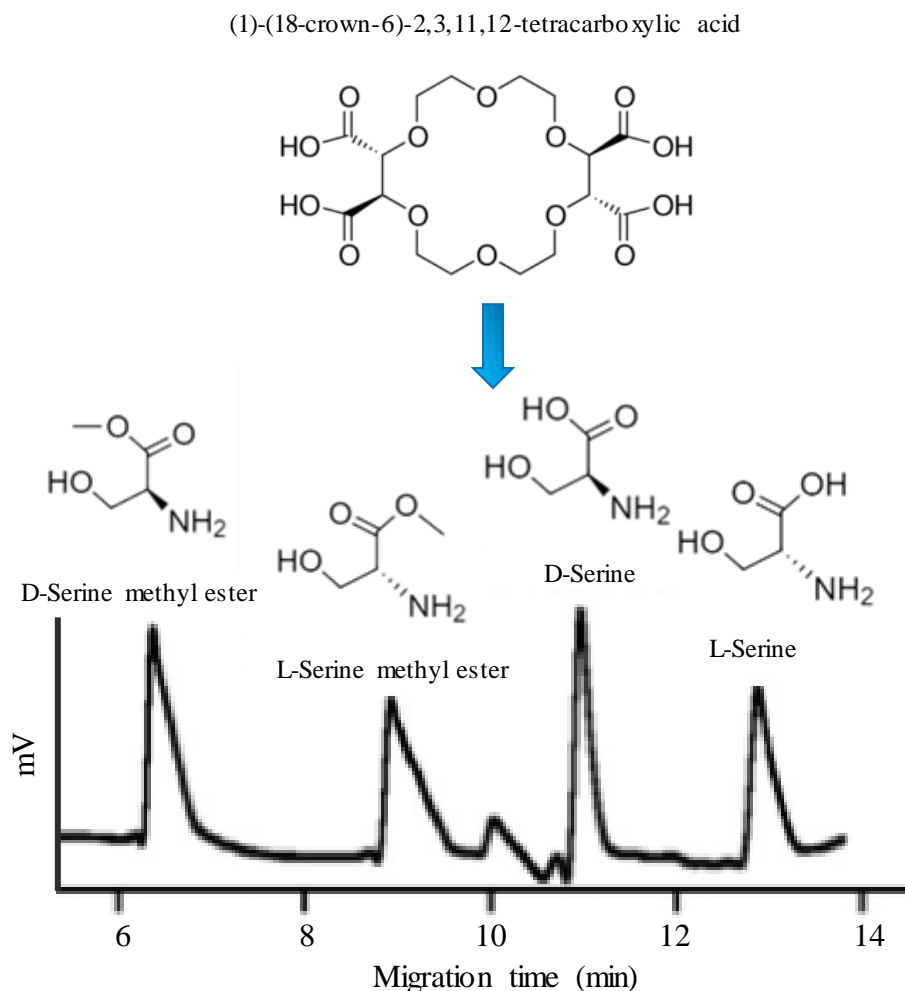


Figure I.10: Electropherogram obtained for the separation of 5 mM D- and L-serine methyl esters as well as 5 mM D- and L-serine using (+)-(18-crown-6)-2,3,11,12-tetracarboxylic acid as a chiral selector and C^4D as detector. Adapted from [93] Conditions summarized in Table I.1

The reaction was conducted by mixing PL with DL-SME or DL-threonine methyl esters (TME). The group demonstrated the increased selectivity of PL towards the L-isomers of both amino acid methyl esters when assayed individually. Similarly, the enantioselectivity of PL was compared to that of wheat germ lipase (WGL) using DL-SME hydrolysis. A consensus was established for the favored production of L-serine by both PL and WGL with PL being more selective and having a higher reaction rate.

Between TME and SME, PL activity was higher towards the L-isomers of TME. This selectivity was related to a single structural difference manifested by a methyl group unique to threonine and not to serine. Indeed, separation of molecules that differ only in their three-dimensional

configuration (stereoisomers) was possible with CE [94]. This was also demonstrated in the examples utilizing lipases to catalyze enantioselective hydrolysis of chiral substrates. Therefore, this separation of desirable enantiomers from a racemic mixture is possible and may be used to detect impurities in pharmaceutical prescriptions.

Recently, Y. Choi *et al.* described an HPLC-based analytical method to determine the integral stereoselectivity of lipases towards TG and DG [95]. This stereoselectivity considers the preference of lipase hydrolysis towards all three ester bonds on the acylglycerol (TG and DG) species. In order to separate the different enantiomers of the hydrolysis reactions, a special chiral-phase column was used consisting of amylose tris(3,5-dichlorophenylcarbamate). Their detection required derivatization of the hydrolysis products with 4-nitrophenyl isocyanate (4-NPI). In order to determine the integral stereoselectivity of porcine PL, *Chromobacterium viscosum* lipase (CVL) and, *Pseudomonas fluorescens* lipase (PFL), the enantiomeric excess of 1,2-DG over 1,3-DG was measured at different stages of the hydrolysis reaction. Figure I.11a represents the HPLC coupling to UV and evaporative light scattering detector (ELSD). The 1,2- and 2,3-DG enantiomers were quantified using HPLC-UV at $\lambda = 285$ nm after their derivatization. The percentage hydrolysis was calculated at different reaction times by measuring the number of moles of FFA released relative to the initial number of moles of the TG substrate using HPLC-ELSD. Furthermore, regioisomers of DG and MG were also analyzed by HPLC-ELSD. Using this method, it was shown that PL demonstrated no preference towards ester bonds at positions (pos) 1 or 3 of the TG substrate, hydrolyzing them equally. Pos 2 ester bonds were not hydrolyzed by PL. Moreover, a similar trend was observed for the hydrolysis of DG into MG. For CVL, a contrast between the stereoselectivity towards ester bonds of TG and DG was observed where the enzyme preferred pos 3 ester bonds over pos 1 in TG and the inverse in DG. As was the case for PL, CVL did not hydrolyze ester bonds at pos 2. Finally, PFL demonstrated hydrolysis of pos 2 ester bonds of TG. The stereoselectivity was thus in the order of ester bonds at pos 1, 2 and 3 of TG. The method did not permit the determination of the exact stereopreference of PFL towards DG isomers due to the presence of two possible hydrolysis sites on each isomer. These results are represented in Figure I.11b. The HPLC-based methods demonstrated the ability to separate the different DG and MG isomers with good resolution and separation factor (> 1). The isomers were then quantified using either HPLC-UV or HPLC-ELSD which permitted the assessment of integral stereoselectivity of lipases from three biological sources.

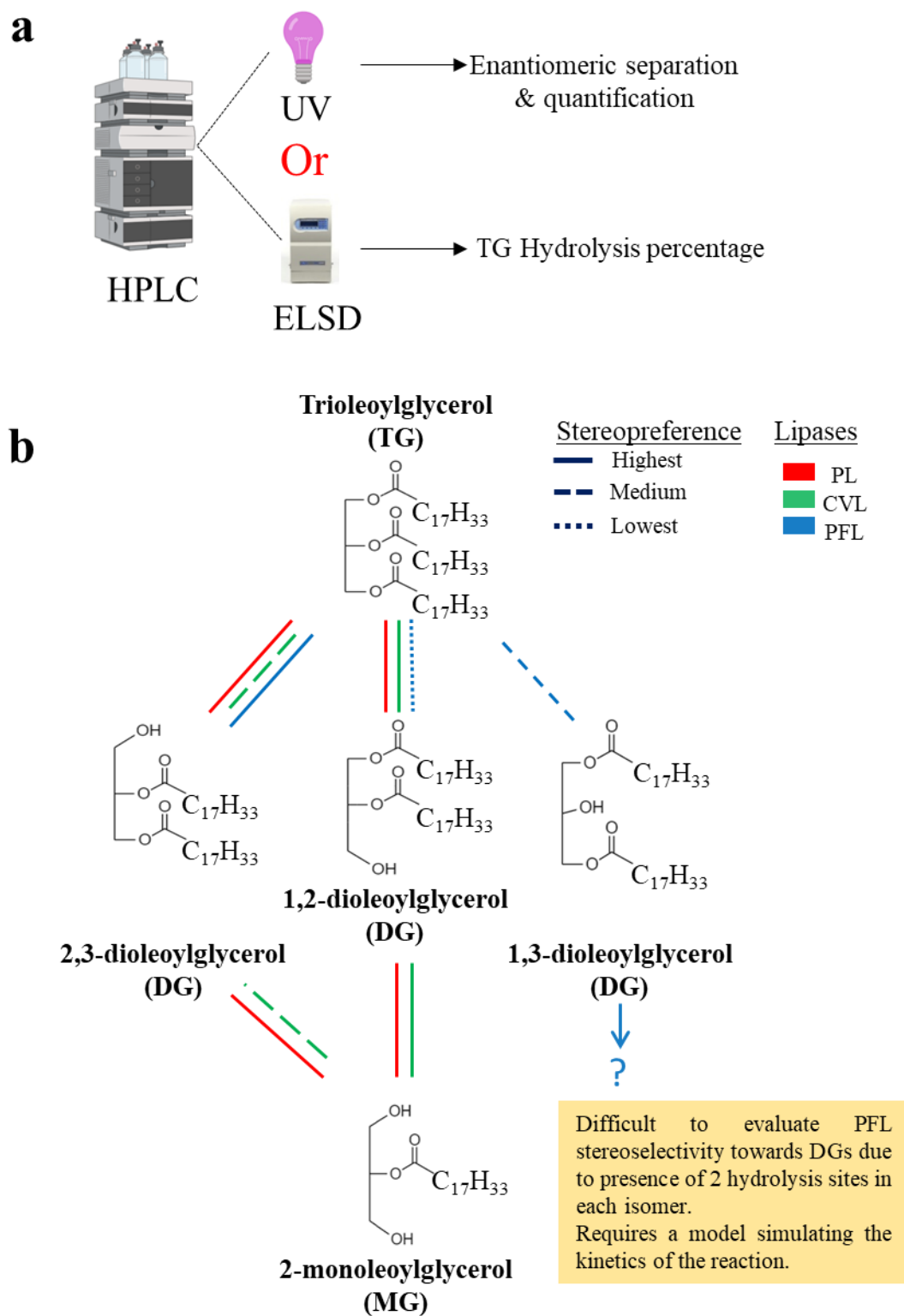


Figure I.11: Quantification of enantiomeric isomers and determination of TG hydrolysis percentage by HPLC-UV and HPLC-ELSD, respectively (a) and stereoselectivity of 3 different lipases towards TG and DG enantiomers (b)

A drawback of the method was the need for isomer derivatization. Furthermore, although all three DG isomers derivatives were detected in 13 min, the detection of MG isomers required the analyses time to be extended to over 20 min. The injection volume (10 μ L) as well as the reaction volume for HPLC-UV analyses (300 μ L) were elevated compared to CE-based assays. The previous examples demonstrate the efficiency of using CE for enantiomeric separation of molecules, simply by adding a chiral selector in the BGE, and its power to separate products obtained after enzymatic reaction in a relatively short time with minimal volume requirement. It should also be mentioned that chromatographic techniques are more adapted for preparative analyses compared to CE-based approaches.

A drawback of HPLC is the high consumption of organic solvents. A powerful chromatographic technique to be used for enantio-resolution is supercritical fluid chromatography (SFC) where supercritical carbon dioxide, possessing properties of both liquid and gas, is used as the mobile phase. This technique requires a reduced percentage of organic solvents compared to conventional LC approaches introducing advantages such as reduced mobile phase viscosity, reduced analyses times and higher separation efficiency as well as a reduction of the environmental impact resulting from excess use of organic solvents [96].

IV.c Organic synthesis

The use of CE to monitor synthesis reactions is a promising prospect given the flexibility of the technique and advantageous merits especially that a miniscule specimen is required to measure the yields of a reaction. Furthermore, lipases have been used in biocatalyzed organic synthesis reactions given their high catalytic activity, wide range of substrate specificity and most importantly, their tolerance to high organic media [97].

W. Liu and colleagues [98] compared the activities of porcine PL immobilized onto different forms of porous materials (metal-organic framework (MOF) and SBA-15) by CE-UV through monitoring the formation of anticoagulant-molecule, warfarin. Immobilization of PL onto the support was confirmed using FT-IR spectroscopy. The PL catalyzed synthesis reaction was carried out by incubating PL with 4-hydroxycoumarin and benzylideneacetone, in methanol for 1 day at 50°C (Figure I.12a). At the end of the reaction, the solution was centrifuged for 5 min to separate the produced warfarin and residual substrates into the supernatant and the carrier-PL complex into the residue. Reaction and CE conditions are summarized in Table I.1.

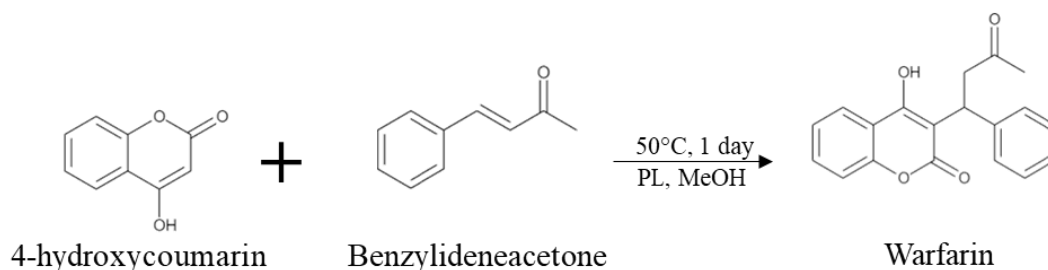
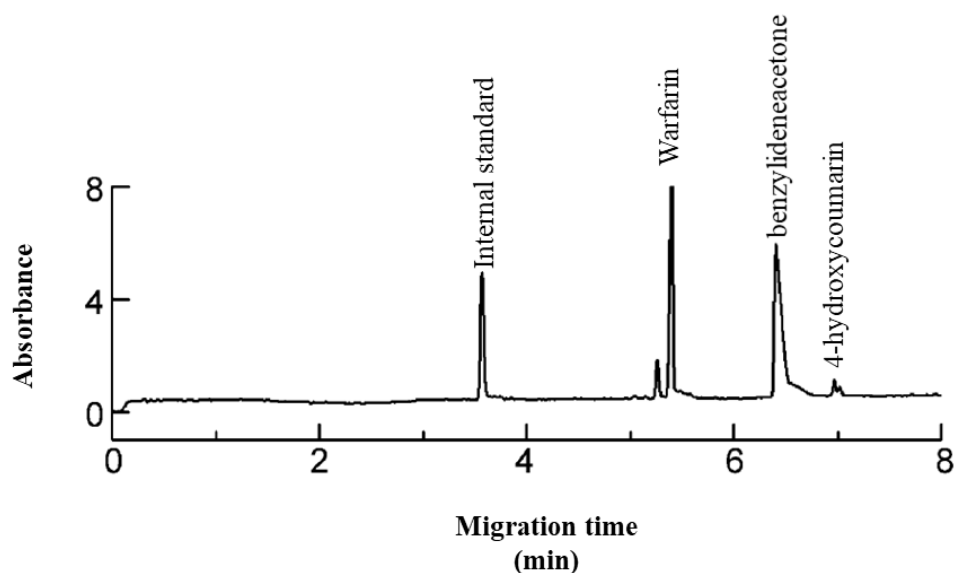
a**b**

Figure I.12: PL catalyzed reaction for warfarin synthesis from 4-hydroxycoumarin and benzylideneacetone (**a**) and electropherogram of the PL-MOF reaction mixture analyzed by CE-UV at $\lambda = 214 \text{ nm}$ (**b**). Adapted from [98]. Reaction and CE conditions are summarized in **Table I.1**

This allowed the reusability of the immobilized PL. The supernatant was injected into the capillary (0.5 psi x 3 sec; 3 nL) and a separation voltage of 28 kV was applied to separate the warfarin product from the substrates using a borax buffer containing sodium dodecyl sulfate (SDS) as BGE (pH 8.5). An example of the obtained electropherograms with PL immobilized onto MOF is presented in Figure I.12b. The warfarin yields by each of the PL immobilized onto 4 different MOFs and SBA-15 in addition to in-solution PL were compared to assess catalytic activity and storage and catalytic stability of the immobilized enzyme. Compared to in-solution, all immobilized PL had higher activities reflected by higher warfarin yields that did not change dramatically upon reusing after 5 cycles. PL-MOFs had higher warfarin synthesizing activities compared to PL-SBA-15. The majority of warfarin yield (65%) were maintained by PL-MOFs

after storage for 35 days at 4°C. Additionally, the RSD of warfarin yields using three batches of each PL-MOFs and their use across five cycles was inferior to 3 % reflecting high catalytic stability. With 104 µL total reaction volume, 3 µL injection volume and the ability to reuse the immobilized enzyme, the CE method for monitoring warfarin synthesis was highly economic providing highly efficient and rapid separation of the warfarin product from the other reactants in under 8 min.

CE was used to monitor the yields of organic synthesis reactions catalyzed by lipases, either in-solution or immobilized onto different supports. The reactants and products were successfully separated in under 8 min. It would be interesting to further expand this type of utility of CE-based assays to measure the yields of organic reactions. Also, the miniaturization of such organic reactions onto microchip systems with continuous flow conjugated to appropriate detection techniques should be considered due to the advantages provided at such scales especially the shorter reaction times [99]. Such miniaturized systems will be discussed in an upcoming section.

Table I.1: CE-based lipase assays

Enzymatic reaction				CE separation			
Enzyme	Substrate	Inhibitor	Incubation buffer (IB)	Reaction conditions	Background electrolyte (BGE)	CE conditions	
[76]	Palastase 20000 L (Commercial lipase from <i>Rhizmucor miehei</i>)	Cream fat	-	Cream matrix, maintained at pH 7.0 through the addition of 0.1 N NaOH	<p><u>Offline reaction</u></p> <p>5 mL of lipase added to 1000 g of cream</p> <p>Incubation at 40°C for 60 min with constant stirring at 60 rpm.</p> <p>10 g of reaction mixture aliquoted at different time points (0-60 min).</p> <p>Reaction was stopped by heating at 95°C for 5 min</p> <p>Aliquoted samples were mixed with 10 mL MeOH, shaken for 1 min and filtered.</p> <p>4 mL of the filtrate was mixed with 1 mL of 100 mM tris, 50 mM p-ainsate and 5 mM β-CD before CE injection</p>	<p>20 mM Tris</p> <p>10 mM p-anisate</p> <p>1 mM trimethyl β-CD (pH 8.0)</p>	<p>Uncoated fused-silica capillary: 80.5 cm \times 50 μm i.d.; 72 cm effective length</p> <p>Temperature: 30°C</p> <p>Separation voltage: +30 kV</p> <p>Injection: 0.7 psi \times 10 s (11 nL)</p> <p>Detection: indirect UV FFA at λ = 270 nm</p>
[81]	rLipAO (lipase from <i>Aspergillus oryzae</i> fungi)	Glycerol tributyrate Or tributyrin	-	<p>50 mM MOPS/KOH</p> <p>10 mM MgCl₂</p>	<p><u>Offline reaction:</u></p>	<p>50 mM ammonium acetate (pH 8.5)</p>	<p>SMILE (+) coated capillary 120 cm \times 50 μm i.d.</p>

Enzymatic reaction				CE separation		
Enzyme	Substrate	Inhibitor	Incubation buffer (IB)	Reaction conditions	Background electrolyte (BGE)	CE conditions
			10 mM KCl (pH 7.2)	20 µL lipase (7 µg) added to 100 µM tributyrin in 200 µL IB Incubation at 37°C for 1 and 5 h Aliquots of 50 µL were collected and diluted with 50 µL MeOH to stop the reaction The sample was filtered <i>via</i> ultrafiltration with a 5,000 Da cutoff before injection into LC or CE-MS		Separation voltage: -30 kV Detection: ESI-MS Butyrate ($m/z = 87.045$) Sheath liquid: 5 mM ammonium acetate in 50% (v/v) MeOH/H ₂ O Negative ionization mode Capillary voltage: 3.5 kV Dry gas: N ₂ at 10 psi
[85]	Porcine pancreatic lipase (PL), type II Covalently immobilized onto the capillary walls <i>via</i> cross-linking	4-nitrophenyl acetate (4-NPA) Orlistat (10 ⁻⁴ -0.5 µM) Ten ethanolic plant extracts (extracted by ultrasonic-assisted extraction) used in Chinese medicines (10 mg mL ⁻¹)	10 mM Na ₂ HPO ₄ (pH 8.0) adjusted with 1 M H ₃ PO ₄	<u>Immobilized enzyme microreactor (IMER)</u> Capillary rinsed with 10 mM Na ₂ HPO ₄ for 3 min 1 mM 4-NPA with or without orlistat or plant extract injected at 0.7 psi × 5 sec; 64 nL Incubation at 25°C for 4 min Reaction was stopped by the application of the separation voltage	10 mM Na ₂ HPO ₄ (pH 8.0) adjusted with 1 M H ₃ PO ₄	APTES/GA activated (16.5 cm) and uncoated fused silica (16.5 cm) capillary connected by a 0.5 cm Teflon tubing 33 cm × 75 µm i.d.; 8.5 cm effective length Temperature: 25°C Separation voltage: +15kV Injection: 0.7 psi × 5 s (64 nL) Detection: UV 4-NP at λ = 400 nm

Enzymatic reaction					CE separation	
Enzyme	Substrate	Inhibitor	Incubation buffer (IB)	Reaction conditions	Background electrolyte (BGE)	CE conditions
[87]	<i>Candida rugosa</i> lipase (CRL) immobilized onto Fe ₃ O ₄ @TiO ₂ NP by electrostatic interactions.	4-nitrophenyl palmitate (4-NPP)	Orlistat 6 methanolic plant extracts used in Tibetan medicine 11 compounds isolated from <i>Oxytropis falcate</i>	20 mM NaH ₂ PO ₄ (pH 4 – 10) 300 µL 4-NPP (0.4 – 1.2 mM) added to a solution of 150 µL of immobilized CRL NP For inhibition assays, 100 µL extracts (50 or 100 mg mL ⁻¹) or isolated compounds (50 or 100 µM) were added to the mixture Incubation at 60°C for 15 min Reaction was stopped by separating immobilized CRL NP using a magnet	Offline reaction 20 mM Na ₂ B ₄ O ₇ ·10H ₂ O (pH 9.0) adjusted with 1 M HCl	Uncoated fused-silica capillary (33 cm × 50 µm i.d.; 24.5 cm effective length) Temperature: 20°C Separation voltage: +20 kV Detection: UV 4-NP at λ = 405 nm
[92]	<i>Candida antarctica</i> lipase B (CALB)	3-(benzyloxy)-1,1-difluoropropan-2-ol	-		22 mM NaOH + 35 mM H ₃ PO ₄ (pH 2.5) + 1.5 mM sulfobutyl ether β-cyclodextrin (β-CD)	Uncoated fused-silica capillary (40.6 cm x 50 µm; 30.2 cm effective length) 15°C +20 kV Injection: 0.1 psi x 5-10 s (1-2 nL) Detection: UV

Enzymatic reaction					CE separation		
Enzyme	Substrate	Inhibitor	Incubation buffer (IB)	Reaction conditions	Background electrolyte (BGE)	CE conditions	
[100]	Porcine pancreatic lipase (PL) Wheat germ lipase (WGL)	DL-Serine methyl ester (DL-SME) DL-Threonine methyl ester (DL-TME)	-	200 mM NaHCO ₃ (pH 7.8)	Ten mg racemic mixture of DL-SME or DL-TME to 1 mL IB, for hydrolysis of individual methyl esters or 5 mg of both for determining selectivity between both amino acid methyl esters 0.5 mL PL (5 mg mL ⁻¹) Incubation at 37°C for 2 days Aliquots taken at different time points for CE analysis	2 M acetic acid + 5 mM chiral crown ether 18C6H4 [(1)-(18-(crown-6)-2,3,11,12-tetracarboxylic acid)]	racemic substrates and products at $\lambda = 206$ nm Uncoated fused-silica capillary 50 cm x 50 μ m i.d.; 45 cm effective length Separation voltage: +15 kV Injection: manual at 10 cm elevation for 10 s Detection: C ⁴ D DL-SME, DL-TME, DL-serine and DL-threonine
[98]	Porcine pancreatic lipase (PL) immobilized onto 4 metal-organic frameworks (MOFs) or mesoporous silica (SBA-15)	4-hydroxycoumarin and benzylideneacetone	-	MeOH	2 or 5 mg PL (immobilized or in-solution) mixed with 1 mg 4-hydroxycoumarin and 4.5 μ L benzylideneacetone in 100 μ L IB Incubation at 50°C for 1 day Centrifugation at 10K RPM for 5 min to separate the immobilized PL for recycling	132.5 mM sodium tetraborate 15 mM SDS (pH 8.5)	Uncoated fused-silica capillary 60 cm x 50 μ m i.d.; 50 cm effective length Separation voltage: +28 kV Injection: 0.5 psi x 3 s (3 nL) Detection: UV Warfarin, substrates and thiourea at $\lambda = 214$ nm

V. CE- and LC- nucleoside kinase assays

In this segment will be reviewing CE-based assays of nucleoside kinases and their applications to scientific and pharmaceutical research.

In 1996, S. Banditelli *et al.* described a CE-based assay to monitor phosphotransferase activities associated with cytosolic 5'-nucleotidase, a bifunctional enzyme catalyzing both the hydrolysis of nucleoside monophosphates into nucleoside and phosphate and, the transfer of phosphate from a donor to an acceptor [101]. Through the use of a single assay, both activities of 5'-nucleosidases purified from calf thymus were monitored simultaneously by CE-UV at $\lambda = 254$ nm. The method, summarized in Table I.2, demonstrated an efficient separation of a mixture consisting of several bases, nucleosides and nucleoside mono, di and triphosphates in under 12 min. Different phosphate donors as well as acceptors were tested and ranked according to their influence on the phosphorylation activity. 5'-deoxy guanosine monophosphate (dGMP) was chosen as the phosphate donor and inosine was chosen as the acceptor substrate. A comparison between the absence and presence of an acceptor nucleoside shows that dGMP conversion to dG was higher in the presence of a nucleoside acceptor such as inosine. This observation suggests that the overall activity (phosphatase + kinase) of the enzyme increases in the presence of a nucleoside acting as a phosphate acceptor. In the absence of such nucleoside, the intermediate enzyme phosphate complex, formed by hydrolytic cleavage of a nucleoside monophosphate (NMP), dissociates resulting in the formation of a nucleoside and phosphate. The study demonstrated a shift in the optimal pH of the enzymatic reaction, from 6.5 to 7, upon addition of inositol. This was attributed either to the binding of inositol to amino acid residues that are not involved in the hydrolysis reaction or to the binding of the phosphate group to those residues. Moreover, phosphorylation of deoxycoformycin, an analog of adenosine used as a chemotherapeutic drug, by 5'-nucleotidase was demonstrated for the first time. This CE-UV method was simple, rapid and required no labeling or modification of the substrate. Additionally, the detection and efficient separation of the substrates and the products of the nucleotidase and kinase activities of cytosolic 5'-nucleotidase allowed the determination of the reaction rates corresponding to each activity in a relatively short time (12 min) without the need of large sample quantities (10 nL).

H.-F. Tzeng *et al.* developed a CE-UV assay for measuring the activities of both thymidine kinase (TK) and thymidine monophosphate kinase (TMPK), simultaneously [102]. The method was optimized for the detection of TMP, the product of thymidine phosphorylation by TK, and

thymidine diphosphate (TDP), the product of TMP phosphorylation by TMPK. A fused-silica bubble cell capillary with an extended light path length of 150 μm ensured high sensitivity detection at $\lambda = 267 \text{ nm}$. Ethylenediaminetetraacetic acid (EDTA) was added in order to chelate Mg^{2+} co-factor ions which were censured for the considerable ATP peak fronting due to the formation of an ATP- Mg^{2+} complex. This addition resolved the ATP and TDP peaks which migrated close to one another. Furthermore, the apparent mobility difference of ATP and TDP anions was the greatest when using 20 mM sodium tetraborate BGE at pH 9.1. This mobility difference was interpreted as two resolved peaks in the electropherogram. Higher pH values resulted in longer migration times due to the increased electrophoretic mobilities of the anionic species acting at the opposite direction of the electroosmotic flow, *i.e.* towards the anodic inlet. Lower pH values resulted in higher currents and consequently excess production of Joule heat which could have a negative impact on the quality of peaks and their resolution. Mixing the analyzed sample with NaCl and 66.7% ACN (*v/v*) prior to CE injection brought about several improvements to the CE separation efficiency, peak shapes and mediated a sample stacking effect. Slightly lower currents were achieved with ACN in addition to a 73% increase in the apparent mobility difference between TDP and ATP species, enhancing the resolution of their peaks by more than 100%. A 3-fold increase in the theoretical plate counts was achieved upon addition of 20 mM NaCl to the sample treated with ACN. A separation voltage of 23 kV was chosen as a compromise to achieve the shortest migration times whilst maintaining good peak resolution. The method was then applied to simultaneously detect TK and TMPK activities of the white spot syndrome virus (WSSV) by infecting an insect cell line with a recombinant version of the virus followed by a protein extraction procedure. Conditions of the enzymatic reaction as well as CE separation are summarized in Table I.2. After 10 min incubation of the protein extract with TK reaction buffer at 37°C, TMP and, to a lesser extent, TDP were detected confirming the presence of both TK and TMPK activities (Figure I.13). An additional 10 min incubation period at 37°C demonstrated a 170% increase of TDP production, verifying the presence of TMPK activity in WSSV-infected cells. The CE method provided a highly efficient separation of dAMP (internal standard), TMP, TDP and ATP peaks in around 6 min with high intraday (RSD < 5%, n = 5) and interday (RSD < 8.5%, n = 5) migration time and corrected peak area repeatabilities. Furthermore, the method was validated by its application to qualitatively and quantitatively detect kinase activities in lysated cells infected with WSSV.

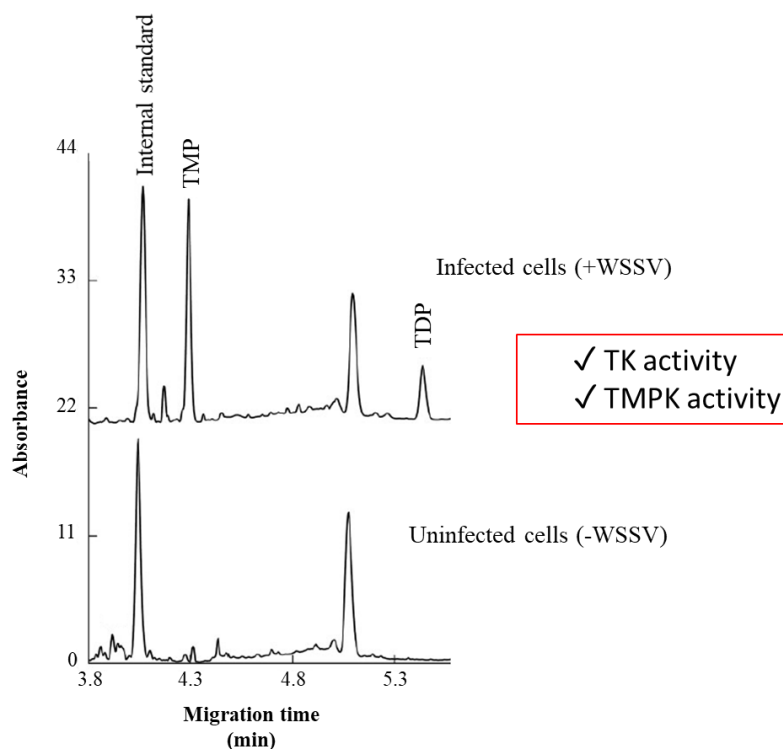


Figure I.13: Electropherograms obtained for the detection of TMP and TDP from insect cell lines after infection with White spot syndrome virus (WSSV) indicating TK and TMPK activities of the virus, respectively. Adapted from [102]. Reaction and CE conditions are summarized in **Table I.2**

In 2005, C. C. Liu *et al.* described a CE-ESI-MS assay to monitor the phosphorylation of lamivudine, an anti-retroviral drug, in human cell lines [103]. The BGE was chosen as ammonium acetate as it provided faster separations compared to ammonium carbonate of the same concentration. pH 10 provided the best resolution of most of the peaks. Furthermore, the concentration of the BGE was fixed at 25 mM to reduce ion suppression and hence enhance the sensitivity for the detection of the nucleoside analytes and to obtain peaks of high resolution. The analysis was carried out at the negative ionization mode as it provided similar sensitivities for unphosphorylated and phosphorylated nucleosides whereas in the positive ionization mode, the higher sensitivities were reserved for unphosphorylated dideoxy nucleosides. Under these conditions, the method was able to resolve GMP nucleotides from dGMP, differing only by the presence of a hydroxyl group in GMP, in around 12 min (Figure I.14a). The developed method was then applied to monitor the production of phosphorylated lamivudine metabolites in human cell line extracts. Lamivudine is a cytosine analogue that is phosphorylated sequentially by cellular kinases into active lamivudine triphosphate which competes for incorporation into the RNA by

reverse transcriptases of viruses such as the human immunodeficiency virus (HIV) or hepatitis B virus (HBV), blocking their replication. The cells were incubated in a medium containing 100 μM lamivudine at 37°C for 10 h. The cells were then extracted using MeOH and the extracts were preconcentrated before the CE-MS analysis. Conditions of the enzymatic reaction and CE-MS analysis are summarized in Table I.2.

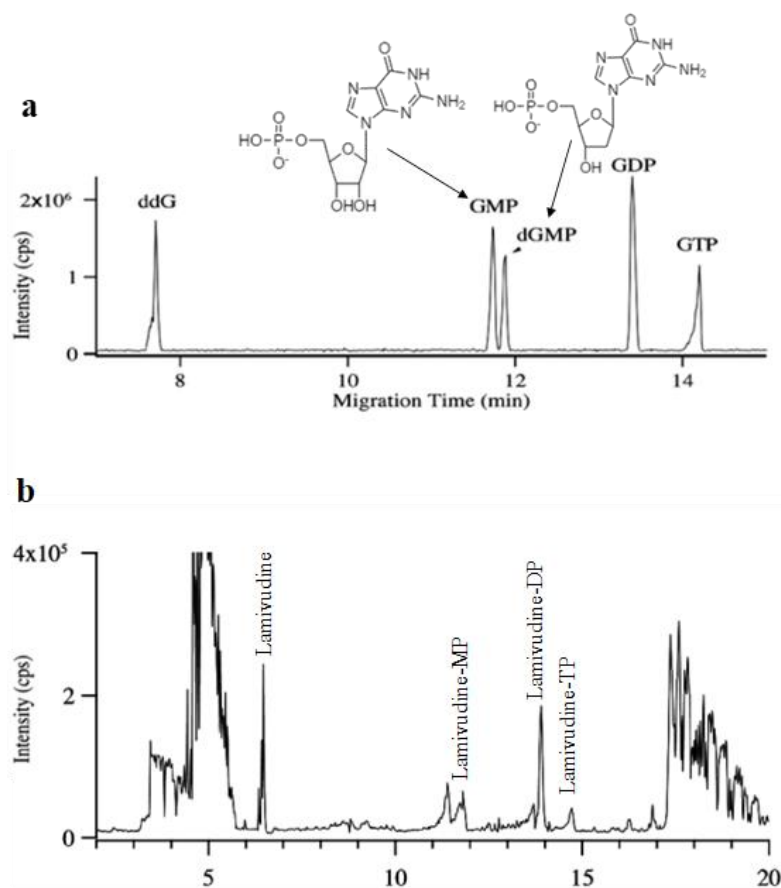


Figure I.14: electropherogram representing the separation of various Guanosine nucleoside phosphates in addition to the resolution of dGMP from GMP (a) and electropherogram of the CE-MS analysis of cell extracts incubated in lamivudine-containing medium demonstrating cellular phosphorylation activity (b). Reaction and CE-MS conditions are summarized in Table I.2. Adapted from [103]

All three phosphorylated metabolites of lamivudine as well as lamivudine itself were detected and separated in under 15 min verifying its activation in the human cell lines (Figure I.14b). The method also demonstrated its capability to detect and quantify endogenous nucleotides in human cell lines untreated with lamivudine. CE-MS was demonstrated for its use in monitoring the activities of *in-cellulo* kinases providing means to evaluate the effectiveness of anti-viral drugs through the detection of their metabolites.

In 2006, J. Iqbal *et al.* described the development of three CE-based methods to assay the activity and inhibition of bovine liver adenosine kinase (AK) [104]. In the first method (Method A), the micellar electrokinetic chromatography (MEKC) mode was implemented through the use of 30 mM borate buffer (pH 9.5) containing 100 mM SDS. The analytes interact differentially with SDS which acts as a pseudo-stationary phase. The SDS is present at a concentration higher than its critical micellar concentration (≈ 8 mM), allowing the formation of micelles in the solution. A series of seven adenosine nucleoside analogs, differing in the nature of substitution at position 2, were tested as alternative substrates of adenosine for AK catalyzed phosphorylation using the offline CE mode (Figure I.15a).

a

Method A	Substrate	% phosphorylation
Testing nucleoside substrates offline	Adenosine	100 \pm 2
	2-Ethylaminoadenosine	3 \pm 1
	2-Isopropylaminoadenosine	4 \pm 0
	2-Isopropylamino-N6-isopropyladenosine	81 \pm 3
	2-Benzylaminoadenosine	4 \pm 0
	2-Cyclohexylaminoadenosine	3 \pm 0
	2-(Pyrrolidin-1-yl)adenosine	53 \pm 2
	2-(4-Benzylpiperazin-1-yl)adenosine	3 \pm 0

b

Method B	AK Inhibitor	K _i value (nM)			
		Offline CE-UV (Method B)	Online-CE-UV (Method C)	Radioactive method	
Testing AK inhibitor offline	ABT-702	1.4 \pm 0.04	1.7 \pm 0.07	3.4 \pm 0.03	
	5-IT	30.6 \pm 1.7	n.d.	29 \pm 6.1	
Method C	Testing AK inhibitor online	A-134974	0.09 \pm 0.006	0.06 \pm 0.031	0.07 \pm 0.006
					0.06 \pm 0.07

Figure I.15: The percentage phosphorylation obtained for 8 substrates of bovine AK using offline CE (**a**) and, K_i values obtained for 3 AK inhibitors using offline and online CE as well as a conventional radioactivity assay using bovine and human AK (**b**). Reaction and separation conditions for all three methods are summarized in Table I.2

Only two amongst the seven tested analogues showed relevant phosphorylation by AK, namely pyrrolidinyl- and isopropylamino-substituted analogues with 53 and 81% phosphorylation compared to that of natural adenosine (100% phosphorylation), respectively. The separation of the phosphorylated analog products from non-phosphorylated substrates was possible due to their altered mobilities manifested by different migration times of peaks detected by CE-UV ($\lambda = 260$ nm). Using normal polarity (+95 μ A), the analog substrates migrated faster towards the cathode due to their lower electrophoretic mobility compared to that of the monophosphate analog product. The developed method provided means to screen novel AK substrates and quantitative detection of their phosphorylated product thanks to the efficiently separated and resolved reactants and products peaks in relatively short migration times thanks to the combination of alkaline pH and high SDS content of the BGE. The total analysis time will, however, still depend on the charge density and size of the tested substrate and consequently, the product, since both parameters define the electrophoretic mobility of molecules.

The second method (Method B) was used to assess inhibition of adenosine kinase using three standard AK inhibitors (2 adenosine analogs and 1 non-nucleoside). Adenosine, the substrate, was fixed at 100 μ M and incubated with AK and the inhibitors offline prior to CE analysis. The reaction conditions were kept similar to the previous method (Method A) except for the IB, which was changed to 20 mM sodium phosphate (pH 7.5) to obtain high quality peak shapes and the internal standard was UMP instead of TMP which comigrated with the ADP peak when borate buffer was used as the BGE (Table I.2). Then, the extent of diminishing of the AMP product peak, detected at ≈ 7 min, as a result of inhibition was measured relative to a control reaction without inhibitors. The K_i values obtained after the offline inhibition assays agreed with those obtained using a radioactive approach and human AK (Figure I.15b). A-134974, an analog of adenosine, was identified as the most potent inhibitor in all three assays. By increasing the pH of the phosphate buffer from 7.5 to 8.5, migration times were cut shorter by approximately 2 min. This is mainly due to the increased charges of the capillary wall resulting in an increase of the magnitude of EOF which is the predominant driving force sweeping all analytes (even anions) towards the cathode. The second method thus permitted screening AK inhibitors in only 5 min permitting the calculation of kinetic inhibition parameters which could be used to rank AK inhibitors for their effectiveness. The third CE method (Method C) involved carrying out the AK inhibition assay using the EMMA online CE-mode. The capillary was coated with polyacrylamide to neutralize the charges on its

walls and thus suppress the EOF. As previously described [105], this type of coating limits the interaction between charged groups on proteins and the capillary wall, a phenomenon that often causes fluctuations in the EOF and therefore result in poor repeatabilities of migration times. Furthermore, the use of a non-alkaline BGE was necessary, since at high pH values, the neutral coating is less stable. After filling the capillary with the dipotassium hydrogen phosphate BGE (50 mM, pH 6.5), a plug of the Tris-HCl IB (20 mM, pH 7.4) was injected first to separate the reactants from the BGE. The reactants were then injected sequentially starting with the one having the lowest mobility *i.e.* AK, since they migrate more slowly, followed by the reactant with a higher mobility *i.e.* the adenosine substrate, which migrates faster. This was followed by the injection of an IB plug and finally BGE. This partial filling of the capillary with the IB plugs at the beginning and the end of the injection sequence aims to isolate the reaction from the BGE which could interfere with the reaction due the different pH values of the BGE and IB. To mix the reactants, a voltage of -5 kV was applied for 12 s after which it was turned off for 5 min to allow the amplification of the AMP product. After the incubation period, the voltage was turned on at a constant current of -60 μ A to separate the products from the reactants. The reversal of the separation polarity was necessary due to the suppression of the EOF by the neutral coating of the capillary. Thus, the analytes predominantly migrated according to their respective electrophoretic mobilities towards the anode. Two of the three inhibitors assayed offline by method B were mixed in the substrate solution, consisting of adenosine, ATP, MgCl₂, UMP internal standard mixed in 20 mM Tris-HCl (pH 7.4) and injected after the adenosine kinase plug. The AMP peak was the last to be detected due to the low charge capacity of AMP compared to UMP, ADP and ATP. The K_i values of the inhibitors obtained by the online assay agreed with those obtained by the offline assay as well as by conventional radioactive assays using the bovine and human enzyme (Figure I.15b). The developed online assay allowed the adaptation of an automated, more economic form of the inhibition assays. Through this study, the flexibility of CE is demonstrated through the adaptation of different reaction and CE-analysis conditions to achieve the best outcomes.

A year later, the same group introduced an optimized CE-UV approach to assay TK activity of the herpes simplex virus (HSV) [106]. Two methods were developed for the detection of TK phosphorylated products. In the first method, the BGE was chosen as 20 mM sodium phosphate buffer (pH 8.5) due to its UV-invisibility at $\lambda = 260$ nm, the wavelength used for nucleoside detection. The concentration of 20 mM was suitable as to not result in the generation of excessive

Joule heating due to high currents. Furthermore, the BGE's pH (8.5) was suitable to obtain high reproducibility of migration times and peak resolution. UMP was used as an internal standard to correct for low repeatabilities associated with the hydrodynamic injection of low volumes (Figure I.16a).

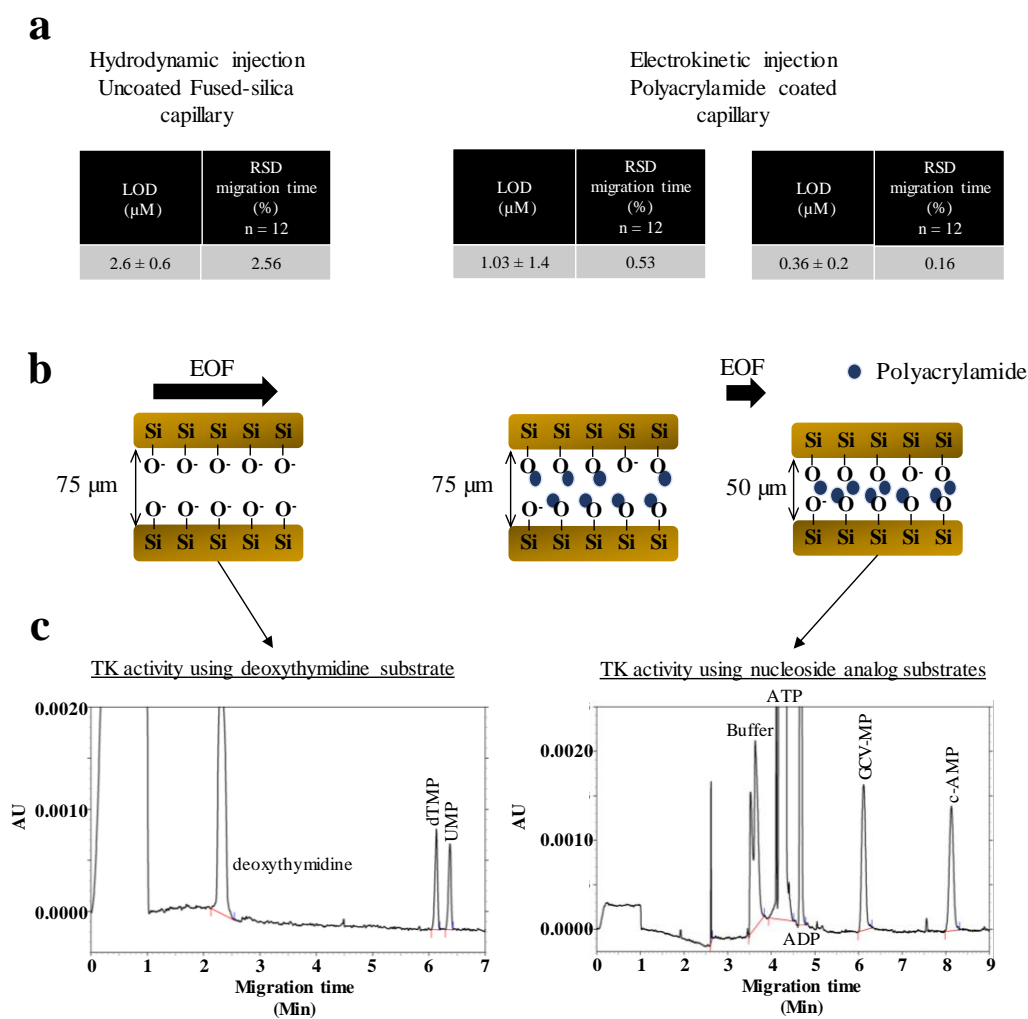


Figure I.16: The LOD of mono-phosphorylated nucleoside or nucleoside analogs and the RSD of migration times between all three types of capillaries used (a), Illustration of the inner polyacrylamide-coated surface of the capillaries (b) and, electropherograms obtained by CE-UV for the phosphorylation of endogenous deoxythymidine (left) and nucleoside analog GCV (right) (c). Conditions of enzymatic reaction and CE separation are summarized in Table I.2. Electropherograms adapted from [106]

The phosphorylated product (dTMP) was detected in less than 7 min followed directly by the UMP standard. Interactions between charged proteins (TK) and silanol groups of the uncoated silica capillary can lead to variations in migration times and diminishing of separation quality and efficiency (Figure I.16c). Therefore, the authors developed a second method where the charged

silanol group were masked by a polyacrylamide coating, resulting in the neutralization of the charges on the capillary wall and the elimination of most protein-capillary wall interactions (Figure I.16b). Indeed, a drastic reduction in the RSD of migration times of dTMP was observed with coated capillaries (16-fold lower, $n = 12$, Figure I.16a). The use of a neutral capillary required the reduction of the BGE's pH to 6.5 since polyacrylamide coating is unstable at high pH [106]. Consequently, the BGE's ionic strength was increased to 50 mM to achieve good peak resolution in short time. Furthermore, a capillary of a shorter length was used to reduce the migration time. The use of electrokinetic injection allowed sample pre-concentration of anionic species and increased sensitivity of the method. The detection wavelength was thus reduced to 210 nm, where nucleoside absorption is higher, since the majority of interfering molecules are eliminated. The LOD of dTMP were approximately 7-fold lower compared to the first method (Figure I.16a). Concerning the inner diameter of the capillary, a higher diameter prompts higher sensitivities. However, when the inner diameter was increased to 75 μm , the migration time repeatabilities of dTMP was higher compared to when using a capillary of 50 μm inner diameter.

The use of electrokinetic injection necessitated the use of an IB of low ionic strength to avoid decrease of the field strength and reduction in the amount of injected analytes. Similarly, the larger inner diameter of the capillary meant that more buffer ions are being introduced into the capillary resulting in decreased sensitivity for the reasons discussed above. The developed method was applied to assess 3 nucleoside analogues, acyclovir (ACV), (E)-5-(2-bromovinyl)-2'-deoxyuridine (BVDU) and ganciclovir (GCV) (Figure I.16c), as substrates of HSV TK. K_m and the turnover number (k_{cat}), the amount of substrate converted to product *per* unit time were determined for each compound and were in good agreement to previously published values. Lastly, by increasing the concentration of ACV and using a constant saturating concentration of endogenous thymidine, the authors demonstrated the competitive nature of ACV inhibition through monitoring the decrease in dTMP, the product of thymidine phosphorylation.

In 2012, N. Malartre *et al.* introduced an HPLC-UV assay for monitoring the phosphorylation activity of several different mutant variants of HSV-TK against deoxythymidine and ACV [107]. TK proteins were incubated at 37°C for 2, 4 and 7 h with deoxythymidine or ACV in the presence of Tris-HCl buffer containing MgCl_2 and ATP. The monophosphorylated form of the substrates were measured using HPLC-UV equipped with a C18 Hypersil ODS column and DAD set at $\lambda = 254$ nm for ACVMP or $\lambda = 266$ nm for dTMP. The seven different mutant versions of the TK

enzyme were obtained through site-directed mutagenesis of the UL23 TK expressing gene. The mutant and the wild-type genes were then overexpressed in *E. Coli* strains and then purified from the cellular lysates to be used in the enzymatic reaction. Based on the phosphorylation activity of the mutant TK towards both deoxythymidine and ACV relative to that of the wild-type TK, the proteins were classified into: altered TK (TK^{alt}) producing no ACVMP and $\geq 15\%$ dTMP, low TK (TK^{low}) producing no ACVMP and $\leq 15\%$ dTMP, Deficient TK (TK^d) producing neither monophosphates and partial TK (TK^{partial}) producing $\leq 15\%$ ACVMP and 100% dTMPK. The detection of the products was linear up to 0.22 mM and the LOD was approximately 0.12 μM . The retention time of ACVMP was 2.8 min and that of dTMP was 4 min. This method provided means to better understand antiviral resistance developed by HSV towards ACV on a genotypic and phenotypic level. The HPLC-UV method was relatively simple and both monophosphorylated products were detected with a high sensitivity and over a relatively wide linearity range in under 5 min. It would be interesting to adapt the concept of the study to online CE where the different TK variants can be tested towards different antiviral drugs as well as endogenous nucleoside substrates in a more economic and automated fashion to correlate the effect of site-induced mutagenesis of the UL23 gene to the activity of the resulting mutant TK. A possible obstacle would be the production of the different TK mutants which could be time-consuming and requires specialized equipment for cell inoculation and culturing.

Recently, our group applied a CE-UV method to determine the catalytic efficiency of human TMPK [108]. The catalytic efficiency is measured as the ratio of K_{cat} to K_m which in turn reflects the effectiveness of the enzyme towards a particular substrate [109]. The catalytic efficiency of TMPK obtained *via* CE-UV ($K_{\text{cat}}/K_m = 0.48 \times 10^5 \text{ M}^{-1} \text{ s}^{-1}$) towards TMP was then compared to that obtained using either flow injection analysis coupled to high resolution mass spectrometry (FIA-HRMS) ($K_{\text{cat}}/K_m = 0.21 \times 10^5 \text{ M}^{-1} \text{ s}^{-1}$) or spectrophotometric assays ($K_{\text{cat}}/K_m = 0.05 \times 10^5 \text{ M}^{-1} \text{ s}^{-1}$). A solution of 80 mM ammonium acetate at pH 9.0 was used as the BGE. This volatile solution was used to maintain similar conditions adaptable for MS analyses. The relatively high concentration of the BGE limits interactions between the solutes and the capillary wall and enhances the buffering capacity of the solution [110]. Furthermore, the alkaline pH ensured that the analytes are negatively charged and their peaks are thus resolved due to the differential electrophoretic mobilities of the anionic species acting opposite to the direction of flow (towards

the anode). The enzymatic reaction was carried out offline by incubating the enzyme with a range of dTMP concentrations in the presence of MgCl_2 and ATP to determine the kinetic parameters (K_{cat} and K_{m}). The concentrations of MgCl_2 and ATP were maintained low, similar to those of FIA-HRMS analyses, to reduce ion suppression and maintain adequate TMPK activity (see Table I.2 for more conditions on the enzymatic reaction and CE analysis). The IB was a more diluted version of the BGE (50 mM ammonium acetate) at pH 7. The lower concentration of the IB compared to the BGE mediates a stacking effect due to the differences in conductivities of the injected sample plug and the surrounding BGE [110,111]. This in turn enhances the shapes of the peaks and the sensitivity of detection. This method demonstrated the feasibility of carrying out kinetic evaluation of kinases using CE-UV without the need of complicated instrumentations where the catalytic efficiency of the TMPK determined by CE-UV was in the same order of magnitude compared to that determined by FIA-HRMS and conventional spectrophotometric assays as depicted in Figure I.17.

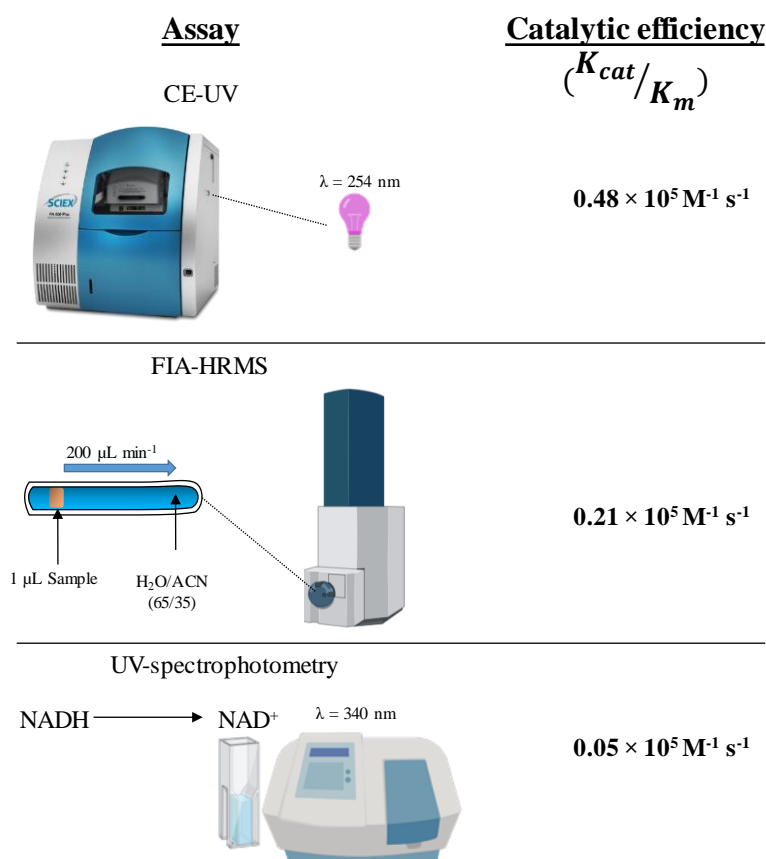


Figure I.17: The value of the catalytic efficiency as a function of the assay used to quantify it

Recently, C. Machon *et al.* introduced the first LC-HRMS assay to study 10 metabolites of 5-fluorouracil (5-FU), a chemotherapeutic drug used to treat several types of cancers [112]. The separation was carried out on a Hypercarb® porous graphitic carbon column. This overcame limitations including difficult retention of nucleotides onto reverse phase columns due to the polarity of the phosphate groups requiring the addition of salt or ion-pairing additives which could hamper detection by mass spectrometry [113]. The LC-MS method was first optimized for the detection of the different metabolites. Six out of the ten metabolites were available as purified standards whilst the remaining four (5-fluorouridine diphosphate (5-FUDP), 5-fluorodeoxyuridine diphosphate (5-FdUDP), (5-FUDP)-Hexose (Hex) and 5-FUDP-N-acetylhexosamines (HexNAc) were either produced in cell lines or from enzymatic reactions. 5-FUDP and 5-FdUDP were produced by incubating the monophosphorylated form of 5-FU or 5-FdU with deoxynucleoside monophosphate kinase (dNMPK) for 30 min before stopping the reaction with a mixture of cold MeOH/water (70/30, v/v) and analysis by LC-MS. The detection of 5-FUDP at $m/z = 420.98550$ in the negative ionization mode and 5-FdUDP at $m/z = 404.99058$ in the negative and $m/z = 407.00514$ in the positive ionization mode in addition to the specific fragmentation profiles confirmed the success of the enzymatic conversion of monophosphorylated 5-FU and 5-FdU into dephosphorylated forms. The retention times of 5-FUMP and 5-FdUMP were spaced by 0.38 min, 4.83 and 5.21 min, respectively. However, the dephosphorylated forms were shown to have the same retention time, 4.5 min for 5-FUDP and 4.49 min for 5-FdUDP. 5-FUMP and 5-FdUMP had slightly better response in the negative ionization mode (2 and 3-fold, respectively) whilst 5-FUDP was not detected in the positive ionization mode and 5-FdUDP had better response in the negative ionization mode (47-fold higher). HCT116 cells, human colon cancer cells, were exposed to 5-FU (or 5-FdU) at 10 or 50 μM for 24 h. 5-FU was phosphorylated sequentially by different cellular kinases into 5-FUTP which was converted into 5-FUDP-Hex by UDP-glucose-pyrophosphorylase and 5-FUDP-HexNAc by UDP-N-acetylhexosamine-pyrophosphorylase. After metabolite extraction from the cell lysate and their analysis by LC-MS, 5-FUDP-Hex was detected at 5.1 min and 5-FUDP-HexNAc at 5.5 min. Similar to 5-FUDP and 5-FdUDP, the response was generally better using the negative ionization mode. Upon analysis of the intracellular anabolism of 5-FU, 5-FdUDP and 5-FdUTP were not detected even after exposition to 5-FdU or using a different cell line. This has been attributed to the possibility that 5-FUMP was a better substrate of cellular UMP-

CMP kinases compared to 5-FdUMP. The method was used to determine 5-FU incorporation into DNA and RNA by LC-MS analysis of metabolites in each of the nucleic acids. Metabolite incorporation into RNA was estimated to be 50 to 100-fold higher than that into the DNA. The developed method was demonstrated to be highly sensitive (in pg), selective (discriminating 5-FU metabolites from endogeneous ones) and linear (over a range of 0.5 - 3 million cells) for the detection of 5-FU metabolites in cells or their incorporation into DNA and RNA. A drawback of this method is common amongst LC-based assays requiring relatively large sample volumes (10 μ L) and organic solvent. Furthermore, although the method demonstrated a great selectivity towards 5-FU metabolites, due to the detection of specific fragmentation patterns of fluorine-containing metabolites, the separation efficiency was rather low since several metabolites were detected at close or identical retention times. This is a common limitation of porous graphitic carbon columns where upon usage, loss of resolution and retention capability was observed [113].

Table I.2: CE-based nucleoside kinase assays

Enzymatic reaction					CE separation	
Enzyme	Substrate	Inhibitor	Incubation buffer (IB)	Reaction conditions	Background electrolyte (BGE)	CE conditions
[101] Cytosolic 5'-nucleotidase /nucleoside phosphotransferase purified from calf thymus	Inosine	-	50 mM Tris-HCl 20 mM MgCl ₂ 1 mM dithiothreitol (DTT) pH 7.4	In a mixture of 140 µL add : 2 mM dGMP 4.5 mM ATP IB 2 mM Inosine 0.3 µg enzyme Incubation at 37°C for 30 min Aliquots of 32 µL drawn at different time intervals and mixed with 48 µL cold MeOH to terminate the reaction and stored at -20°C The aliquot was centrifuged at 10000g for 15 min 50 µL of the supernatant was dried and then reconstituted in 20 µL H ₂ O before CE analysis	50 mM NaH ₂ PO ₄ 40 mM Glycine pH 9.0 adjusted using NaOH	Uncoated fused-silica capillary 50 cm × 50 µm i.d. Temperature: 25°C Separation voltage: +20 kV Injection: 1 psi × 4 s (10 nL) Detection: UV Inosine and dGMP substrates and IMP and deoxyGuanosine products at λ = 254 nm
[102] Thymidine kinase (TK) Thymidine monophosphate kinase (TMPK)	Thymidine Thymidine monophosphate	-	50 mM Tris-HCl (pH 8)	Protein extract from cell lysate mixed 1:1 (v/v) with TK reaction solution containing: 0.4 mM thymidine, 2 mM ATP, 2 mM MgCl ₂ , 0.2 mg mL ⁻¹ bovine serum albumin, 10 mM NaF and 3 mM β-mercaptoethanol in IB (pH 8). Incubation at 37°C for 10 and 20 min	20 mM Sodium tetraborate (pH 9.1)	Uncoated fused-silica capillary bubble cell capillary 45.5 cm × 50 µm; 37 cm effective length; 150 µm path length Temperature: 25°C Separation voltage: +23 kV

Enzymatic reaction					CE separation	
Enzyme	Substrate	Inhibitor	Incubation buffer (IB)	Reaction conditions	Background electrolyte (BGE)	CE conditions
				<p>The reaction was stopped by boiling for 3 min</p> <p>Reaction mixture stored at -20°C until CE analyses</p> <p>The samples were mixed with EDTA, ACN, NaCl and dAMP prior to CE injection</p>		<p>Injection: 0.5 psi × 40 s (52 nL)</p> <p>Detection: UV thymidine, dTMP and dTDP at $\lambda = 267$ nm</p>
[103]	Cellular kinases	Lamivudine	-	<p>Cell incubation media</p> <p>Confluent Hep G2 cells incubated at 37°C for 10 h in a medium containing 100 μM lamivudine.</p> <p>Incubation media was aspirated and the cells washed three times with phosphate-buffered saline (pH 7.4)</p> <p>Cells were lysed by 2 mL of 60% (v/v) MeOH and vortexed overnight then sonicated at 4°C for 1 min</p> <p>The cell lysates were ultrafiltered for 24 h at 6000 g, 10°C and then evaporated to concentrate the extract 100-fold before CE injection.</p>	25 mM Ammonium acetate (pH 10.0)	<p>Uncoated fused-silica capillary 60 cm × 50 μm i.d.</p> <p>Separation voltage: +15 kV</p> <p>Injection: Manual at 18 cm elevation for 30 s</p> <p>Detection: ESI-MS Lamivudine and its phosphorylated metabolites Sheath liquid: 100% MeOH at 2 μL min⁻¹ Negative ionization mode Capillary voltage: -3.6 kV Nebulizing gas flow: 0.41 L min⁻¹ Dry gas flow: 1 L min⁻¹</p>

Enzymatic reaction					CE separation	
Enzyme	Substrate	Inhibitor	Incubation buffer (IB)	Reaction conditions	Background electrolyte (BGE)	CE conditions
[104] Adenosine kinase (AK) from bovine thymus	<p><u>Method A</u></p> <p>7 adenosine nucleoside analogs with different substituents at position 2 of the purine ring</p> <p><u>Method B & C</u></p> <p>Adenosine</p>	<p><u>Method A</u></p> <p>-</p> <p><u>Method B & C</u></p> <p>3 standard AK inhibitors (ABT-702, 5-IT and A-134974)</p>	<p><u>Method A</u></p> <p>20 mM Tris-HCl (pH 7.4)</p> <p><u>Method B</u></p> <p>20 mM Tris-HCl (pH 7.5)</p> <p><u>Method C</u></p> <p>20 mM Tris-HCl</p> <p>0.2 mM MgCl₂ (pH 7.4)</p>	<p><u>Method A & B</u></p> <p>10 µL AK ($C_f = 0.078 \mu\text{g}$) added to the enzyme assay mixture ($V_{\text{total}}: 100 \mu\text{L}$):</p> <p>IB</p> <p>0.2 mM MgCl₂</p> <p>5 mM K₂HPO₄</p> <p>1 mM ATP</p> <p>200 µM substrate in DMSO (1%, v/v) (<u>Method A</u>)</p> <p>OR</p> <p>100 µM adenosine (<u>Method B</u>)</p> <p>20 µM TMP internal standard (<u>Method A</u>)</p> <p>OR</p> <p>20 µM UMP internal standard (<u>Method B</u>)</p> <p>10 µL Inhibitors in DMSO (1%, v/v)</p> <p>Incubation at 37°C for 15 min</p> <p>The reaction was stopped by heating at 99°C for 2 min.</p> <p>Aliquots of 50 µL were then injected into CE.</p>	<p><u>Method A</u></p> <p>30 mM borate buffer</p> <p>100 mM SDS (pH 9.5)</p> <p><u>Method B</u></p> <p>20 mM sodium phosphate (pH 7.5)</p> <p><u>Method C</u></p> <p>50 mM K₂HPO₄ (pH 6.5)</p>	<p>Uncoated fused-silica capillary</p> <p>40 cm x 75 µm i.d.;</p> <p>30 cm effective length</p> <p>Temperature: 25°C</p> <p>Separation current: +95 µA</p> <p>Injection (Offline): 0.1 psi x 25 (37.6 nL)</p> <p>Detection: UV</p> <p>AMP or nucleoside analogue monophosphate at $\lambda = 260 \text{ nm}$</p> <p><u>Method C</u></p> <p>Polyacrylamide-coated fused-silica capillary</p> <p>30 cm x 50 µm i.d.;</p> <p>20 cm effective length</p> <p>Temperature: 37°C</p> <p>Separation current: -60 µA</p> <p>Detection: UV</p> <p>AMP at $\lambda = 210 \text{ nm}$</p>

Enzymatic reaction					CE separation	
Enzyme	Substrate	Inhibitor	Incubation buffer (IB)	Reaction conditions	Background electrolyte (BGE)	CE conditions

Method C1st plug: IB2nd plug: diluted AK3rd plug: 100 μ M Adenosine, 1 mM ATP, 20 μ M UMP (internal standard) and inhibitor in IB4th plug: IB

The reaction was initiated through the application of 5 kV for 12 s

Incubation at 37°C for 5 min

The reaction was stopped by the application of constant current -60 μ A and the analytes were separated

[106]	Herpes simplex virus-1 (HSV-1) thymidine kinase (TK)	Thymidine <u>Method B</u>	<u>Method A</u> -	50 mM Tris-HCl (pH 7.4)	<u>Method A</u> The reaction was initiated by adding 10 μ L TK (4 μ g) to the reaction mixture containing ($V_{total} = 100 \mu$ L): IB 2 mM Thymidine 5 mM ATP 5 mM MgCl ₂	<u>Method A</u> 20 mM sodium phosphate (pH 8.5) <u>Method B</u> 50 mM dipotassium hydrogen phosphate (pH 6.5)	<u>Method A</u> Uncoated fused-silica capillary 40 cm \times 75 μ m i.d.; 30 cm effective length Temperature: 25°C Separation current: 95 μ A
		Acyclovir (ACV)	<u>Method B</u> Acyclovir (ACV)				
		Ganciclovir (GCV)			Incubation at 37°C for 5-120 min		
		(E)-5-(2-bromovinyl)-2'-					

Enzymatic reaction					CE separation	
Enzyme	Substrate	Inhibitor	Incubation buffer (IB)	Reaction conditions	Background electrolyte (BGE)	CE conditions
	deoxyuridine (BVDU)			<p>The reaction was stopped by heating at 99°C for 5 min</p> <p>45 µL of the reaction mixture were transferred to a vial containing 5 µL of UMP (internal standard; 20 µM) before CE analysis.</p> <p><u>Method B (substrate screening)</u></p> <p>The reaction was initiated by adding 10 µL TK (4 µg) to the reaction mixture previously incubated at 37°C for 2 min containing (V_{total} = 100 µL): IB 15.6-1000 µM ACV, GCV or BVDU 1 mM ATP 5 mM MgCl₂</p> <p>Incubation at 37°C for 15 min</p> <p>The reaction was stopped by heating at 99°C for 5 min</p> <p>45 µL of the reaction mixture were transferred to a vial containing 5 µL of UMP or cAMP (internal standard; 20 µM) before CE analysis.</p> <p><u>Method B (Inhibition)</u></p> <p>The reaction was initiated by adding 10 µL TK (4 µg) to the reaction mixture previously incubated at 37°C for 2 min containing (V_{total} = 100 µL):</p>		<p>Injection: 0.1 psi × 25 s (37.6 nL)</p> <p>Detection: UV dTMP at λ = 260 nm</p> <p><u>Method B</u></p> <p>Polyacrylamide-coated fused-silica capillary 30 cm × 50 µm OR 75 µm i.d.; 20 cm effective length</p> <p>Temperature:</p> <p>Separation current: -60 µA</p> <p>Injection: -6 kV for 30 s</p> <p>Detection: UV TMP or monophosphorylated drug analogs at λ = 210 nm</p>

Enzymatic reaction					CE separation	
Enzyme	Substrate	Inhibitor	Incubation buffer (IB)	Reaction conditions	Background electrolyte (BGE)	CE conditions

IB
 100 μM thymidine
 1 mM ATP
 5 mM MgCl_2
 0.0625, 0.5 and 5 mM Acyclovir

Incubation at 37°C for 15 min

The reaction was stopped by heating at 99°C for 5 min

[108]	Human TMPK	dTMP	-	50 mM ammonium acetate (pH 7.0)	0.004 g L ⁻¹ TMPK mixed with a range of dTMP concentrations (0-800 μM), 350 μM ATP and 200 μM MgCl_2 in the IB	80 mM ammonium acetate (pH 9.0)	Uncoated fused-silica capillary (60 cm \times 50 μm i.d.; 50 cm effective length)
					Incubation at 37°C for 5 min		Temperature: 37°C
					The reaction was stopped by heating at 95°C for 5 min		Separation voltage: +15 kV
							Injection: 0.5 psi \times 10 s (12.7 nL)
							Detection: UV dTMP and dTDP at $\lambda = 254$ nm

VI. Microchip-based lipase and kinase assays

Microchips vary in design and fabrication depending on the type of application and the user's preference. Most commonly, microchips are manufactured from glass, certain polymers such as polydimethylsiloxane (PDMS) and poly(methyl methacrylate) or a combination of both [114]. There exist various geometrical designs for microchips with the injection cross geometry being the most common microchip design for microchip electrophoresis (ME) (Figure I.18) [115].

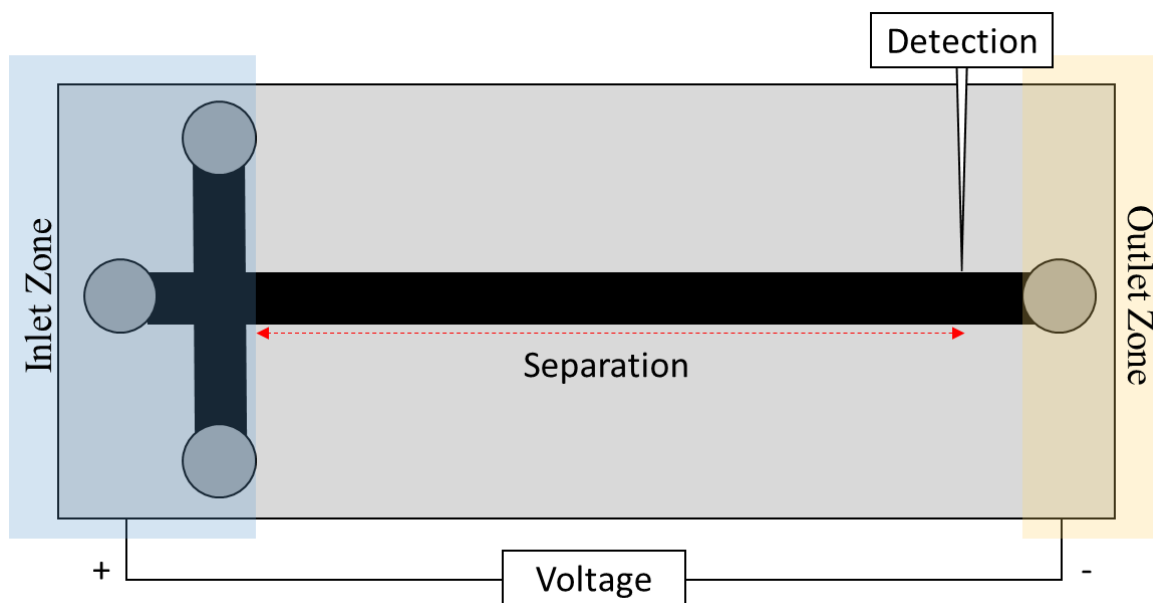
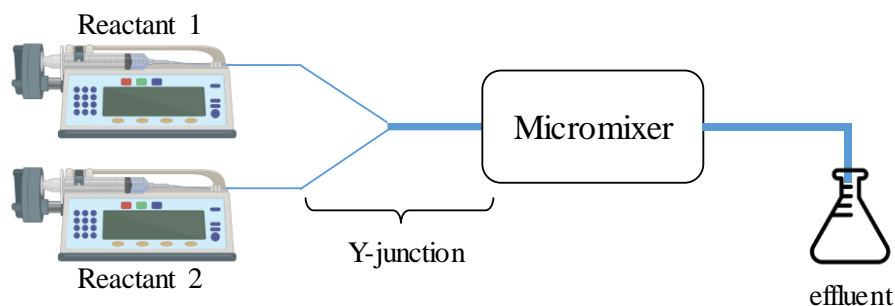


Figure I.18: Schematic presentation of a typical ME device with an injection cross geometry consisting of three inlet and an outlet reservoirs

As far as we know, no recent applications of lipase miniaturized assay involved the use of electrophoretically driven microchips. The applications are almost exclusive to flow-injection microfluidics. Recently, N.N.A. Razak *et al.* demonstrated contrasting kinetic parameters of the lipase catalyzed reaction using a microfluidic flow-injection system compared to macro-scale conventional assays as a result of different hydrodynamic conditions [116]. L.H. Du *et al.* used a similar microfluidic setup for the lipase catalyzed synthesis of β -amino acid esters from aromatic amines and acrylates [117]. The miniaturized device generally consisted of two syringes installed onto syringe pumps used to inject the analytes through a Y-junction into a micromixer (Figure I.19). A different recent application of microfluidic lipase assay was described by H. Yusuf *et al.* for biodiesel synthesis in the form of methyl esters [118].



Micromixer geometries



Figure I.19: An example of a microfluidic device setup involving two reactants mixed in a micromixer with different geometries. Adapted from [116]

The poly(methyl methacrylate) microfluidic chip consisted of a T-shaped inlet leading into a serpentine mixing microchannel that is 400 mm long. The reactants consisting of the lipase enzyme, sunflower oil and methanol substrates and t-butanol solvent were divided into two syringes and introduced to the microchip *via* gravitational flow. Within the context of homogeneous lipase-catalyzed biodiesel synthesis, A. Salic *et al.* described the use of dual microchips connected in series for biodiesel synthesis followed by its purification by glycerol separation. The reactants were introduced into the first polytetrafluoroethylene (PTFE) microchannel *via* two syringes, one containing the methanol substrate and the other containing the lipase, sunflower oil and SDS. The outflow from the first microchannel; containing biodiesel, unreacted oil and methanol and glycerol by product; was directed into the second channel where biodiesel purification took place. A third syringe was used to introduce choline chloride ethylene glycol (ChCl:Etgl), a deep eutectic solvent, to the second microchannel for glycerol separation. The produced biodiesel was quantified using gas chromatography with flame ionization detector (GC-FID). Another microreactor for the lipase-catalyzed biodiesel synthesis has been described using immobilized lipase [119]. The immobilization was carried out using an optimized layer-by-layer method where alternating layers of polyethylenimine (PEI) and lipase are used to coat a PTFE microchannel. The substrates (soybean oil and methanol) in t-butanol solvent were injected

into the microchannel by a syringe and the synthesized methyl ester biodiesel was analyzed using GC-FID. Other recent applications of miniature immobilized lipase assays include quantification of fat in milk samples [120], synthesis of wax esters [121] as well as neohesperidin ester derivatives [122].

Concerning kinases, several miniaturized activity assays have been previously described. Y. Zhang *et al.* described T4 polynucleotide kinase activity assay on a glass electrophoresis microchip. The inhibitory potentials of ammonium sulfate and adenosine diphosphate on T4 polynucleotide kinase were also evaluated [123]. The kinase phosphorylates a labeled double stranded DNA substrate which is then hydrolyzed by an exonuclease. The resulting hydrolyzed DNA was then separated from the non-hydrolyzed one by ME. LIF was used for the detection of the labeled DNA strands. Another approach was described by J. Mao *et al.* using a DNAzyme driven DNA walker biosensor for assaying T4 polynucleotide kinase activity and inhibition [124]. The cleavage of the phosphorylated substrate by an endonuclease initiates a series of cascade reactions ending by the release of labeled DNA which signal is used to determine the T4 polynucleotide kinase activity. A slightly different approach was developed by J. Pagaduan *et al.* [125]. The immune complex between an anti-thymidine kinase-1 (TK1) monoclonal antibody (mAb) and TK1 was detected using a ME assay. The immune complex was detected by LIF after separation of unbound Ab from the immune complex on a PMMA microchip. Although the activity of the enzyme was not directly investigated, the authors suggest a correlation between TK1's activity and the quantity of TK1 isoforms in the medium.

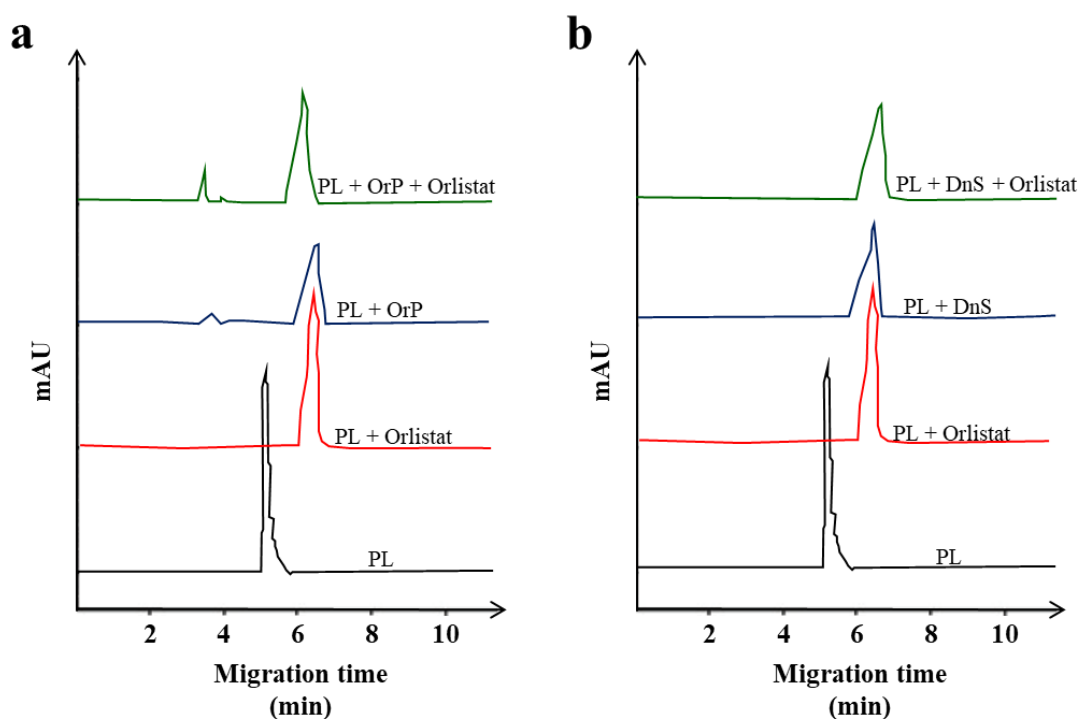
The number of studies utilizing microchip-based enzymatic assays are limited since no fundamental regulations are established. Nonetheless, these miniaturized assays are witnessing an increase in popularity due to the advantages brought about by miniaturization such as reduced sample and reagent consumption, faster analysis times and increased extent of automatization and multiplexing. The microchip-based approach is interesting for applications involving real-time clinical analyses and assays involving single cells.

VII. Binding affinity assays

In 2019, I. Hamdan *et al.* applied CE to monitor changes in the migration times and peak shapes of PL upon binding to certain drugs, orlistat or a combination of both [126]. This mode of CE is known as affinity CE and is often used to study binding interactions occurring between molecules. It was used to confirm findings obtained using conventional spectrophotometric PL inhibition assays and docking studies. Some of the tested drugs demonstrated synergism in inhibitory activity where the addition of orlistat enhanced the overall inhibition. This was attributed to the binding mode of these drugs to PL where the active site, *i.e.* orlistat binding site, remained exposed. Other drugs demonstrated antagonism when combined with orlistat where the overall inhibition diminished due to interferences with orlistat binding to the active site of PL. Orlistat, the tested drugs or both were added to the 50 mM phosphate buffer (pH 6.8) containing 15% (*v/v*) ACN and 16.7% (*v/v*) MeOH as BGE which was then used to fill the capillary. PL was then injected into the capillary. The shift in mobility caused by the formation of a bound complex between PL and the ligands was manifested through changes in the migration times and PL peak shape. As shown in Figure I.20, PL (0.1 g L^{-1}) injected electrokinetically ($18 \text{ kV} \times 15 \text{ s}$) into a capillary filled with blank BGE (no ligands) migrated 5.6 min before reaching the UV detector set at $\lambda = 205 \text{ nm}$. Once orlistat alone was added to the BGE, a shift of PL migration time from 5.6 to 6.5 min was observed. This was attributed to the conformational changes in PL upon binding of orlistat favoring the migration of the complex towards the anode, opposite to the direction of the EOF, and thus slowing down its migration in the capillary by almost 1 min. Similarly, the presence of the tested drugs alone in the BGE resulted in a similar conformational change to PL. When orlistat was present in combination with the drugs in the BGE, the migration times shifts and peak shape changes were more drastic compared to the drugs or orlistat alone (Figure I.20a). One sole drug, dinitrosalicylic acid (DnS), did not demonstrate any significant changes to the electropherograms upon addition of orlistat, an observation that agreed with results obtained using PL inhibition assays and molecular docking studies (Figure I.20b). DnS was shown to bind strongly to Ser-152 of PL's active site which happens to be orlistat's binding site. Thus, the binding of DnS to the active site of PL in addition to its bulkiness minimized the possibility of orlistat binding to PL and thus the overall inhibitory potential was reduced. This study demonstrated the possibility of using CE to gather binding information. Although not the case here, it is possible to determine K_d values of non-covalent interactions which can be used, in addition to catalytic activity assays, to investigate

and rank enzyme-modulating drug molecules.

J. V. Pagaduan *et al.* developed a microchip electrophoresis immunoaffinity assay used to detect and quantify TK-1 in an immunocomplex with anti-TK-1 antibody (Ab) [127]. The assay was coupled to laser-induced fluorescence for the detection of fluorescein isothiocyanate (FITC)-coupled Ab. The microchip device was fabricated using poly(methyl methacrylate). The surface of the device was coated dynamically with 1% methyl cellulose (MC) of different molecular weights in 20 mM Tris-HCl buffer in order to prevent non-specific adsorption of proteins to the surface.



c Structures of PL inhibitor compounds

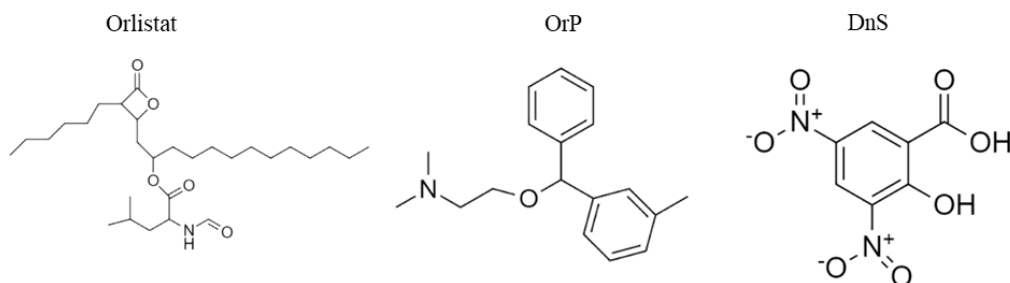


Figure I.20: Electropherograms obtained for the analysis of PL alone (**Black**), PL + Orlistat (**Red**), PL + orphinadrine (OrP) (**Blue**) and PL + OrP + Orlistat (**Green**) (**a**) and, PL alone (**Black**), PL + Orlistat (**Red**), PL + dinitrosalicylic acid (DnS) (**Blue**) and PL + DnS + Orlistat (**Green**) (**b**) and the structures of the investigated PL inhibitory compounds (**c**). Adapted from [126].

The separation buffer chosen was $0.5 \times$ phosphate buffered saline (PBS) at pH 7.4 since sample flow was successful at low currents when a separation voltage of +850 V was applied, compared to other buffers. Increasing the separation distance increased peak broadening due to the increased longitudinal diffusion of the sample plug with increased analysis times and reduced peak heights. The most suitable distance was 5 mm as it was sufficient for the separation of the unbound Ab from the TK-1/Ab immunocomplex. This resolution of bound and unbound species was achieved through the use of MC with a MW of 88000 Da. Due to the increased viscosity of the solution, the electrokinetic injection time was ultimately increased from 30 s for MC 14000 to 60 s for MC 88000 at +350 V. Increasing the concentration of TK-1 increased the intensity of the immunocomplex peak and the detection limit of TK-1 was determined as 80 nM where at lower concentrations, the immunocomplex peak was not detected. The miniaturized assay was able to detect low concentrations in 20 s requiring only 10 μ L of sample volume. This assay however, was not applicable in its current form for the detection of TK-1 in serum samples since the physiological or pathological concentrations of the enzyme were far lower than the assay's detection limits (in the order of pM). Sample pre-concentration is one approach that would allow the application of the developed miniaturized ME assay for determination of TK-1 in serum which in turn can be used for screening of certain types of cancers where TK-1 is overexpressed.

An interesting biophysical technique on the rise and used to evaluate biomolecular binding affinities is microscale thermophoresis (MST) [128]. MST is based on the differential thermodiffusion of bound and unbound species which is governed by the size, charge and solvation of the analytes [128–130]. It has been previously applied for the evaluation of interactions between *E. Coli* AK and ligands [131] as well as nucleoside diphosphate kinase (NDPK) and nucleoside analogs [132]. Additionally, our group used MST to evaluate the binding affinity between human neutrophil elastase (HNE) and ursolic acid, a reference inhibitor of HNE ($K_d = 2.72 \pm 0.66 \mu\text{M}$). The technique is non-separative allowing the determination of K_d with high sensitivity (in pM) in under 30 min and consuming miniscule amounts of samples ($\approx 4 \mu\text{L}$ for each ligand concentration). Furthermore, using MST provides the analyst with the freedom of choice of the buffer where practically any convenient solution or complex biological fluids can be used.

These types of binding affinity assays reveal information limited to the binding interactions between enzymes and ligands. The bound ligand may activate or inhibit the enzyme's catalytic activity. How the binding of these ligands influences the catalytic activity of the enzyme can be

obtained through the use of enzymatic activity assays such as those based on CE. Therefore, the complementary use of catalytic activity (such as CE) and binding affinity (such as MST) permits a better understanding of the molecular mechanism behind ligand binding and catalytic activity modulation.

VIII. Conclusion

In this Chapter, we attempted to describe the different modes and possibilities linked to the use of CE in applications involving enzymatic assays. Offline and online reactions, immobilized and in-solution enzymes and a variety of detection techniques were all considered in the examples. Furthermore, and in order to demonstrate the power of CE-based assays, two enzymes, lipases and nucleoside kinases were used as models of CE-based enzymatic assays due to the vast differences of the reactions they catalyze in addition to the different requirements of the reactions. We compared the CE-based assays to LC-based and miniaturized assays from an objective points of view highlighting both strengths and limitations of the assays. The use of lipases and kinases as model enzymes, having different mechanisms of action, allowed us to demonstrates the versatility and power of using CE for assaying enzymatic activities and screening for potential modulators. In-solution as well as immobilized enzymes were successfully assayed using both offline and online CE modes coupled to different detection techniques such as UV spectrophotometry, C⁴D and MS. The use of a wide array of synthetic and natural substrates was possible and the modulation assay involved the use of modulatory samples that ranged in complexity from crude extracts to isolated and purified molecules. A possible drawback encountered in some of the examples is associated with the use of complex samples which sometimes led to unreliable results especially using online CE-based assays, where in-capillary mixing of the analytes would be complicated in the presence of such samples.

Affinity-based assays were also briefly discussed. These assays answer two broad questions: i) does the molecules bind to the enzyme and, ii) how strong is this binding interaction. However, the bound ligands may induce or inhibit the catalytic activity of an enzyme and such information can be obtained through the use of enzyme activity assays such as those based on CE. Furthermore, the use of affinity- and activity-based assays complementarily allows the better understanding of the molecular mechanism behind ligand binding to the enzyme and modulation of its activity which is advantageous for drug screening and pharmaceutical applications.

References

- [1] S. M. Cuesta, S. A. Rahman, N. Furnham and J. M. Thornton, *Biophys. J.*, 2015, **109**, 1082–1086.
- [2] G. Kapoor, S. Saigal and A. Elongavan, *J Anaesthesiol Clin Pharmacol*, 2017, **33**, 300–305.
- [3] Z. Lou, Y. Sun and Z. Rao, *Trends Pharmacol. Sci.*, 2014, **35**, 86–102.
- [4] A. Sreedhar and Y. Zhao, *Biomed Rep*, 2018, **8**, 3–10.
- [5] R. Nehmé, H. Nehmé, T. Saurat, M.-L. de Tauzia, F. Buron, P. Lafite, P. Verrelle, E. Chautard, P. Morin, S. Routier and H. Bénédicti, *Anal. Bioanal. Chem.*, 2014, **406**, 3743–3754.
- [6] B. Bonamichi, E. B. Parente, R. B. dos Santos, R. Beltzhoover, J. Lee and J. E. N. Salles, *J. Obes. Eat. Disord.*, 2018, **4**, 1–10.
- [7] S. Fayad, P. Morin and R. Nehmé, *J. Chromatogr. A*, 2017, **1529**, 1–28.
- [8] J. Strelow, W. Dewe, P. W. Iversen, H. B. Brooks, J. A. Radding, J. McGee and J. Weidner, in *Assay Guidance Manual*, eds. S. Markossian, G. S. Sittampalam, A. Grossman, K. Brimacombe, M. Arkin, D. Auld, C. P. Austin, J. Baell, J. M. M. Caaveiro, T. D. Y. Chung, N. P. Coussens, J. L. Dahlin, V. Devanaryan, T. L. Foley, M. Glicksman, M. D. Hall, J. V Haas, S. R. J. Hoare, J. Inglese, P. W. Iversen, S. D. Kahl, S. C. Kales, S. Kirshner, M. Lal-Nag, Z. Li, J. McGee, O. McManus, T. Riss, P. Saradjian, O. J. J. Trask, J. R. Weidner, M. J. Wildey, M. Xia and X. Xu, Bethesda (MD), 2004.
- [9] H. Bisswanger, *Perspect. Sci.*, 2014, **1**, 41–55.
- [10] H. Bisswanger, in *Practical Enzymology*, Wiley-Blackwell, 2012.
- [11] M. Zeilinger, F. Pichler, L. Nics, W. Wadsak, H. Spreitzer, M. Hacker and M. Mitterhauser, *EJNMMI Res.*, 2017, **7**, 13.
- [12] P. J. Tonge, *Infect. Dis.*, 2019, **5**, 796–808.
- [13] J. Chapman, A. E. Ismail and C. Z. Dinu, *Catalysts*, 2018, **8**, 1–26.
- [14] P. J. T. Dekker, D. Koenders and M. J. Bruins, *Nutrients*, 2019, **11**, 1–14.
- [15] F. N. Niyonzima and S. More, *Prep. Biochem. Biotechnol.*, 2014, **45**, 233–258.
- [16] N. S. El-Safory, A. E. Fazary and C. K. Lee, *Carbohydr. Polym.*, 2010, **81**, 165–181.
- [17] M. Stoytcheva, G. Montero, R. Zlatev, J. Á. León and V. Gochev, *Curr. Anal. Chem.*, 2012, **8**, 400–407.

- [18] C. A. Espinosa-Leal and S. Garcia-Lara, *Planta Med.*, 2019, **85**, 535–551.
- [19] J. F. Glickman, in *Assay Guidance Manual*, eds. S. Markossian, G. Sittampalam, A. Grossman, K. Brimacombe, M. Arkin, D. Auld, C. P. Austin, J. Baell, J. M. M. Caaveiro, T. D.Y. Chung, N. P. Coussens, J. L. Dahlin, V. Devanaryan, T. L. Foley, M. Glicksman, M. D. Hall, J. V. Haas, S. R.J. Hoare, J. Inglese, P. W. Iversen, S. D. Kahl, S. C. Kales, S. Kirshner, M. Lal-Nag, Z. Li, J. McGee, O. McManus, T. Riss, P. Saradjian, O. J. J. Trask, J. R. Weidner, M. Jo Wildey, M. Xia and X. Xu, Eli Lilly & Company and the National Center for Advancing Translational Sciences, Bethesda (MD), 2004, pp. 1–19.
- [20] Y. Wang and H. Ma, *Drug Discov. Today Technol.*, 2015, **18**, 1–8.
- [21] S. Lanka, A. Pradesh, J. Naveena and L. Latha, *Int. J. Biol. Chem.*, 2015, **9**, 207–219.
- [22] C. Peña-García, M. Martínez-Martínez, D. Reyes-Duarte and M. Ferrer, *Comb. Chem. High Through. Scr.*, 2016, **19**, 605–615.
- [23] F. Hasan, A. A. Shah and A. Hameed, *Biotechnol. Adv.*, 2009, **27**, 782–798.
- [24] R. Nehmé and P. Morin, *Electrophoresis*, 2015, **36**, 2768–2797.
- [25] J. P. Hughes, S. S. Rees, S. B. Kalindjian and K. L. Philpott, *Br. J. Pharmacol.*, 2011, **162**, 1239–1249.
- [26] C. Zhang, A. G. Woolfork, K. Suh, S. Ovbude, C. Bi, M. Elzoeiry and D. S. Hage, *J. Pharm. Biomed. Anal.*, 2020, **177**, 112882.
- [27] S. A. P. Pereira, P. J. Dyson and M. L. M. F. S. Saraiva, *Trends Anal. Chem.*, 2020, **126**, 1–15.
- [28] M. Cheng and Z. Chen, *J. Pharm. Anal.*, 2018, **8**, 226–233.
- [29] Y. Wang, D. I. Adeoye, E. O. Ogunkunle, I. A. Wei, R. T. Filla and M. G. Roper, *Anal. Chem.*, 2021, **93**, 295–310.
- [30] S. El Deeb, H. Wätzig and D. A. El-Hady, *Trends Anal. Chem.*, 2013, **48**, 112–131.
- [31] C. Zhang, E. Rodriguez, C. Bi, X. Zheng, D. Suresh, K. Suh, Z. Li, F. Elsebaei, D. S. Hage, E. Fawzi and D. S. Hage, *Analyst*, 2018, **143**, 374–391.
- [32] V. Kairys, L. Baranauskiene, M. Kazlauskiene, D. Matulis and E. Kazlauskas, *Expert Opin. Drug Discov.*, 2019, **14**, 755–768.
- [33] T. W. Speer, in *Encyclopedia of radiation oncology*, eds. L. W. Brady and T. E. Yaeger, Springer, Berlin, Heidelberg, 2013.
- [34] F. Gomez and M. Fernanda Silva, *Methods Mol. Biol.*, 2019, **1906**, 197–206.

- [35] A. Wuethrich and J. P. Quirino, *Anal. Chim. Acta*, 2019, **1045**, 42–66.
- [36] F. Pena-Pereira, C. Bendicho, D. M. Pavlović, A. Martín-Esteban, M. Díaz-Álvarez, Y. Pan, J. Cooper, Z. Yang, I. Safarik, K. Pospiskova, M. A. Segundo and E. Psillakis, *Anal. Chim. Acta*, 2020, 1–31.
- [37] O. Caen, H. Lu, P. Nizard and V. Taly, *Trends Biotechnol.*, 2017, **35**, 713–727.
- [38] A. Y. Chang and W. F. Marshall, *J. Cell Sci.*, 2017, **130**, 819–826.
- [39] N. Banke, K. Hansen and I. Diers, *J. Chromatogr. A*, 1991, **559**, 325–335.
- [40] H. Nehmé, Etude des réactions enzymatiques par électrophorèse capillaire, PhD Thesis, Université d'Orléans, 2013.
- [41] J. Bao and F. E. Regnier, *J. Chromatogr. A*, 1992, **608**, 217–224.
- [42] B. J. Harmon, D. H. Patterson and F. E. Regnier, *Anal. Chem.*, 1993, **65**, 2655–2662.
- [43] H. Nehmé, R. Nehmé, P. Lafite, S. Routier and P. Morin, *J. Sep. Sci.*, 2013, **36**, 2151–2157.
- [44] H. Nehmé, R. Nehmé and P. Lafite, *Anal. Bioanal. Chem.*, 2013, **405**, 9159–9167.
- [45] H. Nehmé, R. Nehmé, P. Lafite, S. Routier and P. Morin, *Anal. Chim. Acta*, 2012, **722**, 127–135.
- [46] A. Taga and S. Honda, *J. Chromatogr. A*, 1996, **742**, 243–250.
- [47] V. Okhonin, X. Liu and S. N. Krylov, *Anal. Chem.*, 2005, **77**, 5925–5929.
- [48] S. Van Dyck, A. Van Schepdael and J. Hoogmartens, *Electrophoresis*, 2001, **22**, 1436–1442.
- [49] H. Nehmé, S. Chantepie, J. Defert, P. Morin, D. Papy-Garcia and R. Nehmé, *Anal. Bioanal. Chem.*, 2015, **407**, 2821–2828.
- [50] H. Nehmé, R. Nehmé, P. Lafite, S. Routier and P. Morin, *J. Chromatogr. A*, 2013, **1314**, 298–305.
- [51] S. Fayad, R. Nehmé, M. Tannoury, E. Lesellier, C. Pichon and P. Morin, *J. Chromatogr. A*, 2017, **1497**, 19–27.
- [52] J. Schejbal, G. Zdeněk and Z. Glatz, *J. Sep. Sci.*, 2018, **41**, 323–335.
- [53] J. Iqbal, S. Iqbal and C. E. Müller, *Analyst*, 2013, **138**, 3104–3116.
- [54] B. Lindshield, in *Intermediate Nutrition*, New Prairie Press, Manhattan, 2018, pp. 443–445.
- [55] F. J. Contesini, M. G. Davanço, G. P. Borin, K. G. Vanegas, J. P. G. Cirino, R. R. de

- Melo, U. H. Mortensen, K. Hildén, D. R. Campos and P. de O. Carvalho, *Catalysts*, 2020, **10**, 1–33.
- [56] F. I. Khan, D. Lan, R. Durrani, W. Huan, Z. Zhao and Y. Wang, *Front. Bioeng. Biotechnol.*, 2017, **5**, 1–13.
- [57] T. Zisis, P. L. Freddolino, P. Turunen, M. C. F. Van Teeseling, A. E. Rowan and K. G. Blank, *Biochemistry*, 2015, **54**, 5969–5979.
- [58] B. Andualema and A. Gessesse, *Biotechnol.*, 2012, **11**, 100–118.
- [59] R. Sindhu, S. Shiburaj, A. Sabu, P. Fernandes, R. Singhal, G. Marina, I. C. Nair, K. Jayachandran, J. Vidya, L. P. de S. Vandenberghe, I. Deniz, A. Madhavan, P. Binod, R. K. Sukumaran, S. S. Kumar, M. Anusree, N. Nagavekar, M. Soumya, A. Jayakumar, E. K. Radhakrishnan, S. G. Karp, M. Giovana, M. G. B. Pagnoncelli, G. V. de M. Pereira, C. R. Soccol, S. Dogan and A. Pandey, in *Innovative Food Processing Technologies: A Comprehensive Review*, Elsevier, Amsterdam, ND, 2021, vol. 3, pp. 191–215.
- [60] N. B. Melani, E. B. Tambourgi and E. Silveira, *Sep. Purif. Rev.*, 2020, **49**, 143–158.
- [61] N. Sarmah, D. Revathi, G. Sheelu, K. Y. Rani, S. Sridhar, V. Mehtab and C. Sumana, *Biotechnol.*, 2018, **34**, 5–28.
- [62] A. Houde, A. Kademi and D. Leblanc, *Appl. Biochem. Biotechnol.*, 2004, **118**, 155–170.
- [63] D. Deville-bonne, C. El, P. Meyer, Y. Chen, L. A. Agrofoglio and J. Janin, *Antivir. Res.*, 2010, **86**, 101–120.
- [64] A. Larsson, P. Bendahl, K. Aaltonen, S. Jansson, C. Forsare, M. Bergqvist, C. Levin, T. Jørgensen and L. Rydén, *Sci. Rep.*, 2020, **10**, 1–11.
- [65] S. Gattu, C. L. Crihfield, G. Lu, L. Bwanali, L. M. Veltri and L. A. Holland, *Methods*, 2018, **146**, 93–106.
- [66] S. Huang, P. Paul, P. Ramana, E. Adams, P. Augustijns and A. Van Schepdael, *Electrophoresis*, 2018, **39**, 97–110.
- [67] M. Cheng and Z. Chen, *J. Pharm. Anal.*, 2018, **8**, 226–233.
- [68] C. M. Ouimet, C. I. D’amico and R. T. Kennedy, *Expert Opin. Drug Discov.*, 2017, **12**, 213–224.
- [69] W.-F. Wang and J.-L. Yang, *Electrophoresis*, 2019, **40**, 2075–2083.
- [70] S.-Y. Shi, Y.-P. Zhang, X.-Y. Jiang, X.-Q. Chen, K.-L. Huang, H.-H. Zhou and X.-Y. Jiang, *TrAC Trends Anal. Chem.*, 2009, **28**, 865–877.

- [71] A. De Simone, M. Naldi, M. Bartolini, L. Davani and V. Andrisano, *Chromatographia*, 2019, **82**, 425–441.
- [72] S.-M. Fang, H.-N. Wang, Z.-X. Zhao and W.-H. Wang, *J. Pharm. Anal.*, 2012, **2**, 83–89.
- [73] C. J. Malherbe, D. De Beer and E. Joubert, *Int. J. Mol. Sci.*, 2012, **13**, 3101–3133.
- [74] J. S. Hill, R. C. Davis, D. Yang, J. Wen, J. S. Philo, P. H. Poon, M. L. Phillips, E. S. Kempner and H. Wong, *J. Biol. Chem.*, 1996, **271**, 22931–22936.
- [75] U. Bornscheuer, O. W. Reif, R. Lausch, R. Freitag, T. Scheper, F. N. Kolisis and U. Menge, *Biochim. Biophys. Acta*, 1994, **1201**, 55–60.
- [76] B. Vallejo-Cordoba, M. A. Mazonra-Manzano and A. F. González-Córdova, *J. Capill. Electrophor.*, 1998, **5**, 111–114.
- [77] L. Szente, J. Szejtli, J. Szemán and L. Kató, *J. Incl. Phenom. Macrocycl. Chem.*, 1993, **16**, 339–354.
- [78] G. Amores and M. Virto, *Separations*, 2019, **6**, 1–22.
- [79] M. Lubary, G. W. Hofland and J. H. ter Horst, *Eur. Food Res. Technol.*, 2011, **232**, 1–8.
- [80] G. Hao, L. Yang, I. Mazsaroff and M. Lin, *J. Am. Soc. Mass. Spectr.*, 2007, **18**, 1579–1581.
- [81] T. Koseki, S. Asai, N. Saito, M. Mori, Y. Sakaguchi, K. Ikeda and Y. Shiono, *Appl. Microbiol. Biotechnol.*, 2013, **97**, 5351–5357.
- [82] X. Chen, S. Xue, Y. Lin, J. Luo and L. Kong, *Anal. Chim. Acta*, 2020, **1099**, 94–102.
- [83] U. Guzik, K. Hupert-kocurek and D. Wojcieszynska, *Molecules*, 2014, **19**, 8995–9018.
- [84] W. Z. Tang, J. T. Liu, Q. Hu, R. J. He, X. Q. Guan, G. B. Ge, H. Han, F. Yang and H. W. Lin, *J. Nat. Prod.*, 2020, **83**, 2287–2293.
- [85] Y. Tang, W. Li, Y. Wang, Y. Zhang and Y. Ji, *J. Sep. Sci.*, 2019, **43**, 1003–1010.
- [86] S. Kollipara, G. Bende, A. Á. Ema and Á. Regulatory, *Chromatographia*, 2011, **73**, 201–217.
- [87] J. Liu, R.-T. Ma and Y.-P. Shi, *J. Chromatogr. A*, 2020, **1615**, 1–8.
- [88] C. Ruiz, S. Falcocchio, E. Xoxi, L. Villo, G. Nicolosi, F. I. J. Pastor, P. Diaz and L. Saso, *J. Mol. Catal. B Enzym.*, 2006, **40**, 138–143.
- [89] Y. Zhu, X. Ren, Y. Liu, Y. Wei, L. Qing and X. Liao, *Mater. Sci. Eng. C*, 2014, **38**, 278–285.
- [90] S. Bernardo-Bermejo, E. Sánchez-López, M. Castro-Puyana and M. L. Marina, *Trends*

- Anal. Chem.*, 2020, **124**, 1–18.
- [91] K. K. Bhardwaj and R. Gupta, *J. Oleo Sci.*, 2017, **66**, 1073–1084.
- [92] K. Pomeisl, N. Lamatová, V. Šolínová, R. Pohl, J. Brabcová, V. Kašička and M. Krečmerová, *Bioorganic Med. Chem.*, 2019, **27**, 1246–1253.
- [93] A. Schuchert-Shi and P. C. Hauser, *Chirality*, 2010, **22**, 331–335.
- [94] B. Chankvetadze, W. Linder and G. K. E. Schriba, *Anal. Chem.*, 2004, **76**, 4256–4260.
- [95] Y. Choi, J.-Y. Park and P.-S. Chang, *J. Agric. Food Chem.*, 2021, **69**, 325–331.
- [96] C. West, *Trends Anal. Chem.*, 2019, **120**, 1–9.
- [97] A. Kumar, K. Dhar, S. S. Kanwar and P. K. Arora, *Biol. Proced. Online*, 2016, **18**, 1–11.
- [98] W. L. Liu, N. S. Yang, Y. T. Chen, S. Lirio, C. Y. Wu, C. H. Lin and H. Y. Huang, *Chem. Eur. J.*, 2015, **21**, 115–119.
- [99] S. F. Y. Li and L. J. Kricka, *Clin. Chem.*, 2006, **52**, 37–45.
- [100] A. Schuchert-Shi and P. C. Hauser, *Chirality*, 2009, **22**, 331–335.
- [101] S. Banditelli, C. Baiocchi-ii, R. Pesi, S. Allegrini, M. Turriani, P. L. Ipata, M. C. A. M. Ici and M. G. Tozzi, *Int. J. Biochem. Cell Biol.*, 1996, **28**, 711–720.
- [102] H. Tzeng and H. Hung, *Electrophoresis*, 2005, **26**, 2225–2230.
- [103] C. C. Liu, J. S. Huang, D. L. J. Tyrrell and N. J. Dovichi, *Electrophoresis*, 2005, **26**, 1424–1431.
- [104] I. Jamshed, J. C. Burbiel and C. E. Müller, *Electrophoresis*, 2006, **27**, 2505–2517.
- [105] R. Nehmé, C. Perrin, V. Guerlavais, J. A. Fehrentz, H. Cottet, J. Martinez and H. Fabre, *Electrophoresis*, 2009, **30**, 3772–3779.
- [106] J. Iqbal, L. Scapozza, G. Folkers and E. M. Christa, *J. Chromatogr. B*, 2007, **846**, 281–290.
- [107] N. Malartre, R. Boulieu, N. Falah, J. C. Cortay, B. Lina, F. Morfin and E. Frobert, *Antivir. Res.*, 2012, **95**, 224–228.
- [108] J. Ferey, D. Da Silva, C. Colas, R. Nehmé, P. Lafite, V. Roy, P. Morin, R. Daniellou, L. Agrofoglio and B. Maunit, *Anal. Chim. Acta*, 2019, **1049**, 115–122.
- [109] R. Roskoski, in *Reference Module in Biomedical Sciences*, Elsevier, 2015.
- [110] H. Whatley, in *Clinical and Forensic Applications of Capillary Electrophoresis*, eds. J. Petersen and A. A. Mohammad, Humana Press, Totowa, NJ, 2001, pp. 21–58.
- [111] D. Heiger, *High performance capillary electrophoresis*, 2000.

- [112] C. Machon, F. Catez, N. D. Venezia, F. Vanhalle, L. Guyot, A. Vincent, M. Garcia, B. Roy, J. J. Diaz and J. Guitton, *J. Pharm. Anal.*, 2021, **11**, 77–87.
- [113] S. Bustamante, R. B. Gilchrist and D. Richani, *J. Chromatogr. B*, 2017, **1061–1062**, 445–451.
- [114] S. Hendrickx, W. de Malsche and D. Cabooter, in *Microchip Capillary Electrophoresis Protocols. Methods in Molecular Biology*, ed. A. Van Schepdael, Humana Press, New York, 2015, vol. 1274, pp. 3–17.
- [115] J. M. Karlinsey, *Anal. Chim. Acta.*, 2012, **725**, 1–13.
- [116] N. N. A. Razak, S. Firmansyah and M. S. M. Annuar, *Biocatal. Agric. Biotechnol.*, 2020, **27**, 101660.
- [117] L. H. Du, R. J. Long, M. Xue, P. F. Chen, M. J. Yang and X. P. Luo, *Catalysts*, 2020, **10**, 1–14.
- [118] H. A. Yusuf, E. M. Elkanzi, S. M. Z. Hossain, A. Mohammed, A. H. Alhindy, E. Ebrahim, H. Abdulla, E. M. Elkanzi, S. M. Z. Hossain and A. Mohammed, *Arab J. Basic Appl. Sci.*, 2020, **27**, 239–247.
- [119] Y. Bi, H. Zhou, H. Jia and P. Wei, *Process Biochem.*, 2017, **54**, 73–80.
- [120] M. Chakraborty and K. Biswas, *IEEE Trans. Instrum. Meas.*, 2019, **68**, 4526–4534.
- [121] Y. Bi, H. Zhou, H. Jia and P. Wei, *RSC Adv.*, 2017, **17**, 12283–12291.
- [122] L. Shen, H. Wang and X. Luo, *Carbohydr. Res.*, 2018, **455**, 32–38.
- [123] Y. Zhang, J. Zhao, S. Chen, S. Li and S. Zhao, *Talanta*, 2019, **202**, 317–322.
- [124] J. Mao, X. Chen, H. Xu and X. Xu, *J. Electroanal. Chem.*, 2020, **874**, 1–8.
- [125] J. V Pagaduan, M. Ramsden, K. O. Neill and A. T. Woolley, *Electrophoresis*, 2015, **36**, 813–817.
- [126] I. Hamdan I. and H. Zalloum, *Acta Pharm.*, 2019, **69**, 1–16.
- [127] Jayson V. Pagaduan, M. Ramsden, K. O’Neill and A. T. Woolley, *Electrophoresis*, 2015, **36**, 813–817.
- [128] C. J. Wienken, P. Baaske, U. Rothbauer, D. Braun and S. Duhr, *Nat. Commun.*, 2010, **1**, 1–7.
- [129] M. Jerabek-Willemsen, C. J. Wienken, D. Braun, P. Baaske and S. Duhr, *Assay Drug Dev. Technol.*, 2011, **9**, 342–353.
- [130] M. Jerabek-Willemsen, T. André, R. Wanner, H. M. Roth, S. Duhr, P. Baaske and D.

- Breitsprecher, *J. Mol. Struct.*, 2014, **1077**, 101–113.
- [131] H. Mazal, H. Aviram, I. Riven and G. Haran, *Phys. Chem. Chem. Phys.*, 2018, **20**, 3054–3062.
- [132] S. Priet, L. Roux, M. Saez-Ayala, F. Ferron, B. Canard and K. Alvarez, *Antivir. Res.*, 2015, **117**, 122–131.

Chapter II:

**Enzyme modulating molecules: Bioactivities
and biophysical interactions.**

Application to lipases and hyaluronidases

Summary

Nature-derived products have played an important role in the development of drugs and remedies for combating diseases and medical conditions throughout history and amongst different communities and traditions. Drug discovery is a complicated process involving several steps that are both time consuming and expensive. Also, trials of candidate drugs may often end with the drug deemed unsuitable upon reaching clinical trials. Therefore, strategies to rule out unsuitable drugs at the early phases of the drug discovery process are highly desirable. In the first part of this chapter “**Part A**”, a CE-UV/C⁴D (capacitively coupled contactless conductivity detection) based pancreatic lipase (PL) assay is optimized and applied in the offline and online CE modes to screen modulation of natural crude plant extracts and purified molecules. More precisely, in this study, 4-nitrophenyl butyrate was chosen as a substrate of PL which leads to the production of both 4-nitrophenolate (4-NP) and butyrate, detected by UV spectrophotometry (absorption at 400 nm) and C⁴D, respectively. In the second part of this chapter “**Part B**”, we assess the binding affinities of the best PL inhibitors as well as an activator from part A, using microscale thermophoresis (MST). In addition, we demonstrate the importance of using CE activity assays in complementarity with the MST binding assays for elaborating the mechanism of PL modulation by pure molecules. The third part of this chapter “**Part C**” is divided into two sections. In the first section, the effect of molecular crowding, on the activity and modulation of hyaluronidase by original natural or synthetic purified molecules will be investigated *in vitro* using a CE-based offline assay. The second section will involve the use of plant extracts, introduced in **Part A**, as complex samples to investigate their antihyaluronidase bioactivities using a CE-based assay as described in the earlier parts of this chapter, in addition to conventional enzymatic assay kits in order to obtain a clearer image about the extracts’ hypotensive and antioxidant bioactivities. At the end of this chapter, “**Chapter conclusion**”, we highlight the overall inferences from this chapter and propose some perspectives for future work.

Collaborator contributions & acknowledgement

*S. Fayad and A. Marchal (University of Bordeaux, Science institute of vine and wine (ISVV)) planned and performed purification of bioactive compounds from oakwood and wine extracts, L. Orlic, F. Piazza and J. Hamacek (University of Orléans, Center for Molecular Biophysics, CNRS) carried out neocuprine spectrophotometric hyaluronidase assays, C. Lopin-Bon (University of Orléans, ICOA) synthesized biotinylated chondroitin tetrasaccharide inhibitors of hyaluronidase, P. Cao-Ngoc, L. Leclercq, J.-C. Rossi, H. Cottet (University of Montpellier, Max Mousseron institute of biomolecules (IBMM)), J. Hertzog, P. Schmitt-Kopplin (Helmholtz Centre Munich and Technical University of Munich), A.-S. Tixier, F. Chemat (University of Avignon, National institute of agronomic research (INRA)) performed the extraction, characterization and quantification of extracts of *Crataegus oxyacantha* (hawthorn), *Ribes nigrum* (blackcurrant) and *Chrysanthellum americanum*. C. Colas (University of Orléans, ICOA & Center for Molecular Biophysics, CNRS) supervised the HRMS analyses of pancreatic extracts.*

We would like to thank from the University of Orléans, ICOA, F. Coudray for the design and construction of the 3D printed scaffold for the C⁴D cell utilized in CE assays, Dr B. Claude for her aid and advices in lipase purification experiments, Dr D. Da Silva for his aid and advices for MS analyses, Dr. S. Messaili (University of Orléans, ICOA) for her aid in ABTS antioxidant assays and Cedric Maffre for technical support.

Part A:

Screening for pancreatic lipase natural modulators by capillary electrophoresis hyphenated to spectrophotometric and conductometric dual detection

I. Introduction

In the first part of this chapter, we describe the use of capillary electrophoresis (CE) in hyphenation with the conventional ultraviolet (UV) detection and the less conventional capacitively coupled contactless conductivity detection (C⁴D) for assaying pancreatic lipase (PL) activity in the presence of natural modulators. Conductivity detection is desired when ions with low molar absorptivity are involved such as the case for analyses of small inorganic ions where direct UV absorption would be fruitless and indirect detection will require careful choice of buffer and cause reduction of the signal. In this thesis, 4-nitrophenyl butyrate (4-NPB) was used as the PL substrate and is hydrolyzed into two products, 4-nitrophenol (4-NP) and butyrate (Figure II.1). The former absorbs at a wavelength of 400 nm and the latter has no absorption at this wavelength and was detected using C⁴D. This justified the use of dual detection by UV as well as C⁴D, simultaneously, in order to quantify the PL catalyzed reaction using both hydrolysis products.

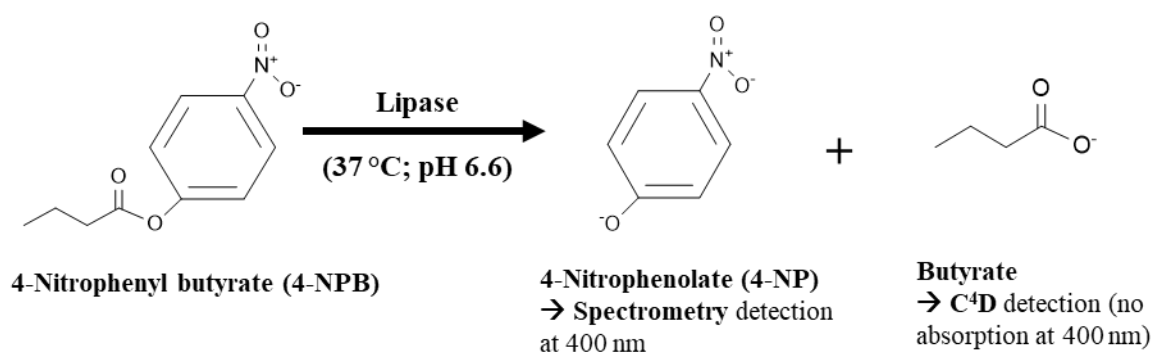


Figure II.1: Hydrolysis of 4-NPB into 4-NP and butyrate catalyzed by PL

Coupling C^4D to CE was introduced for the first time by the groups of Zemann [1] and Fracassi da Silva [2] in 1998. The C^4D cell consists of two electrodes, an excitation electrode and a reception electrode separated by a small gap, corresponding to the detection gap [1,3]. A schematic illustration of the C^4D cell is represented in Figure II.2.

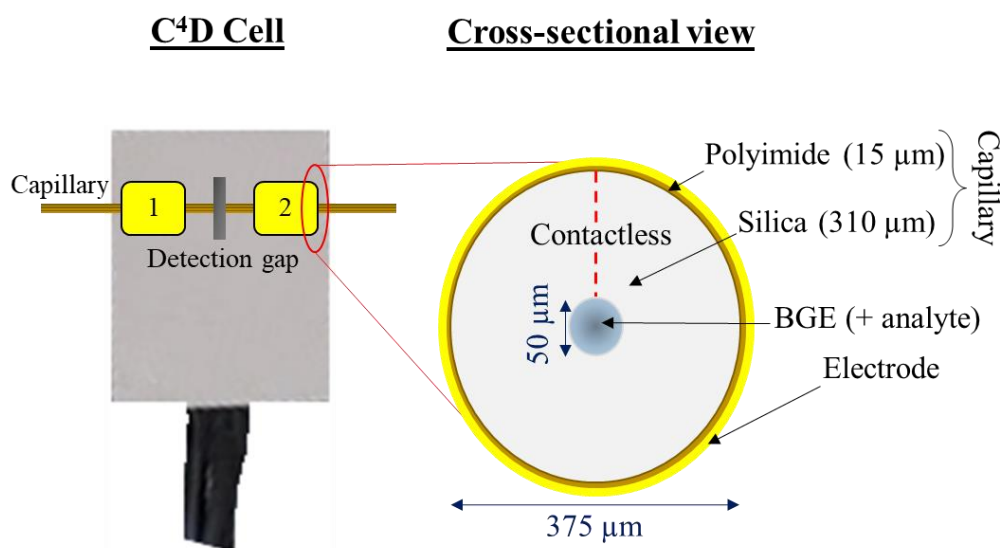


Figure II.2: An illustration of the C^4D cell and a cross-section view of the capillary penetrating the C^4D cell through the electrodes. BGE: background electrolyte, 1: excitation electrode, 2: reception electrode.

This detector comprise two capacitors connected in series where the first capacitor consists of the excitation electrode (electrode 1) and the liquid within the capillary separated by the silica of the capillary which acts as a layer of insulation. Likewise, the silica layer insulates the conductors of the second capacitor which are the liquid within the capillary and the reception electrode (electrode 2). When first developed, a third undesirable system of capacitance was obtained. It consisted of both excitation and reception electrodes as conductors separated by the resistance of air between them and resulted in an increase of background noise and capacitive leakage. This third capacitor was eliminated by the introduction of a thin metal foil between the electrodes [3,4]. The application of a high frequency alternating current to electrode one results in a capacitive transition between this first electrode and the liquid filling up the capillary. The resulting current then crosses the gap between the electrodes where a second capacitive transition occurs this time between the liquid in the capillary, *i.e.* the BGE (+ analytes), and the reception electrode [3].

Moreover, with C_4D , the conductivity of the BGE needs to be as low as possible to lower

background noise. The greater the difference in conductivity between the analyte and BGE, the greater the sensitivity of detection. More precisely, the analytical signal depends on the mobility differences between the analyte and the buffer's co-ion [3]. This difference however, causes electrodispersion and results in asymmetrical peaks. Therefore, the conductivity difference between the buffer's co-ion and the analyte must be a compromise between sufficient detection sensitivities and minimal peak dispersion. The use of C⁴D in hyphenation with CE is advantageous since the detector can be placed anywhere along the length of the capillary without the need of removing the outer polyimide layer of the capillary which increases the risk of the capillary breaking. Furthermore, since the electrodes are not in direct contact with the liquid inside the capillary, the risk of electrode corrosion is reduced and there is no need for regular cleaning or maintenance of the electrodes [5] and the sensitivity of such detectors is greatly enhanced. Using C⁴D hyphenation in a system with circulating coolant liquid can be complicated such as the case with Sciex CE instruments used in this study. To overcome that, a support scaffold was designed and manufactured in our laboratory to fix in place the C⁴D cell (Figure II.3).

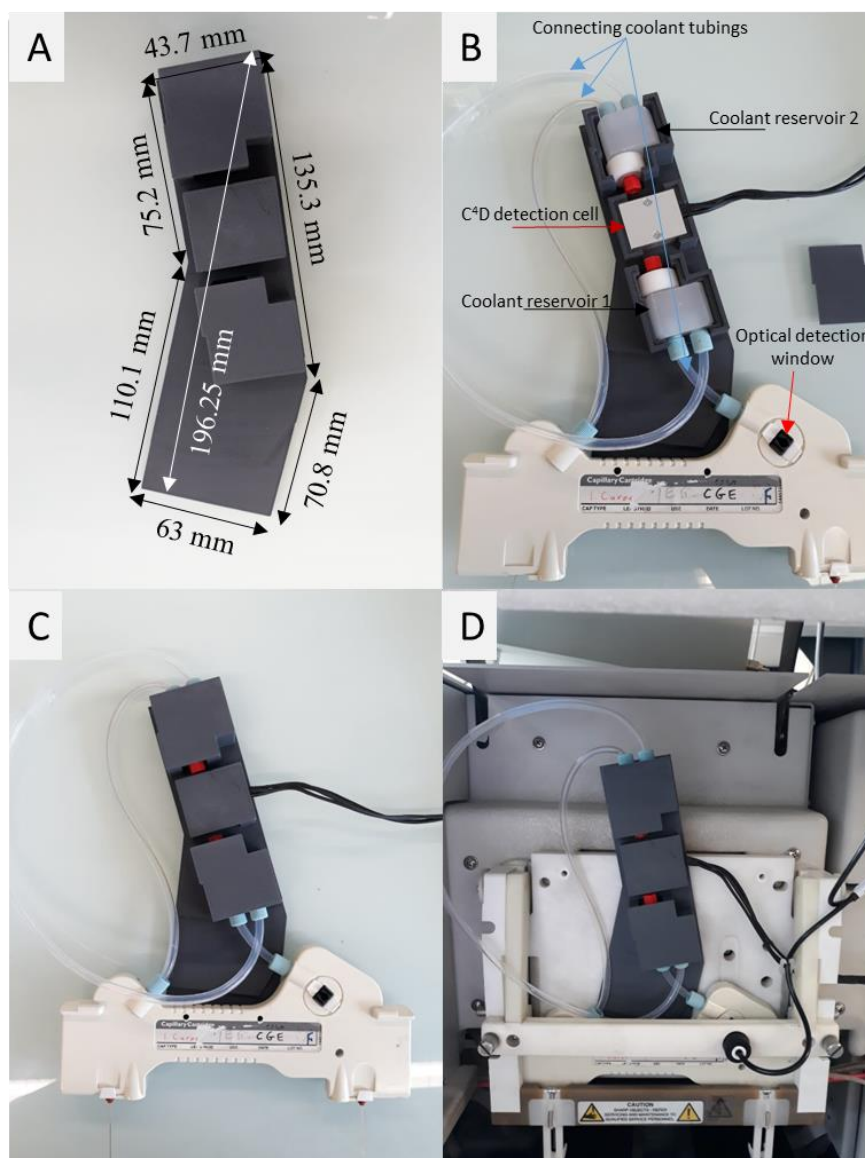


Figure II.3: Capillary cartridge with the connecting tubings and reservoirs supported by a polyacetic acid 3D printed scaffold. The 3D printed scaffold with its dimensions (a), Insertion of all components (two reservoirs, C4D detection cell) into their designated positions in the scaffold (b), Addition of 3D printed clips to fix loose parts of the system in place (c) and, installation of the cartridge into the CE instrument (d)

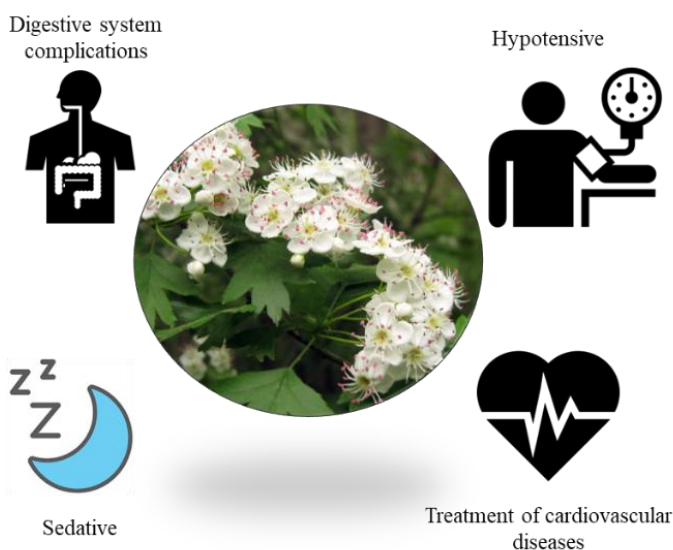
The CE-UV/C⁴D lipase assay we present involves the assay of non-immobilized and unmodified PL by CE using both the offline and online modes. It was optimized at the levels of the choice of the BGE and the incubation buffer (IB) as well as the conditions of the offline and online PL activity assays. The optimized assays were used to firstly determine the kinetic parameters of the PL catalyzed hydrolysis of 4-NPB. The influence of mimicking the lipid-water interface by phospholipidic vesicles on the rate of PL activity as well as on the affinity of PL towards 4-NPB

was investigated. The optimized assays were then used to screen the PL modulation potential of several crude plant extracts and as well as purified molecules extracted from oakwood, wine and grapes.

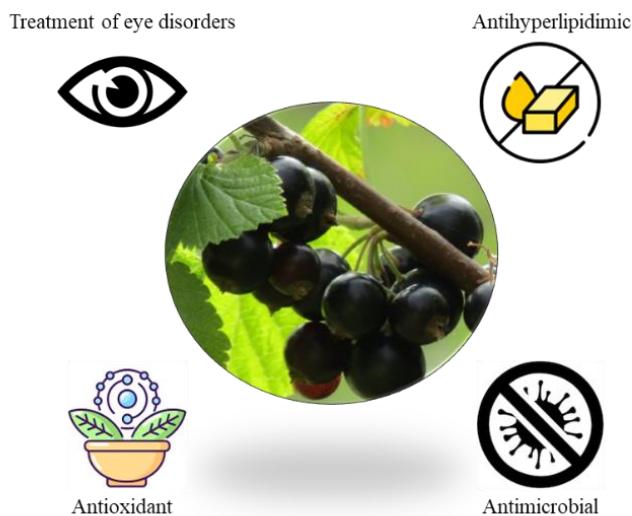
II. Crude aqueous plant extracts

The attainment of extracts from three different plants as well as their molecular characterization will be discussed briefly. Investigation and optimization of plant extraction as well as the characterization of the plant extracts and determination of their chemical composition were conducted by our collaborators [6]. Extracts were collected from different parts of three plants: i) Hawthorn (HAW) flowering tops (leaves + flowers), ii) Blackcurrant (BC) leaves and, iii) *Chrysanthellum americanum* (CA) fibers. These extracts will be investigated for their PL and hyaluronidase modulatory potentials using CE-based enzymatic assays. Additionally, other bioactivities such as hypotensive and antioxidant ones will be evaluated using more conventional spectrophotometric techniques to obtain a more complete image. The choice of the plants was based on their promising medicinal and pharmaceutical properties shown in Figure II.4.

a. Hawthorn (flowering tops)



b. Blackcurrant (leaves)



c. *Chrysanthellum americanum* (fibers)

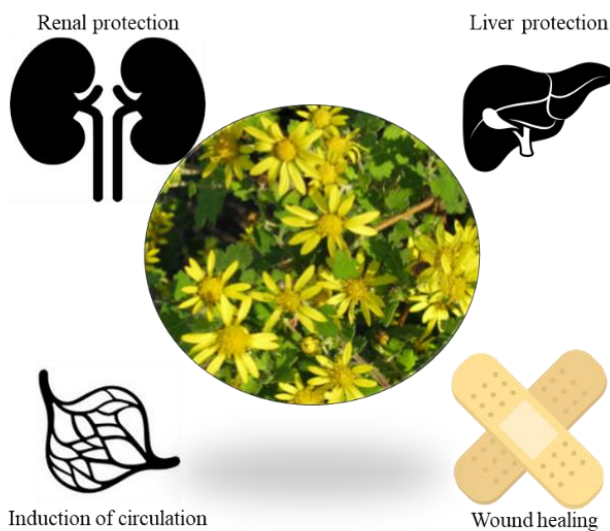


Figure II.4: Representation and therapeutic uses of hawthorn flowering tops (a), blackcurrant leaves (b) and, *Chrysanthellum americanum* fibers (c)

The plant parts were extracted by infusing an appropriate amount of ground plant material in boiling water for 10 min with manual stirring. This extraction mode was found to be the simplest amongst other extraction techniques; using water as the extraction solvent; for day-to-day applications since no special equipment or skills were required. Additionally, infusion-based

extraction mimicked the use of the extracts in the form of herbal tea infusions and thus the extraction parameters were optimized accordingly.

The extracts were characterized through the quantification of the extraction yield, total polyphenols (TPC), flavonoids (TFC) and proanthocyanidin oligomers (OPC) contents (Table II.1).

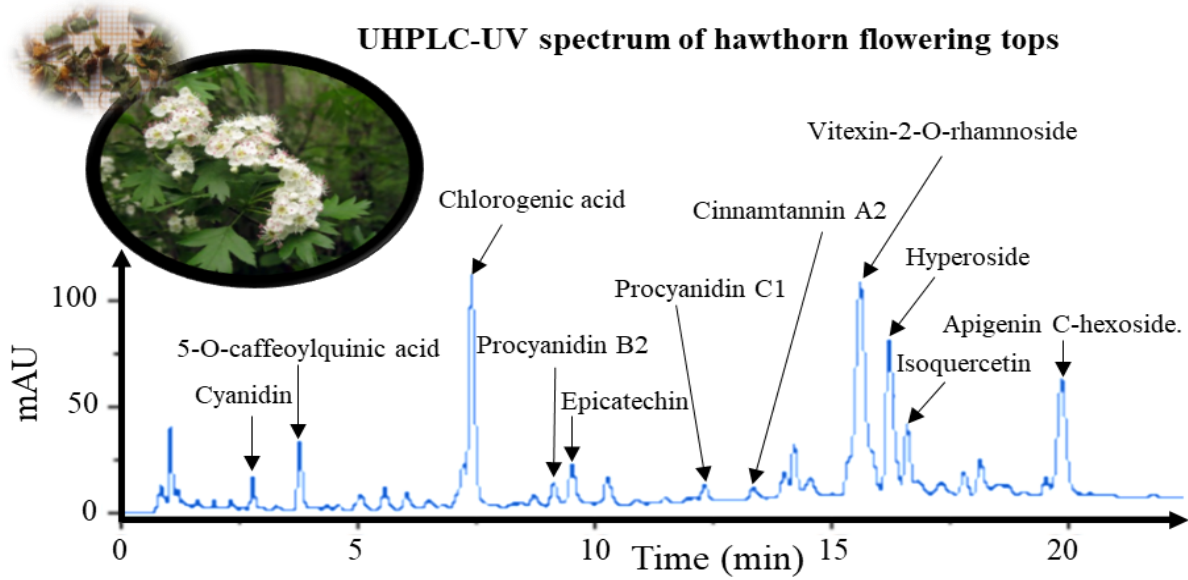
Table II.1: Extraction yield, TPC, TFC, and OPC values in various plant extracts issued from the infusion of ground plant materials (see experimental part for the details). ^a: calculated on 1 experiment. ^b: data extracted from [6]. ^c: in mg eq. gallic acid/g dry extract, ± 1 standard deviation calculated on $n = 3$ repetitions. ^d: in mg eq. quercetin/g dry extract, ± 1 standard deviation calculated on $n = 3$ repetitions. ^e: in mg eq. cyanidin/g dry extract, ± 1 standard deviation calculated on $n = 3$ repetitions

Nature	Lot number	Extraction yield (%)	TPC ^c	TFC ^d	OPC ^e
Hawthorn fresh leaves	Harvested	19.8 ^a	107.7 \pm 4.1	9.8 \pm 0.5	5.0 \pm 0.3
Hawthorn fresh flowers	2020	24.0 ^a	121.3 \pm 6.0	15.7 \pm 0.1	4.8 \pm 0.1
Hawthorn dry flowering tops - Sample A -	20335	23.2 \pm 0.6 ^b	149.5 \pm 4.0	15.4 \pm 0.3	20.0 \pm 1.7
Hawthorn dry flowering tops - Sample B -	CB58120	22.5 \pm 0.3 ^b	96.0 \pm 1.8	13.9 \pm 0.4	8.0 \pm 0.4
Hawthorn dry flowers	20334	21.7 \pm 0.6 ^b	171.4 \pm 3.2	15.9 \pm 0.4	9.0 \pm 0.2
<i>Chrysanthellum americanum</i>	559980	25.9 \pm 0.9	59.9 \pm 0.2	12.8 \pm 0.2	1.6 \pm 0.1
Blackcurrant leaves	55870	28.6 \pm 0.5	138.5 \pm 1.7	15.5 \pm 0.6	5.8 \pm 0.3

The plethora of molecules in each of the extracts were identified by UHPLC-UV, UHPLC-Electrospray ionization (ESI)-MS and high-resolution Fourier transform ion cyclotron resonance (FT-ICR) MS. Figure II.5 delineates the results obtained from the characterization of the chemical constituents of the plant extracts using UHPLC-UV.

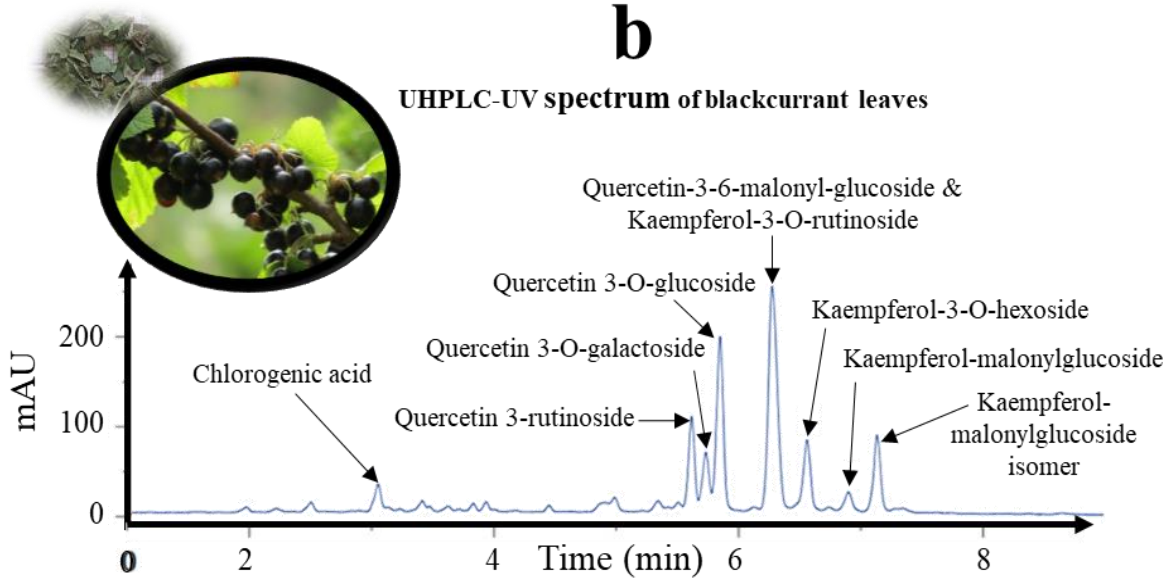
a

UHPLC-UV spectrum of hawthorn flowering tops



b

UHPLC-UV spectrum of blackcurrant leaves



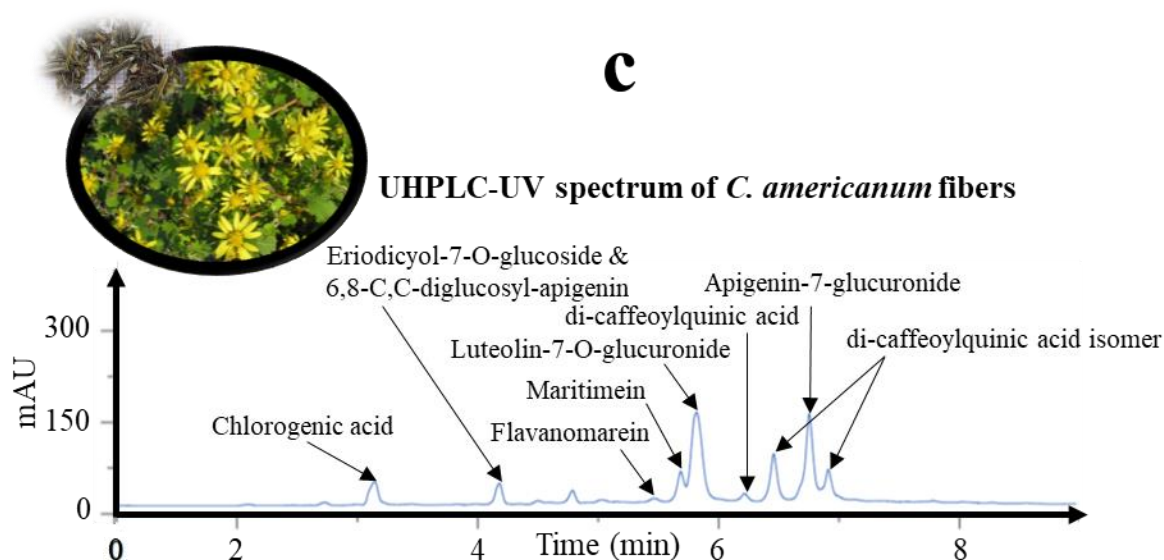


Figure II.5: Identification of molecular constituents based on UHPLC-PDA profiles.

Aqueous extracts from HAW flowering tops (a), BC leaves (b) and, (c) CA fibers were characterized using UHPLC-PDA at a concentration of 4 mg mL^{-1} . The extracts were obtained by infusion in water as described in [6]. **Experimental conditions:** column; Luna® Omega polar C18 column ($1.6 \mu\text{m}$, $100 \times 2.1 \text{ mm}$) for analysis of HAW flowering tops and a Kinetex C18 100A column ($2.6 \mu\text{m}$, $100 \times 2.1 \text{ mm}$) in association with a security guard ultra-cartridge for the analysis of BC leaves and CA fibers. Both columns were thermostated at 35°C . Mobile phase; water/formic acid (1%, v/v) as solvent A and acetonitrile/formic acid (1%, v/v) as solvent B. Gradient program; 5% B, then increase of B to 100% in 30 min with a convex increase; flow rate: 0.4 mL min^{-1} , injection volume: $4 \mu\text{L}$ for HAW analysis, $20 \mu\text{L}$ for BC and CA analyses. UV monitoring was carried out at 280 nm . More details about experimental conditions are found in [6]

The analyses of the plant extracts by ESI(-) FT-ICR-MS are represented by Van Krevelen diagrams (Figure II.6) where the ratios of hydrogen-to-carbon (H/C) atoms are represented as a function of oxygen-to-carbon (O/C) giving an insight about the molecular species present in the extracts as well as their intensities.

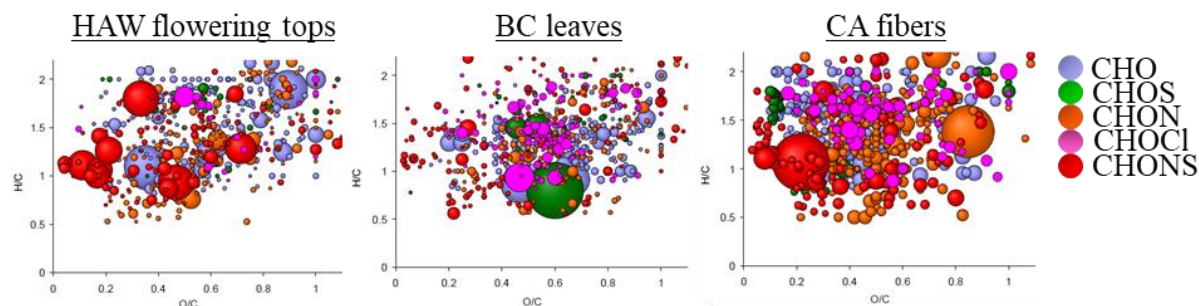


Figure II.6: Van Krevelen diagrams of HAW, BC and CA extracts analyzed by ESI(-) FT-ICR MS demonstrating the hydrogen-to-carbon (H/C) and oxygen-to-carbon (O/C) atomic ratios. Bubbles represent different subtypes of compounds belonging to the same family of compound if they share the same color. The size of the bubbles is relative to the peak intensity

III. Results

The results are detailed in the article titled “**Screening for pancreatic lipase natural modulators by capillary electrophoresis hyphenated to spectrophotometric and conductometric dual detection**” *Analyst* (2021), 146: 1386-1401, DOI: 10.1039/D0AN02234A

Screening for pancreatic lipase natural modulators by capillary electrophoresis hyphenated to spectrophotometric and conductometric dual detection

Ghassan Al Hamoui Dit Banni¹, Rouba Nasreddine¹, Syntia Fayad^{1,2}, Phu Cao-Ngoc³, Jean-Christophe Rossi³, Laurent Leclercq³, Hervé Cottet³, Axel Marchal² and Reine Nehme^{1*}

¹ Institut de Chimie Organique et Analytique (ICOA), CNRS FR 2708 – UMR 7311, Université d’Orléans, 45067 Orléans, France

² Université de Bordeaux, ISVV, EA 5477, Unité de recherche Œnologie, USC 1366 INRA, F- 33882, Villenave d’Ornon, France

³ IBMM, University of Montpellier, CNRS, ENSCM, 34059 Montpellier, France

* e-mail: reine.nehme@univ-orleans.fr.

Keywords

Capillary electrophoresis lipase assay; Contactless conductivity detector; Natural inhibitor screening; TDLFP based on-line enzymatic assay; UPLC/MS molecular characterization of water plant extracts

Abstract

The search for novel pancreatic lipase (PL) inhibitors has gained increasing attention in recent years. For the first time, a dual detection capillary electrophoresis (CE)-based homogeneous lipase assay was developed employing both the offline and online reaction modes. The hydrolysis of 4-nitrophenyl butyrate (4-NPB) catalyzed by PL into 4-nitrophenol and butyrate was monitored by spectrophotometric and conductimetric detection, respectively. The assays presented several advantages such as economy in consumption (few tens of nanoliters for online assays to few tens of microliters for offline assays), no modification of lipase, rapidity (< 10 min) and versatility. Tris/MOPS (10 mM, pH 6.6) was used as the background electrolyte and the incubation buffer for enzymatic reactions. We confirmed that in the conditions of the study (small substrate 4-NPB, 37°C, pH 6.6), the PL was active even in the absence of dipalmitoylphosphatidylcholine (DPPC) vesicles, generally used to mimic the lipid-water interface. This was confirmed by the maximum velocity (V_{\max}) and the Michaelis-Menten constant (K_m) values that were in the same order of magnitude in the absence and presence of DPPC. The developed method was used to screen crude aqueous plant extracts and purified compounds. We were able to identify the promising PL inhibition of hawthorn leaves herbal infusions at 1 mg mL⁻¹ (37%) and PL activation by hawthorn fresh and dry flowers (~24%). Additionally, two triterpenoids purified from extracts of oakwood were identified for the first time as potent PL inhibitors demonstrating 51 and 58% inhibition at 1 mg mL⁻¹, respectively.

Introduction

Lipases catalyze the digestion of the ester linkages of triglycerides (TGs) hydrolyzing them into monoglycerides (MGs) and free fatty acids in the small intestine. This contributes to 50-70% of dietary fat digestion [7]. Lipase is well known to be an enzyme with an interfacial activation mechanism. It is active at a lipid-water interface such as in the intestine [8]. For this, K. Shirai *et al.* [9] evaluated the kinetics of lipoprotein lipase (LpL) in the presence of various vesicles, mainly dipalmitoylphosphatidylcholine (DPPC), using spectrophotometry at 400 nm [10]. They demonstrated an enhancement of LpL activity towards 4-NPB due to an increase of maximum velocity (V_{\max}).

Pancreatic lipase (PL) and its inhibition are trending topics as a way to combat obesity and its ensuing diseases. The community's interest also arises from the scarcity of approved PL inhibitors in pharmaceutical markets. Xenical, also known as orlistat, is the only approved PL inhibitor in Europe and USA used for long term weight management [11]. Orlistat is able to deplete 30% of TG absorption [12] which causes several expected unpleasant effects (such as oily stool, flatulence and diarrhea) [13,14] and more rarely hepatic and renal damages [15–17]. Natural and synthetic molecules capable of inhibiting PL without causing organ damage are needed. For instance, epigallocatechin gallate (EGCG), a flavonoid abundant in green tea demonstrated promising PL inhibition with a half maximal inhibitory concentration (IC_{50}) of $0.8 \pm 0.1 \mu\text{M}$, lower than that determined for orlistat ($IC_{50} = 32 \pm 8.5 \mu\text{M}$) [18]. Saponins, a class of triterpenoids isolated from *Acanthopanax senticosus*, had an IC_{50} between 220-290 μM [19]. On the other hand, some synthetic molecules have been shown to inhibit PL such as rhodanine-3-acetic acid derivatives ($IC_{50} = 5.16 \pm 0.31 \mu\text{M}$) [20] or indole glyoxylamide analogues ($IC_{50} = 4.92 \pm 0.29 \mu\text{M}$) vs $0.99 \pm 0.11 \mu\text{M}$ for orlistat [21]. It is worthy to note that the IC_{50} value for orlistat depends on the used assay [18,21].

Several techniques have been described for assaying the activities of enzymes such as PL. These biocatalysis assays can be divided into heterogeneous and homogeneous assays. In heterogeneous biocatalysis, the enzymes are often immobilized [22,23] which allows better storage stabilities and more tolerance to pH and temperature changes [24]; however a loss in the enzyme's catalytic activity is reported [25]. On the other hand, homogeneous biocatalysis involves the use of free enzymes in a homogeneous phase with the other reactants. A commonly used technique is spectrophotometry using either fluorescence or UV-Vis detectors. Microtiter plates are commonly

used in conjugation with the latter technique for assaying PL activity or screening for novel modulators [26]. Moreover, separative techniques such as capillary electrophoresis (CE) in order to improve the quantification of the product(s) without interferences from the substrate or other reactants in the reaction media. Assaying enzymatic activity and screening for modulators using CE has been widely reported [27–32]. Two common operating modes of CE enzymatic assays are the offline (pre-capillary) [33,34] and online (in-capillary) [35] modes. With the offline mode, the enzymatic reaction takes place in a microvial and the reaction mixture is thereafter injected into the capillary [36–38]. The offline reactions are rather easy to control and optimize. The online mode involves the capillary acting as a nanoreactor into which few nanoliters of the different reactants are injected and mixed. Several modes are available for in-capillary mixing of analytes. Electromigration microanalysis (EMMA) [39] and pressure mediated microanalysis (PMMA) [40] are used to mix analytes according to their electrophoretic mobilities and diffusion coefficients, respectively. In this case, the mixing step can be inefficient when more than two reactant plugs are injected [29,41]. Transverse diffusion of laminar flow profiles (TDLFP) [42] is a more suitable approach to mix multiple reactant plugs. In this mode, the reactants are injected sequentially using high injection pressures and short injection times giving rise to parabolic plugs. The diffusion and mixing of the different plugs is almost exclusively transversal with limited longitudinal diffusion. However, dilution of reactants inside the capillary is a significant drawback of this approach. Compared to offline ones, online reactions consume even less reactants (few tens of nanoliters) and it is possible to automate [43,44]. As mentioned previously, several types of detectors can be hyphenated to CE such as UV/Photodiode array (PDA), laser-induced fluorescence (LIF) [45], mass spectrometry (MS) [46,47] and capacitively coupled contactless conductivity detection (C⁴D) [1,2]. Its use in duality with spectrophotometric detection has been proven to be a powerful way to enhance CE selectivity towards various analytes [48]. An offline CE-C⁴D assay was developed by A. Schuchert-Shi *et al.* [49] to demonstrate the superior selectivity of PL towards the methyl ester substrate of L-threonine compared to L-serine. Y. Tang *et al.* [50] screened PL inhibition potential of ten natural extracts using a heterogeneous online CE enzymatic assay with PL immobilized onto the capillary walls. Using 4-nitrophenyl acetate (4-NPA) as the substrate, the reaction was monitored by detecting at 400 nm the 4-nitrophenol (4-NP) hydrolysis product. Six of the screened extracts showed inhibition of immobilized PL with the ethanolic *Fructus Crataegi* extract at 10 mg mL⁻¹ demonstrating the most relevant inhibition (~ 70%).

In this study, we describe for the first time a homogeneous CE-UV/C⁴D dual detection method for assaying PL activity. 4-nitrophenyl butyrate was chosen as a substrate of the PL which leads to the production of both 4-nitrophenolate (4-NP) and butyrate, detected by spectrometry and by C⁴D respectively (Figure II.1).

Both offline and online homogeneous CE-PL assays were developed. Several parameters were investigated such as the nature of the separation and reaction buffers, preparation of the 4-NPB substrate solution and the effect of DPPC on PL kinetics. Orlistat was used as the reference inhibitor to validate the assays. Furthermore, the developed enzymatic assays were carried out to test the modulatory potential of 11 compounds purified from oakwood, grapes and wine extracts in addition to the aqueous extracts of three different plants, Hawthorn (*Crataegus oxyacantha*), blackcurrant (*Ribes nigrum*) and *Chrysanthellum americanum* extracted by infusion in water to be eventually consumed as herbal tea. Indeed, we have recently [51] demonstrated some promising biological and antioxidant activities of these extracts and characterized their molecular features.

Experimental

Chemicals

Tris(hydroxymethyl)aminomethane (Tris) (C₄H₁₁NO₃, ≥ 99.8%), N-cyclohexyl-2-aminoethanesulfonic acid (CHES) (C₈H₁₇NO₃S, ≥ 99%), 3-(N-morpholino)propanesulfonic acid (MOPS) (C₇H₁₅NO₄S, ≥ 99.5%), sodium butyrate (C₄H₇NaO₂, ≥ 98.5%), 4-nitrophenol (4-NP) (C₆H₅NO₃, spectrophotometric grade), 4-nitrophenyl Butyrate (4-NPB) (C₁₀H₁₁NO₄, purity ≥ 98 %), lipase from porcine pancreas (EC 3.1.1.3, Type II, 100 – 500 units mg⁻¹ of protein), 1,2-dipalmitoyl-sn-glycero-3-phosphocholine (DPPC) (C₄₀H₈₀NO₈P, ≥ 99%), orlistat (C₂₉H₅₃NO₅, ≥ 98%) and lithium hydroxide monohydrate (LiOH.H₂O, ≥ 98%) were purchased from Sigma-Aldrich (Saint-Quentin Fallavier, France). Hydrochloric acid (HCl, 37%) was purchased from Fisher Scientific (Loughborough, UK). HPLC grade methanol (MeOH) was purchased from VWR International (Fontenay-sous-Bois, France). HPLC grade acetonitrile (ACN) and N,N-dimethylformamide (DMF, ≥ 99.8%) were purchased from Carlo Erba (Val de Reuil, France). Water used throughout this study was ultra-pure (18 MΩ-cm) produced by an Elga apparatus (Elga, Villeurbanne, France). Different parts of hawthorn (*Crataegus oxyacantha*, origin France), *i.e.* dry flowering tops (2 lots, number 20335 and number CB58120) and dry hawthorn flowers (lot number: 20334), dry *Chrysanthellum americanum* (origin Ivory Coast, lot number: 559980), and

dry blackcurrant leaves (*Ribes nigrum*, origin Poland, lot number: 55870) raw materials were purchased from France Herboristerie (Noidans-Lès-Vesoul, France). Fresh hawthorn leaves, flowers and flowering tops were harvested on April 24, 2020 on a wild isolated tree in Montpellier (France).

Instrumentation

Experiments were carried out using a Beckman-Coulter P/ACE MDQ CE instrument (Fullerton, CA, USA) equipped with a photodiode array (PDA) detection system and an on-capillary TraceDec C⁴D detection cell (Innovative Sensor Technologies GmbH, Strasshof, Austria). The C⁴D parameters were fixed as follows: frequency medium, voltage 0 dB, gain 100%, offset 010, filter: frequency 1/3 and cut-off 0.02. CE control and the analysis of electropherograms was performed using the 32 Karat software (Beckman Coulter). C⁴D signals were acquired by the Tracemon software (Istech, version 0.07a). Uncoated fused-silica capillaries were purchased from Polymicro Technologies (Phoenix, AZ, USA). The capillaries had a total length of 61 cm, an internal diameter of 50 µm and effective length of 37 cm to the C⁴D detection cell and 51 cm to the optical detection window. The capillary was contained in a system of connecting tubings and reservoirs used for circulating a coolant liquid in a closed circuit within the capillary cartridge. A lab-made 3D printed scaffold was constructed from polyacetic acid using an Ender 3 printer (Creality 3D, Shenzhen, China) and adapted to fix the various components of the C⁴D detection cell and to avoid coolant liquid leakage (Figure II.3). New capillaries were conditioned with 5 mM LiOH, H₂O and BGE for at least 15 min each followed by the application of +30 kV for 15 min. Between analyses, the capillary was rinsed with 5 mM LiOH (5 min), H₂O (1 min), 5 mM HCl (3 min), H₂O (1 min) and BGE (5 min). At the end of each working-day, the capillary was rinsed with 5 mM LiOH and H₂O for at least 15 min each before storing its ends overnight dipped in H₂O vials. All rinse cycles were carried out at 50 psi. The electrophoretic separations were conducted under +30 kV (which corresponded to 5 µA) and at 37°C. The volumes of the injected plugs were estimated using CE expert Lite from Sciex (<https://sciex.com/ce-features-and-benefits/ce-expert-lite>).

UHPLC-PDA system was composed of a Thermo Scientific™ Dionex™ UltiMate™ 3000 BioRS equipment with WPS-3000TBRS auto sampler, TCC-3000RS column compartment set at 35°C and Chromeleon 7 software, (ThermoFisher Scientific, Waltham MA, USA). UHPLC-ESI-MS

system was composed of a Synapt G2-S equipment with ESI operating in resolution mode and MassLynx 4.1 software (Waters Corp., Milford MA, USA). For both methods, a Kinetex C18 100A 100×2.1 mm, 2.6 μm column in association with a security guard ultra-cartridge was used (from Phenomenex Inc., Torrance CA, USA). A binary solvent system was used, consisting of water/formic acid (1%, v/v) mixture as solvent A and acetonitrile/formic acid (1%, v/v) mixture as solvent B. The gradient program started with 95% A, then A was progressively decreased to 0% in 30 min with a convex increase (curve 5 in Chromeleon 7). The flow rate of the mobile phase was set to 0.4 mL min⁻¹ and the injection volume was 20 μL. For the analysis by UHPLC-PDA, the peaks were monitored at 280, 320 and 360 nm and the UV-Vis spectra of the various compounds were recorded between 200 and 500 nm. For the analysis by UHPLC-ESI-MS, positive and negative ionization modes and fast DDA MS methods with automatic MS/MS intensity-based switching parameters, were used. The cone voltage, the extractor voltage and the capillary voltage were set to 30 V, 3 V and 2.4 kV, respectively. The source temperature and the desolvation temperature were 140°C and 450°C, respectively. Ions were scanned between $m/z = 50$ and $m/z = 1200$ to obtain MS spectra.

Solutions

Unless otherwise stated, all solutions were prepared in H₂O and filtered through polyvinylidene fluoride (PVDF) syringe filters of 0.2 μm pore size purchased from Agilent Technologies (Waldbronn, Germany).

Background electrolyte (BGE) and incubation buffer (IB): Tris/MOPS (ionic strength = 10 mM, pH 6.6) was used as the BGE for CE analyses as well as the IB for enzymatic reactions. The pH of solutions was measured using a MeterLab PHM201 Portable pH-Meter (Radiometer Analytical, Villeurbanne, France) and their properties obtained by Phoebus software (Analis, Namur, Belgium) and PeakMaster 5.3 [52].

Reactants: PL stock solutions were prepared daily by suspending the lyophilized enzyme powder in the IB at 10 mg mL⁻¹ followed by 15 min agitation before storage at 0°C. 4-NPB was chosen as the PL substrate due to its similarity to the natural TG substrate in addition to the possibility of following its hydrolysis products using dual detection. The 4-NPB solution was prepared in 100% acetonitrile at a concentration of 1 mg mL⁻¹. Unless otherwise stated, orlistat stock solution was prepared in 70% DMSO at 3 mg mL⁻¹ and was later diluted to 1.5 mg mL⁻¹ in H₂O to prepare the

working solution. The PL modulation by **11** compounds (Table II.2) purified from oakwood, grapes and wine extracts was investigated. These compounds were prepared at different percentages of organic solvents considering their solubilities. The preparation of the different compounds was as follows: compounds **1** to **7** in 70% methanol, compound **8** in 50% ethanol and compounds **9** to **11** in 80% ethanol. All of the purified molecules were prepared at a stock concentration of 40 mg mL⁻¹ and were then diluted to 5 mg mL⁻¹ in H₂O to prepare the working solutions. The modulation of different water extracts from three plants was also investigated. All extracts were prepared before use at 5 mg mL⁻¹ in H₂O and centrifuged at 2000 g for 10 min before isolating the supernatant. The different modulators (purified molecules + aqueous extracts) were assayed at 1 mg mL⁻¹.

Extraction by infusion of different plant parts: The extracts of different parts of *Crataegus oxyacantha* (hawthorn), *Ribes nigrum* (blackcurrant) and *Chrysanthellum americanum* plants were obtained as previously described by P. Cao-Ngoc *et al.* [6]. Unless otherwise stated, plant material was grinded before extraction using a commercial MKM6003 Bosch grinder.

Fresh hawthorn extractions: 20 g of fresh plant material (leaves, or flowers) were infused in 1 L of boiling water using a 'French press' Bodum® (Bistro model, Triengen, Switzerland) under 500 rpm magnetic stirring. After 30 min, the herbal tea solution was filtered first with the Bodum® cover to remove the largest particles, then with Whatman filter paper placed on a Büchner funnel using a vacuum pump (KNF Model N820FT.18, Freiburg, Germany) to remove any residual solid plant particles. Finally, the herbal tea solution was concentrated using a rotary evaporator (down to 20 mL volume) and finally freeze-dried (Cryotec Model CRIOS-80, Saint-Gély-du-Fesc, France) to obtain the dry extract. Lyophilized dry extracts were stored at 4°C.

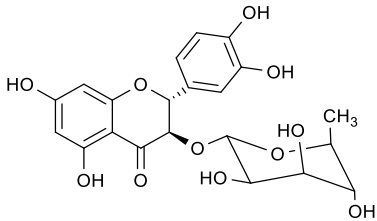
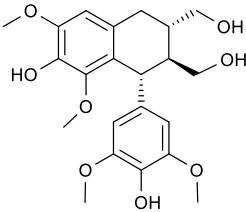
Dry hawthorn extractions: 2.5 g plant material (flowers only: lot No 20334, used as is without grinding, or grinded flowering tops lot No 20335 (sample A) and lot No CB58120 (sample B) were infused in 250 mL boiling water for 10 min using the same equipment as above. The herbal tea solution was then filtered, concentrated, freeze-dried and stored in the same way described above. Blackcurrant and *Chrysanthellum americanum*: the extraction protocol was similar to that of dry hawthorn.

Chemical composition of the plant extracts: The total polyphenols content (TPC), flavonoids content (TFC) and proanthocyanidin oligomers content (OPC) in the various plant extracts were determined by classical colorimetric methods, as previously described [6,51]. UHPLC-PDA and

UHPLC-ESI-MS/MS analyses were performed according to the protocol described in our previous paper [51]. Briefly, 20 mg of plant extract was dissolved in 1 mL water, then strongly vortexed for 2 min. The resulting solution was diluted five times with water, vortexed again for 2 min, and finally analyzed.

Extraction and purification of molecules from oakwood, grapes and wine: 11 natural molecules (Table II.2) were extracted from oakwood, grapes and wine using centrifugal partition chromatography fractionation and HPLC purification [53–57]: **1.** Astilbin ($C_{21}H_{22}O_{11}$, 450 g mol^{-1}), **2.** (-)-Lyoniresinol ($C_{22}H_{28}O_8$, 420 g mol^{-1}), **3.** (+)-Lyoniside ($C_{27}H_{36}O_{12}$, 552 g mol^{-1}), **4.** (+)-lyoniresinol 9'-O- β -glucopyranoside ($C_{28}H_{38}O_{13}$, 582 g mol^{-1}), **5.** Bartogenic acid ($C_{30}H_{46}O_7$, 518 g mol^{-1}) and its glucosyl derivative **6.** 28-O- β -D-glucopyranosylbartogenic acid (Glu-BA) ($C_{36}H_{56}O_{12}$, 680 g mol^{-1}), **7.** 23-O-galloylarjunglucoside (Quercotriterpenoside-I) ($C_{43}H_{62}O_{15}$, 818 g mol^{-1}) and its isomer **8.** (Quercotriterpenoside-III) ($C_{43}H_{62}O_{15}$, 818 g mol^{-1}), **9.** 3-O-[(6-Ogalloyl)- β -D-glucopyranosyl]bartogenic acid ($C_{43}H_{60}O_{16}$, 832 g mol^{-1}), **10.** 3-O-galloylrobural A ($C_{43}H_{60}O_{16}$, 832 g mol^{-1}) and **11.** 3-O-galloylbarrinic acid ($C_{37}H_{50}O_{11}$, 670 g mol^{-1}).

Table II.2: Structures of **11** compounds purified from oakwook and wine extracts and screened for PL modulation potential extracted. The reference PL inhibitor used in this study is orlistat (compound **12**)

Number	Name	Structure	M_w (g mol^{-1})
1	Astilbin		450
2	(-)-Lyoniresinol		420

3	(+) -Lyoniside		552
4	(+) -lyoniresinol 9'-O- β -glucopyranoside		582
5	Bartogenic acid		518
6	28-O- β -D-glucopyranosylbartogenic acid		680
7	Quercotriterpenoside-I		818

8	Quercotriterpenoside-III		818
9	3- <i>O</i> -[(6- <i>O</i> galloyl)- β -D-glucopyranosyl]bartogenic acid		832
10	3- <i>O</i> -galloylrobural A		832
11	3- <i>O</i> -galloylbarrinic acid		670
12 (Reference inhibitor)	Orlistat		495

CE-enzymatic assays

All reactions were performed in triplicates ($n = 3$) at 37°C . The corrected peak areas (CPA) of the reaction products represented the peak areas corrected for migration time. Blank reactions were carried out in the absence of the enzyme, which was substituted with the IB, to estimate the non-enzymatic spontaneous hydrolysis of the 4-NPB substrate. Control reactions were conducted to set the baseline activity of PL which corresponds to 0% PL modulation. The modulatory molecules in control reactions were substituted with their respective solvent. The modulation of PL activity was then calculated relative to the activity of PL observed in control reactions after correction for spontaneous hydrolysis observed in the blank assays. The modulation of PL activity (activation and inhibition) was calculated as follows (Equation II.1):

$$\% \text{ Modulation} = \left| \left(1 - \left(\frac{A_M - A_B}{A_C - A_B} \right) \right) \times 100 \right| \quad \text{Equation II.1}$$

where A_M and A_C are the CPA of the hydrolysis products in presence and absence of the modulator molecules, respectively. A_B is the CPA of the hydrolysis products in the blank assays. This calculation is conducted for UV as well as for C^4D detection.

The residual PL activity is calculated after incubation with inhibitors as follows (Equation II.2):

$$\text{Residual activity \%} = \left(1 - \frac{I}{100} \right) \times 100 \quad \text{Equation II.2}$$

where I is the percentage of PL inhibition, calculated using Equation II.1.

Offline CE-enzymatic assay: 6 μL of PL (1.2 mg mL^{-1}) was pre-incubated with 10 μL of the investigated compounds *i.e.* orlistat (0.3 mg mL^{-1}), natural purified molecules or plant extracts (1 mg mL^{-1}) in 29 μL of Tris/MOPS IB for 5 min. Addition of 5 μL of 4-NPB (0.1 mg mL^{-1}) initiated the enzymatic reaction *i.e.* the incubation step. The linearity of the PL catalyzed hydrolysis reaction was investigated at different incubation times (5, 10, 25, 45, 60, 75, 90 and 120 min). The reaction was found to be linear up to 1 hr. The reaction mixture was thus incubated for 5 min to avoid excess substrate hydrolysis ($\leq 10\%$). At the end of the incubation period, the reaction mixture was moved to a boiling water bath (95°C) for 5 min to terminate the reaction. Then, a bench-centrifuge (model number 250711) (Quirumed, Valencia, Spain) was used to

centrifuge the reaction mixture tube at 2000 g for 5 min. Hydrodynamic injections were carried out at 0.7 psi for 5 s (9 nL).

Influence of DPPC vesicles on PL kinetics: The effect of DPPC vesicles on the kinetics of 4-NPB hydrolysis by PL was investigated using the offline CE-based assay. DPPC vesicles were prepared at 1 mg mL⁻¹ in the IB and then added to the enzymatic reaction. The enzymatic reactions were carried out using 6 different 4-NPB substrate concentrations of (0.3, 0.5, 0.7, 0.9, 1 and 2 mM). Reaction were performed in triplicates (n = 3). The enzymatic reactions carried out in the absence of the vesicles were used to calculate the kinetic parameters of the PL catalyzed hydrolysis of 4- NPB. The initial reaction rate V_i (mM min⁻¹) was calculated as the ratio of products formed *per* time interval in the presence or absence of DPPC vesicles. The nonlinear curve fitting program PRISM® 5.04 (GraphPad, San Diego, CA, USA) was used to determine V_{max} and K_m according to following equation (Equation II.3):

$$V_i = \frac{V_{max} \times [S]}{K_m + [S]} \quad \text{Equation II.3}$$

where V_i is the reaction rate, K_m is the Michaelis constant, V_{max} is the maximal reaction velocity and $[S]$ is the substrate concentration.

Online CE-enzymatic assay: In the optimized conditions, the investigated modulatory compounds (represented by M for online assays) and the enzyme (PL) were mixed together and injected as a single plug. Simulations of plug overlapping by TDLFP and their position in the capillary were done using a software developed by S. Krylov's group [58]. Injection sequence was carried out from the long capillary end (furthest from the optical detection window) as follows: PL + M (0.5 psi × 3 s, 4 nL), 4-NPB substrate (S) (0.5 psi × 6 s, 8 nL), PL + M (0.5 psi × 3 s, 4 nL) and IB (0.5 psi × 90 s, 120 nL) (Figure II.7). Between each injection, the capillary inlet was dipped into the IB to minimize sample carry over [59]. The reactant plugs were mixed inside the capillary and incubated for 5 min. Then, the separation voltage was applied to separate the reaction components and terminate the enzymatic reaction by separating the enzyme from the substrate.

Results and discussion

Before conducting CE-based enzymatic reactions, it is important to ensure that the reaction can be monitored and quantified using suitable separation and detection conditions of both products, 4- NP and butyrate.

The preparation of the 4-NPB substrate was also optimized and a suitable IB was chosen. We mainly focused on the stability of the substrate in the stock solution as well as in the final incubation mixture. The 4-NPB hydrolysis by PL in terms of molecular affinity (K_m) and of reaction rate (V_{max}) was evaluated in the presence and in the absence of DPPC vesicles. The influence of the reference inhibitor orlistat (Table II.2, entry 12) on PL activity was evaluated to validate the developed CE-UV/C⁴D based assays before their use to evaluate the potential bioactivity of six aqueous plant extracts as well as of 11 original compounds purified from oakwood and wine.

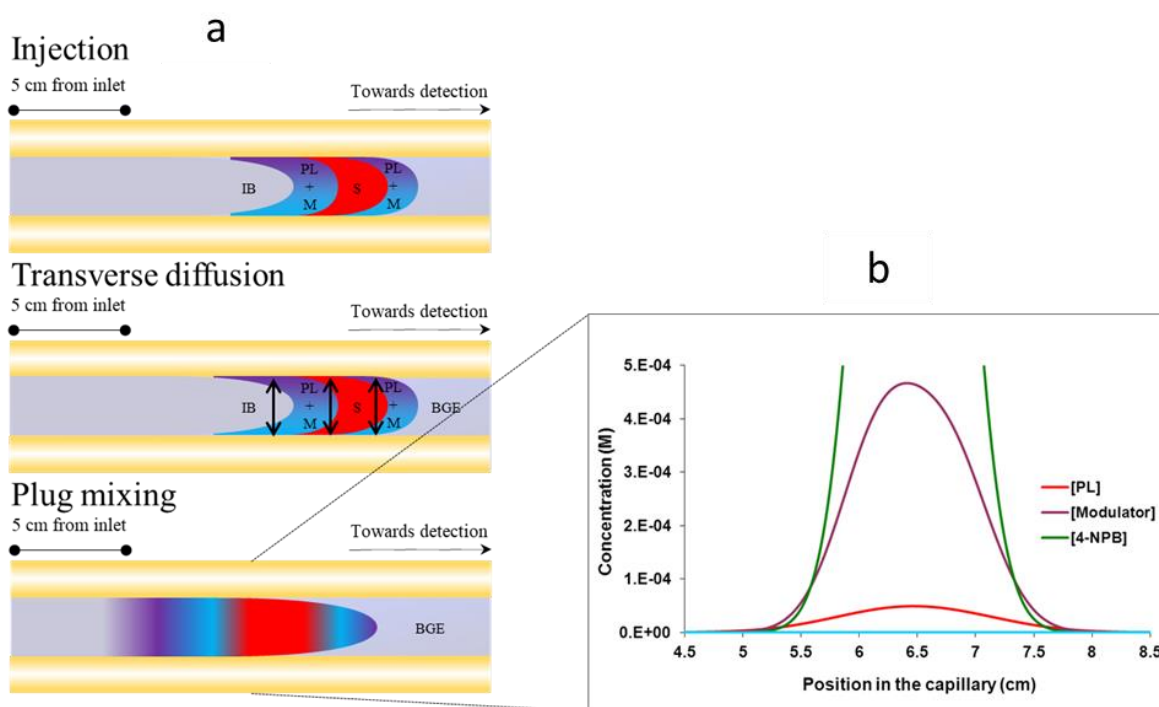


Figure II.7: Schematic representation of the different steps of the online enzymatic reaction (a). *Injection* of the different reactants sequentially into the capillary filled with the BGE as follows; 8 mg mL⁻¹ PL + 1 mg mL⁻¹ of the modulator molecule (M) (0.5 psi × 3 s, 4 nL), 1 mg mL⁻¹ 4-NPB (S) (0.5 psi × 6 s, 8 nL), PL + M (0.5 × 3 s, 4 nL) and IB (0.5 psi × 90 s, 120 nL). *Transverse diffusion* of the different reactant plugs into each other. *Plug mixing* by incubation of the plugs for 5 min at 37°C allowing them to mix to initiate the enzymatic reaction. Simulation of the concentrations of the different reactants relative to their position in the capillary in addition to the overlapping of their plugs using a simulation software developed by Krylov *et al.* [58] (b)

Optimization of the electrophoretic separation buffer (BGE)

The choice of the BGE should be carried out carefully considering its compatibility with the technique of detection as well as the enzymatic reaction. BGE is influential to the sensitivity of analyte detection, peak shape and symmetry and the duration of the analysis [60]. In order to limit the background noise and to avoid interference with the analyte peak, the buffer should have a low conductivity and minimal absorption at the detection wavelength. The use of buffers of different ionic strengths did not appear to exert a significant influence on PL activity in previous reports from the literature [61,62]. With conductometric detection, the analytical response is proportional to the difference between the analyte's and the BGE's co-ion mobilities [3]. However, this difference results in the decline of peak symmetry which relies on the equivalence of these mobilities [63].

The properties of two BGE, 100 mM Tris/50 mM CHES (12 mM, alkaline pH 9.0) and 10 mM Tris/40 mM MOPS (10 mM, slightly acidic pH 6.6) were compared using PeakMaster 5.3 (Table II.4 in the "supplementary information"). Firstly, both buffers had low conductivities and thus were suitable for direct conductometric detection. Additionally, they did not absorb at the wavelength of interest ($\lambda = 400$ nm).

The limits of detection (LOD) of the products were evaluated by injecting different concentrations of standard solutions. The 4-NP peak detected at 400 nm was symmetrical with Tris/MOPS (peak asymmetry of 0.9) and LOD was found to be 30 μ M. Peak symmetry in this case could be explained by the equivalence of the 4-NP mobility and the BGE co-ion's (MOPS) mobility. 4-NP peak was completely distorted with Tris/CHES. In addition, C⁴D was a lot more sensitive to butyrate with Tris/MOPS as BGE (LOD = 0.5 μ M vs 10 μ M). Comparing the mobilities of the butyrate ion to the co-ions mobilities shows that the difference between both mobilities is almost identical in both buffers (Table II.4 in the "supplementary information"). The higher sensitivity with Tris/MOPS is thus probably due to the lower conductivity of this BGE couple compared to Tris/CHES. It is worthy to note that the effective mobility of 4-NP ($\mu_{\text{eff}} = -7.9 \text{ m}^2 \text{ V}^{-1} \text{ s}^{-1}$) is very close to that of MOPS ($\mu_{\text{eff}} = -5.7 \text{ m}^2 \text{ V}^{-1} \text{ s}^{-1}$) which explains that the Tris/MOPS is not suitable for the conductometric detection of the 4-NP.

Additionally, the velocities of the 4-NP and butyrate ions, calculated by dividing the distance from the capillary inlet to the respective detector of the ion over the migration time of each ion, were $0.93 \pm 0.004 \text{ cm s}^{-1}$ and $0.57 \pm 0.002 \text{ cm s}^{-1}$ using Tris/MOPS and $0.03 \pm 1.66 \times 10^{-5} \text{ cm s}^{-1}$ and

$0.15 \pm 0.003 \text{ cm s}^{-1}$ when using Tris/CHES as BGE, respectively. The greater velocities with Tris/MOPS are reflected by shorter migration times and therefore permit rapid analyses (less than 7 min, Figure II.8). Finally, non-enzymatic hydrolysis of nitrophenyl esters is common especially at alkaline pH due to their high reactivities [64]. The extent of spontaneous hydrolysis of the 4-NPB substrate was acceptable with Tris/MOPS at pH 6.6 (< 10%) compared to Tris/CHES at pH 9 where it was about 30%.

For all these reasons, the remainder of the study was carried out using Tris/MOPS (10 mM, pH 6.6).

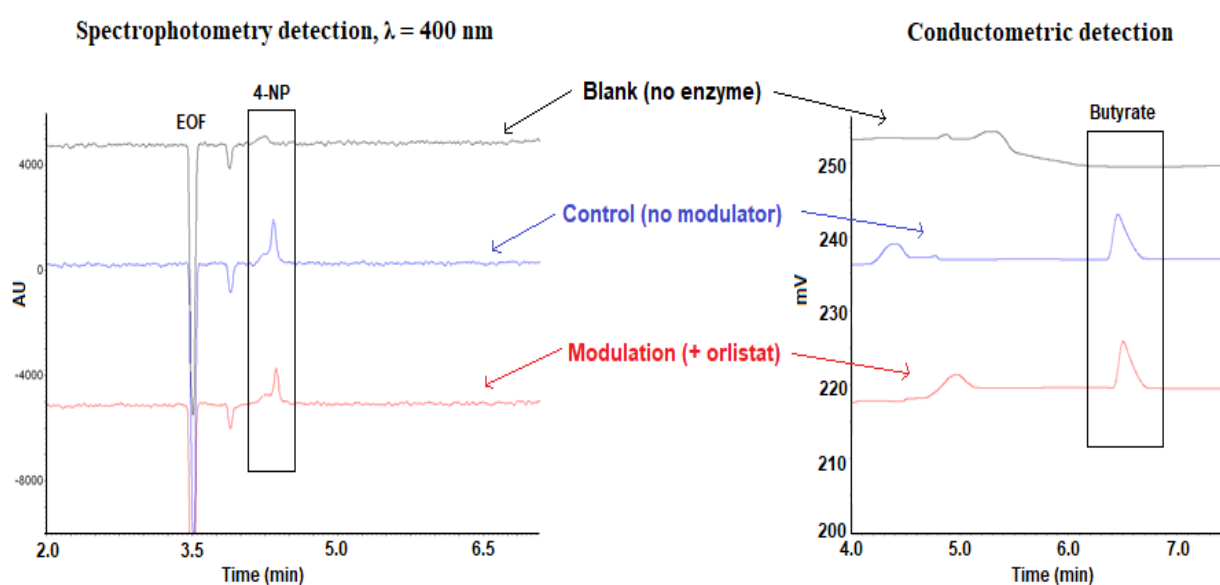


Figure II.8: Electropherograms obtained after monitoring 4-NPB hydrolysis by PL using online CE-UV/C⁴D assay. The injection sequence was carried out as follows: PL + Orlistat (0.5 psi \times 3 s, 4 nL), 4-NPB (0.5 psi \times 6 s, 8 nL), PL + Orlistat (0.5 psi \times 3 s, 4 nL) and IB (0.5 psi \times 90 s, 120 nL). The reactants were incubated for 5 min at 37°C before the application of + 30 kV. BGE/IB: Tris/MOPS (10 mM, pH 6.6). For more details: see “Experimental section”. EOF: electroosmotic flow, AU: absorbance units and mV: millivolts

Optimization of the enzymatic reaction conditions

Choice of the substrate solvent and of the IB: In Figure II.9a, the spontaneous non-enzymatic degradation of 4-NPB prepared in either water or ACN and then diluted in Tris/MOPS buffer at pH 7.5 and pH 6.6 (which corresponds to the BGE tested in the previous section) was observed. The incubation of the different 4-NPB solutions correspond to the offline enzymatic reaction steps (see section “CE-enzymatic assays”) for comparison between spontaneous and enzymatic hydrolysis of 4-NPB. When working at pH 7.5, the degree of spontaneous hydrolysis of the

4-NPB, dissolved in water or ACN, was significant as concluded by comparing the intensities of the yellow colored solutions. Conventionally, Tris adjusted to pH 7.5 is used as the IB to assay PL activity since this conforms to the optimal pH of PL activity [65,66]. At lower pH 6.6, no spontaneous degradation was visually observed with the stock solution prepared in ACN. Owing to its chemical nature, it is a common practice to prepare 4-NPB in organic solvents such as ACN. It is worthy to note that significant hydrolysis of 4-NPB was observed when prepared in DMF, even at 1% (v/v) (results not shown). To further investigate the spontaneous degradation, the 4-NPB solution in ACN diluted in Tris/MOPS pH 6.6 was analyzed by CE at 400 nm.

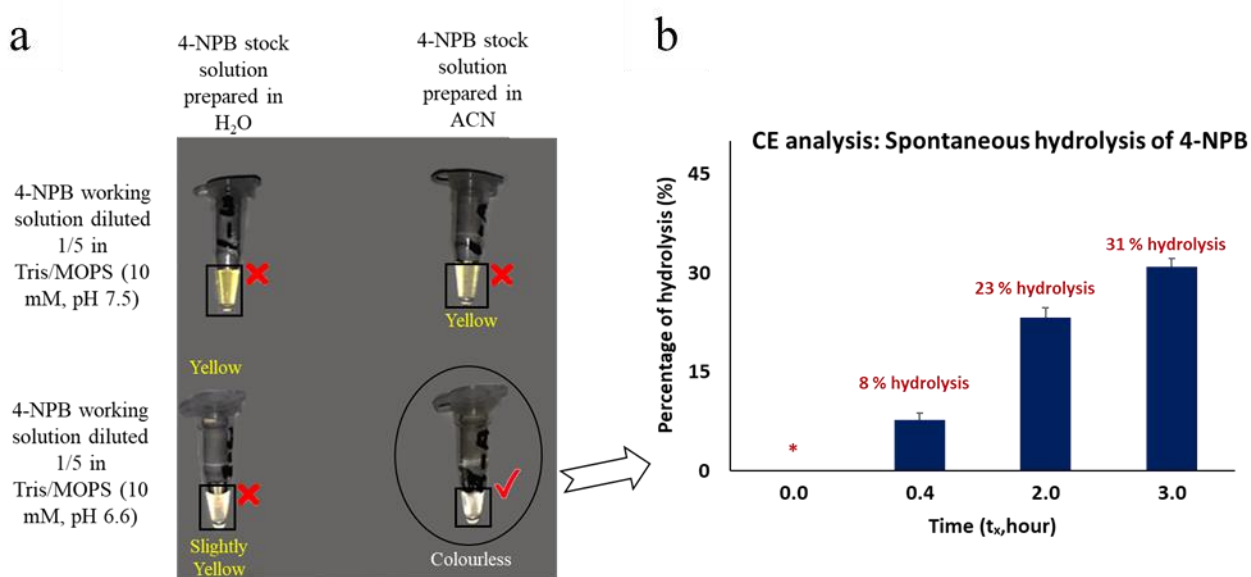


Figure II.9: Visual spontaneous hydrolysis of 4-NPB in the absence of PL (a). The yellow color represents the release of 4-NP as a result of spontaneous 4-NPB hydrolysis. The substrate was prepared at a stock concentration of 5 mM in either water (left) or ACN (right). 10 μ L of 5 mM 4-NPB was then mixed with 40 μ L of 10 mM Tris/ 40 mM MOPS (Ionic strength = 10 mM, pH 7.5 (top row) or pH 6.6 (bottom row)) to have a final substrate concentration of 1 mM and a final volume of 50 μ L. The mixtures were incubated at 37°C for 5 min and then at 95°C for another 5 min before the color of each tube was observed. CE injection at different time points of 4-NPB solution prepared in ACN and diluted in Tris/MOPS (10 mM, pH 6.6) to estimate spontaneous hydrolysis at different times ($t_x = 0.4, 2$ and 3 hr) (b). Y-axis represents the percentage of 4-NPB hydrolysis calculated using the following equation: $100 \times (CPA_{t_x} - CPA_{t_0})/CPA_{t_0}$; where $t_0 = t_{inc} + t_{rinse} + t_{analysis} = 0.4$ hr. *: calculations are relative to the CPA_{t_0}

The results (Figure II.9b) show a time-dependent increase in 4-NP due to the spontaneous degradation of 4-NPB starting from only 8% after 0.4 h to 31% over a period of three hours ($n = 3$). This emphasizes the importance of short CE analysis times of the reaction mixtures after their preparation. Accordingly, the 4-NPB substrate was prepared in pure ACN and diluted in the Tris/MOPS (10 mM, pH 6.6) for the remainder of the study. The ACN quantity in the final reaction

was estimated to be 10%. Being enzymes that function superiorly in the aqueous-organic interfaces, lipases show improved stability in relatively highly organic media rather than purely aqueous ones due to the interfacial activation phenomenon [8,67].

The Tris/MOPS (10 mM, pH 6.6) was also used as the IB. Using 5 min of incubation time confirmed that the activity of the PL in this buffer was satisfactory and the spontaneous substrate degradation was low (8%). Moreover, using the same solution as both the BGE and IB is simpler and of great interest particularly when adapting the online enzymatic assay.

K_m and V_{max} evaluation and influence of DPPC phospholipidic vesicles on PL activity: As mentioned before, PL is active at a lipid-water interface. For this, the offline CE-based assay was conducted using the optimized conditions presented above in order to investigate the effect of phospholipidic DPPC vesicles on 4-NPB hydrolysis by PL in terms of K_m and V_{max}. Both UV and C⁴D results *i.e.* quantification of 4-NP and of butyrate respectively were used.

The results obtained in the absence of DPPC confirmed the substrate-enzyme relationship between 4-NPB and PL as confirmed by K_m values obtained using UV (K_m = 0.57 mM) and C⁴D (K_m = 0.59 mM) (Table II.3). K. Shirai *et al.* [9] found similar K_m value of 0.52 mM for the hydrolysis of 4-NPB by the lipoprotein lipase (LpL). V_{max} was slightly higher for the hydrolysis of 4-NPB by PL in this study as compared to the hydrolysis by LpL (Table II.3).

Table II.3: Kinetic constants of 4-NPB hydrolysis by PL in the presence or absence of 1 mg mL⁻¹ DPPC. The constants were calculated by following the formation of the hydrolysis products, 4-NP and butyrate, using spectrophotometric and conductometric detection, respectively. The constants were compared to those obtained for 4-NPB hydrolysis by LpL as described by K. Shirai *et al.* [9]

(n = 3)		4-NP	Butyrate	4-NP
		UV	C ⁴ D	Lit.[9]
K _m (mM)	-DPPC	0.57±0.03	0.59±0.12	0.52
	+DPPC	1.54±0.01	1.66±0.01	0.55
V _{max} (μM.s ⁻¹)	-DPPC	1.20±0.13	0.71±0.07	0.66
	+DPPC	4.22±0.01	3.68±0.01	2.93

When DPPC vesicles were added to the incubation mixture, the obtained K_m and V_{max} values were in same order of magnitude compared to those obtained in their absence. Indeed, in Shirai's work [9], the K_m value of 4-NPB to LpL was unchanged and the V_{max} was in the same order of magnitude

upon addition of DPPC (Table II.3). These results confirm that in the conditions used in this study, PL was active even in the absence of DPPC.

Moreover, the relative standard deviation (RSD) of the migration times and CPA ($n = 3$) were calculated as 1% and 3% for 4-NP and 2% and 1% for butyrate, respectively. This confirms that the offline method can detect and quantify the PL catalyzed hydrolysis reaction with excellent repeatabilities. The results obtained confirm the choice of the 4-NPB as a substrate for the PL. The good repeatability and the concordance of the results obtained using the dual detection system confirms the reliability of the developed offline CE-UV/C⁴D based lipase assay.

PL inhibition using the reference inhibitor orlistat

Due to its limited solubility, orlistat was tested at a maximum concentration of 0.3 mg mL⁻¹ in 7% DMSO using the offline assay. To assess any non-enzymatic degradation of 4-NPB, blank assays were conducted in the absence of the enzyme, as previously detailed. Control reactions, where no modulatory molecules are involved, were conducted for comparison (Figure II.8).

Offline CE-UV/C⁴D assay to evaluate the effect of orlistat on PL activity: The offline assay consists of four steps: pre-incubation, incubation, termination and centrifugation. The pre-incubation step involves incubating PL with the orlistat. It was found to be essential to allow the establishment of any enzyme-inhibitor interaction as well as for thermal equilibrium of the reaction mixture at 37°C [68]. The presence of 7% of DMSO did not affect the PL activity. In these conditions, the orlistat at 0.3 mg mL⁻¹ was found to inhibit PL activity by $24 \pm 1\%$ ($n = 3$). Both UV and C⁴D results were obtained with excellent reproducibility. This assay was easy to optimize and the quantification could be assessed in a very straightforward manner.

Online CE-UV/C⁴D assay to evaluate the effect of orlistat on PL activity: The online mode combines the enzymatic reaction and the CE analysis into a single automated and very economic process since only few nL of reactants are required. The temperature of the capillary in which the PL reaction takes place was fixed at 37°C (as for offline assays). A plug of the IB is typically injected first into the BGE filled capillary to avoid any denaturation of the enzyme by the BGE. This is known as partial filling [69]. However, since we chose similar BGE and IB (Tris/MOPS 10 mM, pH 6.6), no such precaution was necessary. Furthermore, an IB plug needs to be injected at the end of the injection sequence to improve plugs' overlapping by increasing the lengths of

their longitudinal interfaces. Firstly, an IB plug as long as the sum of the lengths of all the other reactant plugs was used [42]. In these conditions, the injection sequence was as follows: PL (0.5 psi \times 3 s, 4 nL), M (0.5 psi \times 3 s, 4 nL), S (0.5 psi \times 6 s, 8 nL), M (0.5 psi \times 3 s, 4 nL), PL (0.5 psi \times 3 s, 4 nL) and IB (0.5 psi \times 18 s, 24 nL). In the case of control reactions, M plugs were substituted with plugs of the IB. While the simulations using Krylov's program showed good reactant mixing, low detected quantities of 4-NP and of butyrate were indicative of limited PL activity. Thus, the influence of the homogeneity of the temperature along the capillary was addressed. In fact, when conducting online reactions, incubation takes place at the inlet of the capillary, in a non-thermostated part [70]. More precisely, we measured a drop of 10°C of the temperature of the solutions in which the entry of the capillary is dipped after 5 min (corresponding to the time used for enzymatic reactions). This means that PL reactions conducted at the capillary inlet take place roughly at 37°C at the beginning and at 27°C at the end of the incubation time. This important decrease in temperature during the PL reaction may explain the very low enzymatic activity detected [9,70]. To overcome this, the length of the IB terminal plug was increased (injection at 0.5 psi for 90 s, 120 nL) to push all the plugs at least 5 cm into the thermostated region of the capillary (Figure II.7). It is important to mention that the longer the terminal IB plug, the better the reactant mixing but the higher is the dilution of the reactant. This dilution is particularly difficult to measure, which makes quantification and comparison with offline assays challenging [42,71,72]. In these conditions, good enzymatic activity was obtained with the control assay as observed by a 207% increase in the area and 167% increase in the height of the 4-NP product peak relative to the blank assay. Additionally, the RSD of the migration time and CPA were determined as 1% and 5% for 4-NP and 1% and 2% for butyrate, respectively.

Then, the reference inhibitor orlistat was prepared in 20% (v/v) DMSO and injected at 1 mg mL⁻¹. The exact concentration of orlistat in the capillary is difficult to determine. In fact, the dilution factor would be 18-times assuming complete overlapping of all the injected plugs (8 nL of modulator in a total volume of 144 nL). In these conditions, no significant inhibition of PL neither by UV nor by C⁴D was detected. This can be due to the direct contact between the PL's plugs and the high percentage of DMSO in the inhibitor solution before dilution [73]. It can also be due to the absence of a pre-incubation period between the tested inhibitor and enzyme [68]. Subsequently, the injection sequence was replaced by the one presented in the "experimental section" and in which the PL and the modulator plugs were combined into an individual plug by injecting both

reactants from the same solution (Figure II.7a). In these conditions, good inhibition of PL by orlistat was obtained ($32 \pm 5\%$).

Therefore, this method was able to detect modulators of PL activity in an economic automated manner. It is not trivial to compare this result to the one obtained previously by the offline method due to the difficulty of calculating the exact concentrations of the different reactants after using the long terminal IB plug.

Molecular characterization of plant extracts and evaluation of their potential to modulate PL activity

The characterization of the aqueous plant extracts was performed before evaluating their PL modulation potential. The molecular features of fresh hawthorn was characterized in this study whereas *Chrysanthellum americanum*, blackcurrant and dry hawthorn were thoroughly studied in our previous papers [6,51].

Molecular characterization of plant extracts: Global extraction yields, TPC, TFC and OPC results are presented in Table II.1. Concerning hawthorn, the extraction yield was similar for fresh leaves, fresh flowers, and dry flowering tops (20-24%). The values of TPC and TFC from fresh leaves were much lower (107 mg eq. gallic acid/g dry plant extract for TPC and 9.8 mg eq. quercetin/g dry plant extract for TFC) than those from fresh or dry flowers (121-171 mg eq. gallic acid/g dry plant extract for TPC and 16 mg eq. quercetin/g dry plant extract for TFC) and those from dry flowering tops (96-150 mg eq. gallic acid/g dry plant extract for TPC and 14-15 mg eq. quercetin/g dry plant extract for TFC). However, the value of OPC from dry plant (8-20 mg eq. cyanidin/g dry plant extract) was much higher than that from fresh plant (4.5-5 mg eq. cyanidin/g dry plant extract). Those findings are in good agreement with the literature [74,75]. The global extraction yield of *Chrysanthellum americanum* (26%) and of blackcurrant leaves (28.5%) is higher, the former containing much less phenolic compounds (60 mg eq. gallic acid/g dry plant extract for TPC) and proanthocyanidin oligomers (1.6 mg eq. cyanidin/g dry plant extract for OPC) than the two other plants.

UHPLC-PDA and UHPLC-ESI-MS/MS analyses showed that the main compounds found in hawthorn are phenolic acids such as chlorogenic acid and flavonoids such as epicatechin, vitexin 2-O-rhamnoside, pinnatifinoside A, hyperoside, isoquercetin and apigenin-C-hexoside (see Figure II.10, reference [6] and Figure II.13 in the “supplementary information”).

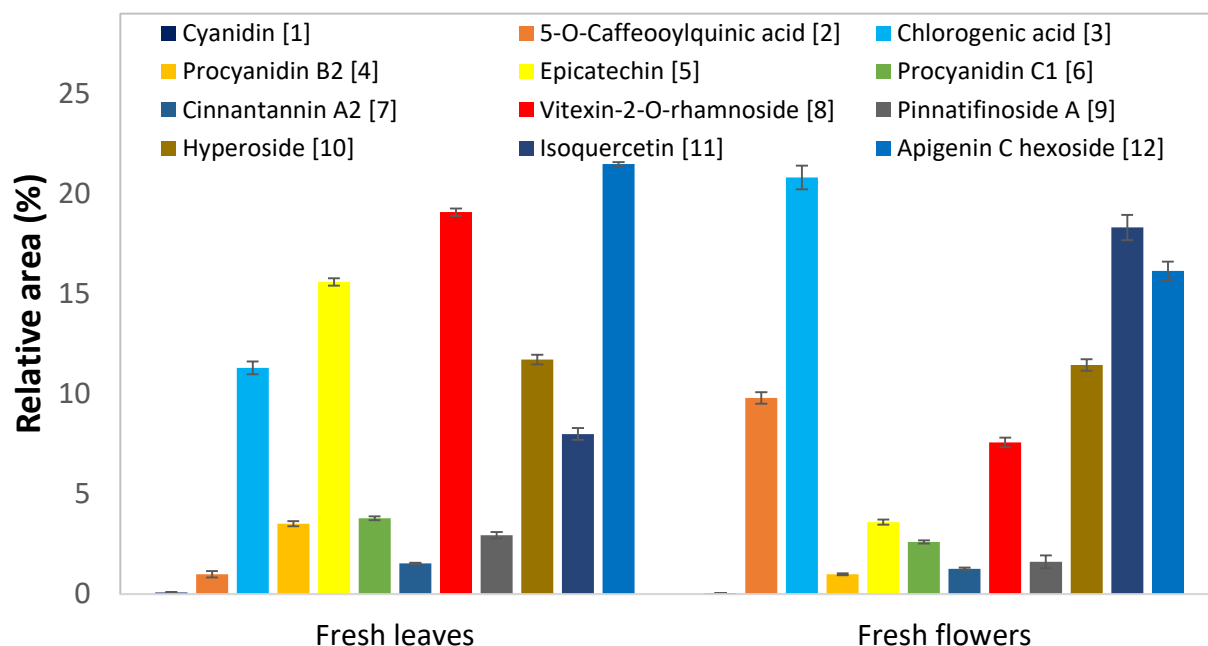


Figure II.10: Relative peak area distributions for the main identified chromatographic peaks according to the nature of hawthorn plant part (grinded fresh leaves or flowers). Same experimental conditions as in Figure II.13. The relative area was calculated by dividing the peak area of each component by the sum of the peak area of the 12 identified components. Error bars: ± 1 standard deviation calculated on $n = 3$ repetitions. 1 = Cyanidin, 2 = 5-*O*-caffeoylquinic acid, 3 = chlorogenic acid, 4 = procyanidin B2, 5 = epicatechin, 6 = procyanidin C1, 7 = cinnamtannin A2, 8 = vitexin-2-*O*-rhamnoside, 9 = pinnatifinoside A, 10 = hyperoside, 11 = isoquercetin, 12 = apigenin C-hexoside

The quantification of several representative compounds for each subfamily such as chlorogenic acid (peak 3 in Figure II.14 in the “supplementary information”), epicatechin (peak 5), vitexin-2-*O*-rhamnoside (peak 8), isoquercetin (peak 11) was determined by external calibration, using commercially available standards as presented in Figure II.14 (“supplementary information” section). Interestingly, for fresh hawthorn leaves, the quantities of epicatechin and vitexin-2-*O*-rhamnoside are 103.2 ± 3.2 mg *per g* of fresh leaves extract and 17.6 ± 0.5 mg *per g* of fresh leaves extract, respectively, which is higher than that in the flowers and flowering tops extracts. On the contrary, chlorogenic acid and isoquercetin are major components in the fresh flowers, with 32.7 ± 0.4 mg *per g* fresh flowers extract and 45.87 ± 1.3 mg *per g* fresh flowers extract, respectively. The main compounds detected by UHPLC-PDA in *Chrysanthellum americanum* and blackcurrant leaves have been previously identified and listed in our previous work [51]. Precisely, nine major peaks were detected in blackcurrant leaves, two of them (chlorogenic acid and quercetin 3-*O*-glucoside (isoquercetin)) were unambiguously identified, while the seven others were tentatively assigned to quercetin 3-rutinoside, quercetin 3-*O*-galactoside, quercetin-3-*O*-malonyl-glucoside,

kaempferol-3-O-rutinoside, kaempferol-3-O-hexoside, kaempferol-malonylglucoside, and kaempferol-malonylglucoside isomer. Ten major peaks were detected in *Chrysanthellum americanum*, one of them (chlorogenic acid) was unambiguously identified and the nine others were tentatively assigned to eriodicyol-7-O-glucoside, 6,8-C,C-diglucosylapigenin, isookanin-7-O-glucoside (flavanomarein), maritimetin-6-O-glucoside (maritimein), luteolin-7-O-glucuronide, di-caffeoylquinic acid, apigenin-7-glucuronide, and di-caffeoylquinic acid isomers.

PL modulation potential of aqueous plant extracts: The six aqueous extracts previously described were screened at 1 mg mL^{-1} using the offline CE-UV/C⁴D based assay and the results are graphically represented in Figure II.11. Firstly, we investigated dry hawthorn flowering tops (two different lots, designated as A and B) and hawthorn dry flowers (without leaves). Surprisingly, PL inhibition was obtained with both hawthorn dry flowering tops lots ($31 \pm 0.3\%$ for lot A and $23 \pm 4\%$ for lot B), while an activation of PL (positive activity, superior to the control assay corresponding to 0%) was noticed with hawthorn dry flowers ($26 \pm 1\%$). We thus suspected that hawthorn leaves and flowers influence PL activity in opposite ways. In a second series of experiments, we decided to test hawthorn leaves and flowers separately by harvesting fresh hawthorn flowering tops and by meticulously separating leaves and flowers before extraction by infusion.

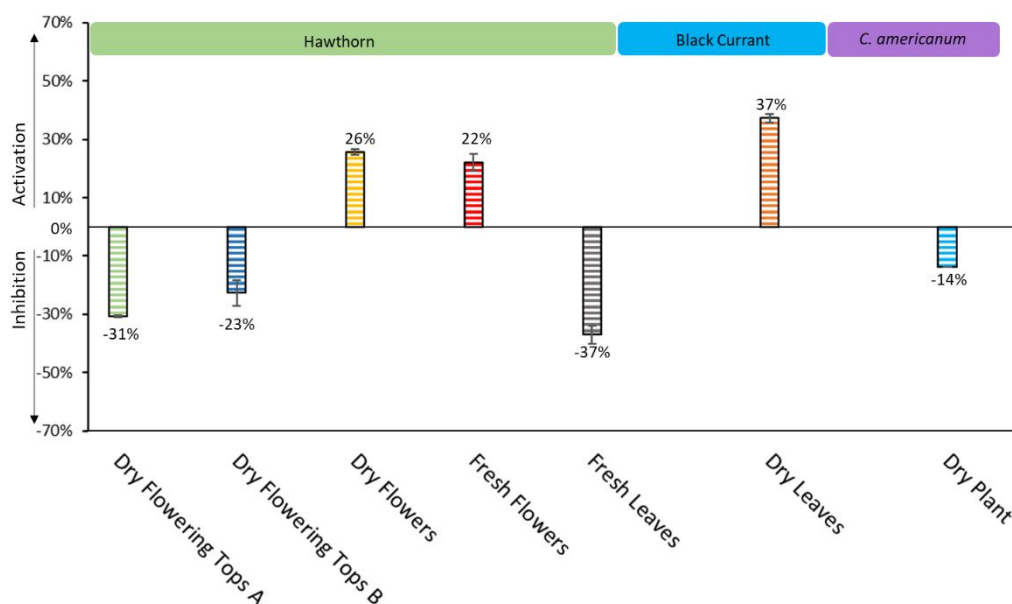


Figure II.11: Modulation of PL activity by aqueous extracts of hawthorn (dry flowering tops, dry flowers, fresh flowers, fresh leaves), dry blackcurrant leaves and dry *Chrysanthellum americanum* at 1 mg mL^{-1} . The percentage of modulation is represented relative to a control reaction conducted in the absence of the extracts. Error bars indicate the standard deviation on PL activity for $n = 3$ experiments

Results presented in Figure II.11 of these fresh samples confirmed an inhibition of the PL enzymatic activity by fresh hawthorn leaves ($37 \pm 3\%$) while the fresh flower activated the PL enzymes ($22 \pm 6\%$). These findings suggest that the inhibitory potential of PL by extracts of flowering tops is mainly due to the leaves which effect is prevailing relative to that of flowers. This difference in PL activity is most likely related to the differences in the chemical compositions of the hawthorn extracts. Certain features were unique to certain parts of hawthorn [6]. For instance, ESI-FT-ICR-MS revealed that CHON species *i.e.* carbon, hydrogen, oxygen and nitrogen-containing species such as amino acids and amino sugars were more abundant in flower extracts of hawthorn. Difference in chemical composition was also studied by UHPLC (see in the “supplementary information” the Figure II.13 for UHPLC traces and the Figure II.14 for the relative peak area) showing an increased presence in fresh flowers of 5-O-caffeoylquinic acid (peak 2), hyperoside (peak 10) and isoquercetin (peak 11), and lower content in vitexin-2-O-rhamnoside (peak 8) compared to fresh leaves.

Extracts of *Chrysanthellum americanum* led to slight inhibition of PL ($14 \pm 0.1\%$), while blackcurrant leaves favored PL activation ($37 \pm 1.5\%$). In our recent study [51], we found that almost 16% of the extracts’ molecular features were unique to each of the three studied plants. Thus, the inhibition or activation can be related to the molecular features and type of compounds in the extracts. Moreover, the application of the online PL assay proved to be tricky to optimize when applied to screen the modulatory effect of these plant extracts. The complex nature of the extracts negatively affected the quality and the repeatability of the reactant mixing by TDLFP.

To conclude, the six aqueous extracts have shown various effects on PL activity. Interestingly, hawthorn leaves extracts induced a specific 37% inhibition of PL, while hawthorn flower promoted PL activity. Recently [50,76], heterogeneous CE-based assay were developed to screen PL modulation by several natural extracts. For instance, at 10 mg mL^{-1} , ethanolic extracts of *Fructus Crataegi* demonstrated PL inhibition of 70% [50]. In another work [76], methanolic extracts of *Oxytropis falcate* Bunge demonstrated 54% and 68.6% PL inhibition at 50 mg mL^{-1} and 100 mg mL^{-1} , respectively. In comparison to these published data, only 1 mg mL^{-1} of the aqueous hawthorn leaves extracts was sufficient to demonstrate 37% inhibition using our developed method. This certainly reflects an interesting inhibitory effect of hawthorn leaves extracts at concentrations 10-100 times lower than that described in the literature for assaying PL inhibition by natural extracts. This also confirms the sensitivity of the CE-UV/C⁴D assay developed in this

study. Moreover, it is interesting to specify that the exact same CE-based PL assay was used to monitor both the inhibition and the activation of the enzymatic activity.

PL modulation potential of natural purified compounds

The influence of **11** purified natural compounds on PL activity was evaluated (Table II.2) using the CE-UV/C⁴D offline based assay. All of these compounds were extracted and purified from oakwood used for wine aging with the exception of compound **1** which was purified from grapes and wine. These compounds can be divided into three groups based on their chemical structures presented in Table II.2: flavonoids (compound **1**), lignans (compounds **2** to **4**) and triterpenoids (compounds **5** to **11**). Figure II.12 represents graphically the effects of the assayed compounds at 1 mg mL⁻¹ on PL activity. Many of the investigated compounds demonstrated activation of PL reflected by a positive activity. Compounds **6** and **10** demonstrated the highest PL activation percentages (37 ± 1% and 40 ± 0.5%, respectively). Compounds **3**, **4** and **7** induced moderate activation of PL (between 20 and 27%) whilst slight PL activation by compounds **1**, **2** and **8** was observed (between 5 and 13%). On the other hand, the compounds **5**, **9** and **11**, induced considerable inhibition of PL. Compounds **5** and **11** demonstrated good inhibition of PL activity; 51 ± 1% and 57 ± 4%, respectively.

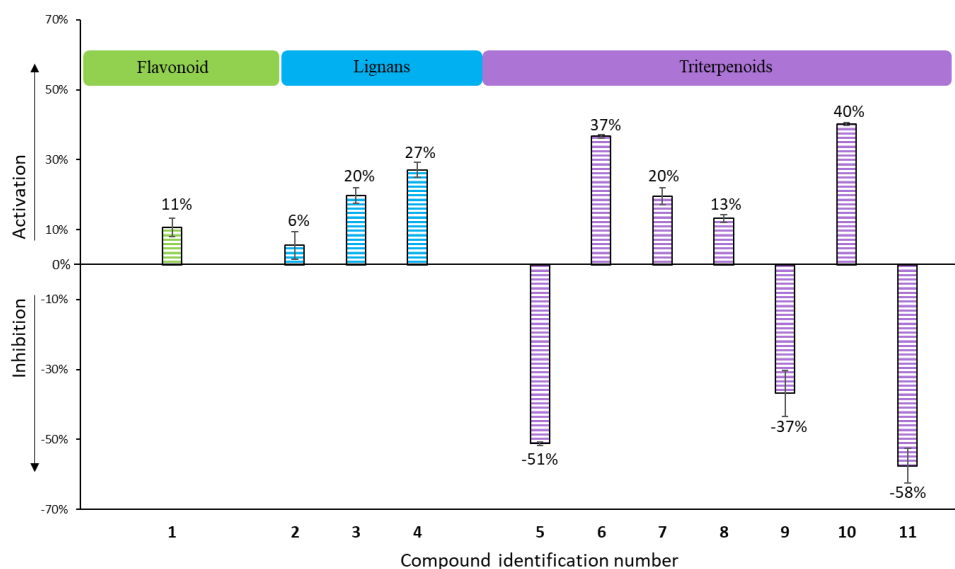


Figure II.12: Modulation of PL activity by **11** compounds purified from oakwood and wine extracts (structures in Table II.2). The compounds were assayed at 1 mg mL⁻¹ using the offline assay (**1-11**). The influence of these compounds on PL activity was relative to control reactions conducted in the absence of the compounds. Error bars indicate the standard deviation on PL activity for n = 3 experiments

The potential of these two compounds was also evaluated by using the online assay previously developed. The results confirm the inhibition potential of both compounds **5** and **11**, however lower inhibition was evaluated ($23 \pm 4\%$ and $40 \pm 5\%$, respectively) due to the dilution phenomena lowering the concentration of the modulators at the time of interaction with the enzyme. The ratios of the residual activities of the online and offline assays were similar, 1.6 for **5** and 1.4 for **11**, demonstrating a constant effect of dilution in the online assay. These ratios also suggest that the dilution factor is not as high as expected probably due to incomplete mixing between all reactant plugs.

The dissimilarity in the bioactivity of the **11** compounds tested is due to the difference in their structure [77]. Compound **5**, bartogenic acid, one of the most potent tested PL inhibitors, is a penta-cyclic triterpenoid having carboxyl groups at positions 24 and 28 bound respectively to C4 and C17. Compounds **6** to **11** all have a common penta-cyclic backbone structure very similar to that of **5**. Compound **6** is carboxylated at position 23 and has a glucosyl moiety attached to position 28. Compared to the bioactivity of **5** against PL, compound **6** resulted in PL activation. Glycosylation and/or the position of the carboxyl group thus appears to play a role in attenuating any enzyme inhibition induced by the molecules. On a similar note, the structures of compounds **9** and **10** differ solely in the positions of the carboxyl groups (position 24 in **9** and position 23 in **10**). Contrasting modulations of PL activity were observed where **9** was found to be an interesting inhibitor whereas the compound **10** was amongst the most activating compounds. Relating these findings to the position of the carboxyl group shows a similar trend to that described for compounds **5** and **6**. Nonetheless, the position of the carboxyl group in the structure does not seem to be the sole contributor to PL modulation. For instance, compound **11** has the carboxyl group at position 23 yet has demonstrated the highest PL inhibition percentage amongst all screened compounds. Interestingly and in contrast to compounds **9** and **10**, compound **11** is galloylated at C3. The presence of galloyl groups in the structure of the compounds has been found to influence competitive inhibition of PL. However, this inhibition was weaker in non-flavonoid compounds compared to flavonoids [78]. Thus, the inhibitory potential of compound **11** can be due to the absence of a glucosyl moiety and/or the presence of a galloyl moiety at C3. This can be further supported by comparing the structures of compounds **7** and **8** which have respectively demonstrated moderate and limited activation of PL despite both containing a galloyl moiety in their structures at position 23 in **7** and attached to C3 in **8**. Both compounds are however,

glycosylated at position 28 thus suggesting that the glycosylation at this position results in decreased inhibition towards PL. In conclusion, glycosylation seems to negate the effects of other substituents such as the galloyl group particularly when this glycosylation is at position 28. Additionally, compounds with glucosyl-galloyl groups on C4 show a modulation of PL activity dependent on the position of the carboxyl groups, demonstrating inhibition when the latter is at position 24 and activation at position 23. In the recent work of J. Liu *et al.* [76], several natural compounds demonstrated interesting PL inhibition using a heterogeneous CE-based PL inhibition assay. Mainly, kaempferol demonstrated the highest PL inhibition; respectively 92% and 96% at 50 mg mL⁻¹ and 100 mg mL⁻¹. In our work, compound **11** was shown to inhibit PL by 58% using only 1 mg mL⁻¹ (50 – 100 times lower compared to literature). On a similar notice to that described for the offline assay, the results described here for modulation of PL activity by purified compounds demonstrate interesting PL inhibition potential of the compounds at merely 1 mg mL⁻¹. Additionally, despite the dilution associate with online CE assays, some molecules demonstrated potent PL inhibition at final concentrations inferior to 1 mg mL⁻¹ reflecting the sensitivity of the online CE-UV/C⁴D assay developed.

IV. Conclusion

In this study, we described for the first time the development and optimization of homogeneous (*i.e.* using non-immobilized enzyme) offline and online CE-based lipase assays hyphenated to dual spectrophotometric and conductometric detection (CE-UV/C⁴D). A lab-made 3D printed scaffold was constructed to hold the C⁴D detection cell while avoiding any coolant liquid leakage. Tris/MOPS (10 mM, pH 6.6) was chosen as the BGE for providing good peak symmetries, low LOD and short analysis times. This buffer was also chosen as the IB as it also proved to be adequate for PL activity. Having the same buffer as both the BGE and IB facilitated the CE online assay as there was no longer need to implement the partial filling technique. It also limited spontaneous non-enzymatic 4-NPB hydrolysis observed at higher pH. The developed offline CE-UV/C⁴D assay was used to screen six aqueous extracts of various parts of different plants for PL activity modulation. These extracts tested at 1 mg mL⁻¹ revealed different PL activity depending on the plant nature (hawthorn, blackcurrant, *Chrysanthellum americanum*) and the part of the plant (leaves *vs* flowers). Hawthorn leaves presented a promising inhibition potential (37%) whereas the flowers had an opposite effect on PL activity (activation by + 22-26%). Furthermore, triterpenoid compounds **5**, **9** and **11**, purified from oakwood used for wine aging, were shown for the first time to have interesting inhibitory effect on PL (up to 57%), which could be considered as comparable to the one induced by the reference PL inhibitor orlistat. The modulation was related to the structures of these compounds where the presence of a glucosyl, galloyl or carboxyl groups at certain positions of the molecule modulated the activity of PL. All these results are very interesting to further develop our structure-activity relationships (SAR) studies, helping to understand and then to predict biological activity toward PL from molecular structure of interesting compounds. Further studies will be conducted in the near future to obtain additional insights into the binding and inhibition mechanisms of the best inhibitors identified. Mainly, microscale thermophoresis will be used as a complementary technique to determine the dissociation constant of inhibition (K_i) of such promising compounds. It would also be interesting to evaluate the influence of the ionic strength of the IB on the bond strength and therefore the potency of the compounds against PL.

A. Supplementary information

Screening for pancreatic lipase natural modulators by capillary electrophoresis hyphenated to spectrophotometric and conductometric dual detection

Ghassan Al Hamoui Dit Banni¹, Rouba Nasreddine¹, Syntia Fayad^{1,2}, Phu Cao-Ngoc³, Jean - Christophe Rossi³, Laurent Leclercq³, Hervé Cottet³, Axel Marchal² and Reine Nehmé^{1*}

¹ Institut de Chimie Organique et Analytique (ICOA), CNRS FR 2708 – UMR 7311, Université d'Orléans, 45067 Orléans, France

² Université de Bordeaux, ISVV, EA 5477, Unité de recherche Œnologie, USC 1366 INRA, F- 33882, Villenave d'Ornon, France

³ IBMM, University of Montpellier, CNRS, ENSCM, 34059 Montpellier, France

* e-mail: reine.nehme@univ-orleans.fr

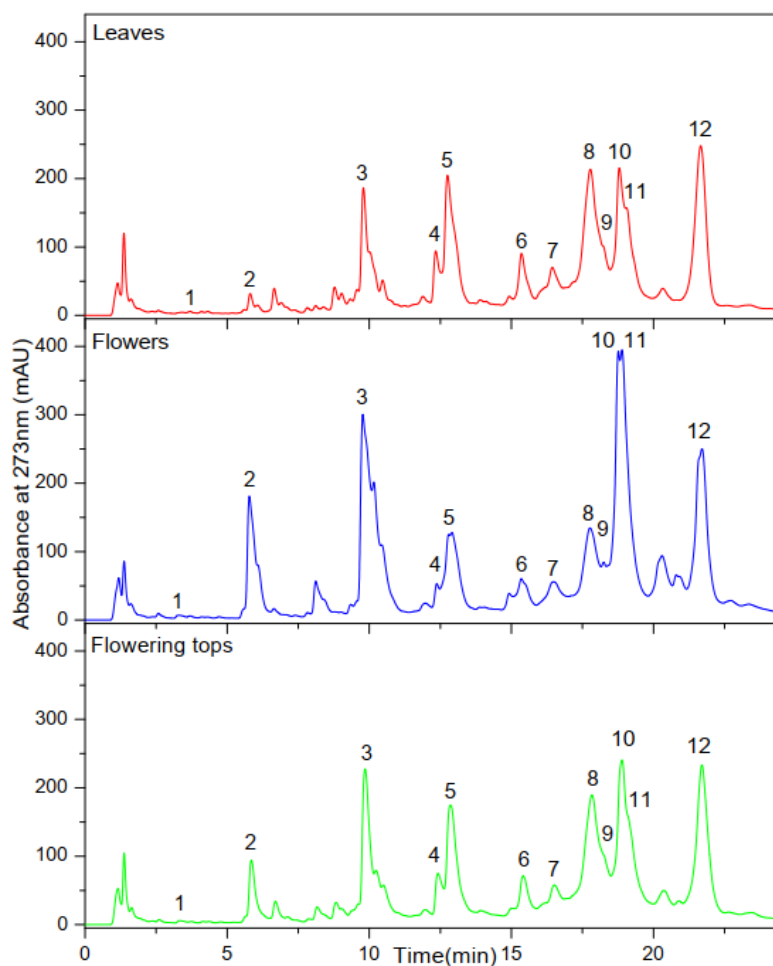


Figure II.13: UHPLC profiles of different parts of hawthorn extracts obtained from infusion extraction modes for ground fresh leaves, flowers and flowering tops (fresh materials harvested in April 2020). Experimental conditions: A Kinetex C18 100A 100×2.1 mm, 2.6 μm column, binary solvent system: water/formic acid (1%, v/v) as solvent A and acetonitrile/formic acid (1%, v/v) as solvent B. Gradient program: 5% B, then increase of B to 100% in 35 min with a convex increase, flow rate: 0.3 mL·min⁻¹, injection volume: 20 μL. Column temperature: 20°C, UV monitoring at 273 nm. UV-Vis spectra recorded between 200 and 550 nm. Peak identification: 1 = Cyanidin, 2 = 5-O-caffeoylquinic acid, 3 = chlorogenic acid, 4 = procyanidin B2, 5 = epicatechin, 6 = procyanidin C1, 7 = cinnamtanin A2, 8 = vitexin-2-O-rhamnoside, 9 = pinnatifinose A, 10 = hyperoside, 11 = isoquercetin, 12 = apigenin C-hexoside

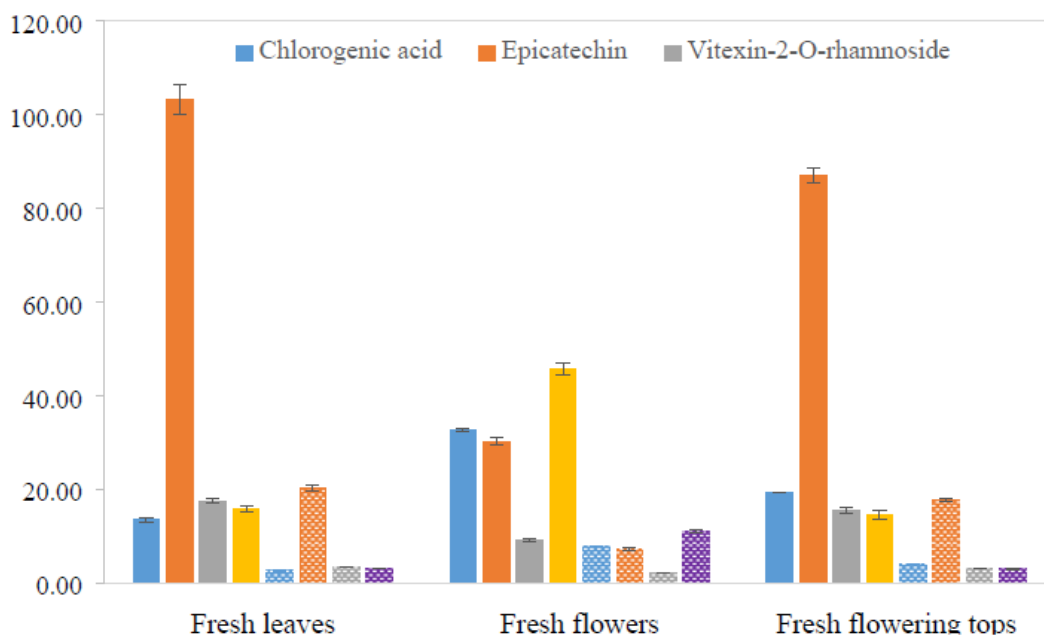


Figure II.14: Quantification of chlorogenic acid (peak 3), epicatechin (peak 5), vitexin-2-*O*-rhamnoside (peak 8), isoquercetin (peak 11) were determined by external calibration, using commercially available standards. Error bars: ± 1 standard deviation calculated on $n = 3$ repetitions. ■■■■, in mg g^{-1} dry extract. ■■■■, in mg g^{-1} fresh plant

Table II.4: Comparison of the conductivities and effective mobilities of both BGEs using PeakMaster v5.3

BGE	Tris/CHES (12 mM, pH 9.0)	Tris/MOPS (10 mM, pH 6.6)
Conductivity (S m^{-1})	0.054	0.046
Effective mobility ($\text{m}^2 \text{V}^{-1} \text{s}^{-1}$)	Co-ion CHES: -5.1	Co-ion MOPS: -5.7
	4-NP: -29.3	4-NP: -7.9
	Butyrate: -30.0	Butyrate: -30.0

Part B:

Microscale thermophoresis, complemented by capillary electrophoresis, to highlight lipase-ligand interactions

I. Introduction

In the second part of this chapter, the investigation of the binding potential of ligands towards lipases present in crude pancreatic extracts was carried out using microscale thermophoresis (MST). Acquiring binding data is as important as acquiring information about enzymatic activity in drug screening and discovery. In fact, the use of both activity and binding data in complementarity is a powerful approach to construct a richer profile about the molecular mechanisms occurring during macromolecular interactions or interactions of proteins with small ligands. Several techniques have been historically used to acquire binding data such as isothermal calorimetry (ITC), surface plasmon resonance (SPR) or nuclear magnetic resonance (NMR). All of the aforementioned techniques have their strengths and weaknesses and can all be used for the evaluation of the binding affinity between an interaction couple represented in terms of the equilibrium dissociation constant K_d [79].

MST is a relative newcomer where the interacting molecules will migrate along a temperature gradient inside a thin capillary as a result of a phenomenon known as thermophoresis or the Soret effect [79–81]. This migration can be monitored using a fluorescence detector, thus requiring labeling of one of the interaction partners, and the fluorescence is traced as a function of time to produce a binding curve from which K_d is evaluated. The temperature difference between two points in space results in the thermodiffusion of molecules from the first point (hot) to the second (cold) (Figure II.15). This can be quantified by the Soret coefficient S_T from Equation II.4 below:

$$C_{hot}/C_{cold} = \exp(-S_T \Delta T) \quad \text{Equation II.4}$$

where C_{hot} and C_{cold} are respectively the concentrations of the molecules in the hot and cold points in space and ΔT is the temperature difference (created by an IR laser).

S_T is calculated by Equation II.5

$$S_T = \frac{A}{kT} \left(-s_{hyd} + \frac{\beta \sigma_{eff}^2}{4\epsilon\epsilon_0 T} \times \lambda_{DH} \right) \quad \text{Equation II.5}$$

where A is the particle surface, kT is the kinetic energy of the particles represented as the product of the Boltzmann constant (k) and the temperature (T), S_{hyd} is the hydration entropy which represents the molecule's hydration shell, λ_{DH} is the Debye length which represents the distance over which the charges of ions or electrons are significantly separated, ϵ is the dielectric constant, ϵ_0 is the vacuum permittivity, σ_{eff} is the particle's effective charge, β is a factor obtained for temperature derivatives considering λ_{DH} and the ϵ .

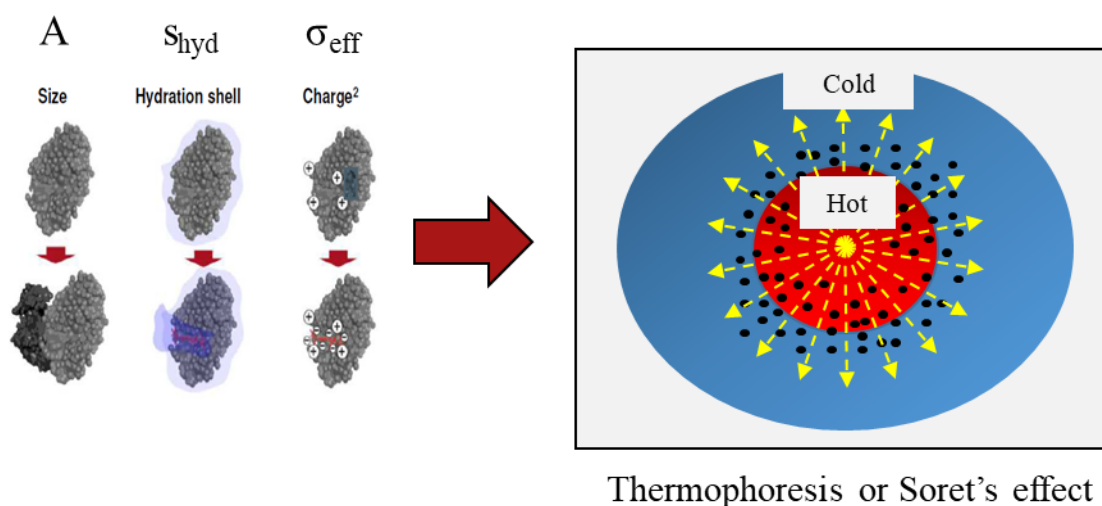


Figure II.15: Factors affecting the Soret coefficient under constant buffer conditions (Left) and, the thermophoretic migration of the labeled targets from hot to cold regions (Right)

Equation II.5 thus states that, under the assumption that the conditions of the MST buffer are not variable, *i.e.* constant pH, ionic strength and temperature, the Soret coefficient depends on three parameters: size, charge and hydration entropy (Figure II.15). The binding of a ligand to a target is granted to induce a change in at least one of these parameters manifested as a detectable variation in the fluorescence response from thermophoretic migration of the bound target compared to the unbound one [80].

MST is considered one of the most sensitive biophysical techniques capable of evaluating K_d as low as few pM [82]. Target labeling with MST is not a prerequisite as long as the target contains fluorescent residues such as aromatic amino acids. Otherwise, the target may be labeled covalently

using commercially available dyes or *via* homemade dyes and fusion proteins [83]. The target needs not to be immobilized using MST and is used free in solution. Another interesting aspect of MST is the possibility to work with complex biological samples such as sera and blood samples [84].

In this work, we optimized an MST binding assay for the determination of the binding affinities of small ligands towards PL from crude porcine pancreatic extracts after appropriate labelling. The importance of carrying out binding assays hand in hand with catalytic activity assays using CE (Part A of this chapter) in order to elaborate the mechanism of ligand modulation in the process of drug screening was pointed out as was presented in Chapter I of this thesis. MST binding affinity analyses were carried out on a Monolith NT.115 Pico from NanoTemper Technologies. Sixteen uncoated capillaries, into which around 4 μL of sample is aspirated, can be scanned individually. The thermal gradient resulting in the Soret effect, or thermophoresis, is generated using an infrared (IR) laser, at a wavelength approximately $\lambda = 1475 \text{ nm}$, which results in a local increase in temperature of the solution in the capillary. The excitation ($\lambda = 605\text{-}645 \text{ nm}$) and the fluorescence emission ($\lambda = 680\text{-}685 \text{ nm}$) of the labeled target (PL*) in the solution are detected through the same objective of the IR laser. Dissociation constants are evaluated by titrating a fixed concentration of the PL* with a range of 16 different ligand concentrations tracing a dose-response curve. An example of a typical MST trace is presented below in Figure II.16 and shows a decrease in the relative fluorescence with time due to the migration of the labeled targets away from the center of the capillary due to thermophoresis.

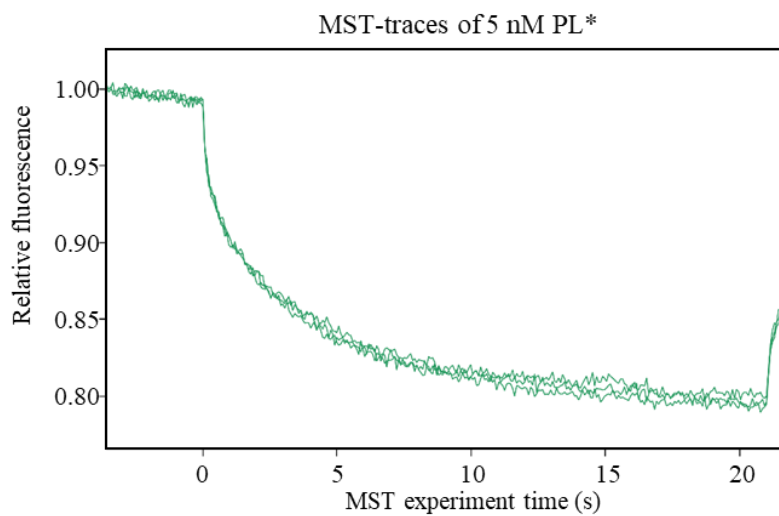


Figure II.16: An example of an MST trace using 5 nM of PL*. MST buffer: 20 mM NaH₂PO₄ + 77 mM NaCl supplemented by 0.05% Triton-X (pH 6.6), LED excitation power: 20%; laser power: medium; temperature: 37°C

II. Results

The results are summarized in the article titled “**Investigation of lipase-ligand interactions in porcine pancreatic extracts by microscale thermophoresis**”, *Analytical and bioanalytical chemistry* (2021), 413: 3667-3681, DOI: 10.1007/s00216-021-03314-7

Investigation of lipase-ligand interactions in porcine pancreatic extracts by microscale thermophoresis

Ghassan Al Hamoui Dit Banni¹, Rouba Nasreddine¹, Syntia Fayad³, Cyril Colas^{1,2}, Axel Marchal³ and Reine Nehmé^{1*}

¹Institut de Chimie Organique et Analytique (ICOA), CNRS FR 2708 – UMR 7311, Université d’Orléans, 45067 Orléans, France.

² Centre de Biophysique Moléculaire, CNRS-Université d’Orléans, UPR 4311, 45071 Orléans CEDEX 2, France

³ Université de Bordeaux, Institut des Sciences de la Vigne et du Vin (ISVV), EA 5477, Unité de recherche Œnologie, USC 1366 INRA, 33882, Villenave d’Ornon, France.

* e-mail: reine.nehme@univ-orleans.fr

Keywords

Binding affinity; Capillary electrophoresis; Enzymatic assays; High-resolution mass spectrometry; Lipase; Microscale thermophoresis

Abstract

The evaluation of binding affinities between large biomolecules and small ligands is challenging and requires highly sensitive techniques. Microscale thermophoresis (MST) is an emerging biophysical technique used to overcome this limitation. This work describes the first MST binding method to evaluate binding affinities of small ligands to lipases from crude porcine pancreatic extracts. The conditions of the MST assay were thoroughly optimized to successfully evaluate the dissociation constant (K_d) between pancreatic lipases (PL) and triterpenoid compounds purified from oakwood. More precisely, the fluorescent labeling of PL (PL*) using RED-NHS dye was achieved *via* a buffer exchange procedure. The MST buffer was composed of 20 mM NaH_2PO_4 + 77 mM NaCl (pH 6.6) with 0.05% Triton-X added to efficiently prevent protein aggregation and adsorption, even when using only standard, uncoated MST capillaries. Storage at -20°C ensured stability of PL* and its fluorescent signal. MST results showed that crude pancreatic extracts were suitable as a source of PL for the evaluation of binding affinities of small ligands. Quercotriterpenoside-I (QTT-I) demonstrated high PL* binding affinity (31 nM) followed by 3-O-galloylbarrinic acid (3-GBA) (500 nM) and bartogenic acid (BA) (1327 nM). To enrich the 50 kDa lipase responsible for the majority of hydrolysis activity in the crude pancreatic extracts, ammonium sulfate precipitation was attempted and its efficiency confirmed using capillary electrophoresis (CE)-based activity assays and HRMS. Moreover, to accurately explain enzyme modulation mechanism, it is imperative to complement binding assays with catalytic activity ones.

Introduction

The process of drug screening is costly and time-consuming starting from several thousands of candidate molecules that are gradually reduced to few tens of molecules demonstrating the highest effectiveness. This effectiveness depends on several factors such as the candidate molecule's affinity to a biological or chemical entity (enzymes, receptors, ion channels), its influence on the inhibition or induction of this entity or unspecific interactions with other targets resulting in toxic and undesirable side effects. When targeting enzymes, two main approaches are implemented to study the efficiency of new drug candidates: by measuring the catalytic activity of the enzyme in the presence of the drug and by evaluating the strength of the binding interaction (or affinity). The binding affinity of a ligand to a target can be evaluated through the measurement of the equilibrium dissociation constant (K_d) [85,86]. The K_d value is used to rank different ligands as a function of their binding likelihood to the target. This helps in the determination of potential hits and its use in complementarity with enzyme activity assays provides a more complete image about the investigated molecules and their physiochemical influence and the subsequent biological effects that ensue. There exists a plethora of conventional techniques described for the determination of binding affinities. Separative techniques such as high performance affinity chromatography (HPAC) and affinity capillary electrophoresis (ACE) involve the separation of the unbound ligand from the ligand-enzyme complex and their consequence detection and quantification [87–93]. However, drawbacks resulting from enzyme immobilization and unspecific interactions between the solid phase and the ligands are associated with HPAC [92] whereas unspecific adsorption of the enzyme to the silica capillary wall [93] is associated with ACE. Isothermal titration calorimetry (ITC) [94–97], surface plasmon resonance (SPR) [98–100] and nuclear magnetic resonance (NMR) [101–103] are all non-separative techniques that involve the detection of changes in certain physiochemical properties, resulting from ligand binding to the enzyme, which are later used to evaluate the binding affinity [104]. Both ITC and SPR are widely used. However, sample consumption is considerable ($\approx 300 \mu\text{L}$) with ITC [97] and immobilization of the target is a prerequisite of SPR which introduces disadvantages such as steric hindrance to ligand binding [100]. NMR provides structural information about the ligand, the enzyme and their complexation product. However, the protein target may require isotopic labeling which represents a limitation of the technique [101].

In this work, we used microscale thermophoresis (MST), a non-separative technique introduced in 2010 by Philipp Baaske *et al.* [105] for binding affinity analyses. It is a user-friendly technique that overcomes limitations of the classical binding affinity analyses techniques with no requirement for target immobilization, low sample and reagent consumption (few μLs), short analysis times and freedom of buffer choice, *i.e.* from chemical buffer solutions to complex biological samples such as cell lysates and serum samples [84]. This technique is particularly well adapted for evaluating interactions between enzymes (large molecules) and modulatory ligands (small molecules) which requires high sensitivities that are not achievable by conventional techniques. With MST, it is possible to evaluate K_d values in the orders of pM [82]. MST has been used for studying biomolecular interactions such as protein-protein [106,107], protein-nucleic acids [108–110] and enzyme-ligand interactions [84,111]. MST involves the diffusion of molecules in a temperature gradient created locally by optical heating provided through an infra-red (IR) laser which results in a 2–6°C temperature increase. This phenomenon is known as thermophoresis and its magnitude and direction are governed by the size, charge and solvation of the molecules [29,112]. The binding of a ligand to a target molecule will modify at least one of these parameters resulting in an alteration of the diffusion rate which is translated into a change in the local concentration of the molecules. Fluorescence plays a crucial role in MST experiments and one of the interaction partners is required to be fluorescent either intrinsically coming from ‘built-in’ fluorescent blocks within the molecule or extrinsically by fluorophores bound to the molecules. The fluorescence of the labeled molecules is monitored in response to thermophoresis and translated to a binding curve from which K_d can be evaluated [80,83,113].

To evaluate the catalytic activity of a target enzyme, several techniques have been used such as colorimetric assays [114], miniaturized microtiter plates assays hyphenated to optical UV or fluorescence detection [115,116], chromatographic based assays [117] and capillary electrophoresis (CE)-based assays [50,76,118]. The latter technique has been extensively used for the determination of enzymatic catalytic activities as well as the influence of drugs on the enzyme activity without any modification of the target [36,111,119]. We have recently described an efficient method for assaying pancreatic lipase (PL) activity using CE hyphenated to dual spectrophotometric and conductometric detection (CE-UV/C⁴D) and for the screening of different modulators of PL activity implementing both the offline and online CE modes [118]. The excessive increase of fat cells in the body due to increased dietary intake, reduced physical activity, genetic

disorders as well as other factors is defined as obesity. It is associated with diseases such as diabetes, hypertension, cardiovascular disorders and some cancers [120]. According to the world health organization (WHO), the number of obese adults between 1975 and 2016 has tripled with an estimate of over 650 million obese adults worldwide [121]. It is thus interesting to study PL given their major contribution to fat digestion and absorption making them targets for drugs used to combat obesity [122]. It is worth mentioning that the term PL refers to more than one lipase enzymes present in the extracts of porcine pancreas. Orlistat is a potent PL inhibitor drug prescribed for the long-term obesity management and is currently the only commercial PL inhibitor in Europe and in the USA [11]. Recently, many natural and synthetic molecules have been screened for PL inhibition with hopes of discovering new alternatives to orlistat due to the side-effects reported amongst patients on orlistat treatment [15,16].

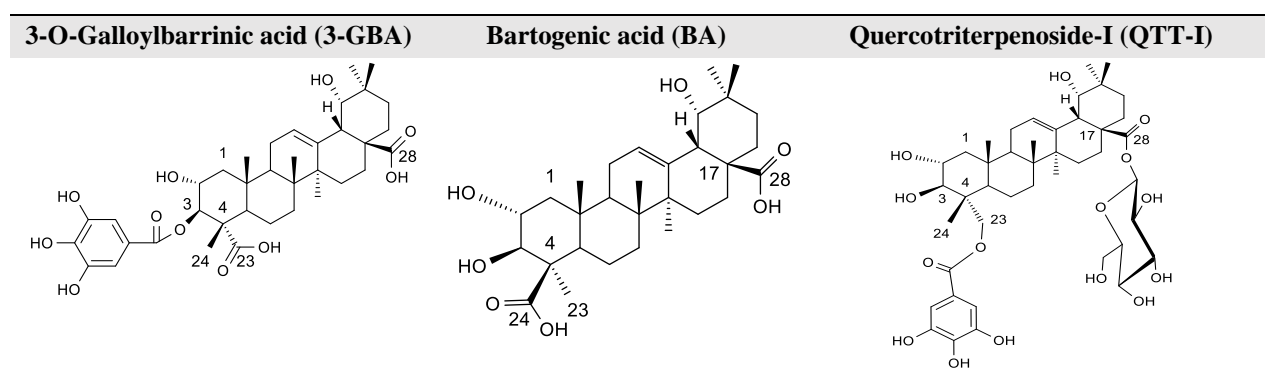
In this work, we describe, for the first time an MST-based assay to evaluate binding affinities of small ligands to PL from crude pancreatic extracts within the context of investigating binding interactions between large molecules and small ligands. Several parameters for the MST analyses were optimized such as the labeling protocol, concentration of labeled PL (PL*), MST buffer additives as well as storage and pre-incubation temperatures. The optimized MST assay was then used to evaluate the PL* binding affinity of three original molecules extracted and purified from oakwood, namely bartogenic acid (BA), 3-O-galloylbarrinic acid (3-GBA) and quercotriterpenoside-I (QTT-I) [55,56] in addition to the reference PL inhibitor, orlistat. We have previously demonstrated an interesting influence of these molecules on PL catalytic activity, as inhibitors and activators, using CE-UV/C⁴D and 4-nitrophenyl butyrate (4-NPB) as a substrate [118]. The complementarity between the results from the CE activity assay and the novel MST binding assay will be addressed. Despite being used by various research groups [21,50,123,124], commercialized PL such as the one used in this study is available in the form of lyophilized, crude porcine pancreatic extracts that contain different proteins such as proteases and other types of lipases [125]. As a result, we attempted to enhance the purity of PL from crude porcine pancreas extracts using precipitation by ammonium sulfate followed by desalting using solid phase extraction (SPE). The effectiveness of this purification protocol was assessed using CE-UV/C⁴D based catalytic assays, and high-resolution mass spectrometry (HRMS).

Materials and methods

Chemicals

Tris(hydroxymethyl)aminomethane (Tris) ($C_4H_{11}NO_3$), 3-(N-morpholino)propanesulfonic acid (MOPS) ($C_7H_{15}NO_4S$), 4-nitrophenyl butyrate (4-NPB) ($C_{10}H_{11}NO_4$), the lipase enzyme used throughout this study was lipase from crude porcine pancreas extracts (EC 3.1.1.3, Type II, 100 – 500 units mg^{-1} of protein), bovine serum albumin (BSA), orlistat ($C_{29}H_{53}NO_5$; MW= 495 $g\ mol^{-1}$), lithium hydroxide monohydrate (LiOH.H₂O), sodium chloride (NaCl) and HPLC grade formic acid (HCOOH) were purchased from Merck (Saint-Quentin Fallavier, France). Ammonium sulfate ((NH₄)₂SO₄) and hydrochloric acid (HCl) were purchased from Fisher Scientific (Illkirch Graffenstaden, France). HPLC grade methanol (MeOH), ethanol (EtOH) and sodium dihydrogen phosphate (NaH₂PO₄·2H₂O) were purchased from VWR International (Fontenay-sous-Bois, France). HPLC grade acetonitrile (ACN) was purchased from Carlo Erba (Val de Reuil, France). Dimethyl sulfoxide (DMSO) was purchased from J.T. Baker (Deventer, Holland). Water used throughout this study was ultra-pure (18 MΩ-cm) produced by a Purelab flex apparatus from Veolia (Aubervilliers, France). Bartogenic acid ($C_{30}H_{46}O_7$; MW= 518 $g\ mol^{-1}$) (BA), 3-O-galloylbarrinic acid ($C_{37}H_{50}O_{11}$; MW= 670 $g\ mol^{-1}$) (3-GBA) and 23-O-galloylarjunglucoside; ‘Quercotriterpenoside-I’; ($C_{43}H_{62}O_{15}$; MW= 818 $g\ mol^{-1}$) (QTT-I) were extracted from oakwood using centrifugal partition chromatography fractionation and purified by HPLC as previously described [55,56] (Table II.5). The pH of the solutions was measured using a MeterLab PHM201 Portable pH-Meter (Radiometer Analytical, Villeurbanne, France). Solutions were filtered through polyvinylidene fluoride (PVDF) syringe filters of 0.2 μm pore size purchased from Agilent Technologies (Les Ulis, France).

Table II.5: Structures of PL modulating ligands purified from oakwood extracts by centrifugal partition chromatography fractionation and HPLC [55,56]



Instrumentation and operating conditions

Microscale thermophoresis (MST) for PL binding assays

The MST analyses were performed on a Monolith NT.115 Pico (NanoTemper Technologies). Standard uncoated capillaries used throughout this study as well as the Monolith protein labeling kit RED-N-hydroxysuccinimide (NHS) 2nd generation containing the RED-NHS dye, labeling buffer (130 mM NaHCO₃, 50 mM NaCl; pH 8.2), Tween 20, buffer exchange column and protein purification column were purchased from NanoTemper Technologies. The LED MST power was set to medium. The excitation and emission wavelengths were 605-645 nm and 680-685 nm, respectively. The temperature at which the MST was carried out was set at 37°C. MST control and data analysis was carried out using MO.Control (v.1.6) and MO.Affinity Analysis (v.2.3) softwares, respectively. The MST buffer used throughout this study was a solution of 20 mM NaH₂PO₄ and 77 mM NaCl adjusted to pH 6.6 using 1 M ammonia.

Different parameters were optimized for MST analyses: PL labeling, PL* concentration, MST buffer additives and temperature conditions.

a. PL labeling: RED-NHS dye was reconstituted in 25 µL DMSO to a concentration of 300 µM. Ten µL of the dye solution were then mixed with 90 µL of PL. These conditions represented a 3-fold dye excess. The PL-dye solution was then incubated in a dark environment at room temperature. During the incubation period, the protein purification column was conditioned incrementally with 8 mL of MST buffer. After incubation, the PL-dye mixture was transferred to the conditioned protein purification column followed by 550 µL of MST buffer. PL* was eluted from the column by 450 µL of MST buffer. We compared PL labeling with and without buffer exchange. For direct PL labeling without buffer exchange, 90 µL of 20 µM PL prepared in MST buffer were mixed with 10 µL of RED-NHS dye at 300 µM and incubated for 15 min or 50 min at the conditions described above. PL* was then purified from unbound dye molecules using the protein purification column as described above. On the other hand, labeling PL with buffer exchange was carried out in three steps illustrated in Figure II.17. The first step involved preparing 20 µM PL in 10 mM Tris/ 40 mM MOPS (pH 6.6) and exchanging this buffer with the labeling buffer using a buffer exchange column (Figure II.17-1st step). Briefly, the buffer exchange column was equilibrated with 300 µL of labeling buffer. The column was then centrifuged for 1 min at 2000 g and the flow-through was discarded. This equilibration was repeated 3 times. Then, 100 µL of PL in Tris/MOPS was transferred to the buffer exchange column and the column was

centrifuged for 2 min at 2000 g. The collected flow-through contains PL constituted in labeling buffer. In the second step, 90 μL of PL in labeling buffer was mixed with 10 μL of RED-NHS dye (300 μM) and incubated for 30 min in the dark and at room temperature. After incubation, PL* was purified using the purification column as described earlier (Figure II.17-2nd step).

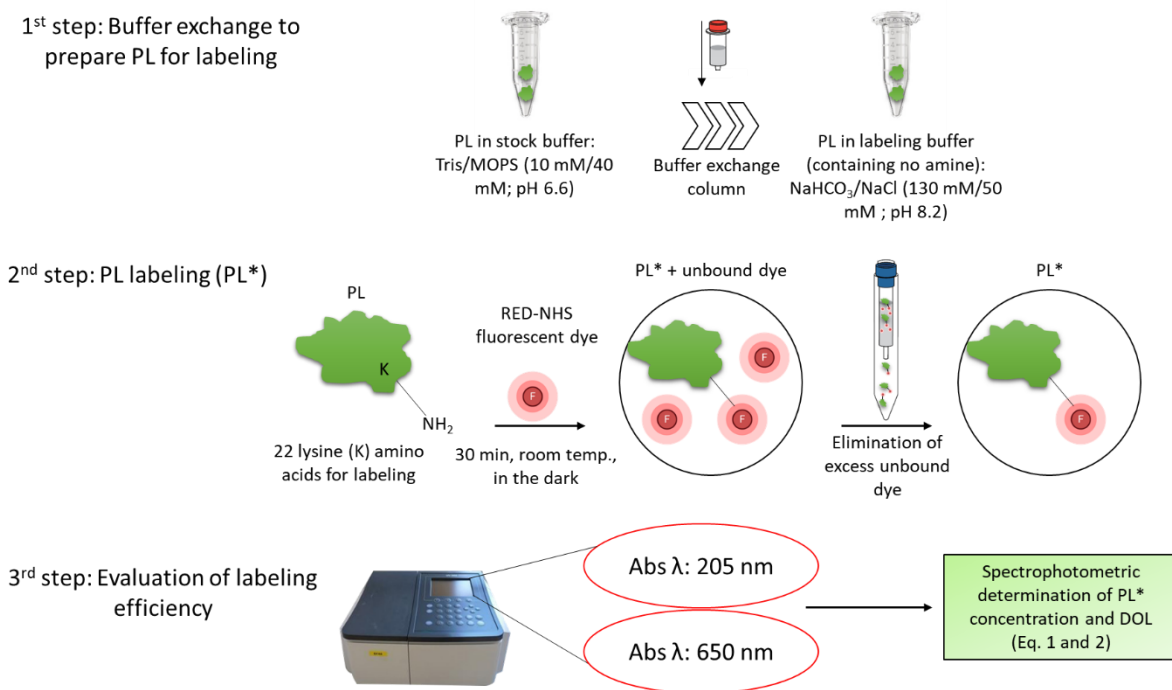


Figure II.17: Illustration of PL labeling for MST binding analysis using buffer exchange from Tris/MOPS (pH 6.6) to $\text{NaHCO}_3/\text{NaCl}$ (pH 8.2)

The third step involved the quantification of PL* concentration and the degree of labeling (DOL), a measurement of the ratio of unbound dye molecules to PL* (Figure II.17- 3rd step). This step was conducted similarly for PL labeled with and without buffer exchange. The PL* solution was transferred into quartz cuvettes with 10 mm optical path length and UV absorption of the solution was measured at a wavelength range of 190-800 nm at fast scan speeds with 0.5 nm sampling intervals using a UV-1800 UV-VIS spectrophotometer (Shimadzu, Kyoto, Japan). The concentration of PL* was calculated using the molecular weight (MW) of PL determined *via* high-resolution mass spectrometry (HRMS) ($\approx 55,374 \text{ g mol}^{-1}$) using the following Equation II.6:

$$C \text{ (M)} = \frac{A_{205} - (A_{650} \times 0.19)}{31 \times MW_{\text{Protein (Da)}}} \quad \text{Equation II.6}$$

where A_{205} is the absorption measured at a wavelength of 205 nm corresponding to the wavelength of absorption of the peptide bond, A_{650} is the absorption measured at 650 nm corresponding to the wavelength of absorption of the RED-NHS dye, 0.19 is the correction factor at 205 nm and 31 is the extinction coefficient of the protein at 205 nm [126].

Then, the DOL was measured using Equation II.7:

$$\text{Degree Of Labeling (DOL)} = \frac{A_{650}}{195,000 \times C} \quad \text{Equation II.7}$$

where $195,000 \text{ M}^{-1} \text{ cm}^{-1}$ is the molar absorbance of the RED-NHS dye and C is the molar concentration of the protein calculated using (Equation II.6).

b. PL concentration:* the fluorescence responses resulting from 3 different PL* concentrations; 1, 2 and 5 nM; were compared in order to choose the appropriate concentration of PL*. The three concentrations were prepared by diluting PL* based on the initial concentration calculated using (Equation II.6) in the MST buffer.

c. MST buffer additives: the influence of adding organic solvents and/or detergents to the MST buffer on the MST response profiles was evaluated using 6 different additives: ACN at 1-10%, EtOH at 1-10%, Tween-20 at 0.05% mixed with either MeOH or ACN at 1%, Tween-20 at 0.01% and 0.05%, and Triton-X at 0.05%.

d. Temperature conditions: both the temperatures of PL* storage as well as the pre-incubation temperatures of PL* prior to MST analysis were evaluated by observing changes in the fluorescence responses of PL*. For the PL* storage, two temperatures were tested, -80°C or -20°C . For the pre-incubation temperatures, PL* was pre-incubated 15 min at either 0°C or 37°C .

Small Ligand-PL* binding assays

The optimized MST method was applied to study the binding affinities of PL modulating small ligands. Three original triterpenoid compounds, BA, 3-GBA and QTT-I, were purified from oakwood extracts [55,56]. BA and QTT-I stocks were prepared, respectively, at 2 mM and 1.2 mM in 70/30 MeOH/H₂O (v/v) and 3-GBA stocks at 1.5 μM in 80/20 EtOH/H₂O (v/v). The binding of orlistat, the reference PL inhibitor, was also investigated. Stock solutions of orlistat were prepared

at 4.4 mM in DMSO. For binding affinity assays, each ligand was serially diluted across 16 tubes in which both the PL* concentration and ligand buffer percentage were fixed. The tubes were incubated for 15 min at 37°C and then centrifuged at 2000 g for another 15 min at room temperature before being transferred into the MST capillaries for analysis. The binding affinity assay of each ligand was repeated twice (n=2) and the data points merged into a single response curve. The fluorescence response was automatically evaluated 1.5 s after the IR laser is on.

The purification of 50 kDa lipase

A lipase purification protocol was adapted from the work of K. Shahani *et al.* [127]. Briefly, 3 g of crude porcine pancreas extract were dissolved in 10 mM cold sucrose solution. After centrifugation at 2000 g, 4°C for 15 min using a Jouan BR4i multifunction centrifuge (Thermo Electron, MA, USA), the obtained supernatant was subjected to precipitation by saturated, cold, ammonium sulfate solution (4 M) on ice with constant stirring for 30 min. The precipitated solution was then centrifuged at 10000 g, -1°C for 30 min and the acquired pellet was rinsed with half saturated, cold ammonium sulfate solution (2 M) and then dissolved in 10 mM cold sucrose. The solution was then subjected to SPE in order to eliminate excess salt carried over from the ammonium sulfate precipitation step. Bond Elut straight barrel C18 SPE cartridges (Agilent technologies) were used with 1000 mg solid phase mass and 40 µm particle size. The SPE cartridge was installed onto a vacuum manifold and sequentially conditioned with 6 mL MeOH, 6 mL ACN and 12 mL H₂O. Then, 10 mL of the salt precipitated solution were transferred into the cartridge. A washing step was then carried out using 12 mL H₂O. The elution solvent was 5 mL of 10 mM Tris/ 40 mM MOPS (pH 8.2) supplemented with 10% ACN. PL activities of salt precipitated crude extracts and SPE eluted samples were assayed using our previously developed CE-UV/C⁴D assay as described in [118] and compared to those of crude pancreatic extracts. Additionally, HRMS analyses were carried out to assess the effectiveness of ammonium sulfate precipitation and SPE on the purification of PL and were compared to HRMS analysis of crude pancreatic extracts. An online-desalting step was also carried out prior to the HRMS analyses to eliminate excess salt since as detailed in the upcoming “HRMS analyses” section.

CE-based assay of PL activity

In this work, an optimized CE-UV/C⁴D PL assay previously developed by our group was implemented to evaluate PL activities of crude pancreatic extracts obtained after ammonium sulfate precipitation and SPE [118].

HRMS analyses

Crude porcine pancreas extracts as well as the ammonium sulfate precipitated and SPE eluted PL fractions were analyzed by HRMS. An Ultimate 3000 RSLC ultra-high-performance liquid chromatography (UHPLC) system composed of an autosampler, a binary pump and a thermostated compartment (Dionex, Germering, Germany) was used to deliver the sample through a MassPREP online desalting cartridge (2.1 x 10 mm) from Waters (Saint-Quentin-en-Yvelines, France) to prevent extensive ion suppression due to excess salt concentrations in all samples, those after salting out only or those after salting out followed by SPE. The mobile phase was composed of H₂O + 0.1% (v/v) formic acid (A) and ACN + 0.1% (v/v) formic acid (B) at a flow rate of 500 µL/min. The mobile phase gradient was as follows: 0-1 min, 5% B; 1-2.5 min, 90% B; 2.5-2.6 min, 5% B; 2.6-2.9 min, 5% B with a switch at 1.5 min from waste to the MS analyzer. Unless otherwise stated, the sample injection volume was 1.5 µL. The MS analysis was carried out on a maXis UHR-Q-TOF mass spectrometer (Bruker, Bremen, Germany) with an electrospray ion source (ESI) working in positive mode. The capillary voltage was set at +4.5 kV. Nitrogen was used as the drying gas at a flow rate of 9 L min⁻¹ heated at 200°C and as nebulizing gas at a pressure of 2 bar. The in-source collision induced dissociation energy was 70 eV. All the MS data were processed using DataAnalysis 4.4 (Bruker). A solution of pure bovine serum albumin was prepared in water at 1 µM and used to validate the HRMS method prior to its use for PL analyses. The mass spectra were deconvoluted using MaxEnt algorithm in order to group together the different charge state ions originating from the same protein.

Results and discussion

This work can be divided into three main headlines. Through exploration of the literature dealing with MST-binding assays, we identified several parameters that can be optimized in order to successfully and efficiently obtain K_d values. For this, we carefully optimized PL labeling, PL* working concentration, MST buffer additives and temperature conditions (storage and pre-

incubation). Then, the optimized MST method was then applied to evaluate the binding affinities of 3 original PL modulatory ligands in addition to evaluating the response of covalent binding of orlistat to PL*. Finally, we attempted to purify a single 50 kDa lipase from crude porcine pancreas extracts by ammonium sulfate precipitation followed by SPE desalting and assessing the effectiveness of this purification using CE-UV/C⁴D, HRMS and MST binding analyses.

I- Optimization of MST analysis conditions

a. Optimization of PL labeling: labeling is a crucial step in MST analysis where one of the binding partners, *i.e.* the target enzyme or the ligand is conjugated to a fluorescent dye. Firstly, we have investigated direct PL labeling without buffer exchange. For PL labeling without buffer exchange, PL was constituted directly in the NaH₂PO₄/NaCl MST buffer which was used previously by our group for MST binding assays of other hydrolytic enzymes. This approach is straightforward and more rapid compared to labeling with buffer exchange. The RED-NHS dye used throughout this study contains a reactive ester group that forms a covalent bond with primary amines on the target molecules. Therefore, PL had to be reconstituted in a buffer that does not contain a primary amine which would interfere with the labelling procedure.

Using UV spectrophotometry, the PL* concentration and DOL for the short incubation period of 15 min were calculated as 671 nM and 0.2, respectively and those for the long incubation period of 50 min were calculated as 887 nM and 0.3, respectively, using Equation II.6 and Equation II.7. On the other hand, for PL labeling with buffer exchange, PL was prepared in Tris/MOPS buffer (pH 6.6) which has been previously used as a reconstituting, incubation and separation buffer when assaying PL activity by CE [118]. Since Tris contains a primary amine in its structure, the aforementioned buffer was not compatible with the labeling protocol and was thus exchanged with the NaH₂CO₃/NaCl labeling buffer *via* a special column as illustrated in Figure II.17-1st step and detailed in the experimental section. The concentration of PL* and DOL with buffer exchange was calculated as 373 nM and 0.9, respectively, using Equation II.6 and Equation II.7.

The differences in PL* concentration and DOL between both protocols, labeling with buffer exchange or without it, were relevantly high. These differences were less significant between short and long incubation periods using direct labeling. Compared to the PL* yield obtained with buffer exchange (373 nM), the yields obtained using direct labeling at short and long incubation periods were higher, at 671 nM and 887 nM, respectively. The DOL values of PL* obtained without buffer

exchange at both short (0.2) and long (0.3) incubation periods were lower than the DOL value obtained after PL labeling with buffer exchange (0.9). The difference in the collected PL* concentrations arises from the fact that both of the labeling and MST buffers differ in their respective compositions and pH. In comparison, PL* collected after direct labeling was prepared directly in the MST buffer. Therefore, the column was exposed only to the MST buffer during the different steps of PL* preparation. This contrast between the solution used for the labeling, conditioning of the purification column and elution of PL* could have been the cause for such a dramatic decrease of PL* concentration observed after buffer exchange.

Moreover, an ideal DOL value ranges between 0.5 and 1. A DOL value above 1 might be indicative of enzyme over-labeling and may negatively affect the protein function. Furthermore, a value below 0.5 may result in reduced signal-to-noise ratio (S/N). However, DOL below 0.5 can still be sufficient for MST analyses given high binding signals and the absence of photobleaching. The DOL values obtained for labeling without buffer exchange, *i.e.* 0.2 and 0.3, were below the ideal DOL range compared to that obtained after buffer exchange, 0.9, which was within the ideal DOL range. This can be expected since the reaction between the amine groups of the protein and the NHS of the dye occurs most efficiently at alkaline pH such as that of the labeling buffer used to label PL after buffer exchange (pH 8.2), while the pH of the MST buffer used in direct labeling was closer to neutral (pH 6.6) [128]. Since PL labeling with buffer exchange provided an excellent DOL value of 0.9 and a PL* concentration (373 nM) sufficient to carry out more than one thousand analyses, all future PL labeling were performed with buffer exchange as illustrated in Figure II.17.

b. Optimization of PL concentration:* the working concentration of PL* to be used for the MST analyses was chosen next by comparing the fluorescence signal intensities of three PL* concentration: 1, 2 and 5 nM. The intensities of the fluorescence responses observed for 1 and 2 nM PL* were relatively low and thus unbecoming to be used for future analyses. The intensity of the fluorescence response at 5 nM PL* was sufficiently high (≈ 6000 counts). Consequently, 5 nM of PL* was chosen as the working PL* concentration for all future MST optimizations and analyses. It is worth mentioning that this very low concentration of PL* is almost 5000 times lower than that used during the CE-UV/C⁴D enzymatic activity assays (24 μ M).

c. Optimization of MST buffer by different additives: using the MST buffer alone, bumpy, distorted MST trace profiles were observed suggesting the presence of PL* aggregation. To counteract this, we investigated the effect of supplementing the MST buffer with various additives on the

thermophoretic curves. The goal was to eliminate PL* aggregates using standard uncoated MST capillaries rather than coated ones which are more expensive. The use of the MST buffer alone or with any of the 6 additives prevented adsorption of PL to the capillary walls, suggested by the asymmetry of the capillary shape profiles. Firstly, the addition of organic solvents to the MST buffer resulted in the elimination of PL* aggregates depending on the nature and concentration of the solvent. For ACN, the aggregates were eliminated with the addition of at least 10% ACN to the MST buffer. Similar results were observed when supplementing the MST buffer with 1% EtOH. Furthermore, the addition of a combination of 0.05% Tween 20 and 1% MeOH to the MST buffer failed to eliminate PL aggregation (Figure II.22a in the “supplementary information”). Similar results were obtained when substituting the 1% MeOH with 1% ACN in combination with 0.05% Tween 20. Likewise, aggregation was still detected after the addition of Tween 20 only at 0.01% or 0.05% to the MST buffer. Finally, adding 0.05% Triton-X to the MST buffer successfully eliminated aggregation (Figure II.22b in the “supplementary information”). 0.05% Triton-X was ultimately chosen as the best additive to the MST buffer for future MST optimizations and analyses as it demonstrated its potential, at a low concentration, to eliminate PL* aggregation.

d. Investigation of temperature conditions: The storage temperature of PL* as well as the temperature at which the 5 nM working PL* solution was pre-incubated before MST analysis were investigated.

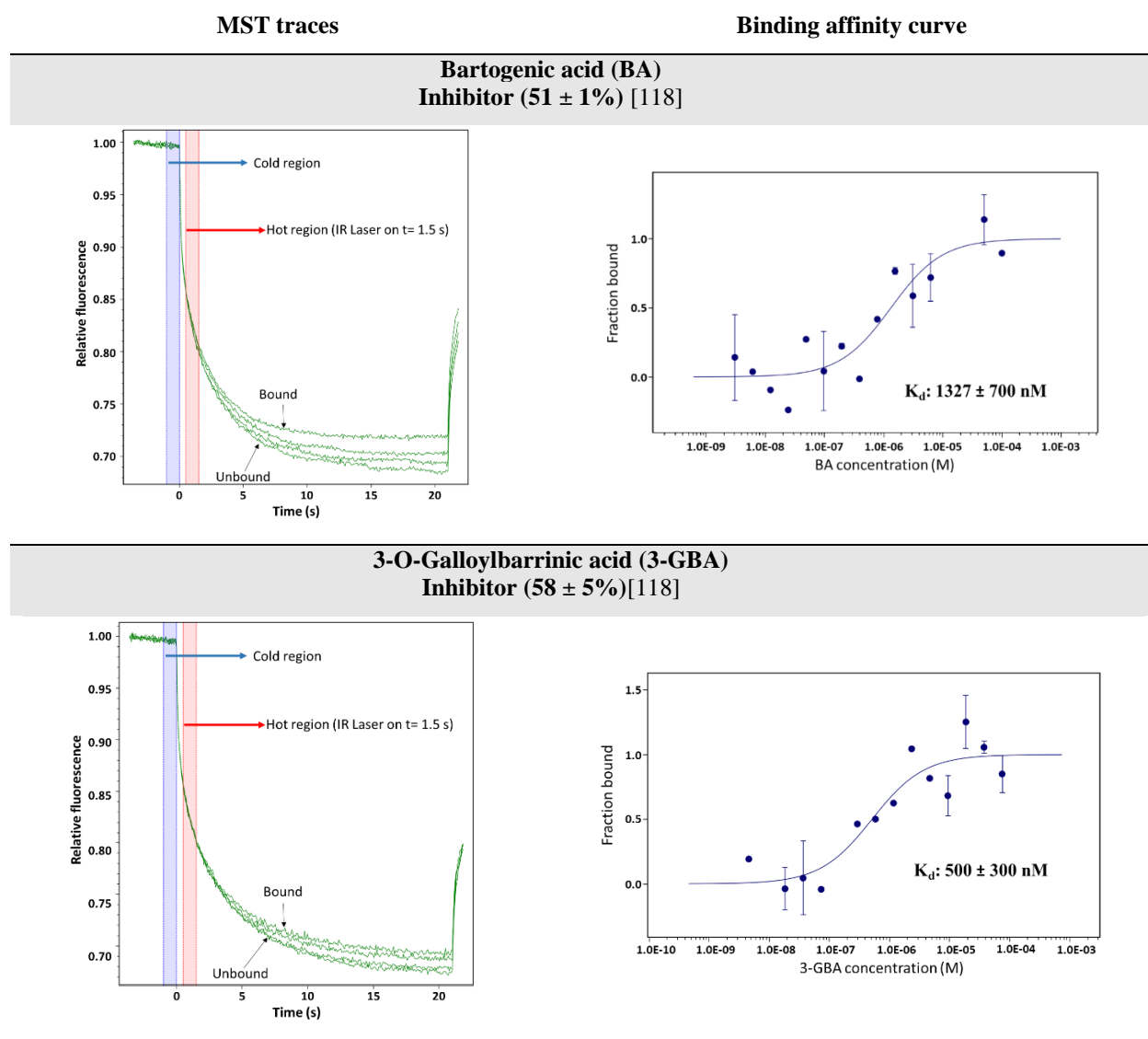
Enzyme storage temperature: Newly labeled PL* was stored in the MST buffer at either -80°C or -20°C. PL* aliquots stored at -80°C demonstrated a decrease in their fluorescence intensity and less symmetrical capillary shape profiles signaling an adsorption issue with time (Figure II.23a in the “supplementary information”). This could result from the formation of fine ice crystals as a result of fast freezing at -80°C which ultimately leads to loss in the enzyme’s activity through denaturation [129]. In contrast, those stored at -20°C displayed good stability of the fluorescence intensity over a period of at least 4 months (Figure II.23b in the “supplementary information”). As a consequence, PL* were aliquoted and stored at -20°C.

Pre-incubation temperature of PL:* Before carrying out the MST binding analysis, PL* is incubated with its potential modulator for a period of time to allow any interaction to take place between the couple. At both tested temperatures of 0°C and 37°C, the thermophoretic response curves were similar with no detection of adsorption or aggregation. Since MST analyses were carried out at 37°C, the PL*-ligand solutions were incubated for 15 min at 37°C. This temperature

also corresponds to the optimal temperature of PL's catalytic activity thus permitting comparison of MST results with CE ones.

II- Binding affinity analysis of small ligands to PL* from crude pancreas extracts

a. Binding analysis of purified triterpenoid compounds: The previously optimized MST assay was applied to evaluate the binding affinities of BA, 3-GBA and QTT-I, triterpenoids shown to modulate the enzymatic activity of PL [118]. The MST traces as well as the fraction bound curves used to evaluate K_d are represented in Figure II.18. With all three assayed ligands, the binding curves were a full sigmoid with lower and upper plateaus representing ligand concentrations where the enzyme is unbound and bound to the ligand, respectively.



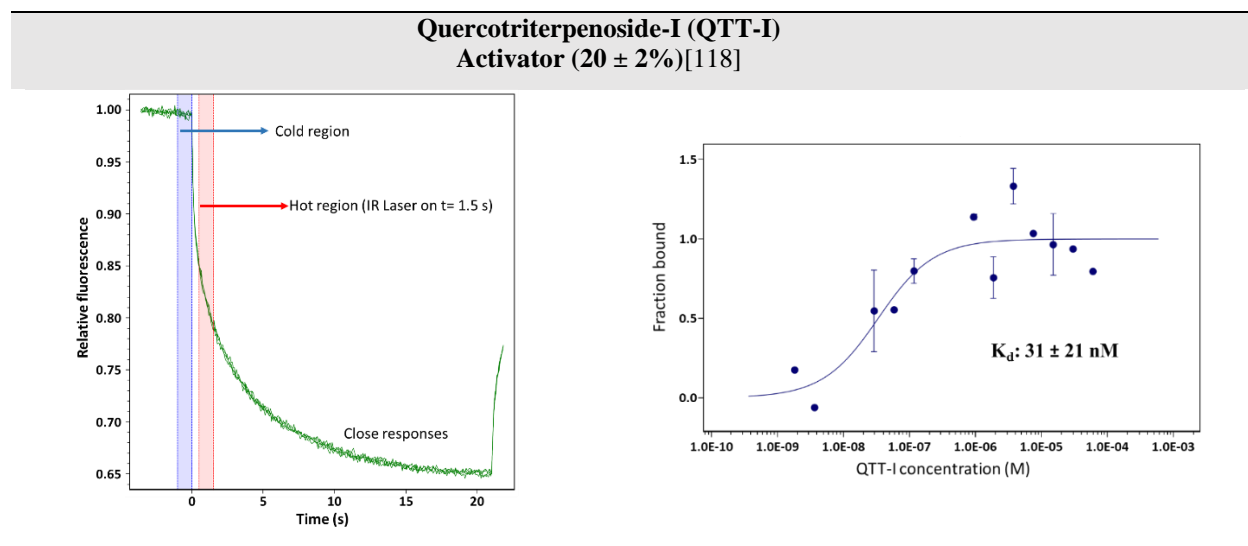


Figure II.18: MST traces and binding affinity curves of 3 triterpenoids modulator of PL activity.

MST traces: The cold region is the pre-IR phase response when IR laser is off, the hot region is the IR-on response when IR is on and was chosen (based on the highest S/N ratio) at $t = 1.5$ s. Binding affinity: the fraction bound curve represents the fraction of the ligand that is bound to PL^* as a function of ligand concentration. Conditions for MST binding analysis are detailed in the experimental section. The modulation of PL activity was assayed in our previous work using CE-UV/ C^4D by monitoring the formation of the hydrolysis products of the 4-NPB substrate in the presence and absence of the ligands [118]. Standard error was calculated using three repetitions ($n=3$)

For BA and 3-GBA, the MST traces demonstrate differences between the high and low concentrations in response to thermophoresis.

Conversely, the MST traces of QTT-I of high and low ligand concentrations were almost overlapping showing little variation in the response between concentrations. K_d of BA binding was evaluated from the binding curve as 1327 ± 700 nM, that of 3-GBA as 500 ± 300 nM and that of QTT-I as 31 ± 21 nM. It can be noticed that the standard deviation values are relatively high. This is probably due to the fact that crude pancreatic extracts were used which represents a complex source of lipases. It has been confirmed that several types of enzymes are present in these extracts including several lipases. Using results from MST, all three ligands demonstrated binding affinities towards PL^* . Without the use of the results of PL activity modulation by CE complementarily, it was not possible to differentiate PL^* binding ligands as inhibitors or activators. Therefore, it was important to complement the MST binding assays with the catalytic activity assays in order to obtain a better understanding of the actual mechanisms involved in the binding of ligands to their targets.

b. Binding analysis of orlistat, a covalent PL inhibitor: The optimized MST assay was then applied to investigate the binding of orlistat, a reference PL inhibitor. The fraction bound curve shows that

the majority of the tested orlistat concentrations are part of the bound orlistat-PL* complex (Figure II.24 in the “supplementary information”). This prevented the formation of a full sigmoidal dose response curve. In fact, orlistat induces inhibition of PL by covalently binding to the enzyme, blocking the access of the substrate to the active site [130]. The fact that orlistat was always bound to PL* with no unbound fraction detected, at most of the tested concentrations, confirms the covalent nature of the binding. The formation of covalent bonds between the binding partners prevents the dissociation of the complex back to the unbound form and therefore K_d cannot be evaluated. Complementing MST binding assays with the CE-UV/C⁴D PL activity assays was important since based solely on the MST result, orlistat would be denoted as a compound that does not bind specifically to PL* since K_d determination was not possible when in reality orlistat was shown to influence PL inhibition [118] thereby confirming the occurrence of an interesting and specific binding interaction.

III- Purification of 50 kDa lipase

In order to improve the efficiency of PL labeling and enhance the MST response repeatability, we attempted to increase the purity of a 50 kDa lipase from crude pancreatic extracts by conducting ammonium sulfate precipitation. In order to alleviate the excess salt concentration, SPE desalting was carried out. The effectiveness of this purification was assessed using CE-UV/C⁴D and HRMS. The optimized MST method was then applied to evaluate the binding affinities of some PL modulatory ligands. This strategy and the main results are summarized in Table II.6 below.

Table II.6: Assessment of PL purification by assaying 4-NPB hydrolyzing activity of the fractions by CE-UV/C⁴D, the detection of PL in their MS spectra by HRMS and evaluation of K_d by MST binding assays. n.r.: Not relevant. It was not possible to distinguish spontaneous 4-NPB hydrolysis due to the alkaline pH of the solvents from that of the enzyme catalyzed one. n.d.: Not determined. The conditions for each of the three assays are detailed in the experimental part

	4-NPB hydrolyzing activity determined by CE-UV/C ⁴ D	Analysis of PL by HRMS	MST binding assays
Extracts after ammonium sulfate precipitation	58 ± 4%	<i>m/z</i> : 55374.33	K_d n.d.
Extracts after ammonium sulfate precipitation and SPE	n.r. (Spontaneous hydrolysis of 4-NPB)	Not detected	K_d n.d. (Protein aggregation)
Crude pancreatic extracts	100%	<i>m/z</i> : 55373.86	K_d evaluated (Figure II.18)

a. CE-UV/C⁴D determination of 4-NPB hydrolyzing activity: For the purification, the lyophilized crude porcine pancreas extract was suspended in cold sucrose solution followed by centrifugation to eliminate insoluble materials. Then, proteins were precipitated using a saturated ammonium sulfate solution. At high salt concentrations, the solubility of proteins is reduced due to increased surface tension of water and reduced surface area of the protein resulting in its precipitation [131]. Ammonium sulfate precipitated extracts demonstrated 4-NPB hydrolyzing activity (58% relative to crude extracts) (Table II.6). The small decrease in the catalytic activity may be due to loss of PL stabilizing or inducing factors during the precipitation or due to a negative effect of the high concentration of the ammonium sulfate salt on the enzymatic reaction or CE separation. Furthermore, the concentration of the precipitated enzyme does not exactly match that of the untreated one as only the pellet of precipitated matter was collected after centrifugation.

Desalting of the precipitated PL solution was carried out using C18 SPE cartridges since ammonium ions are not compatible with labeling by RED-NHS. SPE was carried out using a conventional method described in the experimental part. Precipitated PL solution was loaded at pH 5.3 since at this pH, almost 40% PL retention was observed and only around 7% PL retention was observed when loading PL at pH 6.6. At pH 5.3, the charges on PL are predominantly neutralized enhancing its retention by the C18 support. The extent of PL contribution to 4-NPB hydrolysis of the eluent using Tris/MOPS (pH 8.2) + 10% ACN is difficult to estimate using CE-UV/C⁴D since the elevated pH of the elution solvent resulted in spontaneous non-enzymatic hydrolysis of the 4-NPB substrate during the enzymatic assay [64].

On the other hand, the conductivity of the salt precipitation solution was reduced almost 7-fold, from 7.66 mS cm⁻¹ to 1.5 mS cm⁻¹, after SPE demonstrating the effectiveness of SPE in desalting step.

b. HRMS analysis of PL: In order to validate the results obtained with CE-UV/C⁴D, ammonium sulfate precipitated PL and the SPE eluent (pH 8.2) were analyzed by HRMS and compared to crude porcine pancreatic lipase. PL from crude pancreatic extract constituted in 10 mM sucrose was firstly analyzed at 1 mg mL⁻¹. The mass spectrum demonstrated charge state distribution suggesting the presence of proteins in the analyzed sample (Figure II.19a).

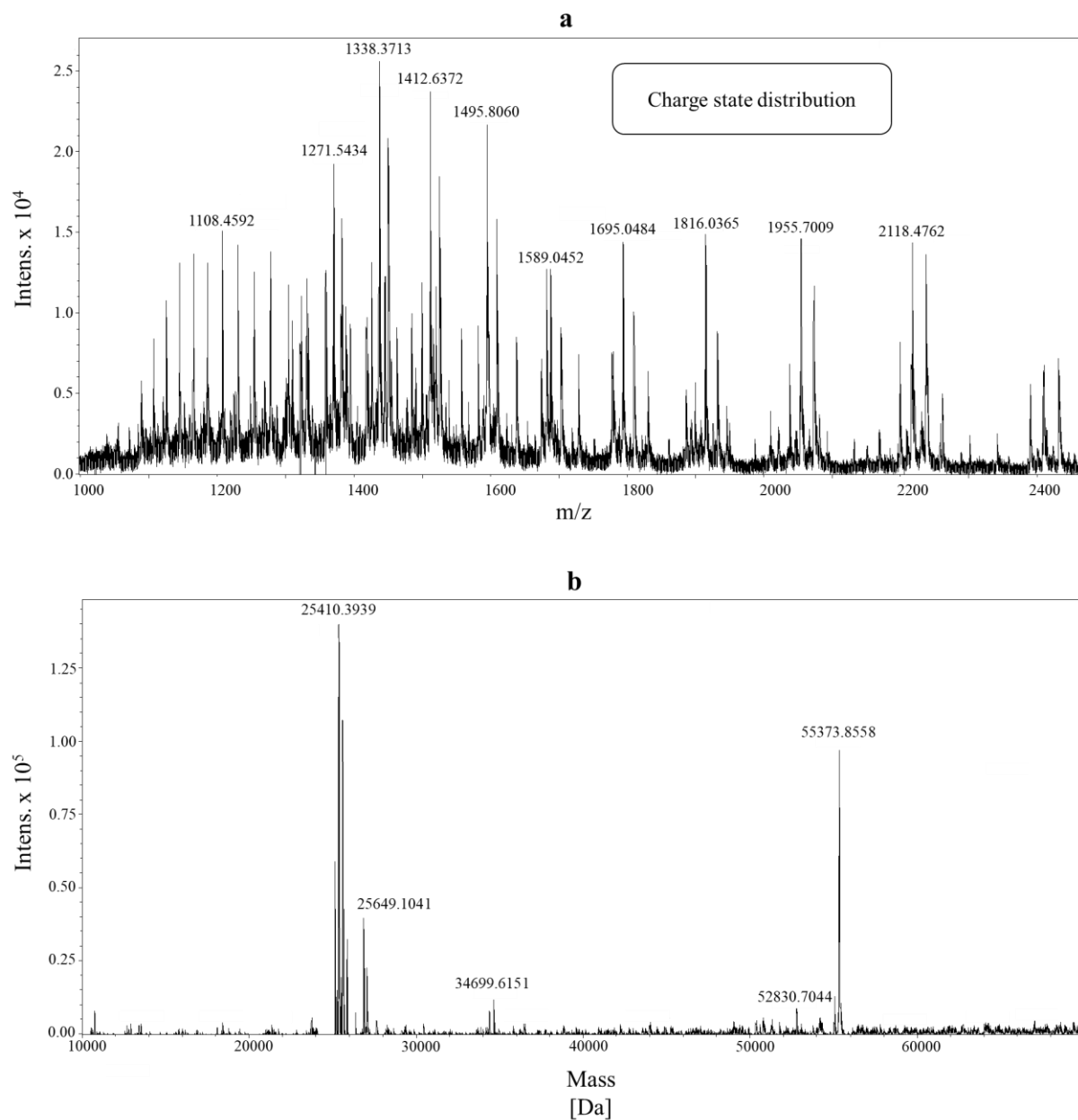


Figure II.19: HRMS analysis of PL from crude porcine pancreas extracts: non-deconvoluted (a) and deconvoluted (b) mass spectra.

Samples were diluted to ca. 1 mg mL⁻¹. Conditions for HRMS analysis are detailed in the experimental section

The deconvoluted mass spectrum revealed the predominance of species with MW of 25410.4 Da followed by 55373.9 Da. Additionally, species with MW 25649.1, 34699.6 and 52830.7 Da were detected at lower intensities (Figure II.19b). The species with MW of 55373.9 Da corresponded to a lipase enzyme with superior triglyceride hydrolysis capabilities (Table II.6). The remaining species may be proteins or other macromolecules as it has been previously reported in crude

extracts of porcine pancreas [125].

Then, PL obtained after ammonium sulfate precipitation, centrifugation and dissolution of the pellet in 10 mM sucrose was analyzed by HRMS at 1 mg mL⁻¹. The charge state distribution confirms the presence of proteins (Figure II.20a) and the deconvoluted mass spectrum (Figure II.20b) reveals the presence of lipase with 55374.3 Da (Table II.6) at higher intensities compared to minor species with lower masses.

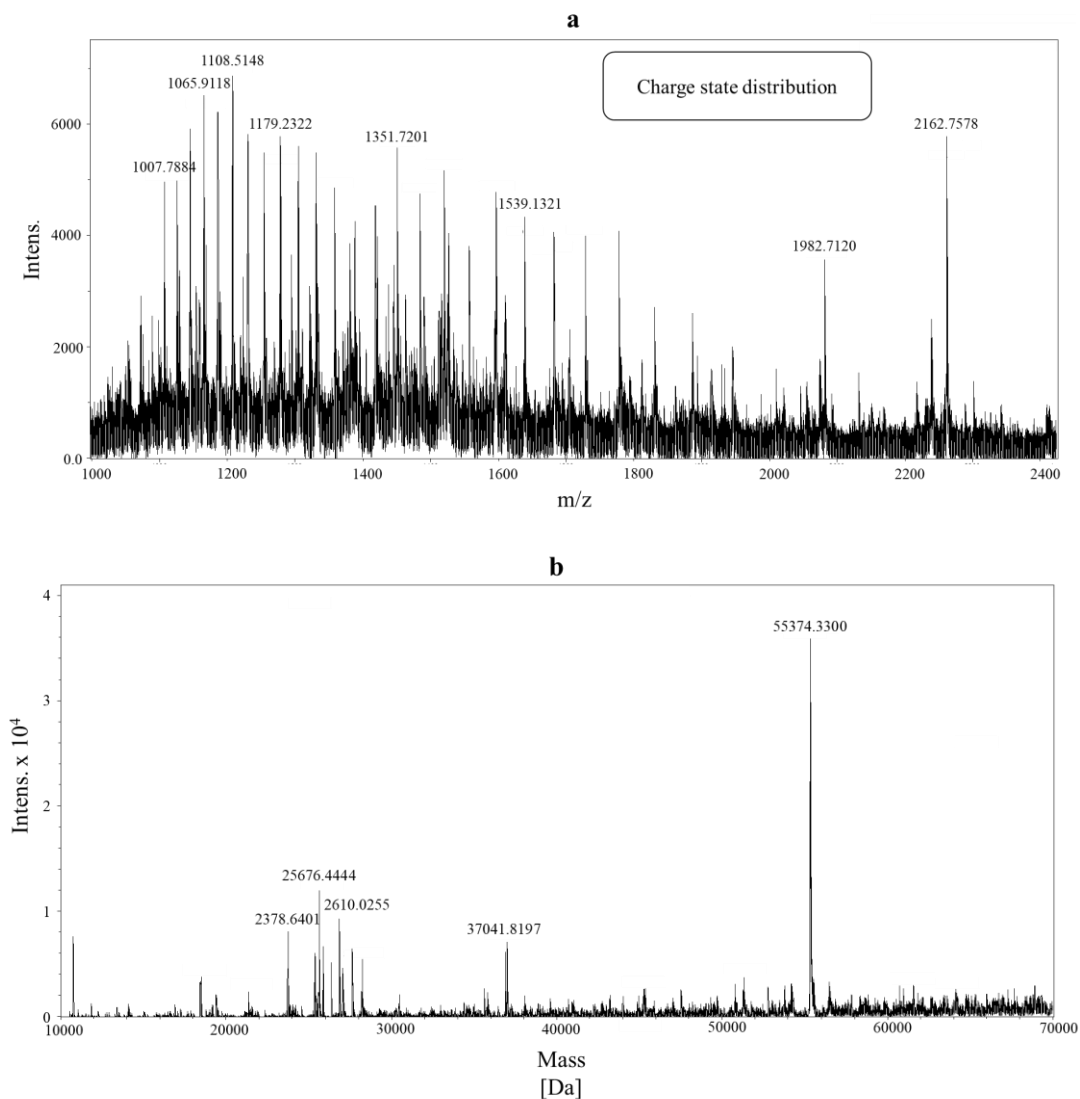


Figure II.20: HRMS analysis of PL precipitated by ammonium sulfate: non-deconvoluted (a) and deconvoluted (b) mass spectra. Samples were diluted to ca. 1 mg mL⁻¹. Conditions for PL precipitation by ammonium sulfate and HRMS analysis are detailed in the experimental section

This demonstrates the efficiency of the fractional precipitation step where PL was precipitated whilst the majority of the contaminants, including the species with lower MW, were still soluble. The intensity of PL in salt precipitated extracts were slightly lower than those of crude extracts,

possibly due to the overestimation of the actual PL concentration (1 mg mL^{-1}) in these extracts. Furthermore, despite passing through an online desalting step, any residual salt in the sample may decrease sensitivity of MS detection due to ion suppression. This slight reduction in PL MS signal goes hand in hand with a decrease of its catalytic activity evaluated by CE.

The effectiveness of the ammonium sulfate precipitation in eliminating PL contaminants present in the extracts was further validated by HRMS analysis of the supernatant (Figure II.25 in the “supplementary information”). Analysis of the SPE eluent by HRMS revealed no characteristic charge state distribution of proteins (Figure II.26 in the “supplementary information”). This confirms that the SPE step resulted in the loss of PL possibly due to failure of its elution from the SPE cartridge. The 4-NPB catalyzing activity of the SPE eluent discussed earlier was thus probably due to the spontaneous hydrolysis of 4-NPB rather than direct enzymatic action as determined by CE (Table II.6).

c. MST binding assay: For the sake of scientific curiosity and in order to observe the nature of MST response of the SPE eluent, the latter was labeled using buffer exchange as previously described in the experimental section and depicted in Figure II.17. The MST traces were uniform in the absence of a ligand, confirming that no aggregates are formed (Figure II.21a). However, upon addition of 3-GBA at different concentrations, aggregation was detected in the majority of the tested capillaries some of which contained very low ligand concentrations (4 nM) (Figure II.21b).

Similar aggregations were also observed in the presence of the reference inhibitor orlistat (results not shown). The abnormal MST responses further validate the results obtained using HRMS and CE-UV/C⁴D analyses of the SPE eluent where PL was most likely not eluted.

The ammonium sulfate precipitated PL fraction cannot be labeled directly for MST analyses as ammonium sulfate and low pH (≈ 5.2) are incompatible with the labeling strategies previously described. It is worth noting that PL bioactivity assays described in literature are conducted using crude pancreatic extracts rather than the purified lipase [21,50,123,124]. This may be due to the fact that lipases in the crude pancreatic extracts may depend on other proteins for their catalytic function. Therefore, although the enrichment of the 50 kDa lipase was successful using ammonium sulfate precipitation, MST labeling was not possible.

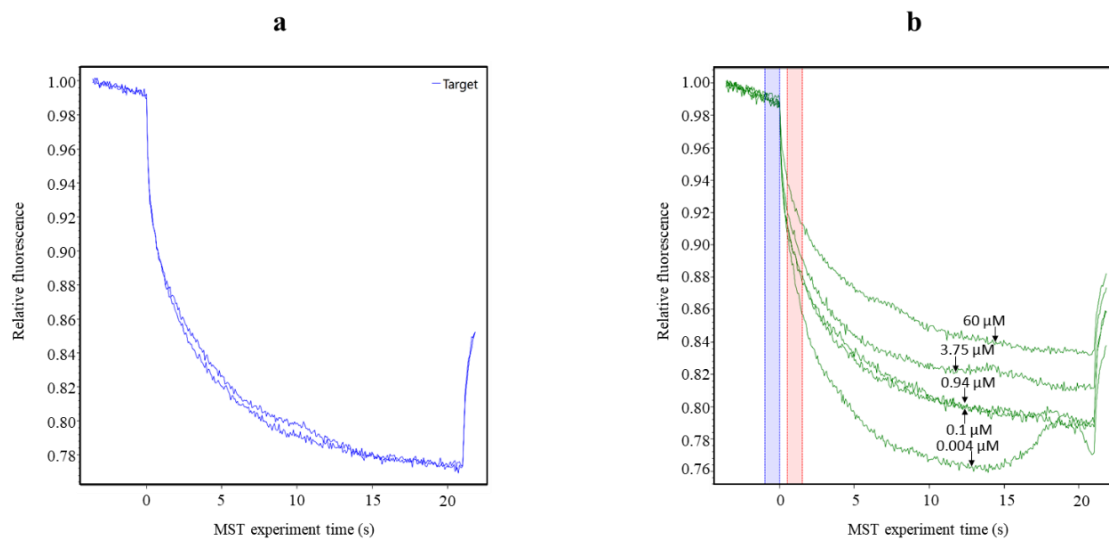


Figure II.21: Ligand induced aggregation after adding different concentrations of 3-GBA.

MST traces of 5 nM labeled SPE eluent: without ligand (a) and, after the addition of various concentrations of 3-GBA (0.004 μM – 60 μM) (b). Excitation power: 100%, other experimental conditions are described in Figure II.17 and in the experimental section

III. Conclusion

Studying binding interactions between large molecules, tens of thousands Da, and small ligands, few hundreds Da, requires highly sensitive techniques capable of detecting the miniscule changes that occurs during the binding. In this work, we described the development and optimization of the first MST assay of PL within the context of investigating the binding of small modulatory ligands. The MST assay required no immobilization of PL. The enzyme was dissolved in a buffer that is appropriate for fluorescent labeling in terms of nature (amine free) and pH (alkaline pH). Few nM of PL* (5 nM) were sufficient to obtain a good MST response demonstrating the sensitivity of the method. When using uncoated standard capillaries, the aggregation and adsorption of PL* were avoided through the addition of a detergent, Triton-X at 0.05%, to the MST buffer. The storage temperature of PL* (-20°C) was found to have an important influence on the stability of the fluorescence response with time. The affinity of 3 triterpenoids towards PL* was evaluated in under 30 min using crude pancreatic extracts. Despite using a complex source of PL, the K_d values were successfully estimated to be 1327 nM for BA, 500 nM for 3-GBA and 31 nM for QTT-I. The nature of the modulation, inhibition or activation, was obtained by complementing the information from MST binding with CE-UV/C⁴D activity assays. Indeed, QTT-I was found to be an activator of PL when using CE, whereas BA and 3-GBA were confirmed as inhibitors. The importance of this complementarity was further confirmed with the reference PL inhibitor, orlistat, where the covalent nature of its binding to PL* could be confused with the absence of any specific binding interaction. Moreover, using CE-UV/C⁴D PL activity assays and HRMS analyses, we have demonstrated the effectiveness of ammonium sulfate precipitation to enrich a single 50 kDa lipase present in porcine pancreas extracts relative to other proteins. It would be interesting to apply the developed assay to screen for other modulators of PL as well as other types of enzymes present in pure forms or in complex samples. For the latter, the intrinsic fluorescence of the matrix must be taken into consideration.

B. Supplementary information

Investigation of lipase-ligand interactions in porcine pancreatic extracts by microscale thermophoresis

Ghassan Al Hamoui Dit Banni¹, Rouba Nasreddine¹, Syntia Fayad³, Cyril Colas^{1,2}, Axel Marchal³
and Reine Nehmé^{1*}

¹Institut de Chimie Organique et Analytique (ICOA), CNRS FR 2708 – UMR 7311, Université d'Orléans, 45067 Orléans, France.

²Centre de Biophysique Moléculaire, CNRS-Université d'Orléans, UPR 4311, 45071 Orléans CEDEX 2, France

³ Université de Bordeaux, Institut des Sciences de la Vigne et du Vin (ISVV), EA 5477, Unité de recherche Œnologie, USC 1366 INRA, 33882, Villenave d'Ornon, France.

* e-mail: reine.nehme@univ-orleans.fr

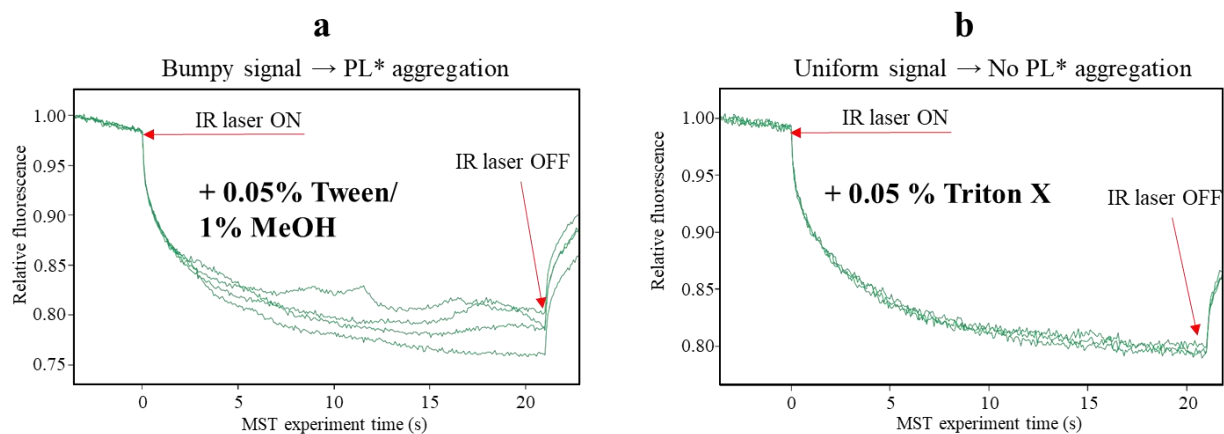


Figure II.22: Influence of MST buffer additives on the quality of MST traces of PL*.

MST buffer contains 0.05% Tween and 1% MeOH (a) or 0.05% Triton-X (b)

MST conditions: 4 standard uncoated capillaries scanned ($n=4$), 5 nM PL*, MST buffer: 20 mM NaH_2PO_4 , 77 mM NaCl (pH 6.6), LED excitation power: 20%; laser power: medium; apparatus temperature: 37 °C. For labeling conditions, refer to Figure II.17 and the experimental section

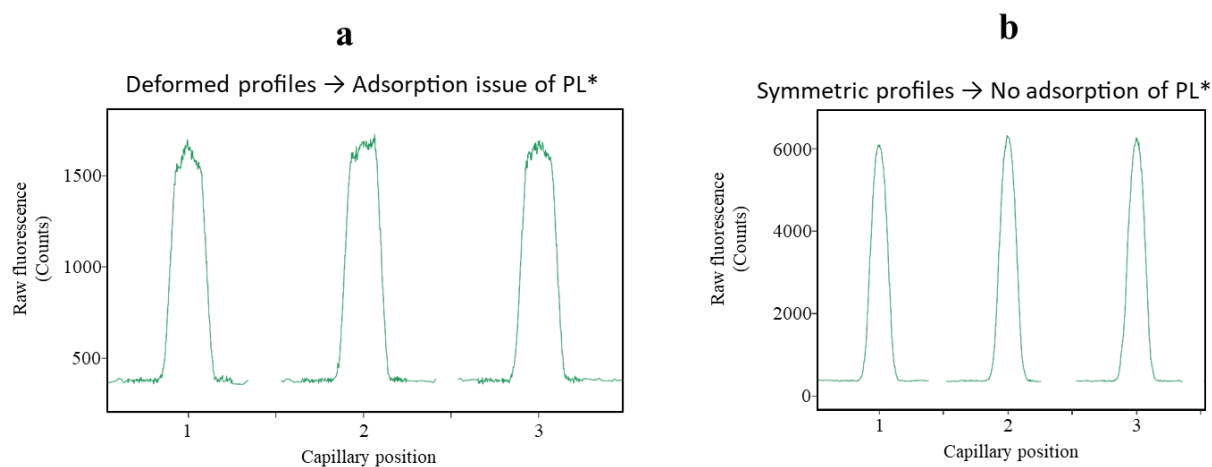


Figure II.23: The influence of storage temperature on the symmetry of capillary shape profiles.

Raw fluorescence of 5 nM PL* in MST buffer obtained after dilution of the PL* stock stored at (a) -80°C or (b) -20°C. MST conditions: 3 standard uncoated capillaries scanned ($n = 3$), 5 nM PL*, MST buffer: 20 mM NaH_2PO_4 , 77 mM NaCl; pH 6.6, LED excitation power: 20%; MST power: Medium; apparatus temperature: 37°C. For labeling conditions, refer to Figure II.17 and the experimental section.

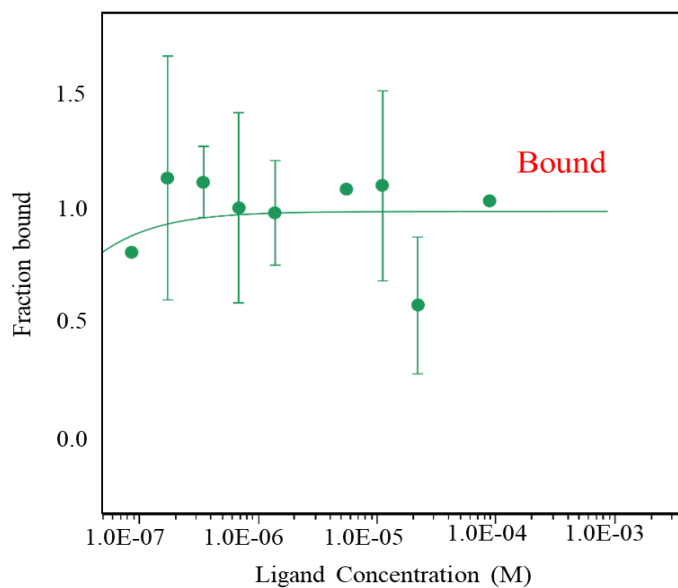


Figure II.24: Analysis of covalent binding of orlistat to PL* at a concentration range of 0.17-88 μM . MST conditions: standard uncoated capillaries, 5 nM PL*, MST buffer: 20 mM NaH_2PO_4 , 77 mM NaCl; pH 6.6 supplemented with 0.05% Triton-X, LED excitation power: 20%; MST power: Medium; apparatus temperature: 37°C. Other MST conditions are detailed in the experimental section of the main manuscript

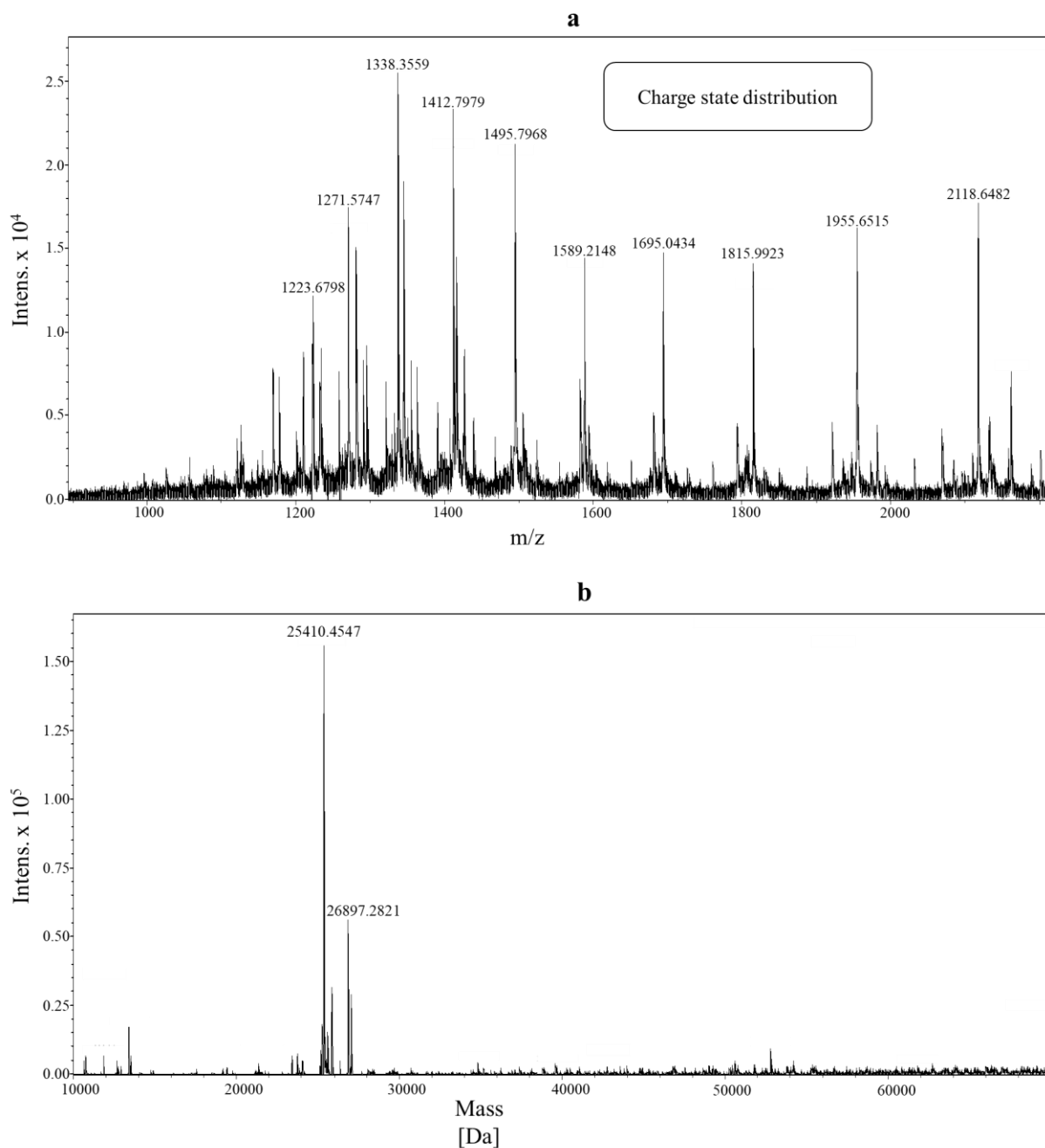


Figure II.25: HRMS analysis of supernatant obtained after PL precipitation by ammonium sulfate: non-deconvoluted (**a**) and deconvoluted (**b**) mass spectra.

The sample was analyzed at ca. 1 mg mL^{-1} . Conditions for PL precipitation by ammonium sulfate and HRMS analysis are detailed in the experimental section of the main manuscript

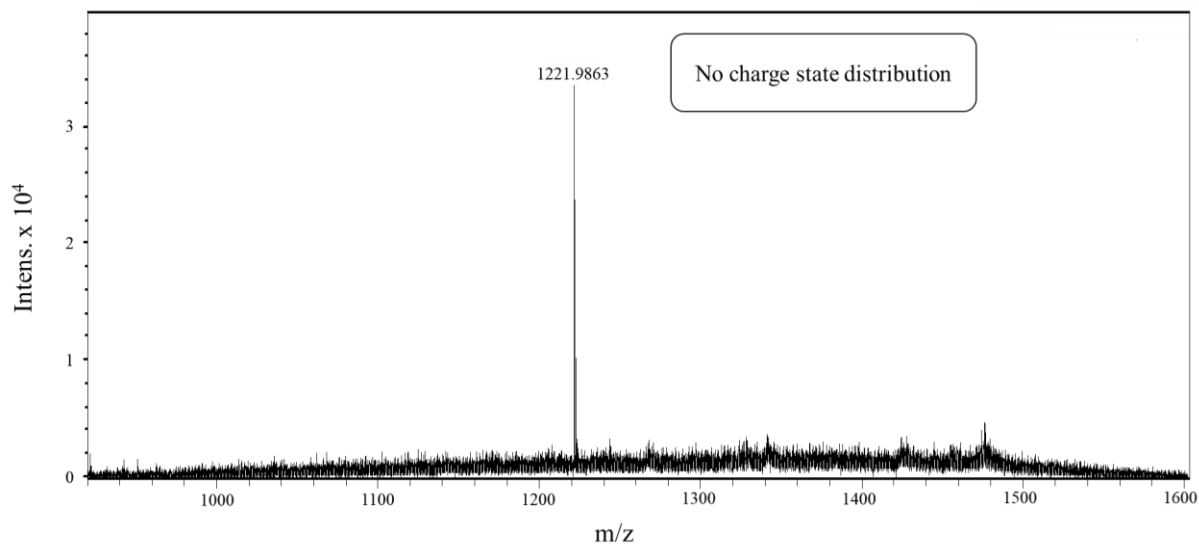


Figure II.26: Non-deconvoluted mass spectrum of HRMS analysis of the SPE eluent. The sample was analyzed at ca. 1 mg mL⁻¹. Conditions for SPE and HRMS analysis are detailed in the experimental section of the main manuscript. Sole peak at m/z: 1221.99 corresponds to Hexakis (1H, 1H ,4H-hexafluorobutyloxy) phosphazine used for lock-mass calibration.

Part C:

Bioactivity assays: investigating the complexity of modulators and reaction environment

Section 1: Investigating the effect of biomolecular crowding on hyaluronidase activity and its modulation by purified molecules

I. Introduction

Hyaluronidases, are enzymes belonging to the glycoside hydrolases family (glycosidases) that are responsible for catalyzing the hydrolysis of hyaluronic acid (HA); a linear, non-sulfated polysaccharide abundant in the extracellular matrix of the skin. HA contributes to the elasticity and hydration of the skin [36,132]. Its cleavage by hyaluronidase results in the production of smaller oligosaccharides implicated in processes such as inflammation and tumor progression in addition to skin dehydration and wrinkling [36,133]. Therefore, molecules demonstrating inhibition of hyaluronidase action have promising potential as anti-inflammatory, anti-cancer and anti-aging agents. HA is made up of several repeating disaccharide units (up to 2500 units) composed of D-glucuronic acid and N-acetyl-D-glucosamine. Hyaluronidase cleaves HA resulting in the formation of oligosaccharides with an even number of motifs (Figure II.27).

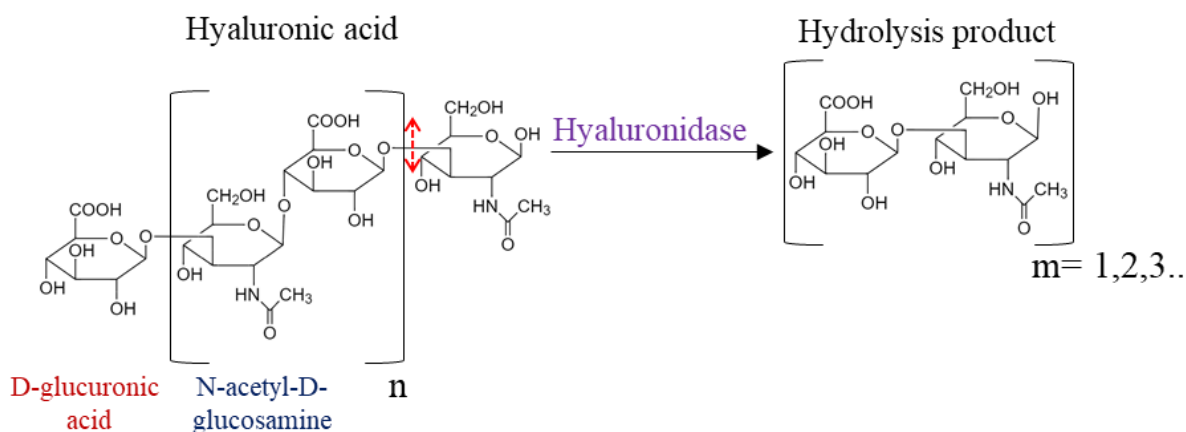


Figure II.27: Illustration of hyaluronidase catalyzed hydrolysis of HA into different lengths of oligosaccharide products.

These oligosaccharides are further hydrolyzed into smaller oligosaccharide units by hyaluronidase. Hexasaccharide (Hex); six sugar units ($m = 3$); are the smallest oligosaccharide hydrolyzed by hyaluronidase. Tetrasaccharide (Tet); four sugar units ($m = 2$); are the final product of the hydrolysis reaction. Although disaccharides (Di); two sugar units ($m = 1$); are also produced from the hydrolysis of HA and smaller oligosaccharide by hyaluronidase, only trace amounts were detected using CE hyphenated to high resolution mass spectrometry (HRMS) [36]. It is thus practical to follow the formation of Tet to assay HA hydrolysis by hyaluronidase. One of the conventional assays used to monitor HA hydrolysis catalyzed by hyaluronidase is the non-separative spectrophotometric neocuproine assay [134]. This assay quantifies all of the oligosaccharide species without discrimination. In order to monitor and quantify oligosaccharides individually, a CE-UV based hyaluronidase assay operated in the offline mode and previously developed in our laboratory [36] was implemented. CE provides selectivity of detection thanks to its high separation efficiency where the oligosaccharides differing in number of constituting units are separated and quantified individually. The results obtained with CE were confirmed using the neocuproine assay complementarily.

An example of the electropherograms obtained for the CE-UV analysis of hyaluronidase-catalyzed HA hydrolysis is presented in Figure II.28.

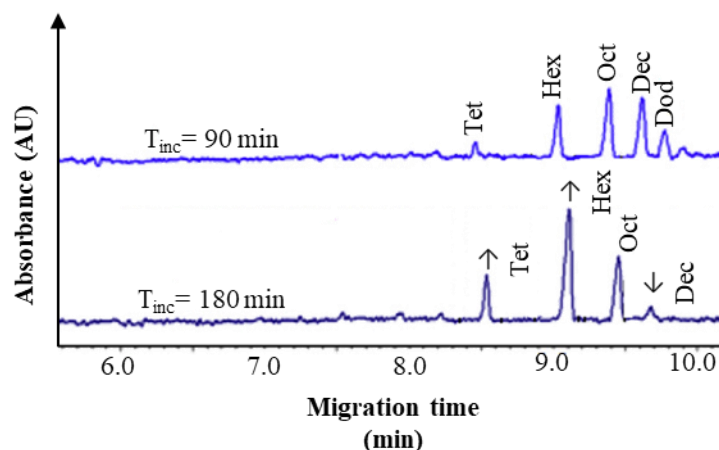


Figure II.28: Electropherograms for CE-UV analysis of hyaluronidase-catalyzed HA hydrolysis. **Oct:** Octasaccharide (8 sugar units), **Dec:** Decasaccharide (10 sugar units), **Dod:** Dodecasaccharide (12 sugar units).

Reaction condition: [HA]: 0.4 mg mL^{-1} , [Hyaluronidase]: 0.2 mg mL^{-1} , IB: 2 mM sodium acetate (pH 4), T_{inc} : 90 and 180 min at 37°C . **CE-UV conditions:** Capillary: uncoated fused-silica ($60 \text{ cm} \times 50 \text{ }\mu\text{m}$ i.d.; 49.8 effective length), BGE: 50 mM ammonium acetate (pH 9), Injection: anodic, $0.5 \text{ psi} \times 5 \text{ s}$ (5 nL), Separation: + 20 kV at 25°C , Detection: UV at $\lambda = 200 \text{ nm}$. Adapted from [36]

As demonstrated in the electropherograms and previously mentioned, several short oligomers are produced as a result of HA hydrolysis, Tet being the final one. Upon increasing the incubation time, the complex mechanism of hyaluronidase action is elaborated. The larger oligomers produced from HA hydrolysis become substrates themselves and are hydrolyzed into smaller oligomers (Tet and Hex). This complex mechanism of hyaluronidase function has been explored in a work recently published by our group [135].

The revelation of this type of information requires a technique such as CE, able to separate the different products of HA hydrolysis and allow their individual quantification. Conventional spectrophotometric assays such as the neocuproine assay only provide information about the system as a whole rather than its individual components.

II. Biomolecular crowding:

Biological processes such as skin aging, blood pressure regulation, oxidation reactions and many others take place in complex environments swarming with macromolecules such as proteins, carbohydrates, nucleic acids *etc.* Therefore, the majority of *in vitro* assays underestimate the effect of a crowded environment on biochemical interactions. Biomolecular crowding refers to the simulation of the cellular environment through the addition of crowding agents. These may be inert proteins such as bovine serum albumin (BSA) or ovalbumin or, polymers such as polyethylene glycol, the most commonly used crowding agent. In crowded environments, enzymes may be stabilized favoring their folded conformation [136,137].

The investigated enzymatic reaction conducted in crowded media may reveal different outcomes compared to those conducted in diluted media. This is of vast importance in drug discovery where drugs thought to demonstrate interesting activities may in fact be inert in crowded media, and thus in actual physiological conditions. This permits the economy of resources and time that would be wasted on the development of such inactive drugs.

The effect of crowding on the activity of hyaluronidase as well as on the modulation of the enzyme's activity by natural and synthetic purified molecules will be investigated *in vitro* using PEG (at 10 and 17%) as a crowding agent. Higher PEG concentrations introduced pipetting issues due to their elevated viscosities and were thus omitted.

One of the natural compounds investigated is a flavonoid abundant in green tea named epigallocatechin gallate (EGCG) and regarded as a reference inhibitor of hyaluronidase. The

Stock solutions of EGCG were prepared at 10 mg mL^{-1} in 2 mM sodium acetate IB (pH 4.3) and then diluted to 5 mg mL^{-1} . QTT stock solutions were prepared in pure MeOH at 40 mg mL^{-1} and then diluted to 5 mg mL^{-1} . HA stock solutions were prepared in the IB at 10 mg mL^{-1} and then diluted to 1.5 mg mL^{-1} . Hyaluronidase stock solutions were prepared in the IB at 10 mg mL^{-1} and then diluted to 2 mg mL^{-1} . The CE-UV assays were complemented by conventional neocuproine spectrophotometric assays used to quantify reducing ends formed as a result of HA hydrolysis catalyzed by hyaluronidase.

IV. Results

The results of antihyaluronidase assays of purified compounds in the presence and absence of crowding agents are detailed in a peer-reviewed article titled “**Polyethylene glycol crowding effect on hyaluronidase activity monitored by capillary electrophoresis**”, *Analytical and Bioanalytical Chemistry* (2020), 412: 4195-4207, DOI: 10.1007/s00216-020-02659-9

Rouba Nasreddine¹, Lucija Orlic^{1,2}, Ghassan Al Hamoui Dit Banni¹, Syntia Fayad^{1,3}, Axel Marchal³, Francesco Piazza², Chrystel Lopin-Bon¹, Josef Hamacek² and Reine Nehmé¹

¹ Institut de Chimie Organique et Analytique (ICOA), CNRS FR 2708 - UMR 7311, Université d'Orléans, 45067 Orléans, France

² Centre de Biophysique Moléculaire, CNRS UPR 4301, Université d'Orléans - CNRS, 45071 Orléans, France

³ Unité de recherche Œnologie, USC 1366 INRA, Université de Bordeaux, ISVV, EA 5477, 33882 Villenave d'Ornon, France

IV.a Type of sample injection into CE

The sample to be analyzed by CE can be injected either hydrodynamically or electrokinetically. With hydrodynamic injection, a pressure gradient draws the sample into the capillary. On the hand, electrokinetic injection is based on the application of a voltage in order to introduce the sample into the capillary. It is known that the injection repeatabilities of electrokinetic injections are lower than hydrodynamic ones. Furthermore, electrokinetic injection suffers from injection bias, were only a handful of charged molecules are injected. Nonetheless, an advantage of such approach is its suitability for injection of viscous solution [139].

Having the reaction media, which already contains viscous HA, crowded by PEG results in further increase in the viscosity. Therefore, both hydrodynamic (0.5 and 1.5 psi × 5 s; 5 and 15 nL) and electrokinetic injections (+/- 5, 10 and 15 kV × 5 s) were compared. Electrokinetic injections resulted in poor CPA repeatabilities, even in the absence of crowding. Similarly, hydrodynamic injection at 0.5 psi × 5 s resulted in poor repeatabilities. At 1.5 psi × 5 s, good CPA repeatabilities were obtained except when HA concentration was higher than 0.5 mg mL⁻¹ in the presence of 17% PEG, where the increased viscosity of the injected sample deteriorated the injection repeatabilities.

Amongst all tested injection approaches, hydrodynamic injection at $1.5 \text{ psi} \times 5 \text{ s}$ resulted in the best CPA repeatabilities and was thus chosen for the remainder of the work.

IV.b Influence of PEG on electrophoretic analyses and hyaluronidase activity

The influence of the addition of 10% (w/w) PEG to the IB was first investigated. Electrophoretic separation of the hydrolysis products was generally unaffected by the presence of PEG. However, the migration times of the products as well as HA were slightly longer due to a small decrease in the electroosmotic flow mobility (μ_{EOF}) owing to the viscosity of PEG (Figure II.30).

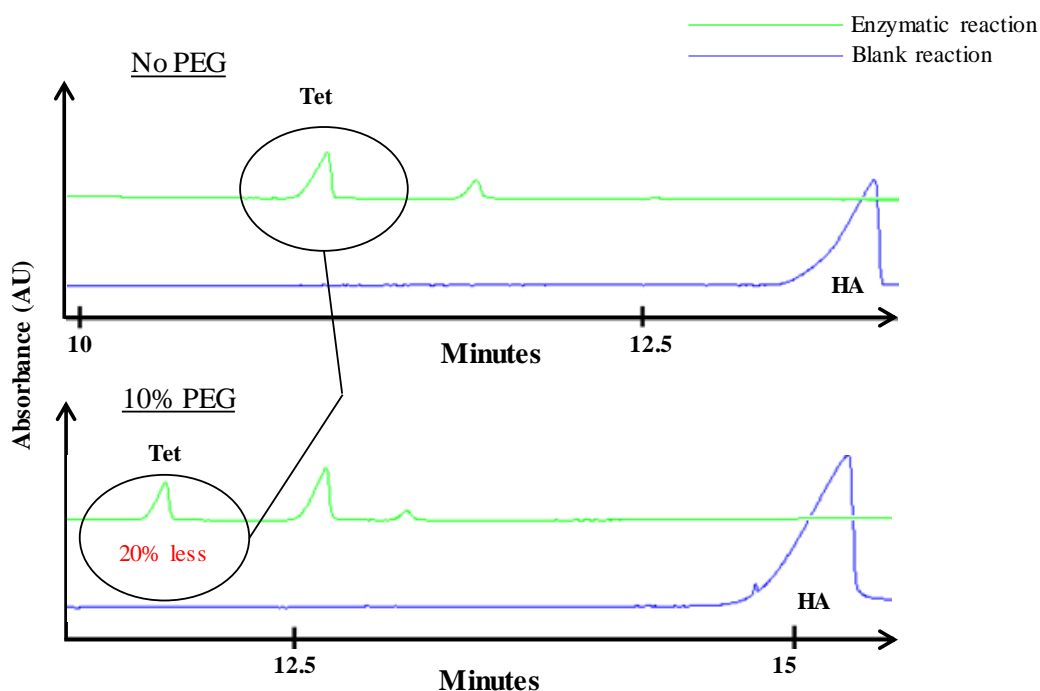


Figure II.30: CE-UV electropherograms at $\lambda = 200 \text{ nm}$ of hyaluronidase catalyzed HA hydrolysis in the absence or presence of 10% PEG. Blank reactions were carried out in the absence of hyaluronidase. $[\text{HA}] = 0.3 \text{ mg mL}^{-1}$. Tet: tetrasaccharide, final product of HA hydrolysis.

Experimental conditions are presented in Figure II.29 and Table II.7

Moreover, hyaluronidase hydrolyzing activity underwent a reduction of almost 20% in the presence of PEG as estimated by comparing the peak areas of the Tet product in the presence and absence of PEG.

The effect of PEG on the analytes' migration times and the HA hydrolysis reaction can be attributed to non-specific interactions between PEG and hyaluronidase as well as to the limitation of hyaluronidase and HA diffusion in the presence of PEG, limiting its catalytic activity towards HA.

IV.c Influence of PEG on the antihyaluronidase activities of purified compounds

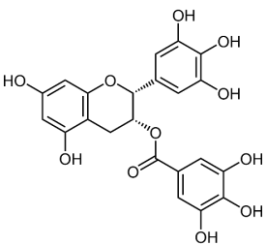
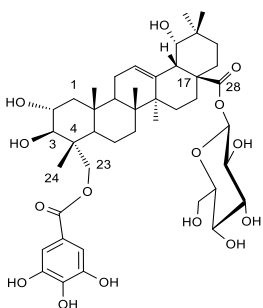
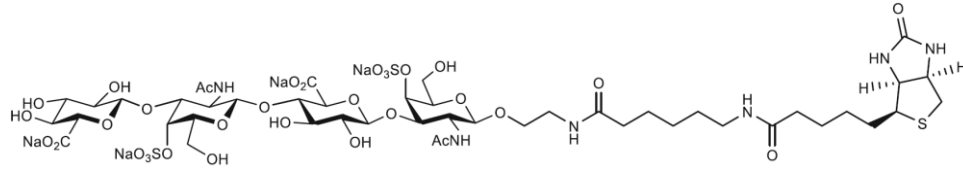
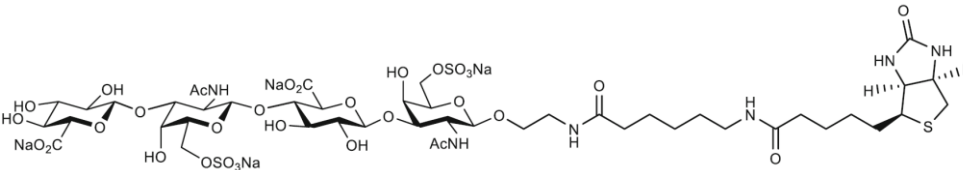
The potential of the two purified compounds, EGCG and QTT-I (structures in Table II.8), at 1 mg mL⁻¹, to inhibit HA hydrolysis by hyaluronidase was evaluated by comparing HA hydrolysis in their presence to that in their absence without the addition of PEG. Hyaluronidase inhibition was 98 and 66% in the presence of EGCG and QTT-I, respectively.

Upon the addition of 10% PEG to the reaction modulated by the purified compounds, the hyaluronidase inhibitory potential was considerably reduced from 98 and 66% to 11 and 2% for EGCG and QTT-I, respectively, considering the 20% contribution of PEG to the reduction in enzymatic activity (Table II.8). Therefore, in crowded media, the influence of both compounds on hyaluronidase activity is negligible.

Moreover, biotinylated, homogeneously sulfated synthetic tetrasaccharides (CS) (structures in Table II.8), previously demonstrated, using a CE-based hyaluronidase assay, to exert an inhibitory effect towards hyaluronidase, were re-evaluated for their hyaluronidase inhibition in the presence and absence of crowding [8]. Hyaluronidase inhibition induced by CS was affected to a lower extent in the presence of PEG compared to EGCG and QTT-I. More precisely, CS-A (a tetrasaccharide sulfated at C4 of N-acetyl-D-glucosamine motifs) exerted 37% hyaluronidase inhibition while CS-C (a tetrasaccharide sulfated at C6 of N-acetyl-D-glucosamine motifs) exerted 39% inhibition, in the absence of PEG. However, in the presence of 10% PEG, the hyaluronidase inhibition potential of CS-A increased by a factor of 1.6 to reach 60% inhibition while that of CS-C remained roughly the same (42%) (Table II.8).

Table II.8: Inhibition percentage of purified natural, EGCG & QTT-I, and synthetic, CS-A & CS-C, in the absence and presence of 10% PEG evaluated using CE-UV. The inhibitory effect contributed by PEG, $\approx 20\%$, was considered when calculating hyaluronidase inhibition in crowded media.

Experimental conditions are presented in Figure II.29 and Table II.7

Inhibitor molecules	Hyaluronidase inhibition (%) 1 mg mL ⁻¹	
	Dilute media	Crowded media
<p>EGCG</p> 	98%	11%
<p>QTT-I</p> 	66%	2%
<p>CS-A</p> 	37%	60%
<p>CS-C</p> 	39%	42%

V. Conclusion

In this section, an offline CE-based assay was used to investigate the influence of purified natural and synthetic molecules on hyaluronidase activity in dilute and crowded media. Biomolecular crowding serves to mimic the real-life environments of the cells and was achieved through the addition of the crowding agent, PEG. Since CE does not involve the use of a stationary phase, different crowding agents can be used without issues associated with unspecific interactions. Furthermore, the CE-based assays were rapid, requiring less than 20 min for the separation of the different products that were detected directly without the need of coupled reactions or modification of the enzyme or ligands. Compared to conventional hyaluronidase spectrophotometric assays such as the neocuproine assay, the CE-UV assay allowed the separation of the oligosaccharide species resulting from HA hydrolysis allowing their individual monitoring and quantification, something which the neocuproine assay is unable to do.

To conclude, crowded media used to mimic the extracellular environment showed an influence on the hyaluronidase activity (20% inhibition) and a greater influence on the inhibitory potentials of EGCG (from 98% in dilute media to 11% in crowded media) and QTT-I (from 66% in dilute media to 2% in crowded media) using a CE-based hyaluronidase assay. This PEG induced modulation of hyaluronidase inhibition can be correlated to the structures of the assayed compounds. EGCG and QTT-I both have similar cyclic and neutral structures that would permit them to significantly interact with PEG in the media, affecting their hyaluronidase inhibition potential. On the other hand, sulfated CS have larger linear, negatively charged structures probably limiting the possibility of strong interactions with PEG and thus the hyaluronidase inhibition potential was less affected (37-39% in dilute media to 42-60% in crowded media). These findings show that molecules such as EGCG, which is considered a reference hyaluronidase inhibitor, will probably yield undesirable outcomes during clinical trials of potential hyaluronidase inhibitors since its inhibitory potential was almost completely lost upon crowding. Such types of *in vitro* crowded assay can thus be beneficial in drug discovery processes to more accurately identify “true hits” that will most likely exert a pharmaceutical affect *in vivo* or during clinical trials.

Section 2: Bioactivity assays based on CE and other conventional techniques

I. Introduction

Nature has served man ever since pre-historic times as a seemingly infinite source of food, clothing and medicine. It is the largest reservoir of secondary, bioactive metabolites abundant in biological tissues. The oldest recorded use of plant-derived drugs in medicine dates back 5000 years where Sumerian clay tablets described recipes of drugs composed of several plants [1]. Since then, the traditional use of plants in medicine and cosmetics in addition to food and condiments has been passed down the generations in different societies and cultures worldwide (Figure II.31).

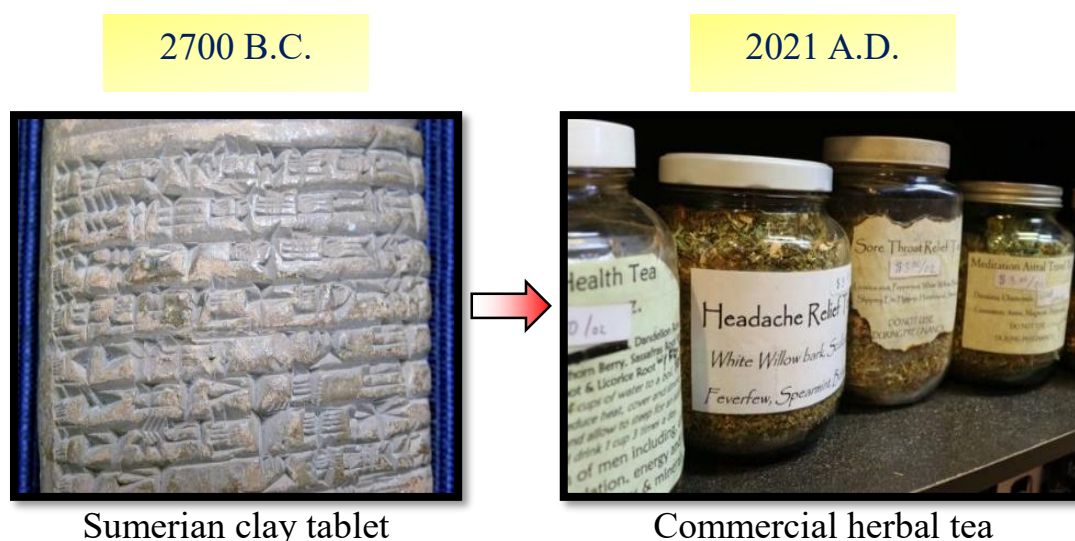


Figure II.31: Conservation of medicinal plant usage with time (2700 B.C. – present day)

Compared to chemically synthesized drugs, bioactive compounds isolated from natural extracts are generally easier to obtain and do not require complicated reaction pathways. Furthermore, they are generally regarded as safer than synthetic molecules and side effects associated with the consumption of natural compounds are more often than not, less adverse [2].

With the recent advances of extraction, fractionation and purification techniques, the identification and isolation of novel modulatory molecules has considerably improved [3–5]. Phytochemical compounds are defined as bioactive when they are involved in the regulation of metabolic processes and promoting desirable effects on the health. The mechanisms with which they

influence metabolism are various and include modulation of the activities of metabolic enzymes and receptors, antioxidation or through their influence on gene expression [6]. In this segment, we describe the bioactivity assays of three plant extracts *Crataegus oxyacantha* (hawthorn; HAW), *Ribes nigrum* (black currant; BC) and *Chrysanthellum americanum* (CA) previously introduced in part A of this chapter (Figure II.4, Figure II.5, Figure II.6 and Table II.1), at three levels: *a.* their antihyaluronidase, *b.* hypotensive and, *c.* antioxidant activities. These three plants have previously demonstrated therapeutic and pharmaceutical potential and represented a degree of sample complexity contrasting that of the molecules investigated in the first section.

a. The antihyaluronidase activities of these plant extracts were investigated using an offline CE-UV-based hyaluronidase assay, described in section 1 of this part of the chapter. The experimental conditions, reaction and CE analysis, are summarized in Figure II.29 and Table II.7.

For the hypotensive and antioxidant activities, conventional spectrophotometric assays were used in order to obtain a more complete picture about the plant's bioactivities.

b. Hypertension is the elevation of arterial blood pressure increasing the risk of strokes, eye, cardiovascular and kidney diseases. Blood pressure is regulated by several mechanisms amongst which the renin-angiotensin system regulates blood pressure through the control of blood volume [10]. An important component of the renin-angiotensin system is the angiotensin converting enzyme (ACE) catalyzing the cleavage of angiotensin I to angiotensin II which in turn induces increased production of antidiuretic hormone (ADH) from the hypothalamus and vasoconstriction of venous and arterial smooth muscles leading to an increase in arterial blood pressure [10,11] (Figure II.32). Compounds capable of affecting the normal function and activity of ACE are therefore hypotensive since they prevent the production of angiotensin II.

c. Lastly, antioxidation is the inhibition of oxidation reactions producing reactive free radicals the can damage cells. The antioxidant capacities of molecules are evaluated based on their ability to sequester reactive oxygen species (ROS). These highly reactive molecules exist in various forms and may be produced in response to various stress agents such as endogenous reactions, drugs, radiation or pollution, and can induce irreversible damage to cell structures such as DNA contributing to the development of metabolic, neuronal and cardiovascular disorders [12,13].

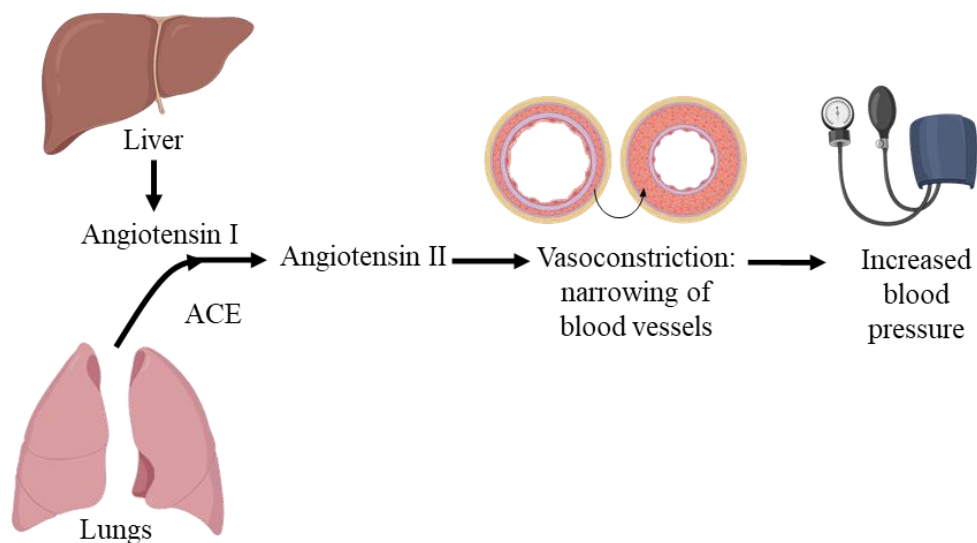


Figure II.32: Illustration of ACE action on angiotensin I and physiological consequence resulting in increased blood pressure

ACE inhibitory potential of the extracts was evaluated in 96-well microtiter plates using reagents provided by an ACE-kit WST purchased from Dojindo Laboratories (Kumamoto, Japan). Similarly, antioxidant assays were also performed in 96-well microtiter plates using a previously described 2,2'-azino-bis(3-ethylbenzothiazoline-6-sulfonic acid) (ABTS) assay [16].

II. Results

The results obtained for antihyaluronidase, hypotensive and antioxidant bioactivities of the plant extracts are detailed in a peer reviewed article titled “**Water-Based Extraction of Bioactive Principles from Blackcurrant Leaves and *Chrysanthellum americanum*: A Comparative Study**”, *Foods* (2020), 9: 1478; DOI: 10.3390/foods9101478

Phu Cao-Ngoc¹, Laurent Leclercq¹, Jean-Christophe Rossi¹, Jasmine Hertzog^{2,3}, Anne-Sylvie Tixier⁴, Farid Chemat⁴, Rouba Nasreddine⁵, Ghassan Al Hamoui Dit Banni⁵, Reine Nehmé⁵, Philippe Schmitt-Kopplin^{2,3} and Hervé Cottet¹

¹ IBMM, University of Montpellier, CNRS, ENSCM, 34093 Montpellier, France;

² Analytical BioGeoChemistry, Helmholtz Zentrum Muenchen, 85764 Neuherberg, Germany;

³ Analytical Food Chemistry, Technische Universität Muenchen, 85354 Freising, Germany

⁴ GREEN Extraction Team, INRA, University of Avignon, 84916 Avignon, France;

⁵ Institute of Organic and Analytical Chemistry (ICOA), CNRS, University of Orléans, 45067 Orléans, France

II.a Antihyaluronidase activity of plant extracts

The influence of the plant material extracted from various parts of three plants on hyaluronidase activity was investigated by offline CE-UV under the same conditions described in Figure II.29 and Table II.7. All of the extracts were assayed at a concentration of 1 mg mL⁻¹ obtained by diluting the extract stock solutions (5 mg mL⁻¹) in deionized H₂O. The absence of interference peaks in the extracts obscuring the Tet product peaks was verified by blank injection of the extracts only (Figure II.33). The percentage of hyaluronidase inhibition by plant extracts was calculated by comparing the CPA of Tet in the presence of plant extracts in the reaction media to their absence as shown in Equation II.8 below.

$$\text{Hyaluronidase inhibition (\%)} = 1 - \frac{CPA_{Sample}^{Tet}}{CPA_{Control}^{Tet}} \times 100 \quad \text{Equation II.8}$$

where CPA_{Sample}^{Tet} and $CPA_{Control}^{Tet}$ are the corrected peak areas of Tet in the presence, or absence of plant extracts, respectively.

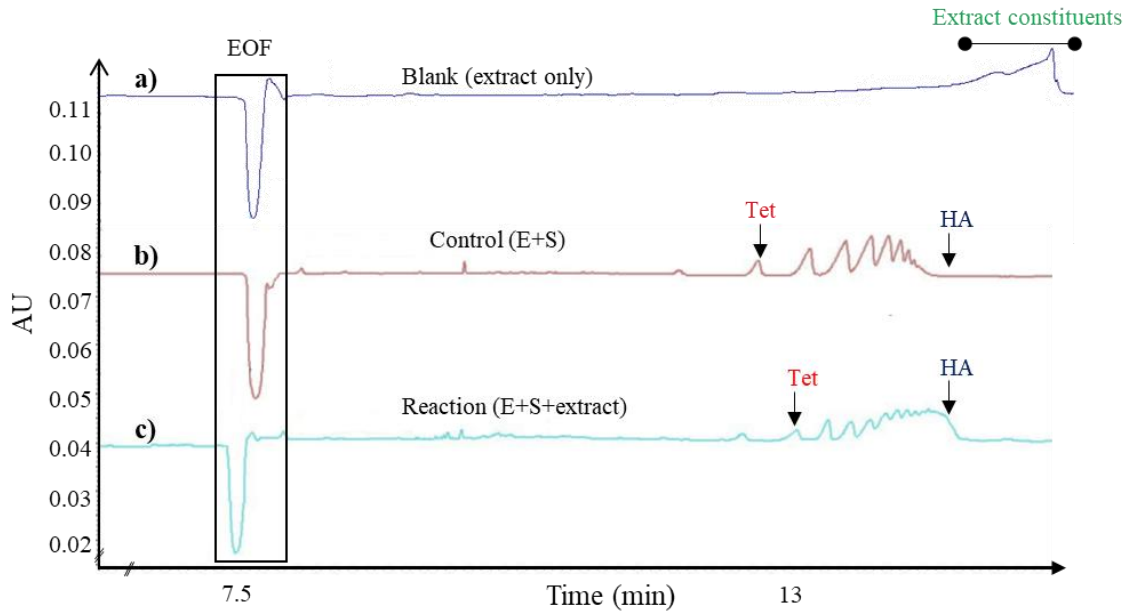


Figure II.33: Electropherograms of hyaluronidase inhibition by *Chrysanthallum americanum* fiber extracts assayed by an offline CE-UV assay. E: hyaluronidase, S: HA and Tet: tetrasaccharide product. **Experimental conditions** are presented in Figure II.29 and Table II.7

The antihyaluronidase activity induced by the extracts was compared to that induced by EGCG, a reference hyaluronidase inhibitor. Results of hyaluronidase inhibition by plant extracts, reported in Figure II.34, show a general trend of inhibition induced by all of the extracts.

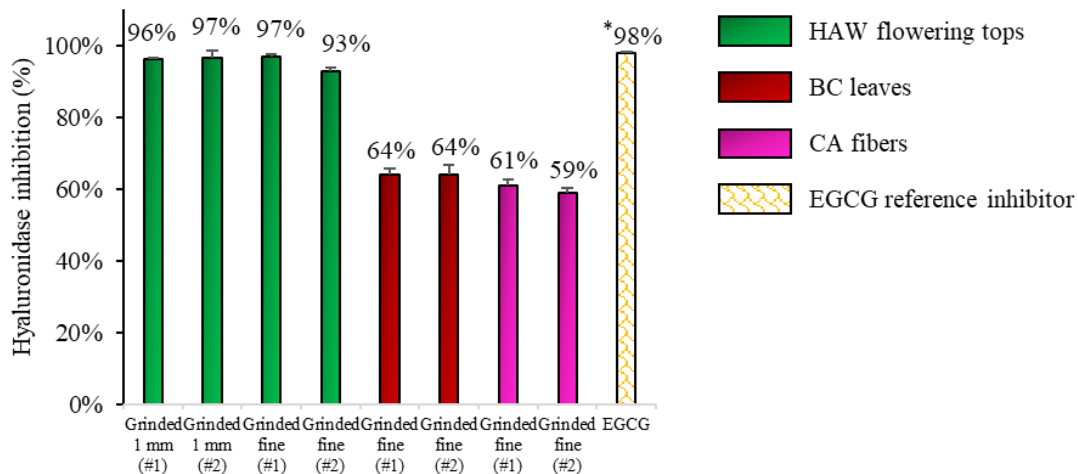


Figure II.34: Percentage of hyaluronidase inhibition induced by extracts from three plants and *EGCG, a reference hyaluronidase inhibitor, at 1 mg mL⁻¹. Assays were carried out in triplicates (n = 3). **Experimental conditions** are presented in Figure II.29 and Table II.7

Compared to inhibition by EGCG (98%), HAW extracts demonstrated the highest hyaluronidase inhibition (93–97%). Inhibition by BC and CA extracts was moderate (64 and 59–61%, respectively).

Furthermore, the degree of extract grinding (fine or at 1 mm) does not seem to influence the extent of hyaluronidase inhibition despite having shown to increase the extraction yield [17]. The differential antihyaluronidase activities of extracts from HAW and those from the other plants are probably attributed to the identity of the molecular features of each extract. BC extracts, for instance, were shown to have the highest TPC (40 mg gallic acid equivalent per g of dry plant) and TFC (4.44 mg quercetin equivalent per g of dry plant) in extracts of their leaves compared to the extracts of HAW and CA but demonstrated the lowest antihyaluronidase activities. Upon further inspection of the UHPLC-UV analysis of chemical composition of extracts from BC leaves (Figure II.5b), there is an abundance in isomers of flavonoids quercetin and kaempferol both of which have been reported to have limited hyaluronidase inhibition [18,19].

Therefore, despite the richness of extracts from BC leaves with polyphenols and flavonoids, both of which have shown to inhibit hyaluronidase, the majority of these molecules belonging to both classes abundant in the extracts may be those inducing limited hyaluronidase inhibition.

The offline CE-based assays of hyaluronidase modulation demonstrate great potential using samples as complex as extracts of plants containing hundreds of molecules. To have a more complete view about the bioactivities of the three plant extracts, conventional tests were used to evaluate their hypotensive and antioxidant activities as will be discussed next.

II.b Hypotensive activity of plant extracts (ACE inhibition)

The extracts were screened for hypotensive properties through their capability of inhibiting ACE using a commercial ACE inhibition kit (ACE Kit-WST, Dojindo laboratories) on microtiter plates. ACE catalyzed the transformation of the 3-hydroxybutyl-Gly-Gly-Gly (3HH-GGG) substrate into 3-hydroxybutyric acid (3HB) product was coupled to a series of secondary reactions terminated by the formation of a colored product (Figure II.35) [20]. The intensity of the yellow color was proportional to the amount of 3HB produced. ACE inhibitors result in reduction of 3HB yields and consequently lower intensity of the final colored product. All necessary reagents were available in the kit. The working enzyme solution, containing ACE catalyzing the conversion of 3HH-GGG into 3-HB-G and aminoacylase catalyzing the conversion of and the latter to 3-

hydroxybutyric acid (3HB), was prepared in deionized water. Similarly, the indicator solution was also prepared in deionized water and contained 3HB dehydrogenase (3HBDH), coenzyme nicotinamide adenine dinucleotide (NAD^+) and 4-[3-(4-iodophenyl)-2-(4-nitrophenyl)-2H-5-tetrazolio]-1,3-benzene disulfonate sodium salt (WST-1) mediator. Plant extracts were dissolved in deionized water at 13 mg mL^{-1} and the resulting solution was centrifuged for 10 min at $2000g$. Similar to the antihyaluronidase activity assays described earlier, the extracts were assayed at 1 mg mL^{-1} and ACE inhibition percentage was calculated by comparing ACE activity in the absence and presence of the extracts. However, since the assay is not a separative one, a reagent blank, containing no ACE or extracts, and in the case of a colored sample, a sample blank, containing the extracts only, were also considered.

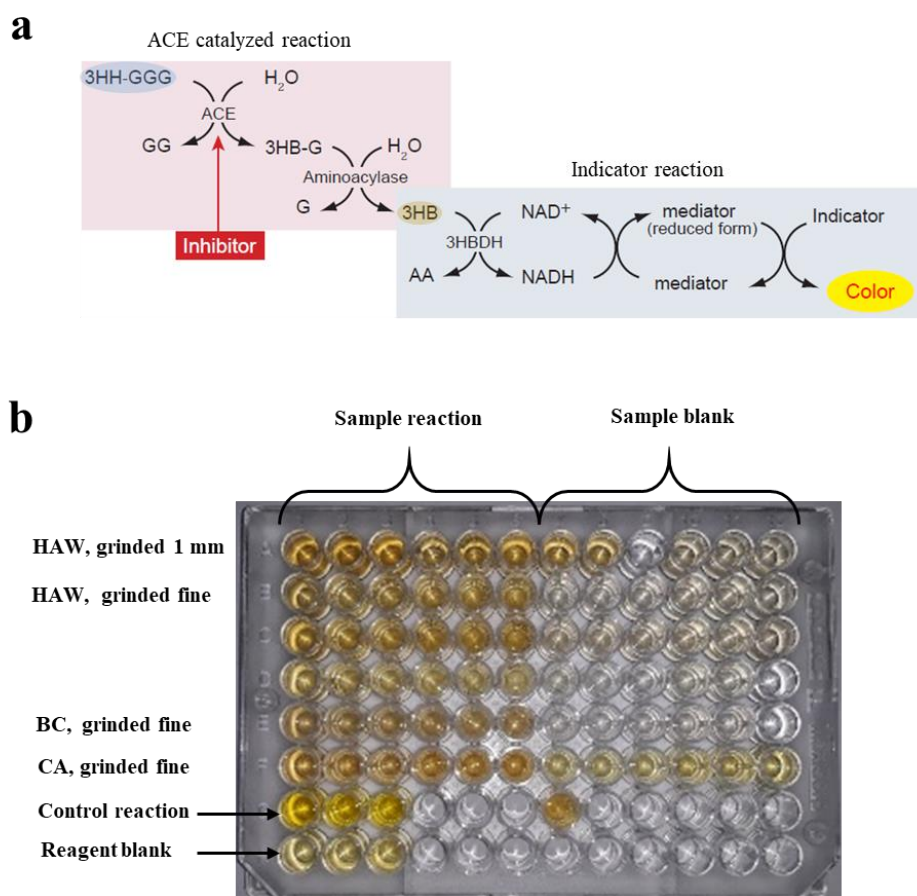


Figure II.35: Illustration of ACE inhibition assay. Illustration of ACE catalyzed hydrolysis of 3HH-GGG to 3HB-G and the subsequent coupled reaction (**a**) and, microplate of ACE inhibition assay (**b**). Final volume in each well $260 \mu\text{L}$, **Sample reaction:** $20 \mu\text{L}$ sample (at 1 mg mL^{-1}) + $20 \mu\text{L}$ 3HH-GGG substrate + $20 \mu\text{L}$ enzyme solution; **Sample blank:** $20 \mu\text{L}$ sample (at 1 mg mL^{-1}) + $240 \mu\text{L}$ H_2O ; **Control reaction:** $20 \mu\text{L}$ water + $20 \mu\text{L}$ 3HH-GGG substrate + $20 \mu\text{L}$ enzyme solution; **Reagent blank:** $40 \mu\text{L}$ H_2O + $20 \mu\text{L}$ 3HH-GGG substrate. The plate was incubated at 37°C for 1 h and $200 \mu\text{L}$ indicator solution was added to each well. The assays were carried out in triplicates ($n = 3$). The plate was read twice ($n = 2$) at $\lambda = 450 \text{ nm}$

ACE inhibition percentage is calculated according to Equation II.9 below:

$$\text{ACE inhibition (\%)} = \frac{(\text{Abs}_{\text{control}} - (\text{Abs}_{\text{sample reaction}} - \text{Abs}_{\text{sample blank}}))}{(\text{Abs}_{\text{control}} - \text{Abs}_{\text{reagent blank}})} \times 100 \quad \text{Equation II.9}$$

where $\text{Abs}_{\text{control}}$, $\text{Abs}_{\text{sample reaction}}$, $\text{Abs}_{\text{sample blank}}$ and $\text{Abs}_{\text{reagent blank}}$ is the absorption of the reaction mixture in the absence of the extracts, the presence of 1 mg mL^{-1} of the extracts, the presence of the extracts but in the absence of ACE, respectively.

The extracts' potential to inhibit ACE at 1 mg mL^{-1} was compared to that of captopril, a reference ACE inhibitor prescribed for the treatment of hypertension, which was previously found to completely inhibit ACE at a concentration 58-fold lower than 1 mg mL^{-1} [21]. Experimental conditions of the ACE inhibition assay are described and the results are presented in Figure II.36. The assay was carried out on 96-well plates in triplicates ($n = 3$) and the absorption of the colored solution was measured twice ($n = 2$) at $\lambda = 450 \text{ nm}$ by a microplate spectrophotometer. All 6 readings of the absorption were then averaged.

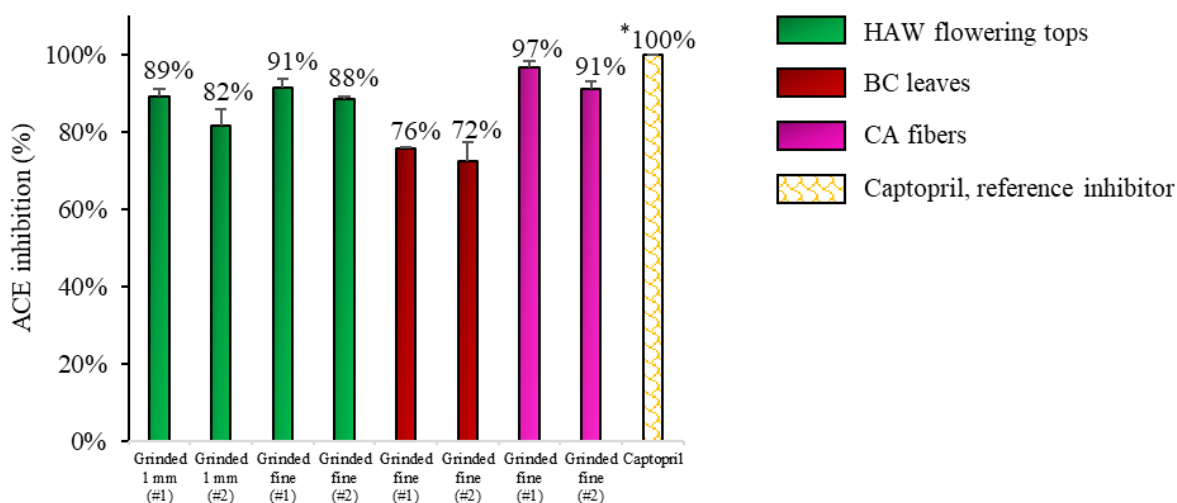


Figure II.36: Percentage of ACE inhibition induced by extracts from three plants at 1 mg mL^{-1} and *captopril, a reference ACE inhibitor assumed to induce complete ACE inhibition at 1 mg mL^{-1} based on the literature [21]. Assays were carried out in triplicates ($n = 3$) and the plate was read twice ($n = 2$)

A general inhibition trend was observed with superior inhibition percentages (72–97%). CA extracts demonstrated the highest ACE inhibition potential (91–97%) followed by HAW (82–91%) and BC (72–76%) extracts. As for hyaluronidase assays seen earlier, the degree of HAW extract grinding did not influence the extent of ACE inhibition since the range of inhibition was similar between extracts with fine and 1 mm grinding.

HAW and BC extracts have been previously described for their positive effects on the cardiovascular system and hypertension [22–24]. Although weak, previous studies have reported an inhibitory effect of HAW extracts towards ACE [25–27]. On the other hand, BC fruit extracts have been previously shown to induce limited ACE inhibition [28] while BC leaves enhanced the activation of endothelial nitric oxide synthase (eNOS), an enzyme contributing, through a signaling pathway, to the reduction of blood pressure [29].

Thus, the moderate ACE inhibitory effect exerted by BC extracts cannot rule out their involvement in blood pressure regulation since the latter seems to take place through a mechanism that does not involve inhibition of ACE.

As far as we know, this was the first time that CA extracts were investigated for their ACE inhibition potential demonstrating almost complete ACE inhibition at the assayed concentration. As a matter of fact, reports on the hypotensive properties of CA were limited to reports of such properties upon intravenous injections of CA were limited to reports of such properties upon intravenous injections of CA extracts which acts as a peripheral vasodilator stimulating the muscular fibers of blood vessels [30].

The observed ACE inhibition trend by the extracts was related to the characterization of molecular features of the extracts by UHPLC and FT-ICR-MS. The inhibition of ACE by all three plant extracts can be attributed to the detection of common compounds such as chlorogenic and caffeic acid shown to induce ACE inhibition of 88 and 63%, respectively, at 0.167 mg mL^{-1} [31]. Similarly, the differential ACE inhibition between the different extracts was explained relative to the ESI(-)FT-ICR-MS phytochemical contents characterization of the extracts. CA extracts showed the highest number and quantities of amino acids, small peptides and amino sugar-like species with a CHON chemical formula and demonstrated strongest ACE inhibition (Figure II.6). Incidentally, BC extracts, demonstrating the lowest ACE inhibition amongst the assayed extracts, showed the lowest number of the aforementioned CHON species. This suggests that the ACE inhibition potential of the extracts is related to the number and concentrations of CHON species.

II.c Antioxidant activities of plant extracts

An ABTS radical cation decolorization assay was used to investigate the antioxidant activities of the plant extracts [16] (Figure II.37a).

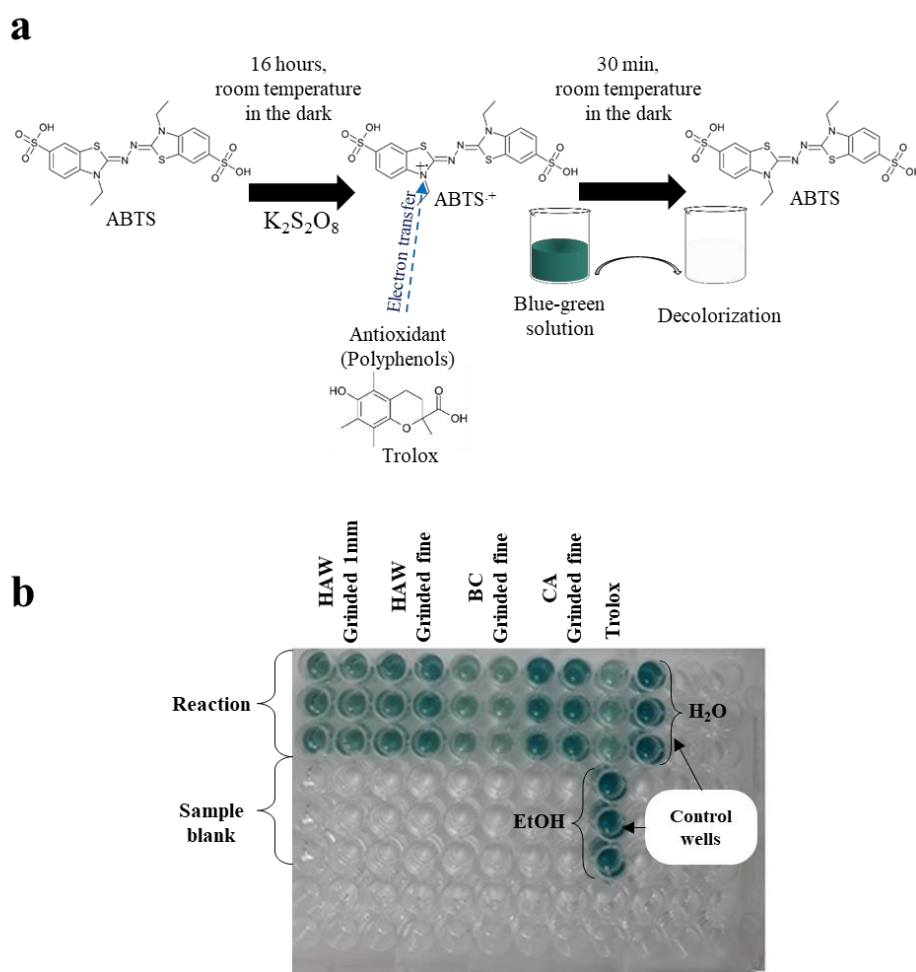


Figure II.37: Illustration of ABTS radical cation antioxidant assay. Illustration of ABTS radical cation formation and decolorization of the ABTS solution induced by antioxidant molecules (**a**) and, microplate of antioxidant ABTS assay (**b**). Final volume in each well 200 μ L, **Reaction:** 10 μ L sample (at 0.01 mg mL⁻¹) + 190 μ L ABTS radical cation solution; **Sample blank:** 10 μ L sample (at 0.01 mg mL⁻¹) + 190 μ L H₂O; **Control wells:** 10 μ L H₂O or EtOH + 190 μ L ABTS radical cation solution. Each sample carried out in triplicates (n = 3). The plate was read twice (n = 2) at $\lambda = 734$ nm to measure the decolorization of ABTS solution in the presence of the samples relative to their absence in the control wells

Briefly, ABTS and potassium persulfate ($K_2S_2O_8$) were mixed and agitated in the dark for 16 h at room temperature to form the blue-green ABTS radical cation solution. The ABTS radical solution was then diluted with ethanol/water (25/75, v/v) at a 1:12.5 volume ratio. Plant extracts were dissolved in water at 20, 2 or 0.2 mg mL⁻¹ and centrifuged for 10 min at 2000g. Trolox, the standard

antioxidant, was prepared in EtOH at 20, 2 or 0.2 mg mL⁻¹. To carry out the antioxidant assays, ABTS was mixed with a solution of plant extracts on a microtiter plate and incubated in the dark for 30 min at room temperature (Figure II.37b). The absorbance of the plate was then measured at $\lambda = 734$ nm. The antioxidant activities of the extracts were evaluated by their ability to decolorize the blue-green ABTS radical cation solution. In other words, the absorption of the ABTS solution in the presence of the extracts was compared to that of the ABTS radical cation solution without the extracts as shown in Equation II.10 below.

$$\text{Antioxidant capacity (\%)}: 1 - \frac{Abs_{\text{Sample}}}{Abs_{\text{Control}}} \times 100 \quad \text{Equation II.10}$$

where Abs_{sample} and Abs_{control} are the absorption of the ABTS solution in the presence, or absence of the plant extracts, respectively. The absorbance of the extracts alone (sample blank) was null and thus was not considered in the calculation.

The antioxidant activity of the extracts was compared to that of trolox, a reference antioxidant compound. The extracts and trolox were first assayed at 1 mg mL⁻¹, the same extract concentration used for antihyaluronidase and ACE inhibition assays. At this concentration, all of the extracts' antioxidant activities were indistinguishable and equivalent to that of trolox ($\approx 100\%$). Thus, the assay was reconducted at a lower concentration.

A 10-fold lower extract and trolox concentration (0.1 mg mL⁻¹) was able to discern CA extracts which demonstrated a lower antioxidant activity of 64%, compared to their activity at 1 mg mL⁻¹, while those of HAW and BC extracts were still high and equivalent to that of trolox ($\approx 100\%$). Therefore, in order to differentiate the antioxidant activities of HAW and BC extracts, the antioxidant assay was carried out at 0.01 mg mL⁻¹ and its results are presented in Figure II.38. BC extracts had the highest antioxidant activity compared to the other extracts (58-64%) and was equivalent to that of trolox (64%). HAW extracts demonstrated a lower range of antioxidant activity (28-45%). The lowest antioxidant capacity was observed once again with the extracts of CA (19-22%). These activities were correlated to the TPC and TFC of the extracts since both polyphenols and flavonoids are known for their antioxidant properties [32]. The highest TPC and TFC were quantified in BC extracts and incidentally these had the highest antioxidant activities equivalent to that of trolox. On the other hand, CA had the lowest TPC and TFC in their extracts and demonstrated the lowest antioxidant activities at 0.1 and 0.01 mg mL⁻¹.

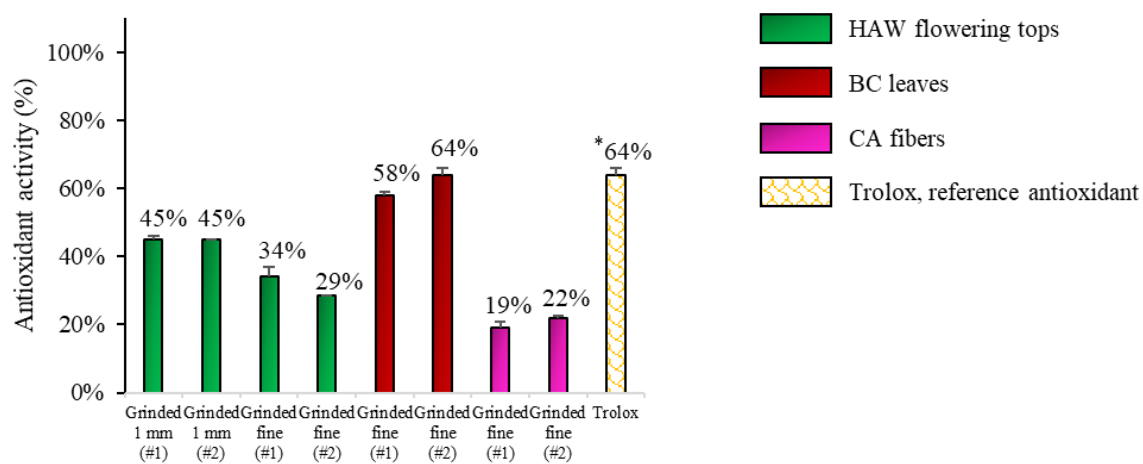


Figure II.38: Percentage of antioxidant activity induced by extracts from three plants and ^{*}Trolox, a reference antioxidant compound at 0.01 mg mL^{-1} . Assays were carried out in triplicates ($n = 3$) and the plate was read twice ($n = 2$) at $\lambda = 734 \text{ nm}$

III. Conclusion

In this section, the hyaluronidase inhibition potential of extracts from three different plants was evaluated using an offline CE-UV assay. CE was demonstrated once again to be a suitable technique for activity assays using ligands varying in their degree of complexity from purified molecules (as seen in the first section) to crude plant extracts containing hundreds of molecules.

The hypotensive and antioxidant properties of the plant extracts were evaluated using conventional spectrophotometric assays in order to gain a clearer insight about the bioactivities of these extracts.

An interesting antihyaluronidase activity similar to that of the reference compound, EGCG, was observed with extracts of HAW flowering tops (> 90% at 1 mg mL⁻¹). CA fiber extracts were shown for the first time to have a strong influence on ACE inhibition (91-97% at 1 mg mL⁻¹). Extracts of BC leaves demonstrated the highest antioxidant capacity equivalent to that of the reference antioxidant compound, trolox, when assayed at three different concentrations: 100% at 1 mg mL⁻¹, 100% at 0.1 mg mL⁻¹ and 58-64% at 0.01 mg mL⁻¹.

Results of the various bioactivities are summarized in Table II.9.

Table II.9: Results of plant extracts bioactivities as well as EGCG, captopril and trolox. *n.r.*: Not relevant, *: theoretical complete inhibition of ACE by captopril. Conditions of all assays are described in Part C of the chapter

	Hyaluronidase inhibition (%) 1 mg mL ⁻¹	ACE inhibition (%) 1 mg mL ⁻¹	Antioxidant activity (%) 0.01 mg mL ⁻¹
EGCG	98%	<i>n.r.</i>	<i>n.r.</i>
Captopril	<i>n.r.</i>	100%*	<i>n.r.</i>
Trolox	<i>n.r.</i>	<i>n.r.</i>	64%
HAW flowering tops (grinded 1 mm)	96-97%	82-89%	45%
HAW flowering tops (grinded fine)	93-97%	88-91%	29-34%
BC leaves (grinded fine)	64%	72-76%	58-64%
CA fibers (grinded fine)	59-61%	91-97%	19-22%

Chapter conclusion

In this chapter, CE was used to investigate the effects of modulators of different complexities (purified molecules or crude extracts) on the activity of PL and hyaluronidase, two model enzymes. It was possible to investigate the effect of different media (crowded or dilute) No modification of the enzyme or ligand was required. Instead, different detection assemblies were coupled to CE to detect products with different physical properties such as UV or UV/C⁴D detectors operated in the offline or the online CE modes.

On the other hand, MST was used successfully to evaluate the binding affinity (K_d) of different ligands towards PL from crude porcine pancreas extracts, a complex source of lipases. K_d were obtained in less than 30 min requiring minimal amounts of target, ligands and reagent volumes. Furthermore, the MST method was optimized to be carried out in standard uncoated capillaries which are much cheaper than coated ones.

The observed effects of the extracts on PL activity were correlated to the chemical compositions as well as previous literature reports of the plant's activity. The effects of purified molecules from oakwood and wine extracts were correlated to their molecular structure establishing a structure-activity relationship.

The purified molecules that have demonstrated either potent inhibition or moderate activation of PL activity in **Part A** have all demonstrated binding affinities of different extents towards PL. Complementing PL binding data from **Part B** with PL catalytic activity from **Part A** allowed the construction of a more complete image of the molecular mechanism that the ligands induce on PL and its activity.

Biomolecular crowding by PEG, investigated in **Part C**, section 1, served to mimic the extracellular matrix, *i.e.* real-life conditions. It has shown to have an interesting effect on the purified modulator compounds EGCG and QTT-I, where their hyaluronidase inhibition potential perished almost completely in crowded media as investigated using a CE-based hyaluronidase assay. On the other hand, the inhibition induced by linear polysaccharides (CS-A and CS-C) was either slightly reduced or unchanged. This has led us to hypothesize that the charge and structure of the molecule plays an important role in determining its inhibitory effect towards hyaluronidase in crowded media due to their interactions with the crowding agents.

It would be interesting to investigate novel synthetic and natural modulators of PL using the CE-UV/C⁴D-MST couple. The application of this binding-activity relationship to crude plant

extracts is more complicated due to the complexity of the sample where several ligands exist simultaneously and several of these ligands may bind or modulate PL activity. However, an alternative would be using CE to assess the overall activities of the extracts as we have shown for PL and hyaluronidase, followed by a thorough examination of the extract's molecular composition and the activities of the isolated constituents prior to MST binding analyses using these purified constituents. The successful use of PL in crude extracts could pave a way for the analysis of PL activity and inhibition in whole cells and cell lysates given the affinity of the substrates and ligands towards PL is sufficient to avoid false-positive results.

The effect of crowding by PEG on hyaluronidase can be expanded to modulators of different structures to gain better insight on the actual mechanism induced by the crowding agent. Furthermore, enzymatic assays with crowded media can be transferred to enzymes other than hyaluronidase to investigate the influence of biomolecular crowding on the stability of the enzyme.

References

- 1 A. J. Zemann, E. Schnell, D. Volgger and G. K. Bonn, *Anal. Chem.*, 1998, **70**, 563–567.
- 2 J. A. Fracassi Da Silva and C. L. do Lago, *Anal. Chem.*, 1998, **70**, 4339–4343.
- 3 A. J. Zemann, *Electrophoresis*, 2003, **24**, 2125–2137.
- 4 H. Nehmé, Etude des réactions enzymatiques par électrophorèse capillaire, PhD Thesis, Université d'Orléans, 2013.
- 5 I. O. Neaga, B. C. Iacob and E. Bodoki, *J. Liq. Chromatogr. Relat. Technol.*, 2014, **37**, 2072–2090.
- 6 P. C. Ngoc, L. Leclercq, J. C. Rossi, I. Desvignes, J. Hertzog, A. S. Fabiano-Tixier, F. Chemat, P. Schmitt-Kopplin and H. Cottet, *Molecules*, 2019, **24**, 1–32.
- 7 R. B. Birari and K. K. Bhutani, *Drug Discov. Today*, 2007, **12**, 879–889.
- 8 F. I. Khan, D. Lan, R. Durrani, W. Huan, Z. Zhao and Y. Wang, *Front. Bioeng. Biotechnol.*, 2017, **5**, 1–13.
- 9 K. Shirai and R. L. Jackson, *J. Biol. Chem.*, 1982, **257**, 1253–1258.
- 10 R. Smith and C. Tanford, *J. Mol. Biol.*, 1972, **67**, 75–83.
- 11 B. Bonamichi, E. B. Parente, R. B. dos Santos, R. Beltzhoover, J. Lee and J. E. N. Salles, *J. Obes. Eat. Disord.*, 2018, **4**, 1–10.
- 12 P. Rosa-Gonçalves and D. Majerowicz, *Am. J. Cardiovasc. Drugs*, 2019, **19**, 349–364.
- 13 A. Zohrabian, *Clin. Outcomes Res.*, 2010, **2**, 63–74.
- 14 J. G. Kang and C.-Y. Park, *Diabetes Metab. J.*, 2012, **36**, 13–25.
- 15 M. M. Beyea, A. X. Garg and M. A. Weir, *Ther. Adv. Drug Saf.*, 2012, **3**, 53–57.
- 16 L. R. Solomon, A. C. Nixon, L. Ogden and B. Nair, *BMJ Case Rep.*, 2017, DOI: 10.1136/bcr-2016-218623.
- 17 T. D. Filippatos, C. S. Derdemezis, I. F. Gazi, E. S. Nakou, D. P. Mikhailidis and M. S. Elisaf, *Drug Saf.*, 2008, **31**, 53–65.
- 18 T. Sergent, J. Vanderstraeten, J. Winand, P. Beguin and Y. J. Schneider, *Food Chem.*, 2012, **135**, 68–73.
- 19 F. Li, W. Li, H. Fu, Q. Zhang and K. Koike, *Chem. Pharm. Bull.*, 2007, **55**, 1087–1089.
- 20 D. Chauhan, G. George, S. N. C. Sridhar, R. Bhatia, A. T. Paul and V. Monga, *Arch Pharm*, 2019, **352**, e1900029.
- 21 S. N. C. Sridhar, S. Palawat and A. T. Paul, *Bioorg. Chem.*, 2019, **85**, 373–381.

- 22 P. Ramana, E. Adams, P. Augustijns and A. Van Schepdael, *Talanta*, 2017, **164**, 148–153.
- 23 N. Drouin, M. van Mever, W. Zhang, E. Tobolkina, S. Ferre, A.-C. Servais, M.-J. Gou, L. Nyssen, M. Fillet, G. S. M. Lageveen-Kammeijer, J. Nouta, A. J. Chetwynd, I. Lynch, J. A. Thorn, J. Meixner, C. Löbner, M. Taverna, S. Liu, N. T. Tran, Y. Francois, A. Lechner, R. Nehmé, G. Al Hamoui Dit Banni, R. Nasreddine, C. Colas, H. H. Lindner, K. Faserl, C. Neusüß, M. Nelke, S. Lämmerer, C. Perrin, C. Bich-Muracciole, C. Barbas, Á. L. González, A. Guttman, M. Szigeti, P. Britz-McKibbin, Z. Kroezen, M. Shanmuganathan, P. Nemes, E. P. Portero, T. Hankemeier, S. Codesido, V. González-Ruiz, S. Rudaz and R. Ramautar, *Anal. Chem.*, 2020, **92**, 14103–14112.
- 24 X. Chen, S. Xue, Y. Lin, J. Luo and L. Kong, *Anal. Chim. Acta*, 2020, **1099**, 94–102.
- 25 J. Iqbal, S. Iqbal and C. E. Müller, *Analyst*, 2013, **138**, 3104–3116.
- 26 C. Serveau-Avesque, R. Verger, J. A. Rodriguez and A. Abousalham, *Analyst*, 2013, **138**, 5230–5238.
- 27 Y. Fan and G. K. E. Scriba, *J. Pharm. Biomed. Anal.*, 2010, **53**, 1076–1090.
- 28 R. Nehmé and P. Morin, *Electrophoresis*, 2015, **36**, 2768–2797.
- 29 S. Fayad, P. Morin and R. Nehmé, *J. Chromatogr. A*, 2017, **1529**, 1–28.
- 30 S. Gattu, C. L. Carihfield, G. Lu, L. Bwanali, L. M. Veltri and L. A. Holland, *Methods*, 2018, **146**, 93–106.
- 31 M. Cheng and Z. Chen, *J. Pharm. Anal.*, 2018, **8**, 226–233.
- 32 W.-F. Wang and J.-L. Yang, *Electrophoresis*, 2019, **40**, 2075–2083.
- 33 N. Banke, K. Hansen and I. Diers, *J. Chromatogr. A*, 1991, **559**, 325–335.
- 34 R. J. Krueger, T. R. Hobbs, K. A. Mihal, J. Tehrani and M. G. Zeece, *J. Chromatogr. A*, 1991, **543**, 451–461.
- 35 J. Bao and F. E. Regnier, *J. Chromatogr. A*, 1992, **608**, 217–224.
- 36 S. Fayad, R. Nehmé, M. Langmajerová, B. Ayela, C. Colas, B. Maunit, J. C. Jacquinet, A. Vibert, C. Lopin-Bon, G. Zdeněk and P. Morin, *Anal. Chim. Acta*, 2017, **951**, 140–150.
- 37 H. Nehmé, S. Chantepie, J. Defert, P. Morin, D. Papy-Garcia and R. Nehmé, *Anal. Bioanal. Chem.*, 2015, **407**, 2821–2828.
- 38 R. Nasreddine, L. Orlic, G. Al Hamoui Dit Banni, S. Fayad, A. Marchal, F. Piazza, C. Lopin-Bon, J. Hamacek and R. Nehmé, *Anal. Bioanal. Chem.*, 2020, **412**, 4195–4207.
- 39 B. J. Harmon, D. H. Patterson and F. E. Regnier, *Anal. Chem.*, 1993, **65**, 2655–2662.

- 40 H. Nehmé, R. Nehmé, P. Lafite, S. Routier and P. Morin, *Anal. Chim. Acta*, 2012, **722**, 127–135.
- 41 E. Farcaş, L. Pochet and M. Fillet, *Talanta*, 2018, **188**, 516–521.
- 42 V. Okhonin, X. Liu and S. N. Krylov, *Anal. Chem.*, 2005, **77**, 5925–5929.
- 43 Y. Fan and G. K. E. Scriba, *J. Pharm. Biomed. Anal.*, 2010, **53**, 1076–1090.
- 44 D. M. Liu, Y. P. Shi and J. Chen, *Chinese J. Anal. Chem.*, 2015, **43**, 775–782.
- 45 T. Kaneta, *Chem. Rec.*, 2019, **19**, 452–461.
- 46 R. Gahoual, E. Leize-Wagner, P. Houzé and Y.-N. François, *Rapid Commun. Mass Spectrom.*, 2019, **33**, 11–19.
- 47 K. Klepárník, *Electrophoresis*, 2013, **34**, 70–85.
- 48 B. Claude, G. Cutolo, A. Farhat, I. Zarafu, P. Ionita, M. Schuler, A. Tatibouët, P. Morin and R. Nehmé, *Anal. Chim. Acta*, 2019, **1085**, 117–125.
- 49 A. Schuchert-Shi and P. C. Hauser, *Chirality*, 2009, **22**, 331–335.
- 50 Y. Tang, W. Li, Y. Wang, Y. Zhang and Y. Ji, *J. Sep. Sci.*, 2019, **43**, 1003–1010.
- 51 P. C. Ngoc, L. Leclercq, J. C. Rossi, J. Hertzog, A.-S. Tixier, F. Chemat, R. Nasreddine, G. Al Hamoui Dit Banni, R. Nehmé, P. Schmitt-Kopplin and H. Cottet, *Foods*, 2020, **9**, 1–26.
- 52 B. Gaš, 2011, <https://web.natur.cuni.cz/gas/PeakMaster 5.4 Relea>.
- 53 A. Marchal, B. N. Cretin, L. Sindt, P. Waffo-Téguo and D. Dubourdieu, *Tetrahedron*, 2015, **71**, 3148–3156.
- 54 A. Marchal, P. Waffo-Téguo, E. Génin, J. Mérillon and D. Dubourdieu, *Anal. Chem.*, 2011, **83**, 9629–9637.
- 55 A. Marchal, A. Prida and D. Dubourdieu, *J. Agric. Food Chem.*, 2016, **64**, 618–626.
- 56 M. Gammacurta, P. Waffo-Teguo, D. Winstel, D. Dubourdieu and A. Marchal, *J. Nat. Prod.*, 2020, **83**, 1611–1622.
- 57 S. Fayad, B. N. Cretin and A. Marchal, *Food Chem.*, 2020, **311**, 125881.
- 58 S. N. Krylov, 2008, <http://www.yorku.ca/skrylov/resources/downloads/TD>.
- 59 M. Pelcová, R. Řemínek, F. A. Sandbaumhüter, R. A. Mosher, Z. Glatz and W. Thormann, *J. Chromatogr. A*, 2016, **1471**, 192–200.
- 60 J. L. Beckers and P. Boček, *Electrophoresis*, 2003, **24**, 518–535.
- 61 J. S. Patton, P. A. Albertsson, C. Erlanson and B. Borgstrom, *J. Biol. Chem.*, 1978, **253**, 4195–4202.
- 62 G. Isaksson, I. Lundquist and I. Ihse, *Gastroenterology*, 1982, **82**, 918–924.
- 63 D. A. Spudeit, S. Gonçalves, L. C. Bretanha, C. A. Claumann, R. A. F. Machado and

- G. A. Micke, *J. Braz. Chem. Soc.*, 2016, **27**, 1974–1979.
- 64 L. Polgár, in *Proteolytic enzymes: tools and targets*, eds. E. Sterchi and W. Stöcker, Springer-Verlag Berlin Heidelberg, 1999, pp. 148–166.
- 65 Q. Zhang, J. Qian, H. Guo, W. Zhang and C. Kuang, *J. Nanosci. Nanotechnol.*, 2018, **18**, 5837–5841.
- 66 B. Liu, X. Peng and X. Meng, *Front. Microbiol.*, 2018, **9**, 615.
- 67 S. Sharma and S. S. Kanwar, *Hindawi*, 2014, **2014**, 15.
- 68 H. Bisswanger, *Perspect. Sci.*, 2014, **1**, 41–55.
- 69 S. Van Dyck, A. Van Schepdael and J. Hoogmartens, *Electrophoresis*, 2001, **22**, 1436–1442.
- 70 M. Dadouch, Y. Ladner, C. Bich, M. Larroque, C. Larroque, J. Morel, P. A. Bonnet and C. Perrin, *Analyst*, 2020, **145**, 1759–1767.
- 71 R. Nehmé, H. Nehmé, T. Saurat, M.-L. de Tauzia, F. Buron, P. Lafite, P. Verrelle, E. Chautard, P. Morin, S. Routier and H. Bénédicti, *Anal. Bioanal. Chem.*, 2014, **406**, 3743–3754.
- 72 S. M. Krylova, V. Okhonin and S. N. Krylov, *J. Sep. Sci.*, 2009, **32**, 742–756.
- 73 W. Tsuzuki, A. Ue and Y. Kitamura, *Biotechnol. Biochem.*, 2001, **65**, 2078–2082.
- 74 A. Alirezalu, P. Salehi, N. Ahmadi, A. Sonboli, S. Aceto, H. H. Maleki and M. Ayyari, *Int. J. Food Prop.*, 2018, **21**, 452–470.
- 75 J. E. Edwards, P. N. Brown, N. Talent, T. A. Dickinson and P. R. Shipley, *Phytochemistry*, 2012, **79**, 5–26.
- 76 J. Liu, R.-T. Ma and Y.-P. Shi, *J. Chromatogr. A*, 2020, **1615**, 1–8.
- 77 N. A. Lunagariya, N. K. Patel, S. C. Jagtap and K. K. Bhutani, *Excli J.*, 2014, **13**, 897–921.
- 78 A. T. M. A. Rahim, Y. Takahashi and K. Yamaki, *Food Res. Int.*, 2015, **75**, 289–294.
- 79 T. H. Scheuermann, S. B. Padrick, K. H. Gardner and C. A. Brautigam, *Anal. Biochem.*, 2016, **496**, 79–93.
- 80 M. Jerabek-Willemsen, T. André, R. Wanner, H. M. Roth, S. Duhr, P. Baaske and D. Breitsprecher, *J. Mol. Struct.*, 2014, **1077**, 101–113.
- 81 S. Duhr and D. Braun, *PNAS is Proc. Natl. Acad. Sci. U.S.A.*, 2006, **103**, 19678–19682.
- 82 T. Schubert and G. Längst, *AIMS Biophys.*, 2015, **2**, 370–380.
- 83 J. M. Rainard, G. C. Pandarakalam and S. P. McElroy, *SLAS Discov.*, 2018, **23**, 225–241.

- 84 C. J. Wienken, P. Baaske, U. Rothbauer, D. Braun and S. Duhr, *Nat. Commun.*, 2010, **1**, 1–7.
- 85 T. W. Speer, in *Encyclopedia of radiation oncology*, eds. L. W. Brady and T. E. Yaeger, Springer, Berlin, Heidelberg, 2013.
- 86 V. Kairys, L. Baranauskiene, M. Kazlauskiene, D. Matulis and E. Kazlauskas, *Expert Opin. Drug Discov.*, 2019, **14**, 755–768.
- 87 R. Mallik, M. Yoo, C. Briscoe and D. Hage, *J. Chromatogr. A.*, 2010, **1217**, 2796–2803.
- 88 C. Zhang, E. Rodriguez, C. Bi, X. Zheng, D. Suresh, K. Suh, Z. Li, F. Elsebaei and D. S. Hage, *Analyst*, 2018, **143**, 374–391.
- 89 D. S. Hage, *Clin. Chem.*, 2017, **63**, 1083–1093.
- 90 H. Whately, in *Clinical and Forensic Applications of Capillary Electrophoresis*, eds. J. Petersen and A. A. Mohammad, Humana Press, New Jersey, 2001, pp. 21–58.
- 91 K. Lipponen, S. Tähkä, J. Samuelsson, M. Jauhiainen, J. Metso, G. C. Karhu, T. Fornstedt, M. Kostianen and M.-L. Riekkola, *Anal. Bioanal. Chem.*, 2014, **406**, 4137–4146.
- 92 G. A. Ascoli, E. Domenici and C. Bertucci, *Chirality*, 2006, **18**, 667–679.
- 93 M. Dawod, N. E. Arvin and R. T. Kennedy, *Analyst*, 2017, **142**, 1847–1866.
- 94 L. Sun, M. J. Gidley and F. J. Warren, *Mol. Nutr. Food Res.*, 2017, **61**, 1–13.
- 95 X. Wu, W. He, L. Yao, H. Zhang, Z. Liu, W. Wang, Y. Ye and J. Cao, *J. Agric. Food Chem.*, 2013, **61**, 8829–8835.
- 96 K. Lin and G. Wu, in *The Hippo Pathway. Methods In Molecular Biology*, ed. A. Hergovich, Humana Press, New York, 2019, vol. 1893, pp. 257–272.
- 97 S. Bjelić and I. Jelesarov, *J. Mol. Recognit.*, 2008, **21**, 289–311.
- 98 S. K. Bhardwaj and T. Basu, *Thin Solid Films*, 2018, **645**, 10–18.
- 99 R. P. Sparks, J. L. Jenkins and R. Fratti, *Methods Mol. Biol.*, 2019, **1860**, 199–210.
- 100 E. Helmerhorst, D. J. Chandler, M. Nussio and C. D. Mamotte, *Clin. Biochem. Rev.*, 2012, **33**, 161–173.
- 101 T. Sugiki, K. Furuuta, T. Fujiwara and C. Kojima, *Molecules*, 2018, **23**, 1–27.
- 102 M. S. Silva and D. Pietrobom, *J. Braz. Chem. Soc.*, 2016, **27**, 1918–1923.
- 103 D. M. Dias and A. Ciulli, *Prog. Biophys. Mol. Biol.*, 2014, **116**, 101–112.
- 104 K. Vuignier, J. Schappler, J. L. Veuthey, P. A. Carrupt and S. Martel, *Anal. Bioanal. Chem.*, 2010, **398**, 53–66.
- 105 P. Baaske, C. J. Wienken, P. Reineck, S. Duhr and D. Braun, *Angew. Chem. Int. Ed.*,

- 2010, **49**, 2238–2241.
- 106 M. Berleth, N. Berleth, A. Minges, S. Hänsch, R. C. Burkart, B. Stork, Y. Stahl, S. Weidtkamp-Peters, R. Simon and G. Groth, *Front. Plant Sci.*, 2019, **10**, 1–15.
- 107 O. B. Torres, A. J. Duval, A. Sulima, J. F. G. Antoline, A. E. Jacobson, K. C. Rice, C. R. Alving and G. R. Matyas, *Anal. Bioanal. Chem.*, 2018, **410**, 3885–3903.
- 108 J. Sloan, J. P. Hakenjos, M. Gebert, O. Ermakova, A. Gumiero, G. Stier, K. Wild, I. Sinning and J. U. Lohmann, *Nat. Commun.*, 2020, **11**, 1–16.
- 109 M. H. Moon, T. A. Hilimire, A. M. Sanders and J. S. Schneekloth, *Biochemistry*, 2018, **57**, 4638–4643.
- 110 M. J. Rubio, M. Svobodová, T. Mairal, T. Schubert, S. Künne, G. Mayer and C. K. O. Sullivan, *Anal. Bioanal. Chem.*, 2016, **408**, 875–884.
- 111 F. Syntia, R. Nehmé, B. Claude and P. Morin, *J. Chromatogr. A.*, 2016, **1431**, 215–223.
- 112 N. Lee and S. Wiegand, *Entropy*, 2020, **22**, 1–24.
- 113 M. Jerabek-Willemsen, C. J. Wienken, D. Braun, P. Baaske and S. Duhr, *Assay Drug Dev. Technol.*, 2011, **9**, 342–353.
- 114 Muntholib, D. Sulistyaningrum, Subandi and M. Siti, *AIP Conf. Proc.*, 2020, **2231**, 1–11.
- 115 X. Du, M. Bai, Y. Huang, Z. Jiang, F. Chen, H. Ni and Q. Li, *J. Funct. Foods*, 2018, **48**, 551–557.
- 116 H. Xu-Dong, S. Li-Lin, C. Yun-Feng, W. Yi-Nan, Z. Qi, F. Sheng-Quan, W. Da-Chang, Z. Shi-Zhu, C. Lu, B. Yue, G. Guang-Bo and H. Jie, *Chin. J. Nat. Med.*, 2020, **18**, 369–378.
- 117 G. Hao, L. Yang, I. Mazsaroff and M. Lin, *J. Am. Soc. Mass. Spectr.*, 2007, **18**, 1579–1581.
- 118 G. Al Hamoui Dit Banni, R. Nasreddine, S. Fayad, P. C. Ngoc, J. C. Rossi, L. Leclercq, H. Cottet, A. Marchal and R. Nehmé, *Analyst*, 2021, **146**, 1386–1401.
- 119 H. Nehmé, R. Nehmé, P. Lafite, S. Routier and P. Morin, *J. Chromatogr. A*, 2013, **1314**, 298–305.
- 120 K. Panuganti, M. Nguyen and R. Kshirsagar, in *StatPearls*, StatPearls Publishing, Treasure Island (FL), 2020.
- 121 World Health Organization, Obesity and overweight, <https://www.who.int/news-room/fact-sheets/detail/obesity-and-overweight>, (accessed 6 December 2020).
- 122 T. T. Liu, X. T. Liu, Q. X. Chen and Y. Shi, *Biomed. Pharmacother.*, 2020, **128**, 1–29.

- 123 R. Huang, Y. Zhang, S. Shen, Z. Zhi, H. Chen, S. Chen and X. Ye, *Food Chem.*, 2020, 126785.
- 124 Q. Hu, X. Q. Guan, L. L. Song, H. N. Wang, Y. Xiong, J. L. Liu, H. Yin, Y. F. Cao, J. Hou, L. Yang and G. B. Ge, *Ecotoxicol. Environ. Saf.*, 2020, **192**, 110305.
- 125 R. L. Segura, L. Betancor, J. M. Palomo, A. Hidalgo, G. Fernández-Lorente, M. Terreni, C. Mateo, A. Cortés, R. Fernández-Lafuente and J. M. Guisán, *Enzym. Microb. Technol.*, 2006, **39**, 817–823.
- 126 N. J. Anthis and G. M. Clore, *Protein Sci.*, 2013, **22**, 851–858.
- 127 K. M. Shahani, I. M. Khan and R. C. Chandan, *J. Dairy Sci.*, 1976, **59**, 369–375.
- 128 W. R. Algar, in *Chemoselective and bioorthogonal ligation reactions: concepts and applications, Volume 1*, eds. W. R. Algar, P. Dawson and I. Medintz, Wiley-VCH Verlag GmbH & Co. KGaA, Weinheim, Germany, 2017, pp. 3–36.
- 129 I. Roy and M. N. Gupta, *Biotechnol. Appl. Biochem.*, 2004, **39**, 165–177.
- 130 A. M. Heck, J. A. Yanovski and K. A. Calis, *Pharmacotherapy*, 2000, **20**, 270–279.
- 131 P. Wingfield, *Curr. Protoc. Protein Sci.*, 2001, **Appendix 3**, 1–10.
- 132 S. Fayad, Développement d’outils ultra-performants de criblage enzymatique de produits naturels par électrophorèse capillaire, PhD thesis, Université d’Orléans, 2017.
- 133 K. Girish, K. Kemparaju, S. Nagaraju and B. Vishwanath, *Curr. Med. Chem.*, 2009, **16**, 2261–2288.
- 134 K. P. Vercruyssen, A. R. Lauwers and J. M. Demeester, *Biochem. J.*, 1995, **310**, 55–59.
- 135 R. Nehmé, R. Nasreddine, L. Orlic, C. Lopin-Bon, J. Hamacek and F. Piazza, *Biochim. Biophys. Acta. Gen. Subj.*, 2021, **1865**, 1–7.
- 136 B. Akabayov, S. R. Akabayov, S. J. Lee, G. Wagner and C. C. Richardson, *Nat. Commun.*, 2013, **4**, 1–10.
- 137 I. M. Kuznetsova, K. K. Turoverov and V. N. Uversky, *Int. J. Mol. Sci.*, 2014, **15**, 23090–23140.
- 138 G. Al Hamoui Dit Banni, R. Nasreddine, S. Fayad, C. Colas, A. Marchal and R. Nehmé, *Anal. Bioanal. Chem.*, 2021, In-Peer.
- 139 J. R. Catai and E. Carrilho, *J. Braz. Chem. Soc.*, 2004, **15**, 413–420.

Chapter III:

Hyphenation of capillary electrophoresis to mass spectrometry. *Application to metabolomics and nucleoside kinase assay*

Summary

This final chapter of my thesis introduces the work done on CE hyphenated to mass spectrometry (MS). This coupling takes advantage of the high efficiency of separation provided by CE and the high sensitivity and selectivity of MS detection to analyze a wide range of analytes for various applications. Following an “**Introduction**” on MS and the hyphenation of CE to MS, “**Part A**” of this chapter will introduce a recent interlaboratory collaboration partook by our laboratory demonstrating the strength of CE-MS for the analysis of small metabolites in biological samples and using electrophoretic mobility rather than migration time scales to overcome poor reproducibilities. “**Part B**” will briefly introduce the reaction pathways of nucleoside kinases and their involvement in vital biological processes and viral infections. Additionally, the involvement of such enzymes in the activation of antiviral and anticancer drugs will be discussed. Results of the optimizations performed using CE-UV and CE-MS for studying nucleoside kinase catalyzed reactions will be presented. Finally, the “**General conclusion**” will highlight the important results obtained in this chapter and propose ideas and perspectives for the future.

Collaborator contributions & acknowledgements

Dr. D. Da Silva, Dr. J. Ferey and Pr. L. Agrofoglio (University of Orléans; ICOA) provided the necessary nucleoside kinases and advices for MS analyses, Dr. V. Roy, Pr. L. Agrofoglio and Dr. N. Biteau (University of Orléans; ICOA) synthesized the thymidine monophosphate analogues, Dr. C Colas (University of Orléans, ICOA & Center for Molecular Biophysics, CNRS) aided in and supervised CE-MS analysis and method development, Dr. R. Ramautar and Dr. N. Drouin (University of Leiden, Leiden academic centre for drug research) oversaw the Metabo-Ring interlaboratory study and provided the samples and necessary instruction

I. General Introduction to MS

Mass spectrometry (MS) is a powerful physico-chemical technique used for the detection and quantification of ionizable samples at high sensitivity. The technique has found applications in many branches of natural sciences such as metabolomic analyses, space exploration, environmental analyses, clinical and forensic sciences and many others.

The samples analyzed by mass spectrometry are first ionized into gas phase ions. These ions are then separated based on their mass to charge ratio (m/z) in the mass spectrometer and the abundance of each species is detected and plotted against the m/z ratio [1].

The word mass spectrometry is vaguely used to describe the synergic function of several instruments. Generally, a typical mass spectrometer is made up of three main components: the ionization source, the mass analyzer and the detector.

The ionization source is where the analytes are ionized prior to their transfer onto the mass analyzer. Several types of ionization techniques are available and the choice of the appropriate one depends on the properties of the analytes. Thermally fragile samples or samples with low volatility will often fragment using hard ionization techniques such as electron (EI) or chemical dissociation ionization (CDI). Alternatively, soft ionization techniques are described for thermally labile, biological samples introduced in a liquid phase. The most common soft ionization source is electrospray ionization (ESI). The introduction of soft ionization techniques was an important step in coupling liquid flow techniques such as liquid chromatography (LC) and capillary electrophoresis (CE) to mass spectrometry [2,3].

The ions produced in the ionization source are then transferred to the mass analyzer where they are separated based on their m/z ratios. Several type of mass analyzers exist that separate ions based on different physical properties such as the velocities of the ions (time of flight (TOF) mass analyzers), their momentum (magnetic sector) or stability of their trajectory (quadropole) [2,4]. Resolution is often used to characterize mass analyzers based on their ability to differentiate ions of very similar m/z ratios [5].

The final component of a mass spectrometer is the detector which converts the analogue signals produced by the incident ions to electric currents relative to their abundance. Mass detectors are usually coupled to signal amplifiers to produce a sufficiently high response that could be translated onto a mass spectrum. [2,6,7]

MS instruments are normally operated under vacuum to prevent the deviation of analyte ions from their trajectory as a result of collision with particles in air. Additionally, unspecific reactions of the air particles with the analyte ions would overwhelm the mass spectrum with contaminant peaks [2].

The concept of modern mass spectrometry was achieved through incremental discoveries and improvements in a span of almost a decade. The discovery of positive ions in gaseous phase by E. Goldstein in 1886 and the electron by J. J. Thomson in 1897 were thought to have kicked off the development of the modern-day mass spectrometer¹. Figure III.1 represents a specimen of mass spectrometry pioneers and their significant contribution.

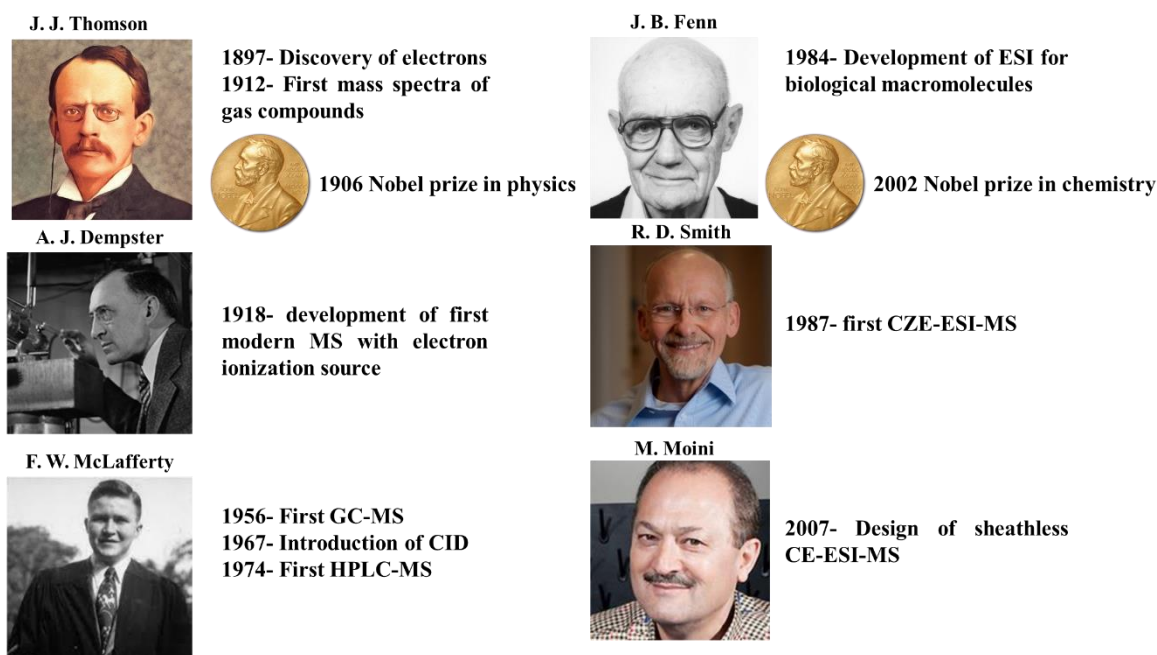


Figure III.1: A representation of iconic names in the field of mass spectrometry and their contributions

Throughout the course of this thesis, MS was used in the context of hyphenation to CE or for obtaining structural information about lipases as previously demonstrated in Chapter II, **Part B**. This coupling exploits the advantages of both techniques such as the high separation efficiency of CE and the high detection sensitivity and selectivity of MS rendering a synergistically robust technique for the analysis of complex samples and a wide range of biomolecules. An ESI source was used to ionize the analytes flowing into it from the capillary. The ionized particles are then

¹ History of Mass Spectrometry, www.ms-museum.org

transferred to a UHR-Q-TOF maXis-ETD mass analyzer (Bruker) where they are separated based on their velocities in the flight tube. Finally, the ions are detected by an electron multiplier (EM) and the signal is amplified and converted into a mass spectrum. In the next segment of this general introduction, the principles and features of the ESI ion source, TOF mass analyzer and EM detector used will be discussed emphasizing on their use in conjunction of CE to MS.

1.a Electrospray ionization

Following its development by J.B. Fenn in 1984 [8], ESI has rapidly increased in popularity becoming one of the most common MS ion sources. The requirement of samples in the liquid phase has promoted the use of ESI in online coupling to flow-based chromatographic or electrophoretic analytical techniques such as LC and CE. Molecules several hundreds of thousands of Da in size such as proteins can be analyzed thanks to the formation of multiple ionic charges. Additionally, ESI MS has also been widely used for the analysis of much smaller analytes.

The process of ion formation in the ESI source can be described in three steps:

(i) Accumulation of charges at the liquid's surface: The application of a strong potential difference (3-6 kV) between the capillary introducing the sample solution and the counter electrode under atmospheric pressure results in the accumulation of charges on the meniscus of the liquid protruding from the capillary. The nature of these charges, *i.e.* their sign, depends on the polarity of the applied potential, *i.e.* positive or negative voltage. At a certain point, the electrostatic repulsion forces between the charges will exceed the surface tension of the liquid where it assumes the form of a cone, called a Taylor cone, at the exit of the capillary (Figure III.2) [2,9].

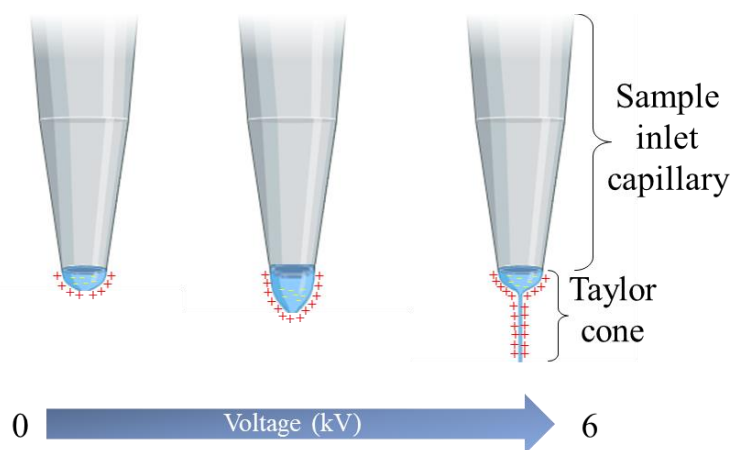


Figure III.2: Illustration of Taylor cone formation after charge accumulation at the surface of the sample solution

(ii) formation of smaller charged droplets: a stream of charged droplets is emitted from the Taylor cone. The size of these first generation droplets decreases by the evaporation of the solvent through the action of the nebulizer gas (flow = 1.1 bar in our study using positive ionization mode), the heated drying gas from the inlet of the MS orifice and by successive fission of the droplets into smaller offspring ones. This is due to increased electrostatic repulsions of like charges over the surface tension as a result of desolvation resulting in a “Coulomb” explosion of the unstable droplet into smaller stable ones. The smaller droplets then undergo the same process dividing into droplets of smaller size and charge [3,9];

(iii) desorption: a stream of heated nitrogen gas (200°C at a flowrate of 4 L min⁻¹ in our study using positive ionization mode) originating from the inlet of the MS analyzer permits the desorption of the charged species from a liquid phase to a gaseous one. The newly formed gaseous cations (or anions) are then transferred from the ESI source at into the MS analyzer through a series of focusing funnels [3,9,10].

Both steps (ii & iii) are depicted in Figure III.3 below.

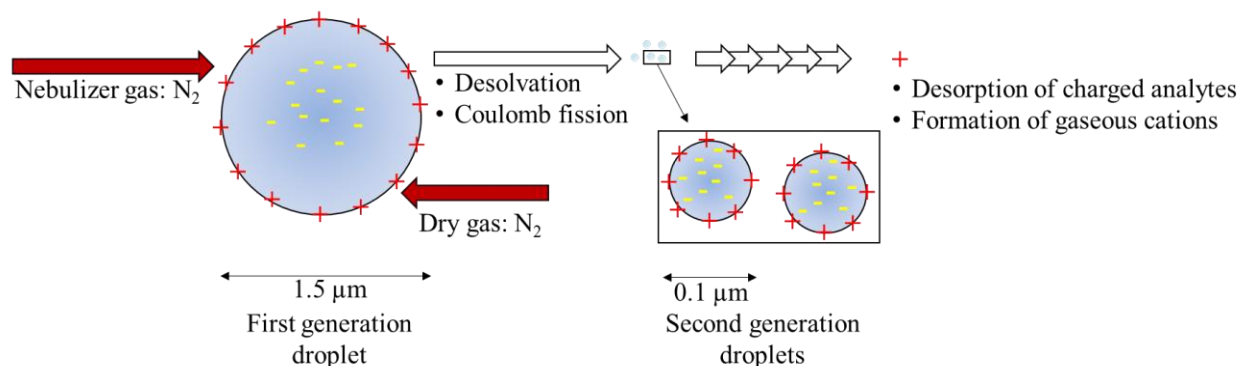


Figure III.3: Illustration of the formation of small charged droplets from larger ones through Coulomb fission occurring during electrospray ionization

1.b Q-TOF Mass analyzer

Following the trajectory of the analytes, now in the form of gas phase cations, leads us to the Q-TOF mass analyzer. As a matter of fact, the Q-TOF system is a hybrid system composed of two mass analyzers, quadrupole and TOF. This coupling introduces enhancement to resolution, scan speeds and accuracy in mass measurements. The system resembles that of a tandem triple quadrupole were the third quadrupole (Q3) is substituted by the TOF analyzer.

Q1: The first quadrupole (Q1) represents the first mass analyzer encountered by the charged ions. The ions can be filtered, allowing the transmission of analytes with a specific ion mass or within a mass range. Otherwise, total transmission of all ions, within a preset mass range, through Q1 is possible through the use of radio frequency (RF) only mode without the application of direct current (DC) rendering Q1 an ion guide [2,4,11].

Q2: The second quadrupole (Q2) represents a collision cell where ion fragmentation is induced through the collision of these ions by particles of an inert gas such as nitrogen. This fragmentation process is known as collision induced dissociation (CID). As for Q1, Q2 can be operated in RF only mode when fragmentation of the ions is not desired [11].

TOF: As soon as the charged ions exit the collision cell (Q2), they are accelerated by an applied electric field into a field-free flight tube. The kinetic energies of the ions are equal and their separation is based on their velocities in the flight tube evaluated by the time taken to transverse the known distance of their trajectory in the tube. Ions with larger masses tend to reach the end of the flight tube later than lighter ones. Kinetic energy dispersion during ion acceleration results in variations in the velocities of ions causing different flight times of ions with the same m/z . In order to circumvent this, modern TOF mass analyzer employ a reflectron situated in the flight tube and into which highly energetic ions penetrate deeper and thus traverse a longer trajectory than ions with lower energies and same m/z [2,11]. In addition, modern commercial Q-TOF-MS instruments are often coupled to continuous sources of ionization such as ESI orthogonally where ions transmitted from the source are accelerated along a new trajectory perpendicular to their initial one into the TOF analyzer [2,12].

Both Q1 and the collision cell functioned as ion guides and the TOF flight tube, equipped with a reflectron, was situated orthogonally to the direction of ion flow from the source as far as the mass analyzer was concerned in this PhD thesis.

I.c Electron multiplier detectors

Being the most common detectors used in MS instruments, electron multipliers were used to detect particles (electrons, ions and neutrons). They are able to convert the contact with individual particles or photons to a secondary flux of electrons (10^6 electrons from a single contact). Microchannel plate detectors are made up of separate miniaturized electron multipliers. They are suitable to TOF analyses and provide spatial resolution due to the presence of multiple separate channels [2,6,13].

II. Hyphenating CE to MS

Hyphenation between CE and MS is most commonly, yet not exclusively, carried out *via* an ESI source. The first CE coupling to MS through an ESI source was carried out by the group of R.D. Smith in 1987 for the analysis of several ionic compounds [14]. Analytes reaching the ionization source would have already begun to ionize by the background electrolyte (BGE), which is at the heart of the principle of CE separation. Therefore, the ESI source serves to desolvate and vaporize the analytes before their transfer to the mass analyzer.

If one wishes to hyphenate CE directly to ESI-MS, they will encounter two main dilemmas that complicates the realization of this coupling:

(1) Incompatible flow rates: Most ESI sources operate at flow rates in the order of $\mu\text{L min}^{-1}$ as to produce a stable electrospray. On the other hand, the CE effluent traverses a 50 μm i.d. capillary at a rate of a few hundred (100 – 300) nL min^{-1} . Thus, this vast difference in the flow rates of each of the techniques prevents their coupling without appropriate measures due to failure in the formation of a stable spray.

(2) Electrical connections: CE separation requires the application of high voltages to the capillary inlet by an electrode dipped into a vial containing the BGE. The circuit is closed by dipping the ground electrode into an outlet BGE vial. For the CE-MS hyphenation, the circuit cannot be closed using an outlet BGE vial. Furthermore, electrospray formation in ESI sources requires high voltages of its own applied between the outlet of the capillary and the inlet of the MS. Therefore, the electrode at the capillary outlet should close the CE circuit and supply the electrospray voltage in order to maintain both functions simultaneously [15].

II.a Sheath liquid (SL) interface

Both inconveniences may be resolved through the use of a CE-ESI interface used to introduce an additional sheath liquid (SL). A number of interface models have been described. The interface used throughout this PhD consisted of three concentric co-axial capillaries, the central one being the separation capillary of CE (Agilent Biotechnologies) (Figure III.4). The second and third capillaries surround the central one and are made out of stainless steel. The SL flows through the second capillary supplied by a syringe or a LC system. It converges as it exits the capillary and mixes with the liquid exiting the capillary. The third capillary contains the nebulizing gas which contributes to the desolvation and fission of the charged droplets. SL is introduced at a flow rate

(few $\mu\text{L min}^{-1}$) that is compatible with ESI processes resulting in the formation of a spray. However, this gain in spray stability is at the expense of sensitivity since the analytes are considerably diluted by the SL. The SL composition is variable and permits the enhancement of the ionization, desolvation and closure of the CE electrical circuits due to the presence of electrolytes. Therefore, the nebulizer is electrically grounded for both the CE and ESI-MS circuits to prevent leakage of current between them [16]. The CE capillary is protruded a distance between 0.05 to 0.25 mm (0.25 mm in our conditions) from the interface. This protrusion of the capillary affects the mixing of the analytes with the SL and thus affects spray stability and ionization efficiency [17]. Furthermore, the polyimide layer in the portion of the capillary in contact with the SL is typically removed to prevent polyimide swelling which can cause issues in current transmission [18].

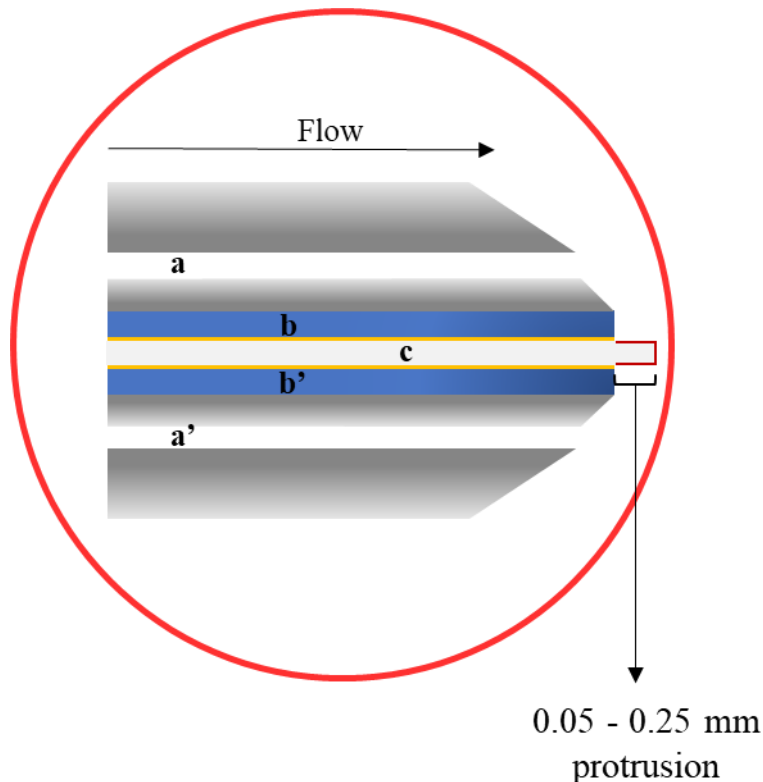


Figure III.4: An illustration of the sheath liquid CE-ESI-MS interface. a and a': Nebulizing gas capillary, b and b': SL capillary and, c: separation CE capillary

Working with SL interfaces often imposes restrictions on the separation electrolyte. Inorganic buffers providing high separation capacity with CE are avoided in CE-MS applications as they contaminate the ion source resulting in ion suppression. They are instead substituted by volatile solutions such as acetic acid or ammonium acetate BGE.

II.b Sheathless interfaces

Although not used in this PhD, it is important to note that CE coupling to MS can be achieved without the use of SL thus avoiding the dilution effect introduced by the addition of SL. These approaches couple CE to the ESI-MS system *via* sheathless interfaces. With this approach, the tip of the capillary is often modified by mechanical or chemical etching to reduce its diameter. This is important for the generation of a stable spray that is compatible with the low flow rates of CE [19].

Moreover, the electrical contact required to close the CE circuit and induce spray generation can be achieved in sheathless interfaces by encasing the outlet tip of the separation capillary with a conductive coating, insertion of a metal wire into the capillary outlet or into pores made close to the outlet or through the air between the outlet and the MS orifice [19,20].

Most of sheathless approaches to couple CE to ESI-MS have demonstrated enhanced sensitivities. Nonetheless, these interfaces often suffer from poor stability and reproducibility [21]. In 2007, Mehdi Moini developed a sheathless CE interface known nowadays as CESI-MS [22]. A segment of the capillary's outlet was etched with concentrated hydrofluoric acid, producing conductive porous walls. The capillary is inserted into a stainless-steel needle filled with a conductive liquid, *i.e.* the BGE, connected to the outlet electrode of the CE apparatus. The electrical contact is thus achieved and the CE circuit is closed. The spray is generated from the tip of the porous capillary which is typically protruded from the needle [16,19]. The sheathless interface was purchased and patented by Beckman-Coulter, now Sciex, and commercialized under the name CESI-MS for the analysis of various biomolecules such as monoclonal antibodies [23,24], proteins [22,25,26] or metabolomics analysis of complex biological samples [27]. R. Haselberg *et al.* demonstrated the potential of CESI-MS compared to a SL interface in the analysis of intact proteins [26]. The peak intensities of the four proteins displays an enhanced sensitivity with CESI compared to SL CE-ESI as a result of the elimination of analyte dilution by the SL. The limits of detection (LOD) were improved 4-20 times using CESI sheathless interfaces (Figure III.5).

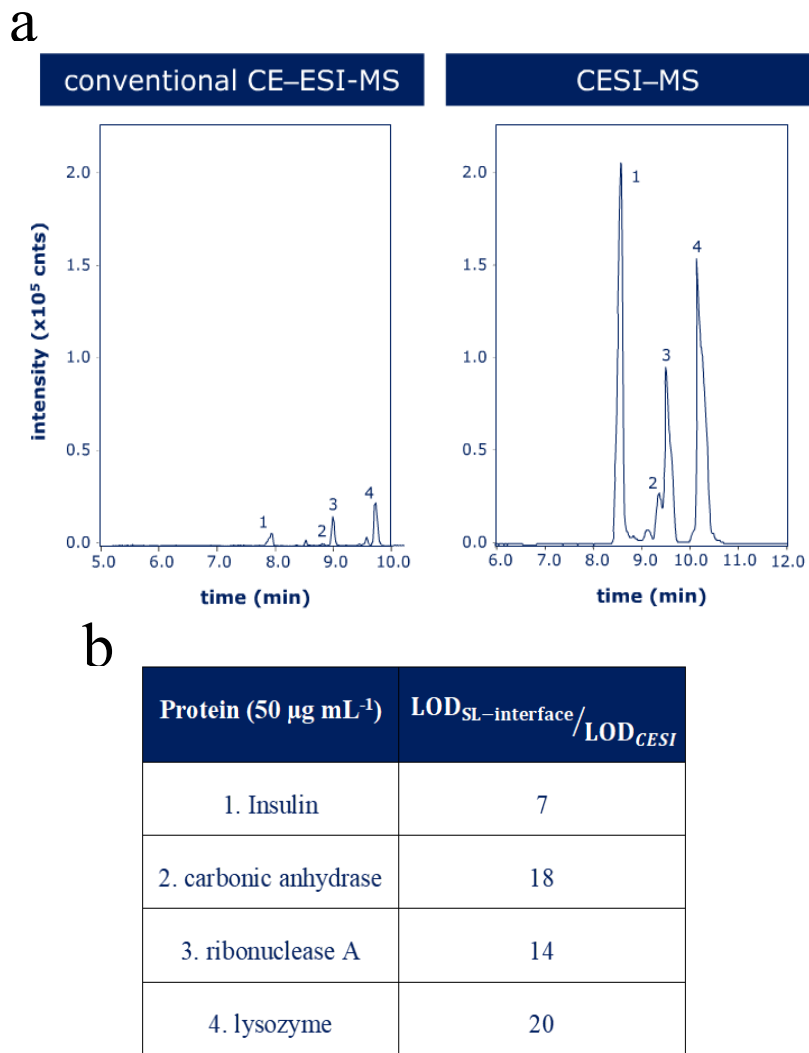


Figure III.5: Comparison of the analysis of four intact proteins (1. Insulin, 2. Carbonic anhydrase, 3. Ribonuclease A and 4. Lysozyme) by R. Haselberg *et al.* using conventional CE-ESI-MS SL interface and sheathless CESI-MS [26]. Peak intensities of the four intact proteins (**a**) and ratio of LOD of the four intact proteins with SL to sheathless interfaces (**b**)

Part A:

Capillary electrophoresis-mass spectrometry at trial by Metabo-Ring: effective electrophoretic mobility for reproducible and robust compound annotation

I. Introduction

Metabolomics involves the study of compounds in very complex biological samples. Due to the overwhelming number of metabolites, MS demonstrates powerful potential to detect the different compounds with high sensitivity and short analyses times. Coupling MS detection to a separative analytical technique further refines the process of metabolite detection [39]. In comparison to other separative techniques used in hyphenation with MS such as LC-MS and GC-MS, the use of CE-MS in metabolomics is quite limited. This may be due to the perceived difficulty of hyphenating CE to MS and the poor reproducibilities in migration times observed with CE [40]. Migration times of the same analyte analyzed by CE can vary due to fluctuations in the EOF, temperature, buffer properties, interactions with the capillary surface in addition to other factors [41]. These variations stand in the way of a wider use of CE in metabolomics since the reproducibility of migration time is important for the identification of metabolites or comparing metabolomic profiles. The migration time of an analyte can be represented, relative to the migration time of an internal standard, as the relative migration time (RMT). This approach can correct for migration time variations due to changes to the dimensions of the separation capillary, separation voltage and viscosity but has little influence on EOF-related variations [42]. Another interesting approach involves the conversion of the migration time scale into an effective electrophoretic mobility scale (μ_{eff}). μ_{eff} is an intrinsic property of an analyte and is directly proportional to the analyte's charge (q) and inversely proportional to its hydrodynamic radius (r_s) as well as the viscosity of the media (η) as shown in Equation III.1 below:

$$\mu_{\text{eff}} = \frac{q}{6\pi\eta r_s} \quad \text{Equation III.1}$$

Being an analyte-specific quality, μ_{eff} does not vary in response to fluctuations in the EOF and thus their use as substitutes to migration times can prove valuable for CE-MS in metabolomics [43].

With more than 40 contributors from 13 different international institute, the Metabo-ring study was an ambitious effort to demonstrate, on a large scale, the viability of using CE-MS for metabolomics. The migration time reproducibilities of CE-MS were assessed and two approaches, relative migration time (RMT) and electrophoretic mobility (μ_{eff}), were used to identify metabolites and compared across the different laboratories. Twenty different CE-MS platforms across the different participating laboratories were set to carry out CE-MS analyses of the same samples. SL, sheathless and home-made CE-MS interfaces as well as CE and MS instruments from different manufacturers were used. The contributors were free to use their habitual experimental conditions. This allowed a large-scale and accurate assessment of reproducibilities. The BGE, however, was imposed and injections were to be carried out hydrodynamically without analyte stacking as both the composition of the BGE and stacking of the analytes are sources of μ_{eff} variation. The BGE used was a 10% solution of acetic acid (pH 2.2) due to its ease of preparation, low currents with CE and its stability over extended time periods [41].

II. Experimental conditions

The CE-MS analysis of the different metabolites was carried out in our laboratory using a PA800+ CE instrument (Sciex) coupled to a MaXis UHR-QTOF mass spectrometer (Bruker Dalton) using a SL co-axial interface (Agilent Technologies). The SL was supplied to the interface *via* an ultimate 3000 HPLC pump (Dionex).

Standard CE-MS conditions in both the positive and the negative ionization modes were previously established in our lab and were used as a starting point. Some conditions, such as the separation pressure, nature and flowrate of the SL, the nebulizer gas pressure and dry gas flow were tested at different levels and the values resulting in the best CE current stability, electrospray stability and best MS detection of the analytes were chosen. The final conditions are presented in Table III.1 below and used to realize the CE-MS analyses. Twenty-one cationic, twenty-one anionic in

addition to neutral standard metabolites were diluted in water (standard mixture), human plasma or urine matrix (sample mixture). The samples, *i.e.* metabolites in plasma and urine, were prepared in three dilutions of each respective matrix in the sample mixture: 0, 5 or 10-fold dilutions. The human plasma matrices were deproteinized in organic solvent.

Table III.1: Parameters and conditions used for CE-ESI-MS.

CE	Capillary	Type	Uncoated fused silica
		Length	90 cm
		Inner diameter	50 μm
	Temperature	Type	CE-MS cartridge
		Cartridge	25°C
	Initial capillary conditioning (72.5 psi)	Ammonium hydroxide (10%, v/v) (10 min) H ₂ O (10 min) BGE (10 min)	
	Capillary washing (72.5 psi)	H ₂ O (2 min) Ammonium hydroxide (10%, v/v) (2 min) H ₂ O (2 min) BGE (2 min)	
	Hydrodynamic injection	Polarity	Reverse
		Pressure	1.5 psi
		Time	10 s
Volume		20 nL	
Separation voltage	Polarity	Normal or Reverse	
	Voltage	+/-15 kV	
	Ramp up	0.17 min	
	Pressure	2 psi at inlet	
Capillary voltage	Negative ionization	-4.5 kV	
	Positive ionization	+4.5 kV	
SL	Composition	MeOH + 0.1% formic acid	
	Flow-rate	10 $\mu\text{L}/\text{min}$	
Nebulizer gas	Composition	Nitrogen	
	Pressure	0.1 bar (negative ionization) or 1.1 bar (positive ionization) for negative or positive	
Dry gas	Composition	Nitrogen	
	Temperature	200°C	
	Flow-rate	4 L min ⁻¹	
End-plate voltage	Voltage	500 V	
Acquisition rate	Rate	0.5 Hz	
ESI-HRMS			

The polyimide coating of the CE capillary was stripped along the length of 1 cm from the outlet (protruding into the ESI source) using a flame source to prevent polyimide swelling and mediate formation of a stable spray [44]. Additionally, an opaque detection window was created at 10 cm from the inlet (sample injection end). Although UV detection was not used in this study, it was a necessary step for the configuration of the device.

The CE cartridge used for CE-MS was similar to that used in conventional CE analyses but was adapted for hyphenation with external detectors by connecting longer coolant liquid tubings as described in **Part A** of this chapter. With this type of cartridge, the outlet side (closest to optical detection window) was the true inlet as shown in Figure III.6. Therefore, the polarities of certain operations had to be reversed. For example, in conventional CE, a reverse polarity implies that the inlet side is the cathodic side and the outlet side is the anodic one. Nonetheless, since the inlet side is omitted in the configuration shown in Figure III.6, the capillary traverses from the cartridge's outlet directly into the ESI source and the cathodic end is actually towards the MS.

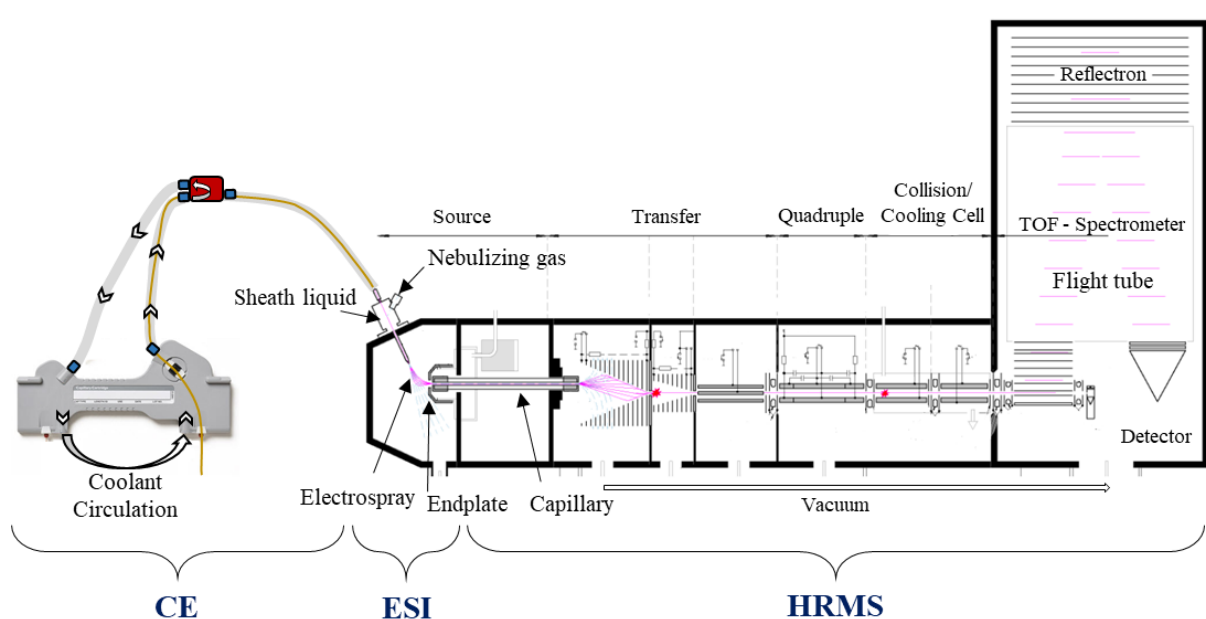


Figure III.6: Illustration of the CE-ESI-HRMS system used throughout this chapter.

The separation voltage was supported by applying a separation pressure of 2 psi at the same time in order to reduce the time of analyses since the velocity of the EOF was small. The ramp time is the time during which the voltage increases gradually to reach the final pre-set voltage value.

The end-plate voltage refers to the potential difference applied between the spray shield, where the MS orifice is located, and the capillary cap in order to focus the ions onto the glass capillary inlet [45]. The acquisition rate is the number of acquired mass spectra *per* second.

III. Results

The results of the interlaboratory CE-MS study investigating the capability of using CE-MS in metabolomics by comparing the reproducibilities of RMT and μ_{eff} were published in an article titled “**Capillary Electrophoresis-Mass Spectrometry at Trial by Metabo-Ring: Effective Electrophoretic Mobility for Reproducible and Robust Compound Annotation**”, *Analytical Chemistry* (2020), 92:14103-14112, DOI: 10.1021/acs.analchem.0c03129

III.a Choice of CE-MS conditions

Several conditions were trialed for the separation of the different metabolites by CE-MS. Parameters were assessed based on the stability of the electrospray and the detection sensitivity of the different metabolites in the standard mixture.

Firstly, different SL were compared: (i) MeOH + 0.1% formic acid delivered by an HPLC pump, (ii) MeOH + 5 mM acetic acid and, (iii) Isopropanol/water (50/50, v/v) + 5 mM acetic acid delivered by a syringe pump to facilitate switching of SL when needed. MeOH + 0.1% formic acid was chosen as the SL for both positive and negative ionization modes since compared to the other, it provided the highest sensitivity of detection, thus lowest ion suppression, whilst maintaining the CE current.

The flow rate of the SL was set at 10 $\mu\text{L min}^{-1}$ after comparing it to 3 and 5 $\mu\text{L min}^{-1}$. At this flow rate, sample dilution is expected but the highest stability of the electrospray was achieved.

The nebulizing gas pressure was set at 0.1 Bar in the negative ionization mode and 1.1 Bar in the positive ionization mode. This parameter influences the in-source droplet formation and thus the ionization efficiency and electrospray stability.

The drying gas flow was set at 4 L min^{-1} since higher flow rates decreased the stability of the electrospray.

During the separation phase, a relatively low voltage (+/-15 kV) was applied to separate the metabolites. With the application of such low voltages, relatively lower peak resolution and higher migration times are expected. However, low voltage in combination with reduced inner diameter and a BGE of low ionic strength resulted in lower Joule heating. Application of higher voltages (>15 kV) caused the capillary to break or fracture at the level of the optical detection window where the polyimide layer was stripped and the coolant liquid had no access, both of which play

an important part in the dissipation of Joule heat [35]. The separation voltage was assisted with a 2 psi separation pressure applied at the capillary inlet. This was necessary to reduce the migration times due to the use of relatively long capillaries by pushing all analytes towards the MS especially during reverse polarity (- to +) where the EOF migrated away from the MS.

Both positive and negative ionization modes were compared for the detection sensitivity of the cationic, anionic and standard metabolites.

For the negative ionization mode, a mixture containing cationic, anionic and neutral compounds was diluted in water at $20 \mu\text{g mL}^{-1}$ except for paracetamol ($30 \mu\text{g mL}^{-1}$). The detection of 6 cationic (L-Arginine, creatine, adenosine, L-Tryptophan, L-Neoptirin and inosine), 6 anionic (Citric acid, GMP, IMP, glucose-6-phosphate, IDP and fructose-1,6-biphosphate) and 2 standard (paracetamol and glucose) compounds was used to evaluate the appropriate ionization mode (positive or negative) and the separation polarities (normal or reverse). With normal separation polarity (+ to -) and +15 kV separation voltage assisted with 0.7 psi applied at the inlet, cationic compounds were detected first followed by neutral and anionic compounds. Anionic compounds were detected at higher sensitivities compared to cationic compounds (Figure III.7a). Upon switching to reverse separation polarities (- to +) using -15 kV separation voltage assisted with 0.7 psi applied at inlet, anionic compounds were detected first followed by neutral and cationic compounds. The sensitivity of detection was globally reduced and amongst the cationic compounds, only inosine was detected. Furthermore, the migration times were much longer compared to normal separation polarity (≈ 30 min). This could be due to the fact that in the former, the direction of the EOF was away from the MS. When the separation pressure was increased to 2 psi, the remaining cationic compounds were detected and the overall analysis time was reduced to 20 min (Figure III.7b).

With the positive ionization mode, a mixture containing two cationic (adenine and L-Arginine), three anionic (AMP, citric acid and glucose-6-phosphate) and paracetamol as a standard compound were prepared at 1 mg mL^{-1} in water. Cationic compounds and paracetamol were detected at higher sensitivities compared to anionic compounds (Figure III.8). As expected, switching to the positive ionization mode greatly enhanced the detection sensitivities of cationic compounds at the expense of anionic compound detection. The bias of each ionization mode towards a particular group of ions is indeed expected since in the negative ionization mode, it is easier to detect deprotonated ions and in the positive ionization mode, it is easier to detect protonated ions or metal adducts. The polarity switching of the MS capillary voltage as well as the different instruments further favors

the detection of either positively or negatively charged analytes depending on the ionization mode.

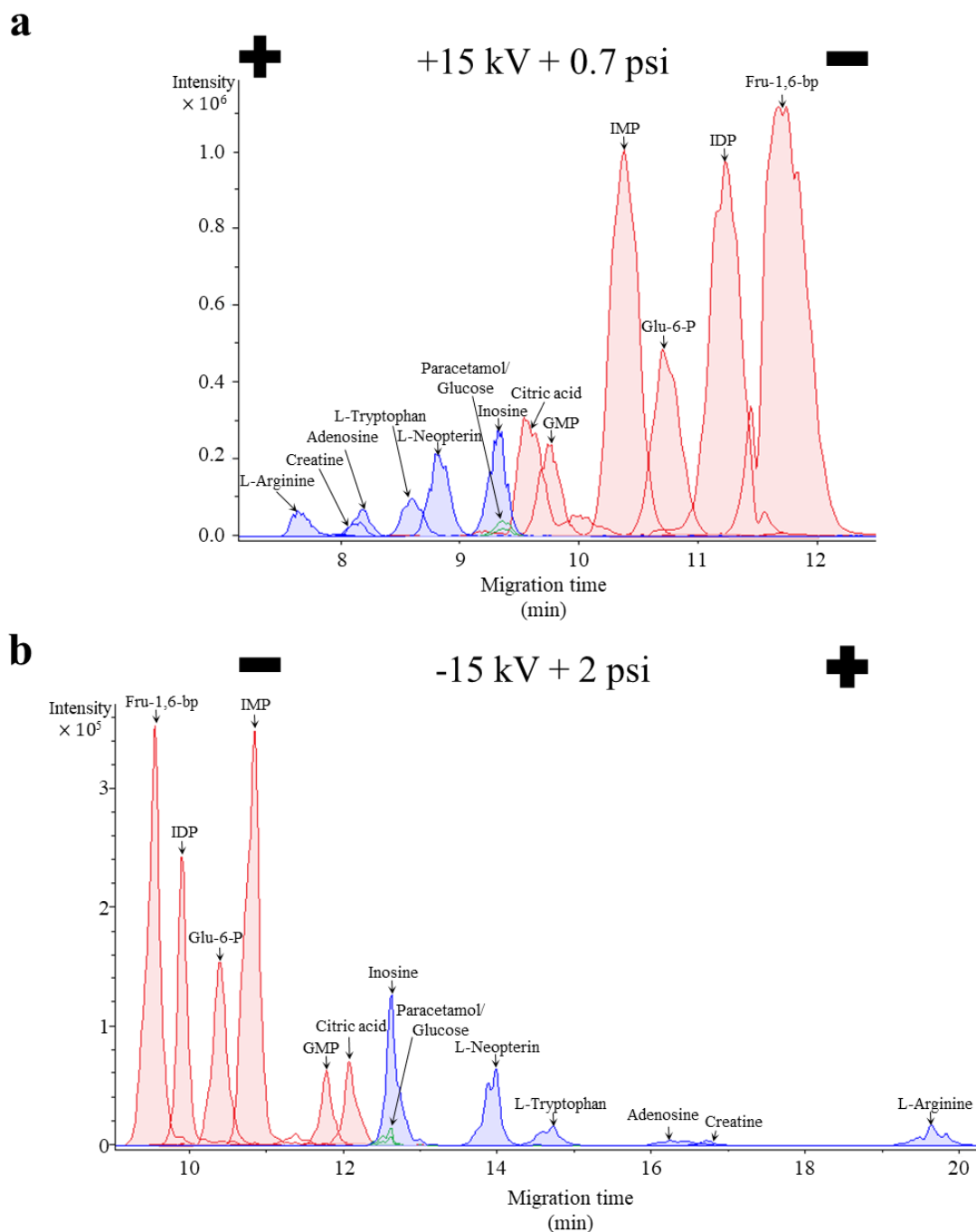


Figure III.7: Electropherograms for the separation of anionic, cationic and standard metabolites in the negative ionization mode: normal polarity (+ to -) at +15 kV with 0.7 psi applied at the inlet (**a**) and, reverse polarity (- to +) at -15 kV with 2 psi applied at the inlet (**b**). CE-ESI-MS conditions are summarized in Table III.1. The metabolites were diluted in water at $20 \mu\text{g mL}^{-1}$ except for paracetamol which was at $30 \mu\text{g mL}^{-1}$.

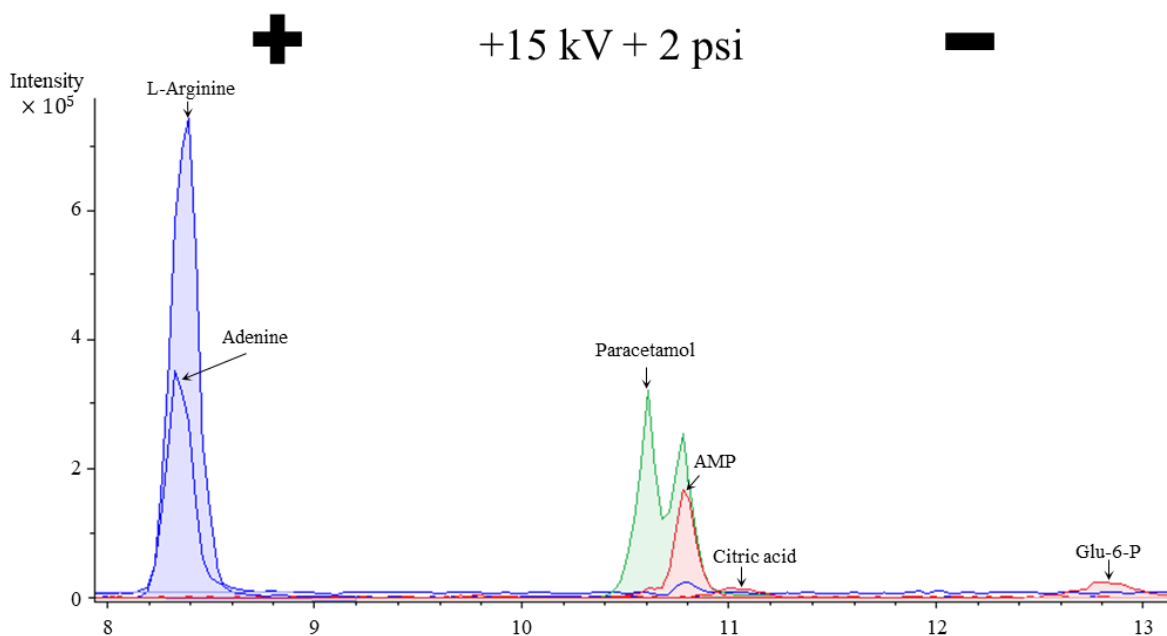


Figure III.8: Electropherograms for the separation of anionic, cationic and standard metabolites in the positive ionization mode: normal polarity (+ to -) at +15 kV with 2 psi applied at the inlet. CE-ESI-MS conditions are summarized in Table III.1. The metabolites were diluted in water at 1 mg mL⁻¹.

Using the conditions mentioned above, the mixture of metabolites was then analyzed in biological fluids, human plasma or urine, at different matrix levels. For the detection of anionic metabolites, negative ionization mode and the negative voltage polarity (- to +) with -15 kV + 2 psi assisted pressure was used. On the other hand, for cationic metabolites, the positive ionization mode and positive voltage polarity (+ to -) with +15 kV + 2 psi assisted pressure was used. Figure III.9 represents detection of anionic compounds in addition to glucose and paracetamol standards at three dilutions of human urine. Similar results were obtained with human plasma. For cationic metabolites, the results were pooled with others from several laboratories to emphasize on the advantage of using μ_{eff} instead of migration time to overcome limitations associated with inconsistencies of the EOF. Figure III.10 represents an example of the electropherograms obtained by one of the participating groups for the detection of cationic and standard compounds. The CE-MS conditions used by the group were different than the ones described above except for the BGE which was fixed for all the participating groups.

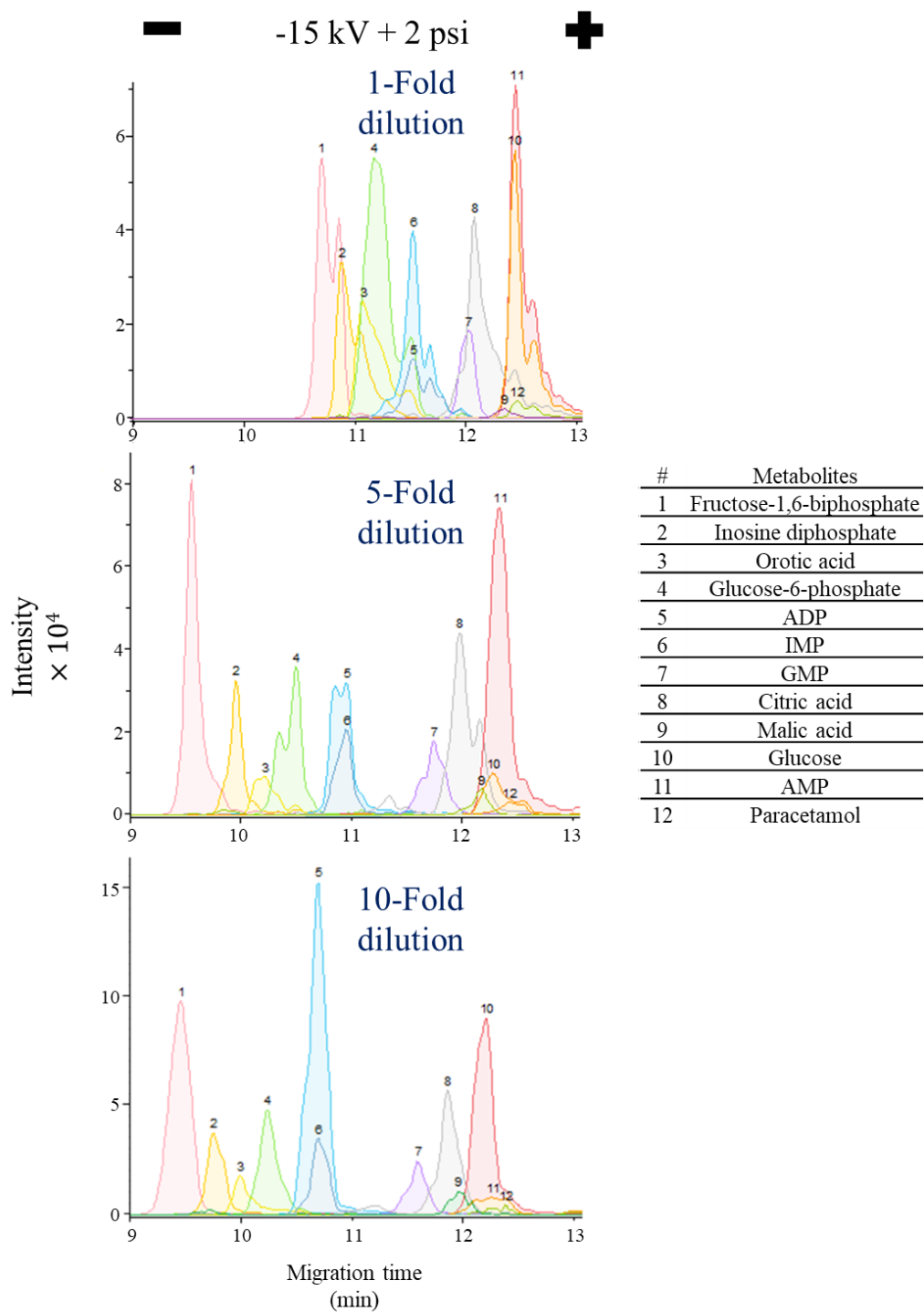


Figure III.9: Electropherograms obtained for the detection of anionic (10) metabolite in addition to 2 standards (paracetamol and glucose) in different concentrations of urine using the negative ionization mode and negative polarity with -15 kV assisted by 2 psi. CE-ESI-MS conditions are summarized in Table III.1.

III.b Influence of standardization of BGE

The relevance of using the same preparation protocol of 10% acetic acid BGE amongst the different participating groups was investigated. An electropherogram obtained after the analysis of the mixture of 23 compounds in water is presented in Figure III.10.

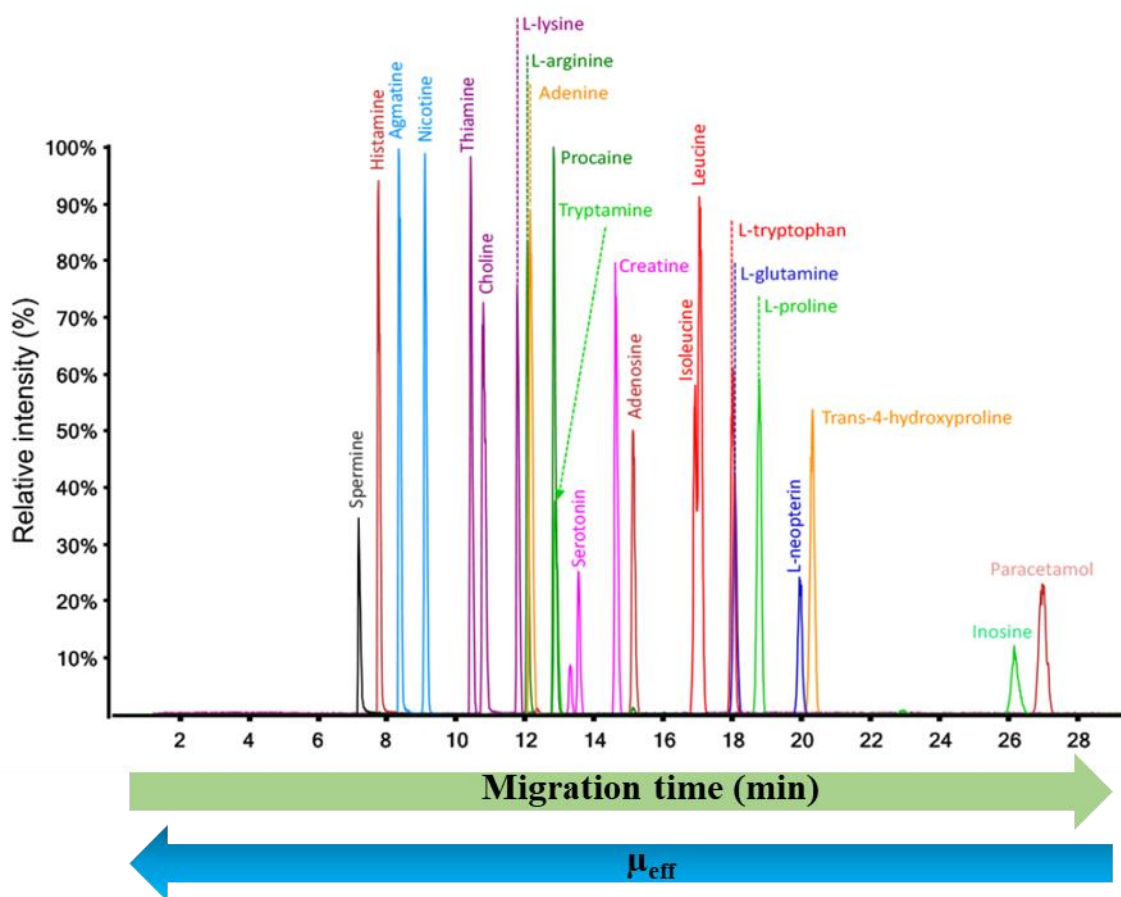


Figure III.10: Electropherogram for the analysis of the mixture of 23 compounds (21 cationic metabolites and 2 standards) diluted in water.

CE conditions: capillary: L = 101.7 cm, i.d. = 50 μm ; BGE: 10% acetic acid (pH 2.2); washing: 1 M NaOH (30 min), H₂O (30 min), BGE (30 min) at 14 psi; injection: 0.7 psi \times 17 s (12 nL); separation voltage: +30 kV (0.1 min ramp time), separation pressure: 0.3 psi; cartridge temperature: 20°C.

ESI-MS conditions: SL: MeOH/H₂O (50/50), 6 $\mu\text{L min}^{-1}$; Nebulizer gas: 10 psi; dry gas: 10 L min^{-1} , 200°C; capillary voltage: 3.5 kV; end-plate voltage: 125 V; acquisition rate: 1.36 Hz.

Interface: G1607 ESI sprayer (Agilent Technologies).

Mass spectrometer: 6224 TOF (Agilent Technologies).

Adapted from [41].

An efficient separation of most peaks was obtained using this BGE. Using the migration time of procaine as reference for calculating RMT, the repeatabilities within each group (interlaboratory) of RMT and μ_{eff} of the standard metabolite mixture diluted in water were below 1% for analyses

in triplicates. Upon pooling the data together, the RMT and μ_{eff} values from the different groups and calculating the average relative standard deviation (RSD) or the intralaboratory reproducibility (standard deviation (SD) divided by the average), a significant variability was observed (4.3% RSD of RMT and 5.7% RSD of μ_{eff}). In order to identify the source of such variation, the RMT and μ_{eff} measured for each compound by each group was compared to the average measured RMT and μ_{eff} by all groups for that compound. This bias error was calculated by the following equation Equation III.2 below:

$$\% \text{ Bias} = \frac{X_m - X_r}{X_r} \times 100 \quad \text{Equation III.2}$$

where X_m is the measured RMT or μ_{eff} of a compound and X_r is the average RMT and μ_{eff} calculated from all of the values measured by the different groups.

Three individual groups measured lower μ_{eff} of slow migrating compounds (longest migration times) compared to the other groups. This was attributed to variations in BGE preparation since μ_{eff} is solely influenced by physicochemical properties of BGE such as its pH and composition. Furthermore, these variations seem more relevant in slow-migrating compounds due to their possession of a basic function with low pK_a or an acidic function with a high pK_a causing them to have a lower charge and thus a lower μ_{eff} . Consequently, any small fluctuation in the pH of the BGE, due to variations in its preparation, influences the μ_{eff} of such slow-migrating compounds [41]. Those three data sets were thus identified as the cause of the interlaboratory variation in RMT and μ_{eff} were thus excluded from further data processing.

III.c Comparison of RMT and μ_{eff} based compound annotation

As mentioned earlier, RMT can be used to correct for variations related to the use of different capillaries, voltages and viscosities. The velocity of the analyte is calculated relative to that of an internal standard by Equation III.3 below.

$$\text{RMT} = \frac{v_a}{v_{\text{IS}}} = \frac{E \times (\mu_{\text{eff}_a} + \mu_{\text{EOF}}) + v_{\text{hydro}}}{E \times (\mu_{\text{eff}_{\text{IS}}} + \mu_{\text{EOF}}) + v_{\text{hydro}}} \quad \text{Equation III.3}$$

where v_a and v_{IS} are the velocities of the analyte and the IS, respectively, E is the magnitude of the electric field; which can be presented as the voltage applied *per* cm of the capillary, μ_{eff_a} and

μ_{effIS} are the μ_{eff} of the analyte and the IS, respectively, μ_{EOF} is the electroosmotic mobility and v_{hydro} is the hydrodynamic movement that occurs through various mechanisms such as the siphoning effect occurring between the capillary inlet and outlet, the vacuum of the atmospheric interface of the MS or due to applied separation pressure [41]. As shown above in Equation III.3, v_{hydro} cannot be corrected accurately by calculating the ratios of v_a to v_{IS} . Nonetheless, if analytes migrate close enough to the IS, they are thought to be experiencing the same variations of v_{hydro} and therefore the RMT approach is much more efficient for those analytes.

μ_{eff} can be alternatively used as it is independent of the BGE and is an intrinsic property of the analyte. In order to calculate the μ_{eff} , one must first determine the magnitude of μ_{eof} through the use of an internal standard known as the EOF marker. This latter standard should be neutral at the tested conditions, effectively having no μ_{eff} . μ_{EOF} can then be calculated using Equation III.4:

$$\mu_{\text{app}} = \mu_{\text{EOF}} = \frac{l}{E \times t_m} = \frac{L \times l}{V \times t_m} \quad \text{Equation III.4}$$

where μ_{app} is the apparent mobility which is the sum of μ_{eff} and μ_{EOF} , L is the total capillary length, l is the effective capillary length (from inlet to detection point), t_m is the migration time and V is the applied voltage.

Then, μ_{eff} can be calculated by subtracting μ_{EOF} from the analyte's μ_{app} calculated using Equation III.4. In this study, paracetamol and procaine were used as the references for μ_{eff} calculations. With the exception of inosine, the reproducibilities (intralaboratory RSD) observed when using μ_{eff} were all below 3.1% for all the metabolites (Figure III.11).

On the other hand, the reproducibilities reached values up to 11% using RMT. This confirms the viability of using μ_{eff} over RMT as it is only dependent on the BGE parameters which are often well controlled.

The trend of reproducibilities across the different migrating metabolites was stable with μ_{eff} ranging from 0.8 to 3.1%. When using RMT however, a plunge in the reproducibility percentage is observed between choline and adenosine. Indeed, the analytes demonstrating lower variations in RMT are analytes that have a close migration time to that of procaine and thus the RMT error is reduced drastically as previously described. Other analytes migrating further from the IS demonstrate higher variations [41,42].

With regards to the percentage of bias when using μ_{eff} , most of measured μ_{eff} values demonstrated

a maximum bias of 5% when compared to the respective average μ_{eff} (Equation III.2) with the exception of inosine. Bias with RMT reached a maximum percentage of 28%.

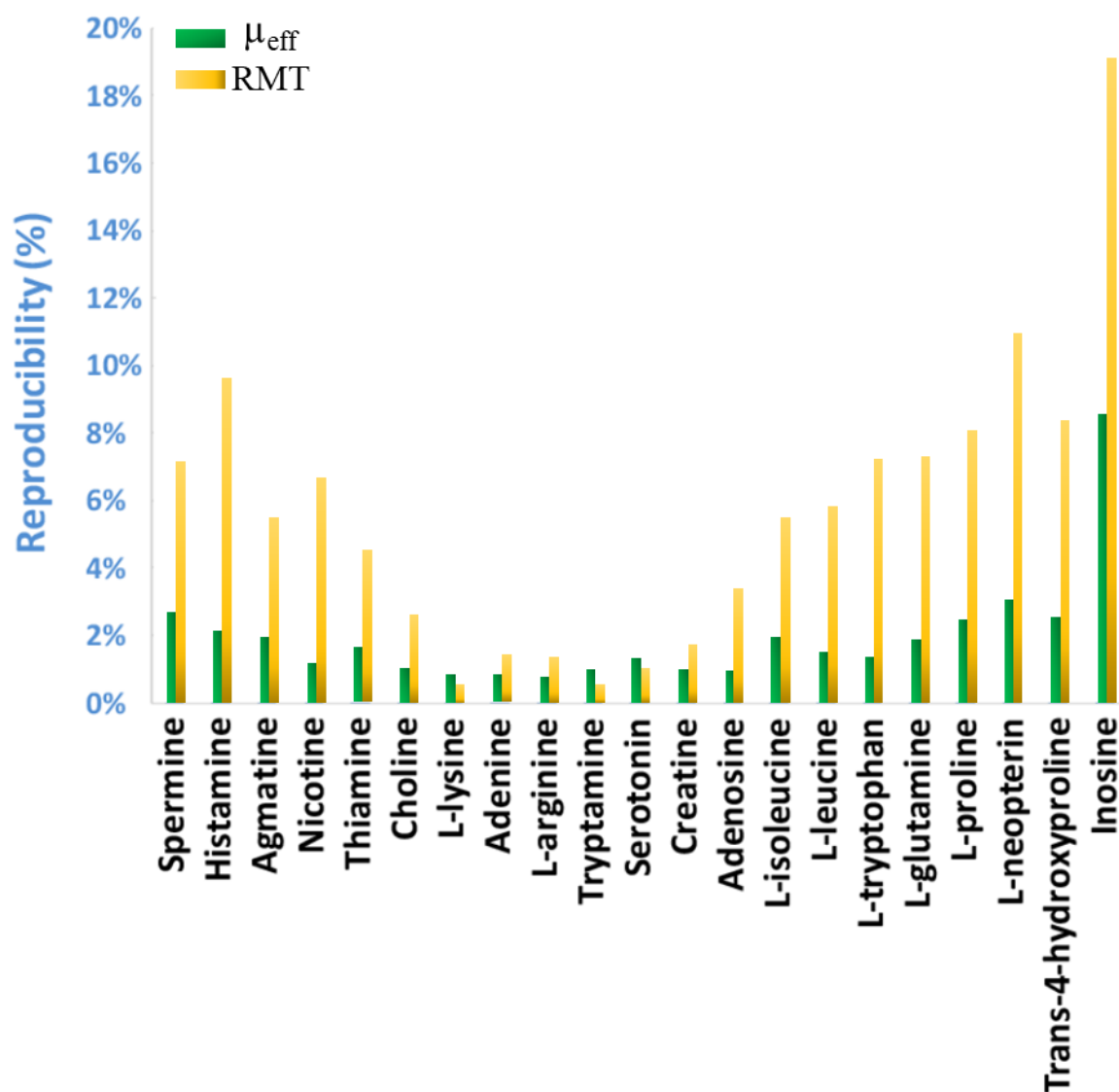


Figure III.11: Presentation of intralaboratory reproducibility percentages (% RSD) for the analysis of 21 cationic metabolites from the standard mixture diluted in water. Green bars represent the reproducibility percentage of μ_{eff} measurements. Yellow bars represent the reproducibility percentage of RMT measurements. Procaine was used as an internal standard to calculate both RMT and μ_{eff} for the 21 compounds

These results thus validate the effectiveness of converting time scales into μ_{eff} rather than RMT to correct for fluctuations in the migration time as the lowest interlaboratory variation for all analytes (except inosine) as well as the lowest bias threshold amongst the two approaches was using μ_{eff} .

III.d Metabolite identification in complex biological fluids

The influence of a complex biological matrix on the reproducibility of the migration indices was addressed by measuring the μ_{eff} of the metabolites at different dilutions of human urine or plasma matrices. The concentration of urine or plasma salts is usually expressed in the terms of adult 24 hr urine and serum sodium, respectively. The reference ranges is 40 – 220 mM for urine sodium over 24 hr and 133 – 146 mM *per* L for serum sodium². High salt concentration in the sample zone can result in deterioration of peak quality and results in variations of the migration times [41,46]. The μ_{eff} reproducibility did not show major changes at the different dilutions remaining under 7% for all metabolites, except inosine, in both urine and plasma matrices. Nevertheless, high bias percentages were observed for fast migrating compound. This can be probably related to the close migration of the metabolites with the highest mobilities to sodium. This proximal migration results in distortion, or in some cases ion suppression, of the analyte's peak rendering it difficult to integrate accurately contributing to deviation of the individual μ_{eff} performed by each laboratory from the average μ_{eff} measurement [41].

III.e Proposition for metabolite annotation using μ_{eff}

A proposition for the annotation of metabolites using μ_{eff} scales was made since they demonstrated their potential in reducing variability. This annotation will be based on a bias threshold range set to determine the confidence level of annotation. The bias is calculated similarly as described before where the individual μ_{eff} measurements are compared to averaged ones. In this case, the average μ_{eff} measurements are substituted with μ_{eff} values in databases harvested in a reliable manner considering sources of possible inter- and intralaboratory variability. The proposal differentiated between fast- and slow-migrating compounds where an analyte is labeled as fast-migrating when it's μ_{eff} exceeded 100 mm² kV⁻¹ min⁻¹ and slow-migrating compounds should have μ_{eff} below this limit. For fast-migrating compounds, a high annotation confidence level is achieved with μ_{eff} bias up to 5% and a low confidence level with bias exceeding 10%. For slow-migrating compounds, the annotation range was expanded reaching 10% bias maxima for metabolite annotation with high confidence level and 20% minima for metabolite annotation with low confidence level. It can be noticed, for example, that inosine, the slowest-migrating metabolite in the mixture, was exempted from most the conclusions and trends experienced by the other metabolites in previous results

² Gloucestershire Hospitals, www.gloshospitals.nhs.uk

discussed above. Yet again this is attributed to the large impact that slight changes in the BGE properties can have on the compound's μ_{eff} resulting in different measurements between the participants. Therefore, bias determinations often tend to be exaggerated for compounds similar to inosine. However, deviation of the absolute μ_{eff} were low across the different platforms reaching a maximum μ_{eff} deviation of about $\pm 10 \text{ mm}^2 \text{ kV}^{-1} \text{ min}^{-1}$. It can be thus concluded that relative measurements of bias and reproducibility are overestimated for such slow-migrating compounds and the use of absolute μ_{eff} thresholds can serve as an alternative to determine confidence levels for metabolite annotation. Based on this, a maximum deviation of $\pm 10 \text{ mm}^2 \text{ kV}^{-1} \text{ min}^{-1}$ from μ_{eff} values in databases was proposed to define annotations with high confidence levels and a minimum of $\pm 20 \text{ mm}^2 \text{ kV}^{-1} \text{ min}^{-1}$ to define annotations with low confidence levels.

IV. Conclusion

Although CE-UV is popularly used as a technique for analysis of pharmaceuticals in pharmacopoeias, the use of CE-MS for metabolomics was often overshadowed by more popular techniques such as LC-MS and GC-MS. Indeed, this is understandable since migration time instabilities can often be frustrating and complicates metabolite identification. Furthermore, coupling CE to MS through ESI sources is a challenge of its own due to the drastic difference between the flow supplied by CE and demanded by ESI. Additionally, two separate electrical circuits should be closed for this coupling. Omitting migration times as indices for metabolite identification and replacing them by ones that are independent of the factors that cause variations in the migration times seems to be cementing CE-MS in metabolomics analyses. Additionally, recent advancements of CE-ESI interfaces such as SL or CESI interfaces confronted the technical challenges and proved merits of CE-MS by the application of such interfaces in the analysis of various biomolecules. The metabo-ring study demonstrated the power of using CE-MS for identifying polar, charged compounds in complex biological mixtures by using μ_{eff} , an intrinsic property unique to each analyte and independent of most of the factors that would normally result in variations of migration times. To do so, the BGE was imposed as 10% acetic acid (pH 2.2). This buffer was easy to prepare, stable over time and fit the requirements of CE-MS coupling. Between the use of RMT and μ_{eff} as substitutes to migration time-based compound annotation, the latter demonstrated the lowest deviation even in complex biological matrices with considerable ionic strengths. Furthermore, a criterion based on relative or absolute deviation, depending on the mobility of the analyte, was proposed for determining the levels of confidence associated with metabolite annotation. Although the study involved cationic metabolites, it could be extended further to investigate anionic ones. Furthermore, a larger library of compounds can be assessed using this method and complementing it by other analytical methods to construct databases of compounds based on their μ_{eff} . This would facilitate the use of CE-MS in complementarity to other techniques for the separation, detection and identification of polar and charged compounds in a complex sample.

Part B:

Capillary electrophoresis- mass spectrometry for monitoring nucleoside kinases activity: Applications to novel anti-viral compounds

I. Introduction

Nucleosides are biomolecules composed of a 5 carbon pentose sugar and a nitrogenous base (nucleobase). The pentose sugar can be either a ribose or deoxyribose, lacking the 2' OH group. On the other hand, nitrogenous bases are structurally divided into two types, pyrimidines and purines. Cytosine, thymidine and uracil are pyrimidine nucleobases composed of a single aromatic heterocyclic ring. On the other hand, adenine and guanine are purines nucleobases given their structure composed of two fused aromatic heterocyclic rings. Nucleotides are phosphorylated derivatives of nucleosides and constitute the building blocks of deoxyribonucleic (DNA) and ribonucleic (RNA) acids. Nucleosides are phosphorylated through the transfer of one, two or three phosphate groups to the C5 of the pentose sugar by nucleoside phosphoryl transferases (kinases). These enzymes contribute to the metabolism of nucleosides and their phosphorylated derivatives in cells. Nucleoside kinases catalyze the transfer of a high-energy phosphate group from a nucleoside triphosphate (NTP) donor, mainly adenosine triphosphate (ATP), to a phosphate acceptor in the presence of a divalent cation metal, such as Mg^{2+} . Nucleoside phosphorylation is crucial for several biological processes such as the synthesis of DNA and RNA, biochemical cell signaling and energy transfer processes. The complexity of such transfer reaction stems from the fact that in addition to the nucleoside substrate, the actual phosphate acceptor, there exists other pseudo-substrates, divalent metal cation and NTP co-factors, both of which are essential for the transformation process. By definition, a co-factor is a molecule that is required for the catalytic activity of the enzyme³. Co-factors may be either inorganic molecules, such as divalent metal cations, or more complex organic molecules, such as NTP, which are then referred to as co-enzymes. Furthermore, the physical properties of the reaction such as the pH, temperature, nature

³ Encyclopedia Britanica, www.britannica.com/science/cofactor

and concentration of the solvent and co-factors, also play a role on the outcome of the phosphotransfer reaction.

Several analytical techniques have been described for monitoring the reactions of kinases, most commonly spectrophotometric and radiometric approaches are utilized. However, these approaches require the use of fluorescent labels, coupled reactions or the use of radiolabeled molecules. Fluorescence labeling or coupled reactions increase the overall time of the reaction. On the other hand, manipulation of radioactive material requires stringent regulations [28]. CE demonstrates great adaptability and versatility for assaying a wide variety of enzymes with different modes of action, such as kinases. Additionally, the minimal volume requirements of CE (few nLs) allows one to conduct a larger number of assays compared to other conventional techniques requiring much greater volumes (μL – mL). This is rather an important parameter to consider since the enzymes that will be discussed later in this part of the chapter, if commercially available, are very expensive. Through careful design and optimization, it is possible to automate the assay and multiplex it allowing simultaneous investigation of multiple enzymes, such as kinases involved in a cascade of phosphorylation reactions (Figure III.12).

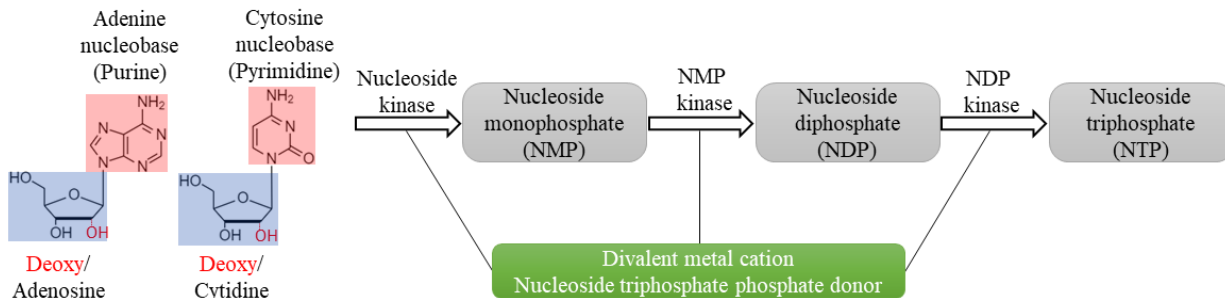


Figure III.12: Illustration of phosphorylation reactions catalyzed by nucleoside and nucleotide kinases

The first chapter of this thesis reviewed most relevant CE and chromatography-based nucleoside kinase assays hyphenated to a variety of detection techniques. This chapter will present the optimizations carried out on CE-based offline assays of two nucleoside kinases, deoxythymidine monophosphate kinase “thymidylate kinase” (dTMPK) and nucleoside diphosphate kinase (NDPK). dTMPK catalyzes the phosphorylation of dTMP into dTDP. NDPK, in addition to other cellular kinases, catalyzes the next phosphorylation step transforming dTDP into dTTP. The latter triphosphate is then incorporated into the DNA chain by DNA polymerase. In addition to endogenous nucleosides, the CE-based method was used to assay dTMPK activity towards

nucleoside analogs.

II. Nucleoside analogs and their therapeutic implications

A nucleoside (or nucleotide) analog is a synthetic molecule that structurally resembles endogenous nucleosides. Due to their similarity to the endogenous molecules, nucleoside analogs are often metabolized in a similar fashion and are therefore phosphorylated by nucleoside kinases. However, since the analogs are not endogenous, the affinities of enzymes towards them is often not the same. Furthermore, analogs are specifically designed so that they take part in therapeutic anti-cancer and anti-viral treatments.

5-fluorouracil (5-FU), for example, is a common anticancer chemotherapeutic drug used for the treatment of several types of cancers, especially colorectal cancer. 5-FU is an analog of uracil (Figure III.13) nucleobases and one of its most important mechanisms of action involves the inhibition of thymidylate synthase, an enzyme that catalyzes the methylation (addition of CH_3) of dUMP to dTMP.

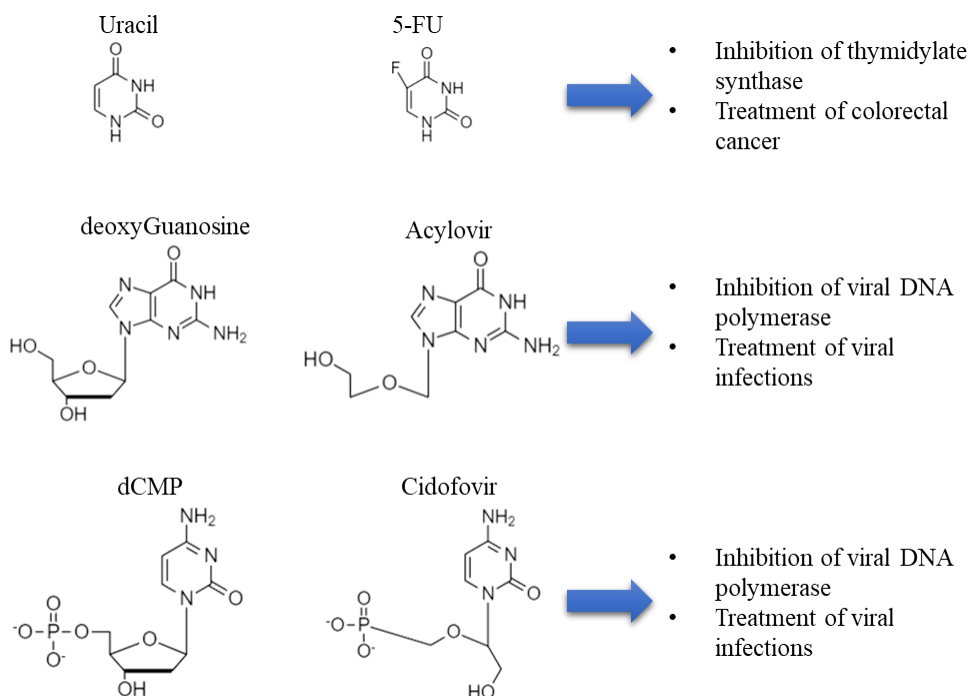


Figure III.13: Structures of endogenous uracil, deoxyguanosine and dCMP compared to their respective analogs, 5-FU, acyclovir and cidofovir as well as their therapeutic uses

The inhibition is brought about by the formation of a ternary structure between the thymidylate synthase enzyme and the 5-FU metabolites in the cell, preventing the binding of dUMP. This results in depletion of dTMP and accumulation of dUMP creating an imbalance in the nucleotide pool. The lack of dTMP prevents the formation of dTTP and its incorporation into the DNA. This consequently results in cell death due to fatal errors in DNA replication [29]. Another example of a nucleoside analog is acyclovir (ACV), used to treat infections caused by herpes simplex virus types 1 and 2 (HSV-1 & 2). ACV is an analogue of guanosine nucleosides (Figure III.13). Once incorporated into the cell, ACV is phosphorylated into ACV-MP by viral TK. The affinity of viral TK towards ACV is much higher than that of human TK and thus this first rate-limiting phosphorylation step occurs almost exclusively in cells infected with HSV. ACV-MP is then phosphorylated to ACV-DP and active ACV-TP by human cellular kinases. The latter is then incorporated into the growing DNA chain by DNA polymerases. The affinity of viral DNA polymerase towards ACV-TP is much higher and thus this incorporation occurs at a grander scale in infected cells. Once inserted into the growing DNA strand, no further nucleotides can be incorporated due to the acyclic structure of the sugar moiety in ACV, lacking the essential 3'OH required for DNA chain growth (Figure III.13). Due to the higher affinities of the viral versions of TK and DNA polymerase enzyme towards ACV, it is a highly specific drug with low toxicity towards uninfected cells [30,31].

The development of resistant viral strains is a common obstacle. For instance, ACV resistance may be brought about by mutations in the viral TK encoding genes which may greatly reduce the affinity of viral TK towards ACV. This could render ACV useless since the first rate-limiting phosphorylation step occurs at a much lesser extent. To overcome this problem, different forms of antiviral analogues can be used instead. For example, using an already phosphorylated analogue, such as cidofovir, overcomes ACV resistance. Cidofovir is an acyclic deoxycytidine analogue (Figure III.13) that is used for treatment of ACV resistant strains of HSV in addition to other DNA viruses by competitively inhibiting viral DNA polymerase. Possible difficulties in cell penetration due to the polarity of the phosphate groups may ensue. The latter can be overcome by masking the polar phosphate groups by a chemical moiety that is later cleaved *in-cellulo* once the analog reaches the cytosol. Although the first phosphorylation step is omitted, cidofovir is still selective since the affinity of viral DNA polymerase towards the activated cidofovir TP is 25-50 times greater compared to the human polymerase [30].

In the context of this thesis, our collaborators have kindly provided us with the nucleoside kinases as well as a series of nucleoside analogs. Human dTMPK and NDPK were overexpressed and purified as described in [32]. Standards of endogenous nucleosides were commercially purchased as sodium salts. C5 substituted but-2-enyl thymine (Figure III.14) were synthesized by our collaborators as described in [33] and demonstrated effectiveness against HSV-1 and HSV-2 in addition to other viruses using cell viability assays.

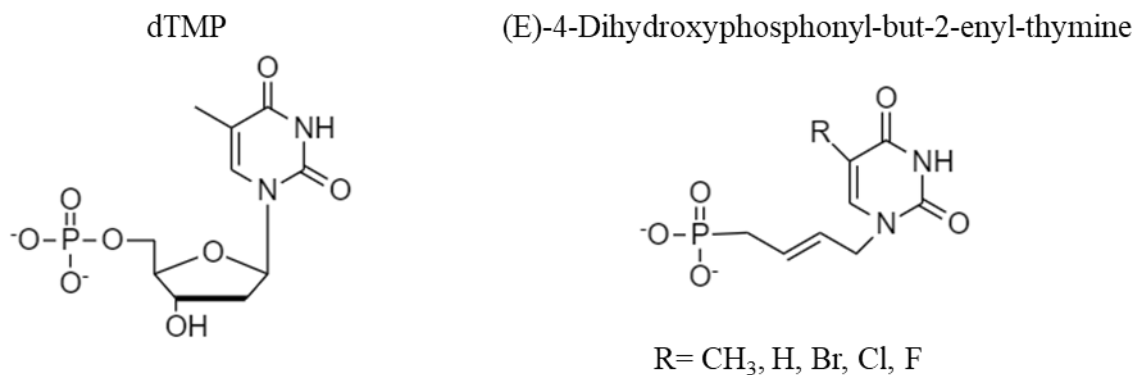


Figure III.14: Structure of dTMP and its chemically synthesized C5 substituted but-2-enyl thymine analogue

III. Results

The optimization of the CE method was carried out in most parts using UV detection. However, the purpose was to develop a method compatible with CE-HRMS to validate results obtained with UV detection. As previously mentioned, hyphenation of CE to MS comes at a price. One of the most important parameters to control is the BGE's nature and concentration. Hyphenation of CE to MS through an ESI source requires the use of volatile BGE's therefore conventional BGE such as borate and phosphate buffers are undesirable. Furthermore, the concentrations of the BGE and certain additives such as co-factors must be controlled to limit ion suppression which results in poor ionization of the analytes.

III.a Choice of BGE and optimization of its parameters

III.a.1 The nature of the BGE: Two of the most commonly used BGE in CE-MS studies, ammonium acetate and ammonium formate, were compared for their use in the separation of a mixture of adenosine and thymidine nucleotides. In fact, both BGEs are volatile which is an important parameter for CE-MS hyphenation permitting facile desolvation and thus enhances analyte nebulization and ionization.

As shown in the electropherograms in Figure III.15, both BGEs resulted in the same migration order of all six nucleotides where TMP migrated the fastest followed by dAMP, dADP, dATP, TDP and TTP.

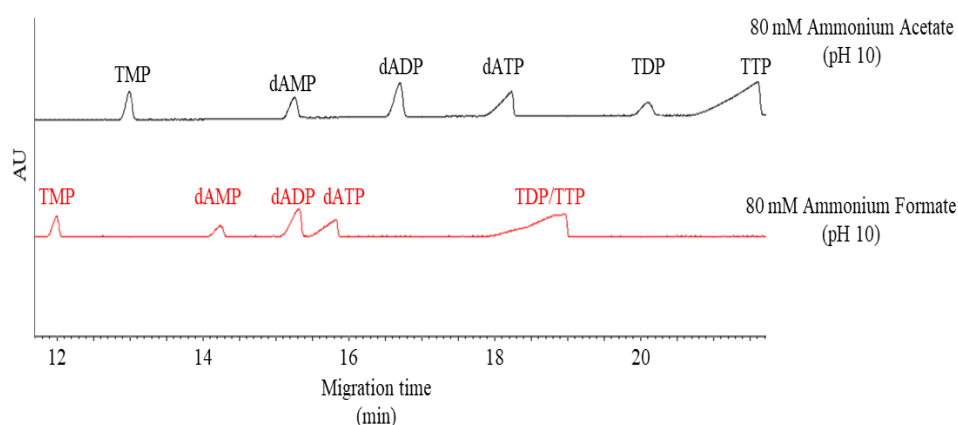


Figure III.15: Electropherograms obtained for the separation of a mixture of 6 nucleotides (dAMP, dADP, dATP, TMP, TDP and TTP) using ammonium acetate (**Black**) or ammonium formate (**Red**) as BGE. **CE conditions:** capillary: (60 cm × 50 μm i.d.; 50 cm effective length); BGE: 80 mM ammonium formate or ammonium acetate (pH 10); injection: 0.5 psi × 10 s (10 nL); separation: +20 kV; detection: UV at λ = 254 nm; [nucleotides]: 100 μM

Adenine nucleotides were investigated since all kinases require a co-enzyme, such as ATP, as a phosphate group donor being converted to ADP in the process. Furthermore, thymidine nucleotides were added to the mix since the investigated enzymes catalyze the phosphorylation of TMP to TDP and the latter to TTP in addition to the sequential phosphorylation and activation of TMP analogs to the tri-phosphorylated form. With formate buffer, the separation efficiencies of NDPs and NTPs were lower than that observed with the acetate buffer where a clear resolution between the dADP and dATP on one hand and TDP and TTP on the other was observed. The migration times were relatively shorter with the ammonium formate buffer possibly due to its higher μ_{EOF} ($4.72 \text{ cm}^2 \text{ V}^{-1} \text{ s}^{-1}$) compared to that of ammonium acetate ($4.39 \text{ cm}^2 \text{ V}^{-1} \text{ s}^{-1}$) as shown in Figure III.15. Ammonium acetate was chosen over ammonium formate as the BGE demonstrated the possibility of efficiently resolving the peaks of the six nucleotides.

III.a.2 pH of the BGE: The electropherograms for the separation of the six adenosine and thymidine nucleotides using ammonium acetate at pH 9.3 and 10 are presented in Figure III.16a. The pH of the BGE plays a key role in controlling the EOF. If the pH is high enough, *i.e.* higher than the pKa of the analytes or *pI* of the proteins, non-specific analyte adsorption to the capillary wall is avoided *via* charge repulsion. Additionally, if the pH is low enough, *i.e.* lower than the pKa of the silanol groups, silanol deprotonation will become limited and the capillary wall will remain largely uncharged preventing the ionic adsorption of analytes onto it. However, this may also largely inhibit the EOF necessitating certain precautions such as reversal of the sense of migration. In addition to the EOF, the pH of the BGE is important for the ionization of the migrating analytes (anionic for nucleotides).

Concerning adenosine species, the abundances of charges were identical at pH 9.3 and pH 10 as determined by simulation using Chemaxon's Chemicalize (Figure III.16b). The migration times of dAMP and dADP were almost identical at pH 9.3 and pH 10 confirming the results of the simulation. Concerning dATP, the migration times were slightly longer at pH 10 compared to pH 9.3. This was contrary to the results of the simulation which suggested identical charge and abundance of charged species at both pH. This might be due to increased charge density of dATP at pH 10.

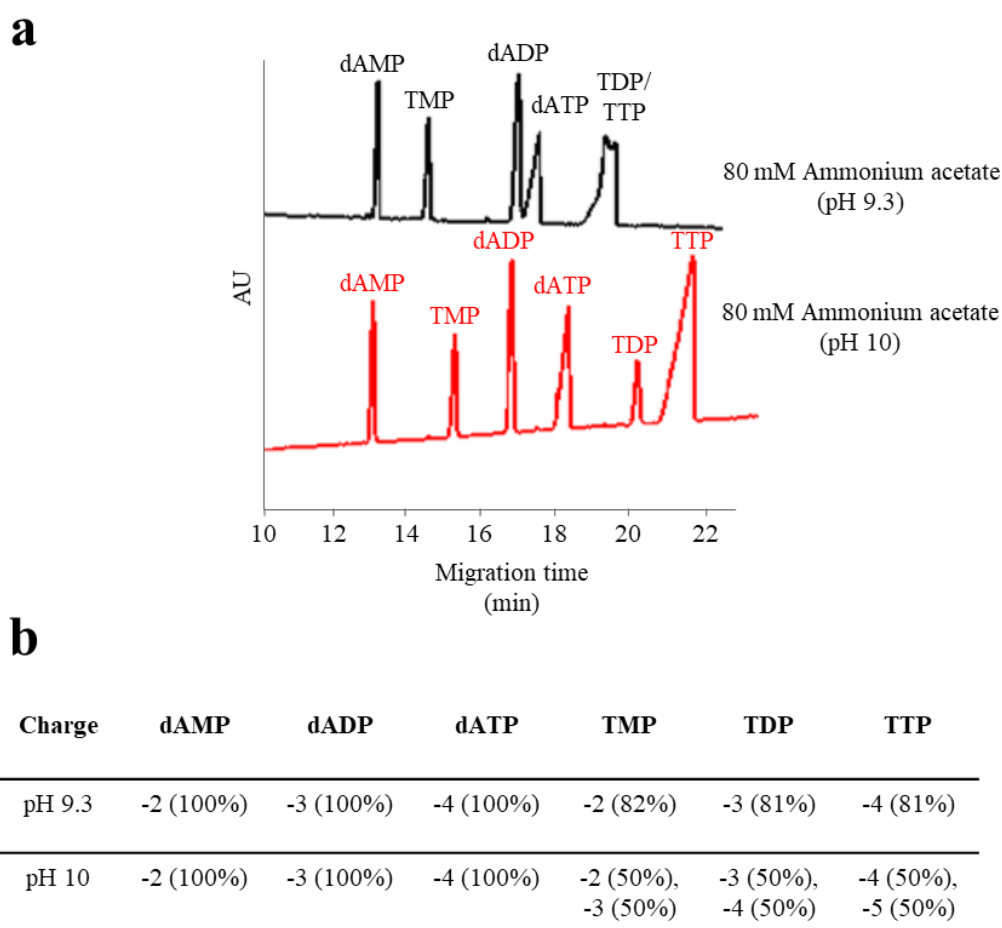


Figure III.16: Electropherograms obtained for the separation of six nucleotide species (TMP, TDP, TTP, dAMP, dADP and dATP) using 80 mM ammonium acetate at pH 9.3 (**Black**) and pH 10 (**Red**) (**a**) and the charges of the nucleotide species as well as their abundance at pH 9.3 and pH 10 (**b**). CE conditions are similar to those described in Figure III.15

Concerning thymidine nucleotides, the charges and their abundances were different at pH 9.3 and pH 10. The migration times of thymidine nucleotides were longer at pH 10 where species bearing higher negative charges emerge. The increase in the migration times is due to the electrophoretic mobilities of these charged species which counteracts the EOF, slowing their migration towards the cathode in the capillary. Furthermore, using 80 mM ammonium acetate at pH 9.3 did not resolve TDP and TTP peaks. It worth noting that pH values lower than those presented in Figure III.16 resulted in an important increase of total migration times possibly due to decrease EOF. The pH of the BGE was chosen as pH 10 since the analytes were well ionized and migrated in their anionic forms, the EOF permitted relatively short analysis times and good peak shape and resolution were obtained.

III.a.3 Ionic strength of the BGE: At ionic strengths of 80 mM, relatively high currents were generated and the migration times were around 22 min as shown in Figure III.15. Nonetheless, ionic strengths lower than 80 mM required the addition of complexation agents such as Mg^{2+} as will be discussed later in segment **III.b.** to enhance the resolution of NDP and NTP peaks. An increase in the ionic strength of the BGE results in the reduction of the EOF and excess generation of Joule heating. The reduction of EOF results in longer migration times whilst excessive Joule heating results in peak dispersion and reduced separation efficiencies [35]. Additionally, and most importantly, a high BGE concentration may result in ion suppression using CE-MS. The ionic strength of the acetate BGE was set at 40 mM as long as Mg^{2+} was added as the complexation agent.

III.b Effect of Mg^{2+} complexation

As mentioned above, the use of 80 mM ammonium acetate BGE may result in undesirable Joule heating and ion suppression. Consequently, the ionic strength was reduced to half, *i.e.* 40 mM ammonium acetate. Complexation between cationic metals and nucleotides have been previously described and investigated by CE [36]. Furthermore, it is well established that the ATP and Mg^{2+} requirement for kinase reactions is actually in the form of a single ATP- Mg^{2+} complex, where Mg^{2+} complexes to ATP facilitating the binding of kinase. At 40 mM BGE, dADP and dATP co-migrated as manifested by the single peak following the dAMP peak. Upon addition of 200 μ M Mg^{2+} as a complexation agent, the peaks of dADP and dATP were well resolved. Such low concentration of Mg^{2+} is a compromise between efficient resolution of NDP and NTP species and ion suppression, as previously described by our group [32].

Additionally, even in the absence of $MgCl_2$ in the sample solution, dADP and dATP were resolved when injected into a capillary previously exposed to Mg^{2+} even after rinsing procedures, from the long capillary end (Figure III.17a). This was further confirmed by using new clean capillaries where the resolution of dADP and dATP peaks was lost. Furthermore, injection of adenosine nucleotides in the absence of Mg^{2+} from the short capillary end, *i.e.* cathodic injection, and using a capillary previously exposed to Mg^{2+} did not demonstrate the same results where dADP and dATP were unresolved as shown in Figure III.17b. The electropherograms reveals limited resolution of dADP and dATP peaks upon addition of 200 μ M Mg^{2+} into the short end of the capillary. These results may be explained by residues of Mg^{2+} that remain in the capillary possibly interacting with the capillary wall. The fact that only long end injection (50 cm to the detector)

and not short end ones (10 cm to the detector) resulted in resolution of dADP and dATP, in the absence of Mg^{2+} added to the sample solution, may support this theory since the distance migrated by the analytes is 5-folds greater increasing the probability of encountering more remnants of Mg^{2+} in the capillary. The final conditions chosen were ammonium acetate buffer (40 mM, pH 10) with 200 μM Mg^{2+} added to the sample solution to complex with nucleotides and induce efficient resolution of their peaks.

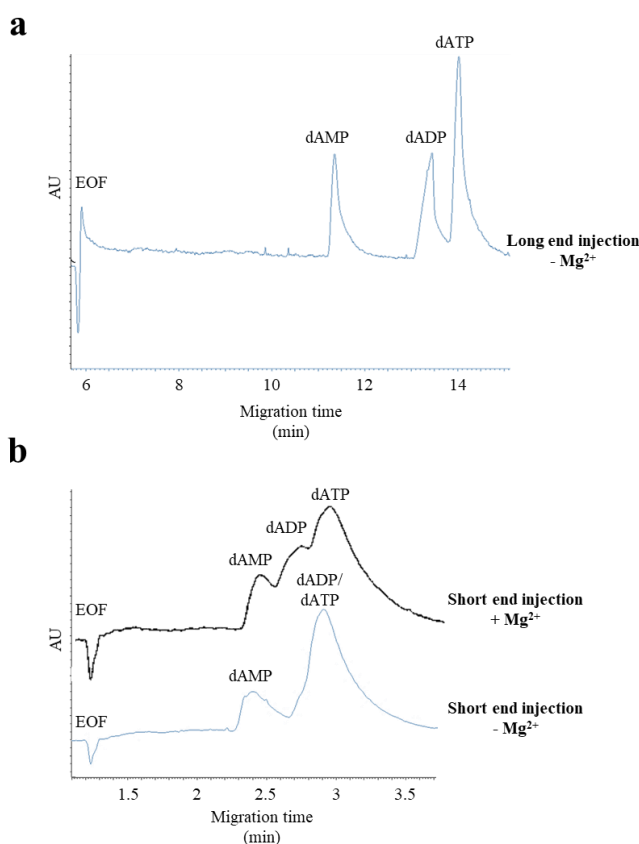


Figure III.17: Electropherograms obtained for the separation of three adenosine nucleotides (dAMP, dADP and dATP); at 50 μM in 40 mM ammonium acetate, pH 10) into a capillary previously exposed to $MgCl_2$ from the long (a) and the short capillary end (b). For injections from the short capillary ends, the mixture of adenosine nucleotides was injected either in the absence (Blue) and presence (Black) of 200 μM $MgCl_2$ into the capillary previously exposed to Mg^{2+} . CE conditions are described in Figure III.16 with ammonium acetate BGE (40 mM, pH 10)

III.c Effect of separation voltage

A high separation voltage goes hand in hand with high peak efficiency and more or less contributes to the resolution and reduced migration times of the analytes unless excessive Joule heating is generated. Another consequence of excessive Joule heating is fracturing or breakage of the capillary at the opaque detection window, rendering the capillary useless. We have noticed a

temporal deterioration of current upon use of relatively high separation voltages (> 15 kV). Upon further inspection, the capillary was broken in most of the cases. Therefore, the separation voltage was limited to a maximum of 15 kV. At such relatively low voltages, the analytes' migration times are expected to be longer. As a result, whenever necessary, separation pressure was combined with the voltage in order to speed up the analyses.

III.d Kinetic parameters of hTMPK and hNDPK

The Michaelis Menten constant (K_m) is a kinetic parameter that reflects the enzymes' (human TMPK and NDPK) affinities towards their substrates (TMP and TDP, respectively). It is calculated from plotting the rate of the enzymatic activity as a function of a range of substrate concentrations. K_m of both enzymes were evaluated using CE-UV in order to assess the stability of the enzymes following a relatively long storage period. The conditions used are summarized in Table III.2 below. The enzymatic reactions were carried out offline using similar conditions as those described in [32] using flow injection analysis (FIA) coupled to HRMS.

Table III.2: Conditions for the offline reaction and CE separation for determination of the kinetic parameters of human TMPK and NDPK

Offline reaction conditions	
Enzymes	[TMPK] or [NDPK] at 0.04 g L ⁻¹
Substrates (Phosphate acceptors)	[TMP] or [TDP] at (0.05, 0.1, 0.25, 0.35, 0.6 & 1 mM)
Co-factors	[MgCl ₂] at 200 μM
Co-enzymes	[ATP] at 350 μM
IB	Ammonium acetate at 50 mM, pH 7
Reaction Steps	10 min pre-incubation at 37°C (Enzyme + IB + ATP & MgCl ₂) Addition of substrate and incubation for 30 min at 37°C Incubation at 95°C in water bath to terminate the reaction Three blanks were conducted
CE conditions	
BGE	Ammonium acetate at 40 mM, pH 10
Injection	0.5 psi × 10 s at 10 nL
Separation voltage	+15 kV
Detection	UV at 254 nm

The electropherograms for the separation and detection of the reactants of the TMPK catalyzed reaction at different substrate (TMP) concentrations is presented in Figure III.18a.

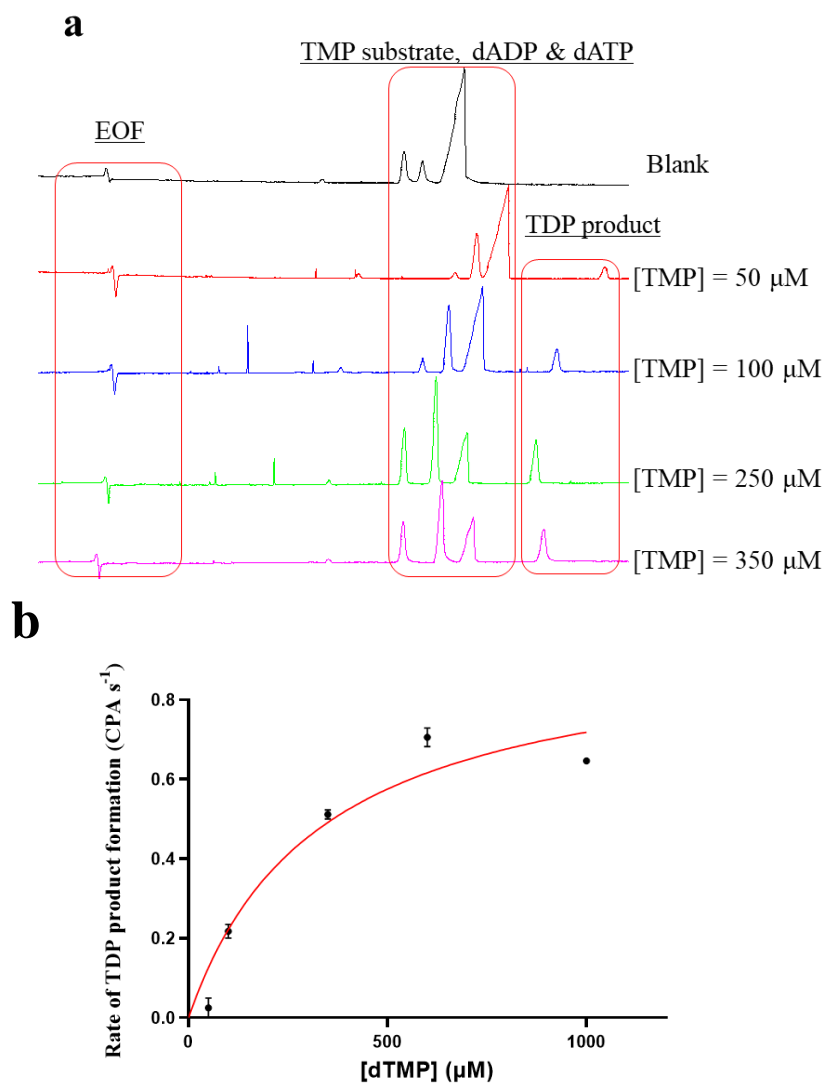
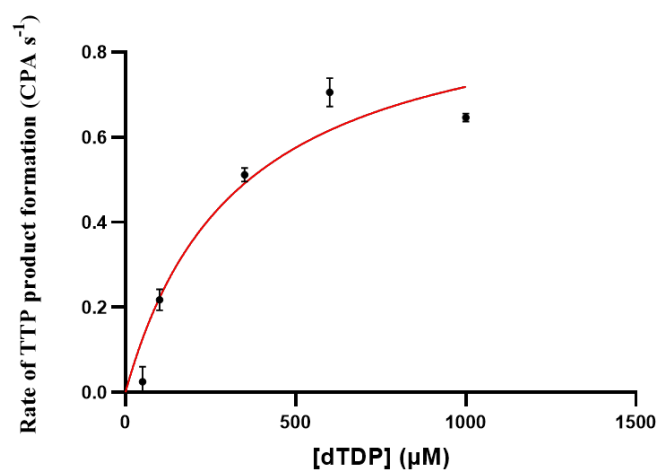


Figure III.18: Electropherogram (a) and the Michaelis Menten plot (b) of TMPK catalyzed phosphorylation of TMP into TDP and K_m values calculated from the plot. These values were compared to those determined by FIA-HRMS [32].

Offline reaction and CE conditions are summarized in Table III.2

The K_m values were calculated using non-linear regression provided by Graphpad prism, and compared to those obtained in [32] (Figure III.18b for TMPK and Figure III.19 for NDPK). The

reaction consisted of pre-incubating all of the reaction components except the substrate at 37°C for 10 min. This step ensures the thermal equilibrium between all the reactants and allows the formation of any complexes. Meanwhile, the substrate was incubated alone at the same temperature (37°C). The reaction was initiated through the addition of the substrate to the reaction medium.



Kinetic parameter	CE-UV (n=2)	Reference (FIA-HRMS) [32]
K_m (μM)	33.2 ± 12.5	93 ± 13

Figure III.19: Michaelis Menten plot of NDPK catalyzed phosphorylation of TDP into TTP and K_m values calculated from the plot. These values were compared to those determined by FIA-HRMS [32]. Offline reaction and CE conditions are summarized in Table III.2

For both enzymes, the reaction rate can be quantified by monitoring the rate of substrate phosphorylation or formation of phosphorylated product. Alternatively, quantification of ATP dephosphorylation or formation of ADP is another viable option. The results demonstrate that K_m of both enzymes towards their substrates, calculated *via* CE-UV, were within the same order of magnitude as those calculated *via* FIA-HRMS. The next section will consider the optimization of the TMPK catalyzed reaction.

III.e Optimization of TMPK reaction

III.e.1 Nature of the incubation buffer: The reaction buffer plays an important role in mediating the suitable conditions for the enzymatic reaction. Up to this point, volatile buffer ammonium acetate was used as the incubation buffer at 20 mM. This solution buffering range is between 3.8-5.8 and 8.3-10.3 based on the pK_a , $-\log$ of the acid dissociation constant, of the acetate ($pK_a=4.8$)

and ammonium ($pK_a=9.3$) components of the buffer, respectively. On another note, human TMPK functions optimally at the physiological pH of 7.1-7.5 [32,38]. At this pH, the buffering capacity of the ammonium acetate solution is expected to be low. In other words, the pH is expected to be unstable and prone to changes during the reaction. HEPES (4-(2-hydroxyethyl)-1-piperazineethanesulfonic acid) is a zwitterionic buffer with $pK_{a1}=7.5$ and thus has useful buffering range between pH 6.5 and 8.5. Therefore, at pH 7, HEPES is expected to be a better buffering solution resisting any changes in the pH upon the enzymatic reaction. Both buffers were compared by calculating TMP conversion by TMPK and the results presented below in Figure III.20.

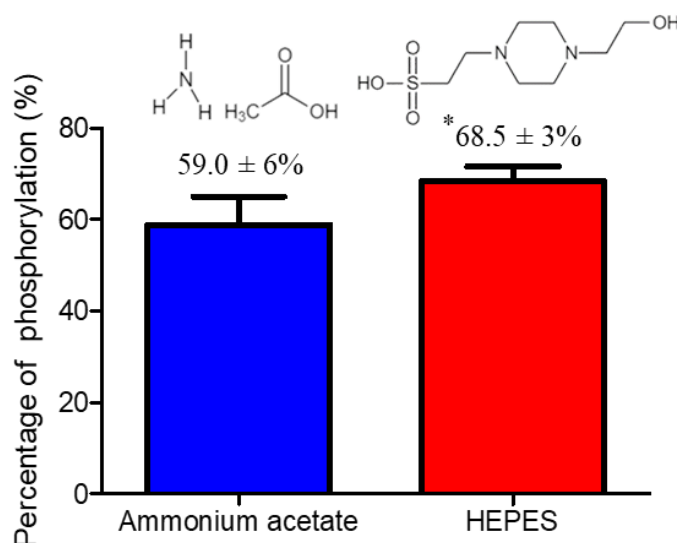


Figure III.20: Percentage of TMPK catalyzed phosphorylation of TMP to TDP in the presence of ammonium acetate or HEPES as IB. Reaction conditions: IB: 20 mM Ammonium acetate (Blue) or 25 mM HEPES (Red) (pH 7), [TMP substrate]: 400 μ M, [TMPK]: 0.04 g L⁻¹, [ATP]: 350 μ M, [MgCl₂]: 5 mM. Pre-incubation of all reaction components except TMP for 10 min at 37°C, reaction initiated through the addition of TMP and incubation for 5 min at 37°C. Reaction was stopped by incubation at 95°C for 5 min.

CE conditions were summarized in Table III.2. Each reaction was repeated six times ($n = 6$)

TMP conversion was estimated by calculating the corrected peak area of TMP in the reaction relative to that in a blank where no enzyme was present. HEPES was used at a concentration of 25 mM and adjusted to pH 7 through the addition of NaOH. Both buffers contained 5 mM MgCl₂. This relatively elevated amount (compared to 200 μ M) was used since very little enzymatic activity was observed in the presence of Mg²⁺ lower than 250 μ M with HEPES as the IB, as will be later discussed. As shown in Figure III.20, the TMPK catalyzed conversion of TMP using HEPES IB was significantly higher (68.5%) than that observed with ammonium acetate as the IB (59%).

Methyl substituted but-2-enyl thymine monophosphorylated nucleoside analogs (structure in Figure III.14) demonstrated much lower conversion rates (31.3%) compared to the natural substrate TMP (68.5%) as shown in Figure III.21.

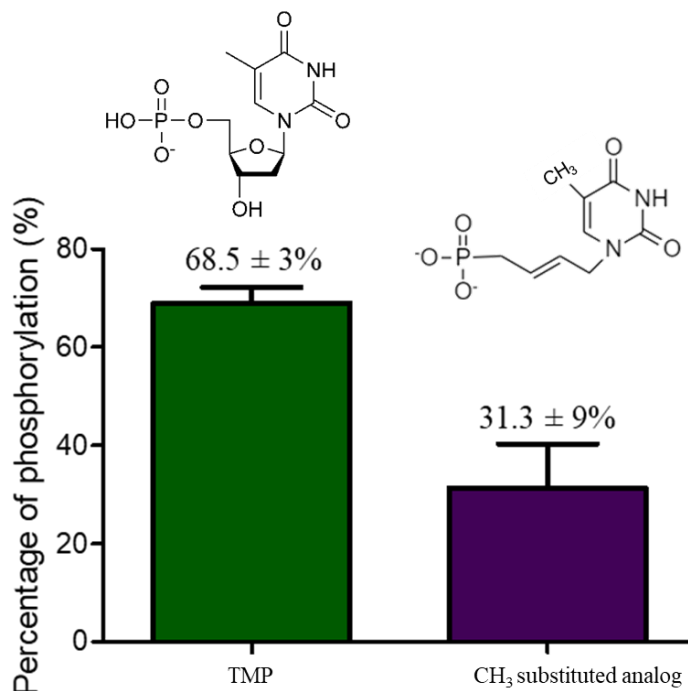


Figure III.21: Percentage of TMPK catalyzed phosphorylation of TMP (Green) or CH₃ substituted analog (Purple) in the presence of HEPES.

Reaction conditions: IB: HEPES (25 mM, pH 7), [TMP or analog substrate]: 400 μM, [TMPK]: 0.04 g L⁻¹, [ATP]: 350 μM, [MgCl₂]: 5 mM. Pre-incubation of all reaction components except TMP for 10 min at 37°C, reaction initiated through the addition of TMP and incubation for 5 min at 37°C. Reaction was stopped by incubation at 95°C for 5 min. CE conditions were summarized in Table III.2. Each reaction was repeated six times (n = 6)

The lower activity of TMPK towards the analog is due to the fact that kinases tend to be less catalytically active towards nucleoside analogues compared to endogenous nucleotides. Despite this lower activity, the highest phosphorylation of the CH₃ substituted analog was obtained using HEPES compared to other buffering agents such as MOPS and TRIS (Figure III.22).

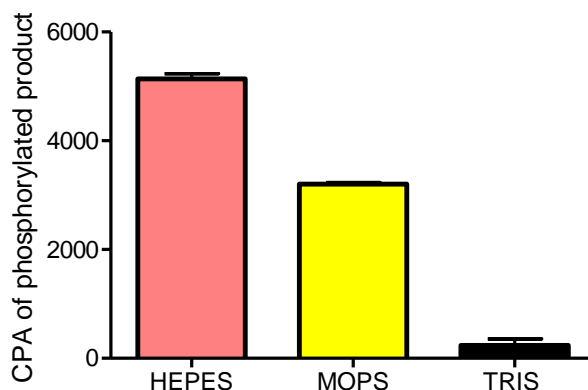


Figure III.22: CPA of CH₃ substituted analog phosphorylation product in the presence of HEPES (Pink), MOPS (Yellow) and TRIS (Black). All buffers were prepared at 25 mM and adjusted to pH 7. Reaction conditions were similar to those described in Figure III.21 for the analog

III.e.2 TMPK concentration and linearity of its reaction: The appropriate enzyme concentration is one which results in measurable product yields with considerations to minimize consumption of the enzyme solution. The linearity of the enzymatic reaction is an important consideration when studying the kinetics of an enzyme catalyzed reaction. It is the period of time in which the increase in the rate of the reaction is linear with the increase of incubation time. Using CE-MS, the most suitable TMPK concentration and incubation times with CH₃ substituted analog as the substrate were investigated simultaneously. The investigated TMPK concentrations were 0.005, 0.04 and 0.2 g L⁻¹. Each concentration of the enzyme was incubated for 5, 15, 20, 60 and 90 min. The results are presented by plotting the area of the phosphorylated analog product as a function of incubation time (Figure III.23). At the lowest tested enzyme concentration (0.005 g L⁻¹), the measured areas were much lower than higher concentration. The enzymatic reaction was however linear for 90 min. At higher concentrations of TMPK (0.04 and 0.2 g L⁻¹) the product yield was higher. Nonetheless, the linearity of the reaction was around 15-20 min. A concentration of 0.04 g L⁻¹ was chosen as a compromise between good product yields and economy in enzyme consumption. The incubation time was set at 5 min since it was within the linearity range of 0.04 g L⁻¹ TMPK.

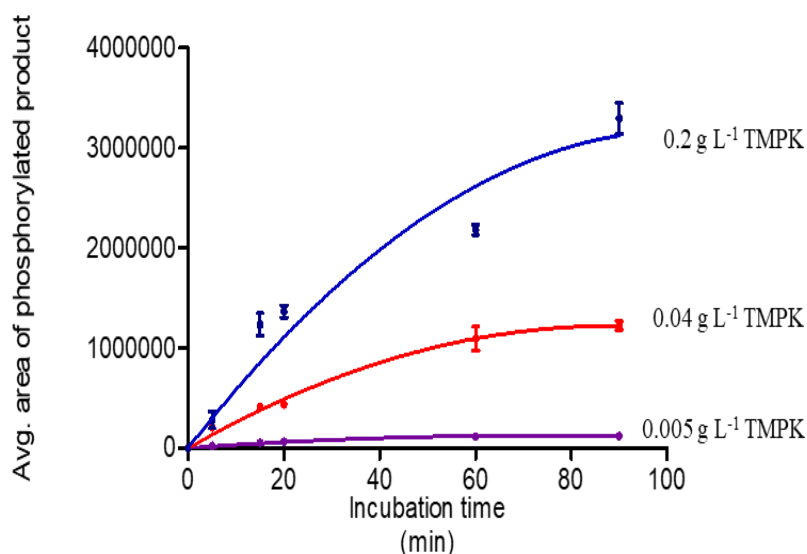


Figure III.23: Plot of the average area of phosphorylated CH₃ substituted analog product as a function of reaction time in the presence of 0.005, 0.04 and 0.2 g L⁻¹ TMPK.

III.e.3 Effect of Mg²⁺ concentration: As discussed earlier, Mg²⁺ is a basic required co-factor for the normal functioning of kinase enzymes. The binding of Mg²⁺ to ATP co-enzyme facilitates its binding to the enzyme. With regards to MS detection, an elevated Mg²⁺ concentration causes important ion suppression were the ionization efficiency of the actual analytes is greatly reduced. The TMPK catalyzed phosphorylation of the CH₃ substituted analog was investigated by CE-UV in the presence of different Mg²⁺ concentrations (0, 0.5, 2.5, 5 and 10 mM) in the IB. Furthermore, the concentrations of the analog substrate and ATP were fixed at 1 mM to saturate the enzyme ruling out any decline in TMPK activity due to depletion of the co-enzyme or cofactor. The results are presented in Figure III.24 as the CPA of the analog phosphorylated product as a function of Mg²⁺ concentration. No phosphorylated product was detected in the absence of Mg²⁺. At 0.5 mM Mg²⁺ the product yields were negligible. At 2.5 mM, 5 mM and 10 mM Mg²⁺, product yields were considerable. Therefore, Mg²⁺ concentration of 5 mM was chosen as a compromise between good activity of the TMPK enzyme and minimal ion suppression.

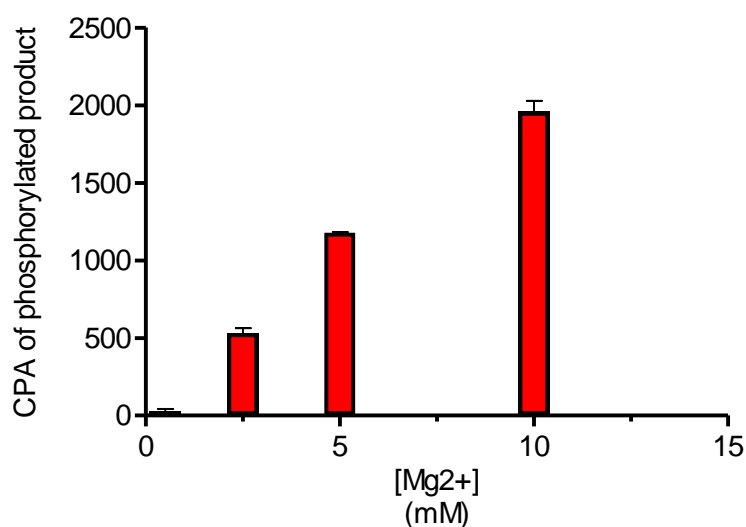


Figure III.24: Investigation of the effect of different Mg^{2+} concentration (0, 0.5, 2.5, 5 and 10 mM) on the TMPK catalyzed phosphorylation of CH_3 substituted analog. Reactions were carried out in triplicates ($n = 3$)

III.e.4 CE-MS assay of TMPK activity: Up until this point, most of the optimizations were carried out using CE-UV with consideration to the regulations required by CE-MS approaches. The aim of this study was to demonstrate the viability of results obtained with conventional CE-UV to those obtained with CE-MS. The reaction conditions were generally kept identical between both platforms. However, technical changes needed to be made due to the differences in both setups. All of the optimized parameters were carried over and applied to the CE-MS approach. The detection of nucleotides was carried out in the negative ionization mode since the analytes were already separated in their anionic forms. CE-MS approaches often require longer capillaries (up to 1 m in length) compared to ones used in conventional CE-UV. This results in an increase of the migration times of the analytes. Furthermore, the applied separation voltage was limited to 15 kV, half of the maximal value, which also contributes to the elongation of the time of analyses. Considering the setup of the CE-MS configuration, it was necessary to reverse the polarities of the applied voltages and pressures since the true inlet is now at the end closest to the UV detection window as shown in Figure III.6.

The reactions were carried out offline similar to CE-UV. In the case of TMP, the natural substrate of TMPK, it was monitored along with its phosphorylated product (TDP) at m/z 321 and 401, respectively. In the case of CH_3 substituted analog of TMP, it was monitored along with its phosphorylated product at m/z 259 and 339, respectively. Using a separation voltage of -15 kV

only, the migration time of the species exceeded 20 min. Therefore, it was necessary to assist the voltage with at-inlet applied pressure to speed up the analyses. Nonetheless, the application of pressure throughout the duration of the separation phase resulted in poorly shaped peaks with low to little resolution. As a result, the separation was split into two phases: i) application of separation voltage and pressure for a particular period of time to push the analytes towards the MS detector significantly reducing their migration times and ii) cessation of separation pressure while maintaining the separation voltage to resolve unseparated peaks. Upon trial of different separation pressures, the best and fastest separation was obtained when -15 kV separation voltage was assisted with 2.5 psi pressure for 5.5 min followed by the application of -15 kV with a lower pressure (0.2 psi) only for 10 min as shown in Figure III.25 below.

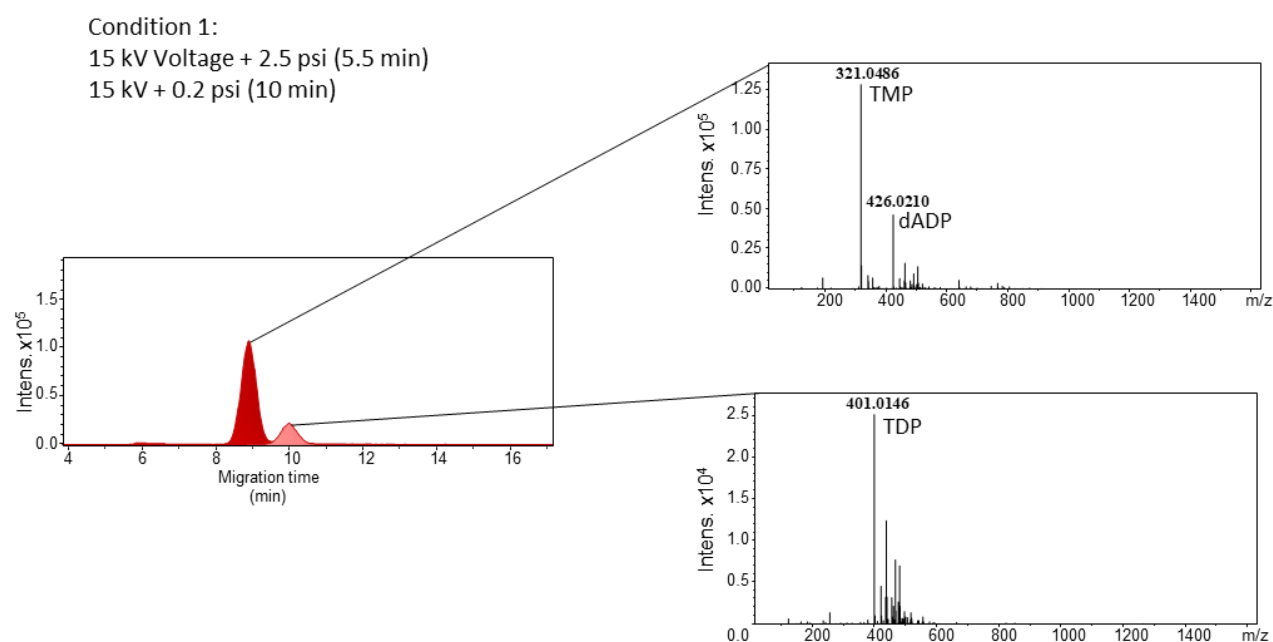


Figure III.25: Electropherogram and mass spectra of TMPK substrate (TMP) and product (TDP) separated and detected by CE-MS using a bi-phased separation method.

Reaction conditions: IB: HEPES (25 mM, pH 7), [TMP substrate]: 1 mM, [TMPK]: 0.04 g L⁻¹, [ATP]: 1 mM, [MgCl₂]: 5 mM. Pre-incubation of all reaction components except TMP for 10 min at 37°C, reaction initiated through the addition of TMP and incubation for 5 min at 37°C. Reaction was stopped by incubation at 95°C for 5 min.

CE-MS conditions: Capillary: uncoated fused silica (90 cm × 50 μm i.d.), BGE: Ammonium acetate (40 mM, pH 10), Injection: 0.5 psi × 10 s, separation: -15 kV + 2.5 psi for 5.5 min followed by -15 kV for 10 min, SL: MeOH + 0.1% formic acid at 10 μL min⁻¹, ionization mode: negative, capillary voltage: -4 kV, nebulizer pressure: N₂ 1.1 bar, dry gas: N₂ heated at 200°C at 4 L min⁻¹

As shown in the electropherogram in Figure III.25, the reaction product migrated at 10 min which is more than two-fold faster than when no pressure was applied at the inlet. Both substrate and

product peaks were well resolved and detected at a considerable intensity. Under such separation conditions, the peak efficiency was reduced. However, the migration time as well as the resolution were improved. This biphased approach was then applied for the separation and detection of CH₃ substituted substrate analog and its phosphorylated product and the results presented in Figure III.26.

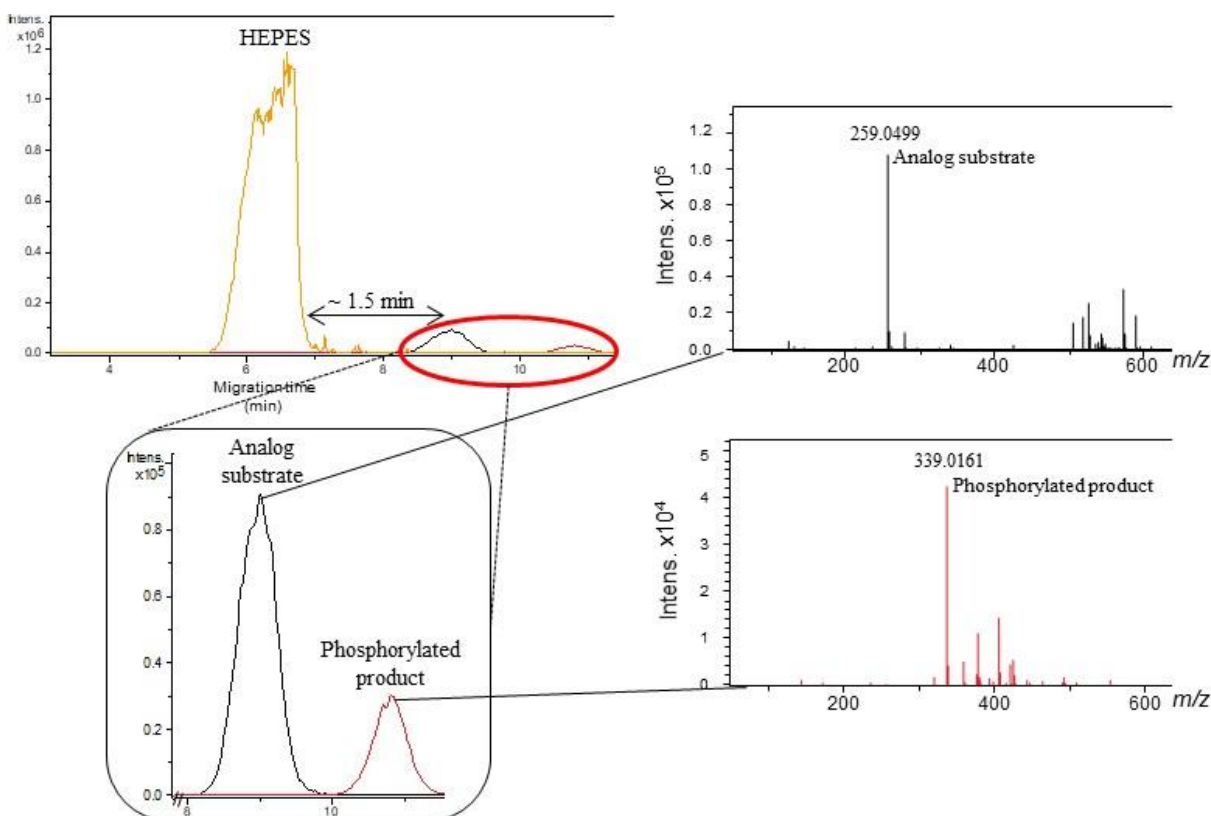


Figure III.26: Electropherogram and mass spectra of CH₃ substituted analog substrate and product separated and detected by CE-MS using a bi-phased separation method. CE-MS Conditions were similar to those describe in Figure III.25

Using the bi-phase separation approach permitted in addition to reduction of migration times and improvement to the peak efficiencies, the separation of the substrate and product peak from HEPES by almost 1.5 min. HEPES was used as the IB since the best phosphorylation rates were observed using it as the incubation buffer at pH 7. It is, however, non-volatile and may induce some ion suppression in the ionization source. With this CE-MS method, HEPES was separated from the substrate and product peaks minimizing the risk of it competing with the ionization of the nucleotides. As shown in the electropherograms of Figure III.26, both substrate and product peaks were well resolved and took around 11 min to reach the MS detector.

IV. Conclusion

This part of the third chapter described the optimizations performed for nucleotide separation using CE-UV and CE-MS. One possible hindrance was the scarcity of commercial availability of the investigated kinases, which required their production from plasmids. This puts further emphasis on a method capable of achieving desirable results rapidly and consuming low reactant volumes. Compared to CE-UV, CE-MS benefits from a higher detection sensitivity and selectivity. Considerations for the hyphenation of CE to MS were taken at the level of the separation as well as the separation. The choice of the BGE was ammonium acetate (80 mM, pH 10) or (40 mM, pH 10, in the presence of complexation agents), since it was volatile, promoted peak resolution and efficient separation of charged species. Complexation of Mg^{2+} resolved NDP and NTP species, thus allowing the reduction of the BGE ionic strength to minimize generation of Joule heating. Separation voltages were limited to 15 kV. CE-UV was used to evaluate K_m of human TMPK and NDPK towards their natural substrates, TMP and TDP, respectively, which were within the same order of magnitude compared to K_m evaluation by FIA-HRMS. With regards to the enzymatic reaction, HEPES was chosen as the TMPK reaction's IB since it provided the highest percentage of phosphorylation of the natural TMP substrate or CH_3 substituted TMP analog. The TMPK concentration was chosen as 0.04 g L^{-1} as a compromise between high product yields and economy in consumption. At this concentration, the reaction was linear up to 20 min and 5 min were sufficient to build up enough phosphorylated products to be detected. The concentration of Mg^{2+} complexation agents was set at 5 mM since lower concentrations resulted in little to no TMPK activities and higher concentration were incompatible with MS.

For CE-MS, the application of separation pressure with the voltage was necessary to speed up the analyses. However, this resulted in peak broadening. Therefore, a bi-phased separation method was put in place where the first phase consisted of application of a high separation pressure (2.5 psi) along with the voltage (-15 kV) for 5.5 min and the second phase involved the reduction of the separation pressure (0.2 psi) whilst maintaining the separation voltage as it is. These conditions sped up the analyses and provided highly resolved substrate and product peaks at the expense of reduced peak efficiency. The method was successfully applied to monitor the TMPK catalyzed reaction towards the natural nucleotide substrate as well as validate the efficiency of CH_3 substituted nucleoside analog as TMPK substrates.

The developed CE-HRMS method can be successfully applied to screen for novel anti-viral molecules that are activated by nucleoside kinases. Additionally, kinases labeled fluorescently for MST binding affinities (as seen in Chapter II; Part B) can be assayed for their activities following labeling to gain insights on the labeling site.

Chapter conclusion

The hyphenation of CE to MS was explored in this chapter in terms of use in metabolomics in addition to assaying the activities and substrate selectivity of nucleoside kinases (TMPK). Poor migration time repeatabilities of CE-MS were overcome by substituting migration time scales with effective mobility scales. Partaken by several laboratories utilizing various CE, CE-MS interfaces and MS detectors, the Metabo-ring interlaboratory study provided interesting insights on the merits of CE-MS in metabolomics through the use of effective mobility scales instead of migration times.

Following the validation of the hyphenation between CE and MS for metabolomics, CE-MS-based nucleoside kinase assays were successfully used to demonstrate the activation of novel anti-viral analogs by human TMPK. The assay was largely developed using conventional CE-UV and then the parameters were transferred to CE-MS. This method transposition from UV to MS hyphenation is another interesting aspect of using CE since it is not possible to carry it out with the same degree of effectiveness using techniques such as HPLC.

Metabolomics of complex cellular extracts may be combined with single-cell enzymatic studies where the enzymes are assayed directly from the cells using CE-MS. Despite the need of a high level of optimizations, this approach can combine the metabolomics approach and the catalytic activity approach in one step. Furthermore, the scarcity of enzymes not commercially available is addressed by further reducing their consumption.

References

- [1] P. L. Urban, *Phil. Trans. R. Soc. A*, 2016, **374**, 1–5.
- [2] E. de Hoffmann and V. Stroobant, *Mass Spectrometry, Principles and Applications*, John Wiley & Sons, Ltd, NJ, USA, 3rd edn., 2007.
- [3] C. Bhardwaj and L. Hanley, *Nat. Prod. Rep.*, 2014, **31**, 756–767.
- [4] A. M. Haag, in *Modern Proteomics – Sample Preparation, Analysis and Practical Applications*, eds. H. Mirzaei and M. Carrasco, Springer International Publishing, Cham, Switzerland, 2016, pp. 157–169.
- [5] F. Xian, C. L. Hendrickson and A. G. Marshall, *Anal. Chem.*, 2012, **84**, 708–719.
- [6] D. W. Koppenaal, C. J. Barinaga, M. B. Denton, R. P. Sperline, G. M. Hieftje, F. J. A. Gregory D. Schilling and J. H. Barnes, *Anal. Chem.*, 2005, **77**, 418–427.
- [7] S. Medhe, *Chem. Biomol. Eng.*, 2018, **3**, 51–58.
- [8] M. Yamashita and J. B. Fenn, *J. Phy. Chem.*, 1984, **434**, 4451–4459.
- [9] L. Konermann, E. Ahadi, A. D. Rodriguez and S. Vahidi, *Anal. Chem.*, 2013, **85**, 2–9.
- [10] P. Kebarle and U. H. Verkerk, in *Reactive intermediates: MS investigations in Solution*, ed. L. S. Santos, Wiley-VCH Verlag, Weinheim, Germany, 2010, pp. 1–35.
- [11] D. R. Allen and B. C. Mcwhinney, *Clin. Biochem. Rev.*, 2019, **40**, 135–146.
- [12] I. V Chernushevich, S. I. Merenbloom, S. Liu and N. Bloomfield, *J. Am. Soc. Mass. Spectrom.*, 2017, **28**, 2143–2150.
- [13] T. Gys, *Nucl. Instrum. Methods. Phys. Res. A*, 2015, **787**, 254–260.
- [14] J. A. Olivares, N. T. Nguyen, C. R. Yonker and R. D. Smith, *Anal. Chem.*, 1987, **59**, 1230–1232.
- [15] R. T. Johnson, PhD thesis, University of Kansas, 2016.
- [16] R. Gahoual, E. Leize-wagner, P. Houzé, R. Gahoual, E. Leize-wagner, P. Houzé and Y. F. Revealing, *Rapid Commun. Mass Spectrom.*, 2018, **33**, 11–19.
- [17] M. Mokaddem, P. Gareil, J. Belgaied and A. Varenne, *Electrophoresis*, 2008, **29**, 1957–1964.
- [18] M. Yamamoto, R. Ly, B. Gill, Y. Zhu, J. Moran-mirabal and P. Britz-mckibbin, *Anal. Chem.*, 2016, **88**, 10710–10719.
- [19] E. J. Maxwell and D. D. Y. Chen, *Anal. Chim. Acta*, 2008, **627**, 25–33.
- [20] H. J. Issaq, G. M. Janini, K. C. Chan and T. D. Veenstra, *J. Chromatogr. A.*, 2004, **1053**, 37–42.
- [21] P. Caludia, S. Filip, B. Daniel M., W. Mullen, A. Vlahou and H. Mischak, *Proteomics*

- Clin. Appl.*, 2015, **9**, 322–334.
- [22] M. Moini, *Anal. Chem.*, 2007, **79**, 4241–4246.
- [23] M. Dadouch, Y. Ladner, C. Bich, M. Larroque, C. Larroque, J. Morel, P. A. Bonnet and C. Perrin, *Analyst*, 2020, **145**, 1759–1767.
- [24] R. Gahoual, E. Leize-wagner and Y. N. Fran, *MAbs*, 2014, **6**, 1464–1473.
- [25] A. M. Belov, R. Viner, M. R. Santos, D. M. Horn, M. Bern, B. L. Karger and A. R. Ivanov, *J. Am. Soc. Mass. Spectrom.*, 2017, **28**, 2614–2634.
- [26] R. Haselberg, C. K. Ratnayake, G. J. De Jong and G. W. Somsen, *J. Chromatogr. A.*, 2010, **1217**, 7605–7611.
- [27] E. Sánchez-lópez, S. M. K. Guinevere, A. L. Crego, M. L. M, R. Ramautar, D. J. M. Peters and O. A. Mayboroda, *Sci. Rep.*, 2019, **9**, 1–9.
- [28] R. Nehmé and P. Morin, *Electrophoresis*, 2015, **36**, 2768–2797.
- [29] D. B. Longley, D. P. Harkin and P. G. Johnston, *Nat. Rev. Cancer*, 2003, **3**, 330–338.
- [30] E. Paintsil and Y.-C. Cheng, in *Encyclopedia of Microbiology (Third Edition)*, ed. M. Schaechter, Academic Press, Oxford, Third Edit., 2009, pp. 223–257.
- [31] G. B. Elion, *Am. J. Med.*, 1982, **73**, 7–13.
- [32] J. Ferey, D. Da Silva, C. Colas, R. Nehmé, P. Lafite, V. Roy, P. Morin, R. Daniellou, L. Agrofoglio and B. Maunit, *Anal. Chim. Acta*, 2019, **1049**, 115–122.
- [33] D. Topalis, U. Pradère, V. Roy, C. Caillat, A. Azzouzi, J. Broggi, R. Snoeck, G. Andrei, J. Lin, S. Eriksson, J. A. C. Alexandre, C. El-Amri, D. Deville-Bonne, P. Meyer, J. Balzarini and L. A. Agrofoglio, *J. Med. Chem.*, 2011, **54**, 222–232.
- [34] S. Fayad, R. Nehmé, M. Langmajerová, B. Ayela, C. Colas, B. Maunit, J. C. Jacquinet, A. Vibert, C. Lopin-Bon, G. Zdeněk and P. Morin, *Anal. Chim. Acta*, 2017, **951**, 140–150.
- [35] D. N. Heiger, *High performance capillary electrophoresis: an introduction : a primer*, Agilent Technologies, Germany, 2000.
- [36] X. Cahours, P. Morin and M. Dreux, *Chromatographia*, 1998, **48**, 739–744.
- [37] H. Tzeng and H. Hung, *Electrophoresis*, 2005, **26**, 2225–2230.
- [38] L. S. Lee and Y. C. Cheng, *J. Biol. Chem.*, 1977, **252**, 5686–5691.
- [39] R. Ramautar, in *Capillary Electrophoresis–Mass Spectrometry for Metabolomics*, The Royal Society of Chemistry, 2018, pp. 1–20.
- [40] R. Ramautar, G. W. Somsen and G. J. de Jong, *Electrophoresis*, 2019, **40**, 165–179.
- [41] N. Drouin, M. van Mever, W. Zhang, E. Tobolkina, S. Ferre, A.-C. C. Servais, M.-J. J. Gou, L. Nyssen, M. Fillet, G. S. M. Lageveen-Kammeijer, J. Nouta, A. J. Chetwynd, I.

- Lynch, J. A. Thorn, J. Meixner, C. Löbner, M. Taverna, S. Liu, N. T. Tran, Y. Francois, A. Lechner, R. Nehmé, G. Al Hamoui Dit Banni, R. Nasreddine, C. Colas, H. H. Lindner, K. Faserl, C. Neusüß, M. Nelke, S. Lämmerer, C. Perrin, C. Bich-Muracciole, C. Barbas, Á. L. González, A. Guttman, M. Szigeti, P. Britz-Mckibbin, Z. Kroezen, M. Shanmuganathan, P. Nemes, E. P. Portero, T. Hankemeier, S. Codesido, V. González-Ruiz, S. Rudaz and R. Ramautar, *Anal. Chem.*, 2020, **92**, 14103–14112.
- [42] P. M. Nowak, M. Woźniakiewicz, M. Gładysz, M. Janus and P. Kościelniak, *Anal. Bioanal. Chem.*, 2017, **409**, 4383–4393.
- [43] N. Drouin, J. Pezzatti, Y. Gagnebin, V. González-Ruiz, J. Schappler and S. Rudaz, *Anal. Chim. Acta*, 2018, **1032**, 178–187.
- [44] R. Gerard, B. Hans, A. Sibylle and W. Christian, *CE/MS principles and applications, a guidebook for novices and practitioners*, 2019.
- [45] Bruker Daltonics, *maXis user manual*, 2008.
- [46] A. Buko, *J. Appl. Bioanal.*, 2017, **3**, 5–20.

Conclusions & perspectives

The objective of this PhD thesis was to bring to light the advantages and limitations of using CE as a technique for enzymatic studies. Through the use of mainly two model enzymes, lipases and nucleoside kinases, in addition to hyaluronidase, CE was demonstrated as a powerful technique for assaying enzymatic activity and modulation since all of the aforementioned enzymes differ considerably in their mechanisms of actions,

The possibility to hyphenate CE separation to various types of detectors such as UV, C⁴D or MS allows one to carry out enzymatic assays by CE taking into account the physical properties of the analytes to be detected, without the prior need of target or ligand modification. The reaction can be carried out offline, before CE analysis or integrated into the CE-separation process by carrying it out directly in the capillary for increased automation. The former offline reaction is straightforward and easy to control and optimize but lacks in automation potential. In contrast, online reactions provide a high degree of automation but are often complicated to control and optimize.

A CE-based lipase assay was developed and optimized using dual detection by UV and C⁴D connected in series to the capillary cartridge and supported by a lab-made 3D scaffold. This dual detection approach allowed the simultaneous detection of the products of 4-nitrophenyl butyrate (4-NPB) hydrolysis reaction, 4-NP and butyrate. The developed offline assay was applied successfully to investigate the catalytic activity of in-solution lipases from crude pancreatic extracts and to screen for modulators of these lipases either in the form of complex plant extracts or purified molecules isolated from oakwood extracts or. The reference lipase inhibitor, orlistat, was used to validate the offline and online assays for use in modulator screening. The developed assay successfully detected both inhibitors and activators of lipases simultaneously. Carrying out online assays especially with complex crude plant extracts proved to be a difficulty. It would be interesting to optimize the online assay so that such complex sample can be screened with a high degree of automation for their lipase modulation potential

The relatively novel biophysical technique, microscale thermophoresis (MST), was used to evaluate the binding affinities of small purified ligands towards lipases from crude pancreatic extracts. These ligands have demonstrated modulation of PL activity using CE. The binding assay was developed and optimized using standard uncoated MST capillaries rather than coated ones, which are far more expensive. The complementarity between PL activity assayed using CE and the binding affinity evaluated using MST was of great importance since the latter technique did not provide any information about the type of modulation exerted by the PL-bound ligand (activation or inhibition) or the degree of this modulation. For instance, the

binding of the covalent PL inhibitor, orlistat, was not detected using MST whereas its inhibitory potential was clearly demonstrated using the developed CE-assay. The purity of the enzyme sample represented a challenging aspect that was reflected on the repeatability of K_d evaluation by MST. For that we have attempted to purify certain lipases from the other proteins in the extracts. Despite this, using either CE-based activity or MST-based binding assay we successfully managed to conclude findings about the modulation and binding of small ligands, respectively.

Biomolecular crowding is the simulation of the real-life environment where enzymatic reactions take place. Dilute *in-vitro* assays are often carried out without accounting the various biomolecular species in the vicinity of the reaction. CE was used to investigate the effect of biomolecular crowding by polyethylene glycol (PEG) on the activity of hyaluronidase and on its inhibition by purified natural and synthetic molecules. A slight decrease of hyaluronidase activity was observed in the presence of PEG. Most interestingly, the effect of PEG on the hyaluronidase inhibition potential of epigallocatechin gallate (EGCG), a natural reference inhibitor of hyaluronidase, was remarkable where the inhibition was almost completely lost in crowded media (from 98 to 11%). This drastic decrease of inhibition upon adaptation of real life-like conditions may suggest that EGCG does not function as well as speculated *in-vivo*. Therefore, the use of crowded *in-vitro* assays may serve the drug discovery processes by eliminating false positive hits that may go unnoticed until clinical trials, thus economizing time and money which are better spent on the investigation of more promising hits. A challenging feature of using the biomolecular crowding approach is the elevated sample viscosity which can be problematic for injection into CE. It is for this reason that the electrokinetic injection approach was attempted as a way to overcome the high sample viscosity but was found to give low injection reproducibilities. It is therefore important to verify the injection repeatabilities upon use of macromolecular crowding to ensure injection of the same sample quantities. It would be interesting to compare the results obtained by induced biomolecular crowding to those obtained in a true ECM *in vivo*.

Understanding the bioactivities of nature-derived therapeutics may come a long way in the development of cures and remedies of various diseases and medical conditions. CE was used to characterize plant extracts for their hyaluronidase inhibitory potential. The three plants: hawthorn, blackcurrant and *Chrysanthellum americanum* have been chosen thanks to their rich therapeutic history. In order to obtain a clearer insight about the plant's bioactivities, their anti-angiotensin converting enzyme (ACE) and antioxidant activities were investigated using conventional spectrophotometric techniques. The results demonstrate the interest of using these

plant extracts as therapeutic herbal tea infusions given their hypotensive, antioxidant and antihyaluronidase bioactivities.

The hyphenation of CE to mass spectrometry (MS) represents important technical and analytical challenges given the difficulty of achieving this type of hyphenation and the relatively poor repeatabilities of migration times. Through an interlaboratory study involving several groups utilizing different methods and approaches, the interest of using CE-MS in metabolomics was explored. Hyphenation difficulties were overcome through the use of special sheath liquid or sheathless CE-MS interfaces. The substitution of migration time scales with those of electrophoretic mobilities provided an answer to the poor repeatabilities since the latter was not dependent on factors resulting in variations of the migration time. Several small anionic and cationic metabolites in human biological fluids were successfully separated, detected and annotated by CE-MS. Concerning the use of CE-MS hyphenation for enzymatic studies, nucleoside kinases were used as model enzymes. A CE-based nucleoside kinase assay was developed using CE-UV and successfully transposed and adapted for CE-MS. Novel C5 substituted thymidine monophosphate analog substrates (such as methyl substituted analogs) were demonstrated as active and effective antivirals *via* their activation by thymidine monophosphate kinase (TMPK). One of the major challenges faced was the commercial unavailability of nucleoside kinases with appreciable catalytic activities, requiring their expression in special vectors. This requires expertise in the field of biomolecular engineering and is often time consuming and the enzymatic yields are small. Therefore, it is important to take into consideration sample consumption during the development of the assay. Fortunately, CE thrives when sample and reagent consumption are involved since only few tens of nLs are injected into the capillary.

The developed CE-based assays, whether those used for lipases or kinases, can be implemented for the discovery of novel substrates or modulators of both enzymes. Although these assays were designed according to the enzymes mechanisms of action, the adaptability of CE for assaying different enzymes was demonstrated and thus it is possible to develop novel assays based on the ones presented herein. Most of the enzymatic reactions presented in this thesis are within the realm of *in vitro* assays, the use of crowded media with CE can be considered as an important transition towards *in vivo*-like conditions. It would be interesting to validate the findings of the hyaluronidase modulation in presence of PEG through the use of modulators that resemble those used in this thesis in addition to new classes of molecules to gain new insight about the mechanism of molecular interactions with the crowding agents. The coupling of catalytic activity and binding affinity assays through the complementary use of CE-based

and MST assays would be an interesting approach to screen for novel drug candidates understanding their binding mechanisms and their modulatory effect on a target enzyme.

Ghassan Al Hamoui Dit Banni

Suivi de l'activité enzymatique et de sa modulation par CE: application à l'étude des lipases et nucléosides kinases

L'électrophorèse capillaire (CE) a montré un potentiel prometteur en tant que technique complémentaire ou alternative aux techniques conventionnelles pour diverses applications pharmaceutiques et thérapeutiques. L'une des applications les plus intéressantes en CE est celle de la miniaturisation des criblages de candidats modulateurs des activités enzymatiques.

Cette thèse visait à démontrer la puissance et la flexibilité de la CE pour le suivi des réactions enzymatiques en l'absence ou en présence de modulateurs naturels (extraits de plantes ou molécules naturelles purifiées) ou synthétiques. Les réactions en mode hors-ligne et en-ligne ont été utilisées après optimisation. De plus, plusieurs techniques de détection telles que l'UV, le C⁴D et la MS, ont été utilisées pour l'étude des enzymes modèles à savoir les lipases et les nucléosides kinases en particulier. La thermophorèse à micro-échelle (MST), été utilisée pour l'évaluation des affinités de liaison entre les lipases et des petites molécules (K_d). La complémentarité entre les résultats de l'affinité moléculaire et ceux de la modulation de l'activité enzymatique obtenus par CE permet l'obtention d'une image plus complète du mécanisme moléculaire par lequel les ligands induisent des changements dans l'activité enzymatique. Par ailleurs, l'important effet de l'encombrement (bio)moléculaire a été démontré par un test de l'activité de l'hyaluronidase en CE. Les dosages de la bioactivité de plusieurs extraits de plantes, utilisant la CE ainsi que plusieurs techniques plus conventionnelles, ont révélé l'intérêt d'utiliser ces extraits sous forme d'infusions compte-tenu de leurs propriétés anti-hyaluronidase, hypotensives et antioxydantes. En plus des dosages enzymatiques, l'application de la CE, plus spécifiquement la CE-HRMS, pour la détection de métabolites dans des échantillons biologiques complexes a démontré une excellente répétabilité en utilisant l'échelle de mobilité effective au lieu de l'échelle de temps de migration conventionnelle. En outre, un test basé sur la CE-MS a été développé et appliqué avec succès pour surveiller l'activité des nucléoside kinases et cribler l'activité de nouveaux substrats antiviraux

Mots-clés : Electrophorèse capillaire, suivi enzymatique, thermophorèse à micro-échelle, spectrométrie de masse à haute résolution, lipases, nucléoside kinases, encombrement (bio)moléculaire, extrait des plantes.

CE platform for assaying enzymatic activity and modulation: application to lipases and nucleoside kinases

Capillary electrophoresis (CE) has shown promising potential to be used as a complementary or an alternative technique to conventional techniques for several pharmaceutical and therapeutic applications. One of the most significant applications of CE is that of screening for enzyme modulating drug candidates.

This thesis was set to demonstrate the analytical and technical power of CE as for monitoring enzymatic reactions in the absence or presence of natural or synthetic modulators. Both offline and online reaction modes were adopted for mixing the different reactants. Additionally, several techniques for analyte detection such as UV, C⁴D and MS, were hyphenated to CE and used for assaying the activities and regulation of model enzymes, mainly lipases and nucleoside kinases. The modulatory molecules ranged in complexity from isolate, molecules purified from natural or synthesized chemically to complex plant extracts. Microscale thermophoresis (MST) was used for evaluation of binding affinities (K_d) between lipases and small ligands. The complementarity between the results from ligand binding and those from ligand modulation of enzymatic activity allow the construction of a more complete image of the molecular mechanism in which ligands bind and induce changes in the enzymatic activity. Biomolecular crowding was shown through an offline CE-based hyaluronidase assay to have a significant effect on the ability of purified molecules to inhibit hyaluronidase. Bioactivity assays of several plant extracts, using CE in addition to more conventional techniques revealed the benefit of using these extracts as herbal tea infusions given their anti-hyaluronidase, hypotensive and antioxidant properties. In addition to enzymatic assays, the application of CE, more specifically CE-HRMS, for metabolite detection in complex biological samples demonstrated enhanced repeatability upon using the effective mobility scale instead of the conventional migration time scale. Furthermore, a CE-MS based assay was developed and successfully applied to monitor the activity of nucleoside kinases and screen the activity of novel anti-viral substrates.

Keywords: Capillary electrophoresis, enzymatic assays, microscale thermophoresis, high resolution mass spectrometry, lipases, nucleoside kinases, biomolecular crowding, plant extracts.



Institut de Chimie Organique et Analytique
Université d'Orléans, CNRS UMR 7311, BP 6759
45067 Orléans Cedex 2, France

